

Regulation of Cytokinesis in Neural Stem Cells During Cerebral Cortex Development

Katrina Colleen McNeely

Nottingham, Pennsylvania

B.S., Biochemistry, Indiana University of Pennsylvania 2012

A Dissertation presented to the Graduate Faculty of the University of Virginia in
Candidacy for the Degree of Doctor of Philosophy

Neuroscience Graduate Program

University of Virginia

February 14, 2020

Noelle Dwyer, Ph.D. (Dissertation Advisor)

Bettina Winckler, Ph.D. (Executive Committee Member)

Xiaowei Lu, Ph.D.

Jung-Bum Shin, Ph.D.

Sarah Siegrist, Ph.D.

Abstract

Mammalian brains have an expanded cerebral cortex, which is essential for many of the processes we consider to be innately human, like consciousness and language. The cerebral cortex contains six layers of neurons that are all derived from the expansion of neural stem cells (NSCs). The neurons within these layers are polarized cells with unique morphologies. The fate decisions that occur during cell division of NSCs to produce specific neurons for each layer is still under intense investigation.

NSCs must make these fate decisions at the correct time during development to produce an exact number of neurons. Errors in neuron production cause developmental disorders like microcephaly. How NSCs can control this cell fate process is still quite mysterious. The coordination of many different processes most likely controls cell fate decisions. In this thesis, we will focus on one cell cycle process, cytokinesis. Cytokinesis, the separation of two daughter cells, can be split into cleavage furrowing and abscission. We will focus on two critical proteins that localize to the midbody during abscission, Kif20b and Cep55. The loss of either of these proteins causes problems with NSC divisions and mouse mutants with small brains. This highlights the importance of regulated NSC cytokinesis for developing a correctly sized and correct structure cortex.

This thesis work furthers our understanding of cytokinesis within the developing cerebral cortex, and the role of two midbody proteins Kif20b and Cep55. We have found that abscission duration and midbody remnant disposal is regulated developmentally. The loss of Kif20b in cell lines causes dysregulated cleavage furrowing and abscission, as well as disrupted ESCRT recruitment. When Kif20b is lost in NSCs, abscission is faster, and there is p53-independent early neurogenesis. Kif20b also affects neuron polarization and outgrowth. Without Cep55 in NSCs, these cells have longer abscission, increased binucleate daughter cells, perturbed ESCRT recruitment, and dysregulated midbody remnant disposal.

These data, taken together, show that slight perturbations from the loss Kif20b or Cep55 cause dysregulated cytokinesis and influence overall brain development. Both proteins are expressed in other cell types, but the brain is the most severely perturbed. This highlights the essential role regulated cytokinesis and midbody remnant disposal play in cerebral cortex development.

Acknowledgements

I want to thank my mentor, Noelle Dwyer, for the opportunity to work in her lab. Noelle has supported and encouraged me over the years to become an independent scientist. It has been a great privilege to work in the lab on topics that I find biologically interesting. Noelle has encouraged me to take on challenging projects, and it has yielded a fun and exciting graduate school experience.

I want to thank members of the Dwyer and Lu labs for the continued support over the years. I want to thank Jessica Neville Little, a former graduate student in the Dwyer lab. Jessica has been a great friend and scientist. I appreciate her thoughtful conversation and review of my project. Working alongside her has pushed me to be a better scientist. Additionally, her support and friendship during the tough times in graduate school made things easier. I want to thank Andre Landin-Malt, a post-doc in Xiaowei Lu's lab, for his continued support as a friend and mentor. I appreciate his enthusiastic personality that has yielded many years of laughter and fun in the lab. I would like to thank our lab technician, Kaela Lettieri, for her help over the past few months with the mouse colony and experiments. It has been a pleasure to mentor her and work with her. Over the years, I have had a pleasure to work with several undergraduates: Sara Martin, Adriana Ehlers, Madison Hecht, Sam Lim, Caitlin Cook, Nitya Khatri, and Naaz Daneshvar. It has been a great experience to mentor them and watch them all grow as scientists.

I want to thank my committee: Bettina, Xiaowei, Sarah, and Jung-Bum, for their continued support over the years. The feedback about papers, data, and presentations have helped to push this project forward. I would also like to thank the NGP and NGP directors (Manoj Patel, Chris Deppmann, and Alban Gaultier) for their support. Particularly, Nadia Badr Cembré has been instrumental in my success as an NGP student, and I am grateful to her for her advice and time.

I have been lucky enough to have an extensive support system during graduate school. I had an excellent incoming NGP class Katie, Jamie, and Ben. These fellow scientists helped to encourage me and made great study partners during classes. Friends both near and far have been essential to my success. I am grateful to Gracie, SaraJane, Kristen, Breanna, and Robyn for their encouragement.

I would not be in graduate school if it weren't for the constant support of my family. My parents, Colleen and David Owens, and my sister, Emily Hess, have always been available to listen to me talk about what I am doing and offering their advice and support. My parents instilled a curiosity and love for science in me as a child, and I will be forever grateful for this. I want to thank my husband, Ryan McNeely, for his unwavering support and love. Ryan has spent the last years, making sure I am well fed; this small gesture means a lot on those days with long hours and disappointing results. He has been my rock, and I am forever grateful for him.

Table of Contents:

<u>Abstract</u>	<i>ii</i>
<u>Acknowledgements</u>	<i>iii</i>
<u>List of Figures</u>	<i>viii</i>
<u>Chapter I: Introduction</u>	<i>1</i>
1.1 Overview	
1.2 Neurogenesis in the Neocortex	
1.2.1 Apical Progenitors	
1.2.2 Basal Progenitors	
1.2.3 Regulation of cell fate through inheritance of various candidate determinants	
A. Apical membrane inheritance is influenced by spindle and cleavage planes.	
B. Inheritance of the Basal Process	
C. Inheritance of Numb and Par complex	
D. Asymmetric Centrosome Inheritance	
E. Midbody Remnants Can Influence Daughter Cell Fate and Epithelial Polarity	
F. Length of the Cell Cycle May Control Types of Divisions (Neurogenic or Proliferative)	
1.2.4 Polarization and Migration of Post-Mitotic Neurons	
1.3 Cytokinesis in the Developing Epithelium	
1.3.1 Cytokinesis: the last step of cell division	
1.3.2 Cytokinesis in an epithelium	
1.3.3 Duration of abscission	
A. Delayed and Failed Abscission	
B. Faster Abscission	
1.4 Kinesin-6 Family Member: Kif20b	
1.4.1 What are the known functions of Kinesin motor proteins?	

- 1.4.2 Kinesin-6 family members have cytokinetic and possible post-mitotic roles
- 1.4.3 The role of Kif20b in abscission of HeLa cells and Neural Stem Cells
- 1.4.4 Kif20b interactors
- 1.4.5 Mouse model of a loss of function mutation in Kif20b causes microcephaly

1.5 Research Objectives

Chapter II: Kinesin-6 KIF20B is required for efficient cytokinetic furrowing and timely abscission in human cells.....42

Introduction

Materials and Methods

Results

Discussion

Figures

Chapter III: Cytokinesis and post-abscission midbody remnants are regulated during mammalian brain development.....76

Introduction

Materials and Methods

Results

Discussion

Figures

Chapter IV: Mutation of Kinesin-6 Kif20b causes defects in cortical neuron polarization and morphogenesis.....105

Introduction

Materials and Methods

Results

Discussion

Figures

Chapter V: Conclusions and Discussion.....139

5.1 Overview	
5.2 Role of abscission duration and midbody remnants in cell fate and cortical development	
5.3 Midbody proteins, Kif20b and Cep55, reveal essential cytokinetic regulation in brain development	
5.4 Microtubule function of Kif20b may explain abscission and axon outgrowth phenotypes	
5.4 Future Directions: Where can we go from here?	
<u>Appendix I: Neural stem cell abscission in the absence of Cep55.....</u>	161
Figures	
<u>Appendix II: Kif20b mutant NSCs undergo premature neurogenesis.....</u>	182
Figures	
<u>Appendix III: HeLa midbody remnants do not influence cell fates of NSCs or neuron polarization.....</u>	195
Figures	
<u>Appendix IV: Diaphanous- 3 (mDIA2) midbody localization is reduced in Kif20b knockdown HeLa cells..</u>	199
Figures	
<u>Appendix V: Kif20b mutant neuron outgrowth phenotypes differ on L1CAM and Laminin.....</u>	208
Figures	
<u>Appendix VI: Shootin1 mutant neurons do not grow longer on L1CAM.....</u>	227
Figures	
<u>References.....</u>	230

List of Figures

Chapter I: Introduction: cytokinesis and the developing brain

Figure 1-1: Spindle angle vs. Cleavage Plane of dividing NESCs.....7

Figure 1-2: Schematic of Kif20b and Cep55 localization during abscission.....21

Chapter II: Kinesin-6 KIF20B is required for efficient cytokinetic furrowing and timely abscission in human cells

Figure 2-1: KIF20B localizes to the central spindle and midbody throughout cytokinesis in HeLa cells.....62

Figure 2-2: KIF20B protein shows overlapping but distinct localization from MKLP1/KIF23 and MKLP2/KIF20A during cytokinesis.....63

Figure 2-3: Cytokinesis defects in KIF20B-depleted asynchronous HeLa cell cultures.....64

Figure 2-4: Cleavage furrow ingression is slower in KIF20B-depleted cells.....65

Figure 2-5: Midbodies tend to be thinner in KIF20B-depleted HeLa cells.....66

Figure 2-6: Midbody assembly appears normal in KIF20B-depleted cells.....67

Figure 2-7: Midbodies of KIF20B-depleted cells show reduced frequency of constriction sites and increased CEP55 intensity.....69

Figure 2-8: Pattern of anillin and VPS4 recruitment are consistent with late-stage maturation defect in KIF20B-depleted midbodies.....70

Figure 2-9: KIF20B depletion delays and dysregulates abscission.....71

Supplemental Figure 2-1: Knockdown efficacy of siRNAs to human KIF20B.....73

Supplemental Figure 2-2: Example deconvolution images of normally organized central spindles.....74

Supplemental Figure 2-3: Spastin recruitment in the midbody does not require KIF20B.....75

Chapter III: Cytokinesis and post-abscission midbody remnants are regulated during mammalian brain development

Figure 3-1: Imaging cytokinesis in neural stem cells of developing cortex.....94

Figure 3-2: In Kif20b mutant brains, a subset of NSCs furrow more slowly.....96

Figure 3-3: Abscission is accelerated in Kif20b mutant cortex.....98

Figure 3-4: Sequential abscissions on both flanks are observed in most NSC divisions, and occur faster in Kif20b -/- brains.....100

Figure 3-5: Midbody remnants (MBR) are detected at the apical membrane, and correlated with early proliferative symmetric divisions.....102

Supplemental Figure 3-1: NSC midbody remnants (MBRs) retain central bulge (marked by CitK or Cep55), but not midbody flanks (marked by Survivin or AurKB).....104

Chapter IV: Mutation of Kinesin-6 Kif20b causes defects in cortical neuron polarization and morphogenesis

<u>Figure 4-1</u> : Cortical neurons show abnormal morphologies in Kif20b ^{-/-} brains.....	127
<u>Figure 4-2</u> : Kif20b expression and localization in cultured cortical neurons.....	128
<u>Figure 4-3</u> : Kif20b mutant neurons are less polarized at 2 days or 4 days in vitro.	129
<u>Figure 4-4</u> : Kif20b mutant axons have reduced enrichment of Shootin1 in the growth cone.	130
<u>Figure 4-5</u> : Morphological changes in Kif20b mutant neurons are not due to cell type.....	132
<u>Figure 4-6</u> : Kif20b mutant neurons that polarize have shorter axons, longer minor neurites, and more axon branches.....	133
<u>Figure 4-7</u> : Kif20b mutant neurons have wider axons and minor neurites than controls.....	134
<u>Figure 4-8</u> : Kif20b mutant neurons' growth cones have longer filopodia.....	135
<u>Figure 4-9</u> : Kif20b mutant axons are more likely to retract and retract farther than controls.....	136
<u>Figure 4-10</u> : Summary of phenotypes of Kif20b mutant neurons seen in culture.....	137
<u>Supplemental Figure 4-1</u> : Morphological abnormalities in Kif20b mutant cells are observed in both Ctip2 ⁺ and Ctip2 ⁻ neurons.....	138

Chapter V: Conclusions and Discussion

<u>Table 5-1</u> : Comparison between Kif20b and Cep55 mutant phenotypes.....	146
<u>Table 5-2</u> : Candidate protein interactions of Kif20b that are of the most interest.....	148

Appendix I: Abscission in the absence of Cep55

<u>Figure App 1-1</u> : Cep55 mutant eyes are similar in size to controls.....	170
<u>Figure App 1-2</u> : Cep55 mutants have a normal proportion of NSCs exiting the cell cycle at E12.5.....	171
<u>Figure App 1-3</u> : Cep55 mutation results in an increased midbody index in apical NSCs.....	172
<u>Figure App 1-4</u> : Cep55 mutant midbodies are shorter in NSCs and thinner in MEFs.....	173
<u>Figure App 1-5</u> : Midbody Remnants are increased at the apical membrane in Cep55 mutants.....	175
<u>Figure App 1-6</u> : Increase in multiciliated NSCs and longer cilia at later developmental stage.....	176
<u>Figure App 1-7</u> : Cilia length is correlated with endfoot size in Cep55 mutants during later developmental stages.....	177
<u>Figure App 1-8</u> : Cep55 mutant MEFs and NSCs have delayed ESCRT recruitment.....	178

Figure App 1-9: Cep55 mutant NSCs have tripolar spindles and tripartite midbodies.	179
Figure App 1- 10: Cep55 mutant cells have a delay in microtubule disassembly.	180
 Appendix II: Kif20b mutant NSCs undergo premature neurogenesis	
Figure App 2-1: Kif20b mutant brains show reduced proliferative symmetric divisions and increased neuron daughters in early corticogenesis.	189
Figure App 2-2: The increased neuronal fate of Kif20b mutant NSC daughters during early cortical development is not p53-dependent.	190
Figure App 2-3: Kif20b mutant cultures have increased NSCs and NSCs have a normal cell cycle.	191
Figure App 2-4: Kif20b mutant endfeet are more asymmetric at E11.5 then E15.5.	192
Figure App 2-5: Apical endfoot asymmetry is a consequence of cell death in the Kif20b mutants.	194
 Appendix III: HeLa midbody remnants do not alter fates of NSCs or neuron polarization	
Figure App 3-1: HeLa cell remnants do not offer cell fate or polarization cues to cultured neural stem cells.	198
 Appendix IV: The formin Diaphanous- 3 (mDIA2) interacts with Kif20b and is a candidate for p53 activation in Kif20b depleted cells.	
Figure App 4-1: Knock-down of Kif20b disrupts mDIA2 localization in the midbody and cleavage furrow.	203
Figure App 4-2: Serum antibodies for mDIA2 are not as specific as Proteintech antibody.	205
Figure App 4-3: Example images of mDIA2 staining in E11.5 or E12.5 NSCs.	206
Figure App 4-4: The loss of Kif20b in HeLa cells does not increase mDIA2 nuclear localization.	207
 Appendix V: Differential axon outgrowth phenotypes between L1CAM and Laminin	
Table App 5-1: Summary of Kif20b mutant phenotypes on different substrate.	218
Figure App 5-1: Kif20b neurons polarize more and grow longer axons on L1CAM.	220
Figure App 5-2: Kif20b mutant neurons have longer axonal branches and rescue the filopodia defect on L1CAM.	222
Figure App 5-3: Kif20b^{-/-} cortical neuron polarization and axon outgrowth is similar to controls when grown on Laminin.	224
Figure App 5-4: Increased ratio of acetylated tubulin to tubulin found in mutant axons is independent of substrate.	225
Figure App 5-5: SiR-Tubulin, a taxol derivative, treatment stops Kif20b mutant axon overgrowth on L1CAM.	226

Appendix VI: Shootin1 Mutant neurons do not grow longer on L1CAM

Figure App 6-1: Shootin1 mutant neurons have normal axon
outgrowth.....229

Chapter I: Introduction

1.1 Overview

The brain is a complex organ that contains billions of neurons. Mammalian brains contain features that are believed to offer cognitive advantages. One of these features is the expanded cerebral cortex, which is thought to play a role in consciousness and language. This dissertation will focus on the development of the mammalian cerebral cortex. The neocortex is made up of six layers of neurons that develop in an inside-out manner. The neurons within these layers are polarized cells with unique morphologies. As a scientific community, we are still dissecting the coordinated processes required to produce the number of neurons needed in the adult brain.

One of these coordinated actions is the well-controlled cell division that occurs in the neuroepithelium. The neuroepithelium is a pseudostratified tissue with a defined apical side and basal side (Farkas and Huttner, 2008). The cells that occupy this space are considered neural stem cells (NSCs) and are responsible for the production of all the neurons and glia in the brain (Farkas and Huttner, 2008). In order to produce enough NSCs to expand the epithelium, these stem cells undergo symmetric division. As expansion ends, neurogenesis and asymmetric division begins and is marked by the transition of NSCs into a progenitor cell known as radial glia (Tan and Shi, 2013). The radial glial phenotype allows the cells to continue to proliferate but confines daughter cell fate to radial glia, neurons, and glia.

Elucidating factors that influence the switch from symmetric to asymmetric division is a continually expanding field. A few of the factors believed to alter division and cell fate are: spindle orientation, inheritance of membrane, segregation of proteins, and cell cycle timing (Tan and Shi, 2013). In this dissertation, we investigate two proposed cell fate determinants: midbody inheritance and duration of abscission (**Chapter III, Appendix I, Appendix II**). We are only starting to understand the mechanisms that coordinate fate decisions.

The regulation of NSC division is crucial for developing a cortex that is the correct size. There are mouse models of mutations that affect NSC division and brain size. One of these models is the loss of Kif20b. Kif20b is a member of the kinesin-6 family and a plus end-directed motor. Kif20b has been shown to have a role in coordinating abscission,

the final step of cell division ((Abaza et al., 2003; Maliga et al., 2013), **Chapter II, III**).

The loss of this kinesin has been shown to produce a small brain phenotype (Janisch et al., 2013). The loss of Kif20b protein dysregulates abscission in both cortical NSCs and HeLa cells ((Janisch et al., 2018), **Chapter II and III**) and disrupts *in vitro* neuron polarization and axon outgrowth ((McNeely et al., 2017), **Chapter IV, Appendix V**).

Another mouse model is the loss of the midbody protein Cep55. Cep55 has been shown in cell lines to be essential for abscission to complete (Zhao et al., 2006). The loss of Cep55 causes a small brain phenotype and abscission delay in cortical NSCs (Little, 2019), **Appendix I**).

1.2 Neurogenesis in the Neocortex of Mammals

In the mammalian neocortex, all excitatory neurons are derived from the same group of stem cells that are located in the ventricular zone of the neuroepithelium. The stem cells have apical-basal polarity, which forms the pseudostratified epithelium. Initially, these stem cells are known as neural stem cells (NSCs), which divide symmetrically to increase the epithelium in size as the neural tube is folding. Eventually, the NSCs transition into a progenitor cell known as radial glial cells (RGCs) which are responsible for neurogenesis. This transition doesn't occur until after the closure of the neural tube. The cells have their apical side facing the ventricle and their basal side facing the outside of the neural tube. Progenitor cells are split into two categories: apical or basal. Cell division of both apical and basal progenitors can be classified into asymmetric and symmetric based on the fate of the daughter cells.

I. Apical Progenitors

Apical progenitor is a broad term encompassing both NSCs and RGCs. NSCs undergo symmetric division to increase the progenitor pool by creating two identical progenitor cells early in development. RGCs undergo asymmetric division and are a part of neurogenesis. Neurogenesis is defined as the creation of neurons either directly or indirectly. Direct neurogenesis is a division that produces a progenitor cell and a neuron. Indirect neurogenesis is a division that produces a progenitor cell and a basal progenitor, which can divide to form two neurons. Indirect neurogenesis amplifies the output of the apical progenitors, which drives the radial expansion of the cerebral cortex.

Apical progenitors undergo *interkinetic nuclear migration* (IKNM) in which the nucleus moves within the ventricular zone as it undergoes different phases of the cell cycle. The nucleus is at the ventricle during mitosis and early cytokinesis. At G1, the nucleus is moving within the cell from the apical side to the basal side, whereas during G2, the nucleus is moving from the basal side to the apical side preparing to enter into mitosis (Farkas and Huttner, 2008). At the earliest stages of development, the migrating nucleus within the VZ reaches the basal lamina (Farkas and Huttner, 2008). During later stages, the nucleus does not reach the basal lamina because the first neurons have migrated and formed the preplate and the VZ is no longer abutting the basal lamina. IKNM is believed to occur to allow more cells to divide in the same tissue as well as expose the cells to an apical-basal distribution of factors (Paridaen and Huttner, 2014).

Apical progenitors maintain polarity within the neuroepithelium. These progenitor cells have a unique bipolar structure in which they have an apical endfoot connecting the cell body to the apical membrane and a basal process that ascends to the pia. Additional establishment of apical and basal polarity in the apical progenitors arises from polarity proteins like the Par complex (Par3, Par6, and aPKC) that is located at the apical side of the cell membrane. The centrosome of the apical progenitor is docked at the apical membrane to be the basal body for the primary cilium (Paridaen and Huttner, 2014). This cilium is protruding into the ventricle where it can sense signals and is important to keep apical polarity as NSCs switch to become RGCs.

A. Transition from NSCs to RGCs

As development progresses, around E11 to E12 in mouse, NSCs begin to transform into the progenitor cell known as radial glial cells (RGC) (Gotz and Huttner, 2005). The progression from NSC to RGC occurs over multiple days, and the details of how it is regulated are still mostly unknown. What we do know are markers that appear that allow us to delineate NSCs from RGCs after the transition is over. RGCs begin expressing intermediate filaments such as nestin, vimentin, and sometimes GFAP (Kriegstein and Alvarez-Buylla, 2009). The transition involves the up-regulation of SLC1A3, an astrocyte-specific glutamate transporter, and FABP7, a fatty acid binding protein (Tan and Shi, 2013). The apical junctions lose tight junctions due to the loss of occludin but maintain

the adherens junctions that mediate cell to cell adhesion using cadherins and catenins (Paridaen and Huttner, 2014).

B. Neurogenesis

Once a cell has adopted an RGC phenotype, it will begin asymmetric division and be a part of the more extensive process of neurogenesis. Neurogenesis begins with the first neurons born in the VZ migrating out to form the preplate. The preplate is split into the subplate and marginal zone by the migration of newly born neurons into the cortical plate. The cortical plate is layers two through six in the neocortex. Cajal-Retzius cells are neurons born around E11-E12 to form the marginal zone, which will become layer one in the postnatal cortex (Kwan et al., 2012). These neurons secrete reelin, which is an essential signal for the proper inside-out layer formation. *Inside-out formation* is when newly born neurons migrate into the cortical plate through the previously born neurons along the radial glial fibers (Kwan et al., 2012). Between E12 to E16 in mouse, layer six through layer two are being born either from an asymmetric division from an RGC or by symmetric division from a basal progenitor. The current model of neurogenesis proposes that once RGCs undergo asymmetric division, they no longer undergo symmetric proliferative division. Further understanding of local signaling and inheritance of fate markers may elucidate this in the future.

II. Basal Progenitors

Basal progenitors also known as intermediate progenitors are born around E12 in mice at the ventricle and migrate out of the ventricular zone to form the sub-ventricular zone (SVZ). These cells express transcription factor genes, Eomes (Tbr2) and Cux1/2, which allow them to be distinguished from apical progenitors (Tan and Shi, 2013). Additionally, basal progenitors take on a multipolar phenotype. Basal progenitors only undergo symmetric division, with randomized cleavage planes, either making two basal progenitors or two neurons (Noctor et al., 2008). Another basal progenitor cell type is the outer subventricular zone progenitors known as basal radial glia (bRG). Work in human fetal tissue revealed that these progenitors originate from apical progenitor divisions that had horizontal or oblique cleavage planes (LaMonica et al., 2013). bRGs have similar behaviors to the RGCs, but only retain the basal processes and lack an apical process

(Fietz et al., 2010). These types of progenitors are poorly understood because of their rarity in the mouse neocortex.

III. Regulation of cell fate through inheritance of various candidate determinants

The type of division, symmetric versus asymmetric, in NSCs has a significant role in determining the cell fate of the resulting daughter cells. Symmetric division of NSCs, where two NSC daughter cells are produced, occurs early in development. Symmetric division also occurs in basal progenitors during neurogenesis to dramatically increase cell number, by either producing two neurons or two basal progenitors. Asymmetric division allows for maintenance of the progenitor pool and the creation of neurons, either directly or indirectly. A direct asymmetric division is when a NSC and a neuron are produced and an indirect asymmetric divisions is where an NSC and a basal progenitor are produced. *For this dissertation, we will refer to all apically dividing cells as NSCs or neural progenitors.* Currently, there are many factors thought to play a role in controlling cell fate. Some of these factors are cleavage plane, spindle angle, apical membrane inheritance, basal process inheritance, asymmetric centrosome inheritance, midbody inheritance, protein segregation, and cell cycle length. Experiments from multiple model systems, reveals the diversity of cell fate factors based on cell type and time in development. The exact mechanism that determines symmetric versus asymmetric fates is not well understood. It is unlikely there is one sole determinant of cell fate, but rather multiple in combination can give the vast diversity of actions needed to form the brain.

A. Apical membrane inheritance is influenced by spindle and cleavage planes.

Spindle angle can range from parallel to perpendicular to the ventricular surface. The cleavage plane will appear in between the spindle poles, determining how much apical membrane each daughter cell will inheritance. A parallel to oblique spindle angle results in a vertical cleavage plane and a perpendicular spindle results in a horizontal cleavage plane (**Figure 1-1**). NSC spindle angles are between parallel and oblique, resulting in mostly vertical cleavage planes in the ventricular zone, regardless of developmental age

(Falk et al., 2017; Kosodo et al., 2004; Noctor et al., 2008). NSC endfeet at the apical membrane are connected through apical junctions. These apical junctions are a hybrid of tight and adherens junctions and are thought to be separated into distinct domains containing polarity proteins and junctional proteins (Marthiens and French-Constant, 2009). The cleavage plane is tightly controlled, and slight changes in the angle could

lead to equal inheritance of the apical domains (bisecting) or asymmetric inheritance (bypassing) of the domains. Asymmetric inheritance would result in separation of junctional proteins from polarity proteins in only one of the daughter cells. Both N-cadherin and Zona-Occludin, junctional proteins, are equally inherited between two daughter cells ((Marthiens and French-Constant, 2009), **Appendix II**). Alternatively, prominin 1, which is a proliferative marker and localizes to the apical membrane has equal inheritance during symmetric divisions which results in more proliferative daughters and unequal distribution of prominin 1 during asymmetric division (Kosodo et al., 2004). Interestingly, there was a small percent of cells that resulted in asymmetric divisions that had an equal division of the membrane and proliferative marker prominin 1 (Kosodo et al., 2004).

The rest of this section will discuss three sets of evidence that the apical membrane is not essential for the ability to carry out symmetric and asymmetric divisions (Konno et al., 2008; Postiglione et al., 2011; Shen et al., 2002). First, we will discuss cell fate consequences of two models of defects in spindle orientation (*LGN* and *Inscuteable* mutants). Second, cell fate of progenitor cells *in vitro* which lack all apical membrane and polarity. Third, description-based studies of bRG that divide without an apical attachment.

LGN and *Inscuteable* are cell polarity proteins that position the spindle orientation during mitosis. *LGN* is believed to link the cell cortex to astral spindle microtubules, through

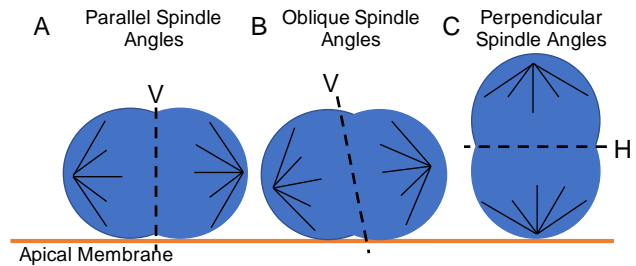


Figure 1-1: Spindle angle vs. Cleavage Plane of dividing NSCs. A. NSC with parallel spindle poles to the apical membrane results in a vertical cleavage plane (V) with equal inheritance of the apical membrane. B. NSCs with spindle poles oblique to the apical membrane will have a vertical cleavage plane that will have unequal inheritance of the membrane. C. An NSC with perpendicular spindle poles to the apical membrane results in a horizontal cleavage plane (H).

interaction with Gai and dynein, to position the spindle in a preferentially parallel manner allowing for a vertical cleavage plane. Inscuteable was found to bind LGN to the Par complex which influences a perpendicular spindle orientation and a horizontal cleavage plane. In the *LGN* knockout, caused by the truncation of the GoLoco domain, the mouse is viable and does not have microcephaly (Konno et al., 2008). With the loss of LGN, the spindle-cell cortex interaction is disrupted, which resulted in random cleavage planes and sacrifice of apical progenitors for non-surface progenitors (Konno et al., 2008). Non-surface progenitors are cells that can divide, express the radial glial marker, Pax6, but do not have an apical attachment (Konno et al., 2008). The authors concluded that LGN was required for parallel spindle orientation to the ventricular surface to keep apical progenitors attached to the membrane but not necessary for maintaining correct numbers of proliferative and neurogenic divisions (Konno et al., 2008). In contrast, the loss of Inscuteable in the mouse caused mostly parallel spindle orientation and more direct neurogenic divisions early on in development. Increase in parallel divisions was at the loss of oblique divisions which the authors suggest are what create basal progenitors. Therefore, this early loss of proliferative capacity through less basal progenitors causes microcephaly (Postiglione et al., 2011). These models tell us that small changes in spindle angle may influence direct versus indirect neurogenic divisions (Inscuteable mutant), but losing the apical membrane attachment (LGN mutant) does not cause cell cycle exit.

Two lines of evidence support the idea that the apical membrane is not essential for production of different cell types in the correct developmental time course. First, when cortical NSCs divide in dissociated cultures, they lack the apical membrane domains as well as the basal process. Surprisingly, the cells can still undergo both symmetric and asymmetric divisions and create layer specific neurons (Cajal Retzius cells, layers six through two) at the right age (Shen et al., 2006). Second, Basal radial glia (bRG) division patterns further supports the idea that spindle orientation may be important for creating a basal progenitor. bRGs are derived from a division of an NSC in which they inherited the basal process but not the apical process (Fietz et al., 2010; Hansen et al., 2010; LaMonica et al., 2013; Wang et al., 2009). bRGs spindle orientation can be vertical to result in a horizontal cleavage plane as described in humans or oblique as described in mouse (LaMonica et al., 2013; Shitamukai et al., 2011). This oblique to horizontal cleavage plane causes one daughter to inherit the basal process and one daughter

without a basal process. The second daughter, still inherits the apical membrane in the mouse and will become a neuron; in humans, the second daughter can regrow a basal process and regain apical progenitor phenotype and divide again (LaMonica et al., 2013; Wang et al., 2009). These data together suggest that apical membrane inheritance is not necessary for a cell to remain proliferative, but raises interesting questions about the basal process.

Spindle orientation and cleavage planes are well-controlled processes. Disruption of these angles can influence the fate of the cell in a highly polarized tissue environment. Interestingly, the disruption of membrane inheritance does not always result in a poorly developed brain. There seem to be some intrinsic signals that control symmetric and asymmetric division that results in proper neurogenic output; regardless of environment. Overall, continuing to unravel the individual effects of proteins involved in cleavage plane, spindle orientation, and the apical membrane will elucidate the importance of these events on cell fate.

B. Inheritance of the Basal Process

Inheritance of the basal process occurs differently across species. In the VZ in mouse E14 slices, multiple groups have shown that the neuron is more likely to inherit the basal process and use it to migrate out of the VZ (Miyata et al., 2001; Tsunekawa, 2012 #1961; Shitamukai et al., 2011). The NSC then regrows its apical process before resuming IKNM (Miyata et al., 2001). In the zebrafish spinal cord, the basal process can split during cytokinesis and then be inherited symmetrically or asymmetrically between the two daughter cells (Kosodo et al., 2008). Interestingly there seemed to be no difference in inheritance patterns between divisions producing two of the same daughter cells or two different daughter cells. The splitting of the basal process was shown less convincingly in mouse neocortex due to difficulty in following the thinning basal process from M phase through cytokinesis and delineating it from the cells around (Kosodo et al., 2008). The most convincing evidence for the splitting of the basal process in the mammalian neocortex was the anillin spot found in the basal process (Kosodo et al., 2008). The anillin spot moves towards the cell body and then localizes to the contractile ring to begin cytokinesis. Cytokinesis machinery in the basal process does support this

idea of splitting the basal process membrane in two. Another hypothesis could be that anillin has a secondary role independent of cytokinesis that has yet to be defined.

It is possible that inheritance of the basal process changes through development. As the neocortex expands, it would become harder to re-grow a process because of the expanding epithelium or split a process because the process becomes thinner. Perhaps with continued improvement of light microscopy and live imaging, we will eventually be able to understand basal inheritance further. For now, we will have to assume basal inheritance to one or both cells can happen and wait to draw any more significant cell fate conclusions.

C. Inheritance of Numb and Par complex

Numb inheritance controls cell fate at different developmental stages. Numb inhibits Notch signaling in the cell. Notch activation in the cell promotes continued cell divisions. A daughter cell that inherits Numb can then block Notch, allowing the cell to differentiate (Shen et al., 2002). At E10.5, dissociated NSCs *in vitro*, have Numb expression segregates symmetrically into daughter cells. At E13.5 and E14.5 Numb segregates asymmetrically into the daughter cell that will become the neuron (Shen et al., 2002). Interestingly the Numb knockout has less P/N divisions than P/P and N/N, which suggests that Numb is important for asymmetric divisions (Shen et al., 2002). Asymmetric divisions are critical during neurogenesis (the peak being around E13-E14 mouse). These data further suggest more than one cue is necessary to “switch” from symmetric to asymmetric fates.

Asymmetric inheritance pattern of Par3, an apical membrane protein, is different in mouse and zebrafish (Alexandre et al., 2010; Bultje et al., 2009). Par3 is an apical membrane protein that helps to establish apical-basal polarity. In mouse, Par3 localizes with Zona Occludin-1 in the apical endfoot of interphase progenitor cells (Bultje et al., 2009). During mitosis, Par3 changes localization to the spindle midzone and can be symmetrically or asymmetrically inherited. In the mouse knockdown of Par3, there is increased neurogenic divisions, and in the overexpression of Par3, there are more proliferative divisions. Interestingly, the level of Notch signaling is coordinated with more or less Par3. The daughter cell that inherits the most Par3 keeps Notch signaling and

remains a progenitor cell in the mouse (Bultje et al., 2009). In zebrafish, Par3 is apically localized, and the neuron inherits this apical attachment and Par3 (Alexandre et al., 2010). This disagreement between these two studies could be the result of the limited understanding of apical progenitors in the zebrafish neural tube and differences across species. Overall, the inheritance of Notch, Numb, and Par3 is temporally and species regulated.

D. *Asymmetric Centrosome Inheritance*

Among the roles of the centrosome are to anchor the NSCs in the ventricular zone, influence mitotic spindle orientation, and prevent up-regulation of p53. Surprisingly, even without the centrosome, the NSCs are still able to divide (Insolera et al., 2014). During G2 of the cell cycle, the centrosome is duplicated and the older (mother) centrosome and newer (daughter) centrosome are segregated to different daughter cells during mitosis. The mother centriole is more mature than the daughter centrioles as defined by the more complex microtubule array seen by electron microscopy (Yamashita et al., 2007). In *Drosophila* male germline, the stem cell inherits the mother centriole, and the differentiated gonialblast inherits the newer centriole in 85% of cells observed (Yamashita et al., 2007). Surprisingly, in the female fly germline, the centriole is segregated opposite to the male fly germline. The differentiated gonialblast inherits the mature mother centriole 70% of the time (Salzmann et al., 2014). The *Drosophila* neuroblast also has an asymmetric inheritance of the centriole, and like the female germline, the mother centriole is inherited by the differentiated cell (16 cells observed, all had the same result). Within the same organism, there are cell-type differences with centrosome inheritance, and it does not appear that inheritance of the mother centriole itself confers proliferative capacity.

In mouse NSCs that are asymmetrically dividing, 78% of the time the mother centriole stays in the ventricular zone and is inherited by the progenitor cell (Wang et al., 2009). The more mature mother centriole not only has the anchor microtubules but also expressed specific proteins like ninein. Ninein localizes to appendages and satellites of the mother centriole (Wang et al., 2009). When ninein was depleted experimentally, there was a premature exit of progenitors from the ventricular zone resulting in more neurons and the loss of Pax6+ cells (Wang et al., 2009). In this case, the centriole

inheritance seems to confer proliferative capacity. Interestingly, the mother centriole inherits a piece of the apical membrane during cell division and this inheritance is important for the establishment of the new cilium (Paridaen et al., 2013). This further supports the idea that the mother centriole is important for maintaining proliferative capacity of the cell remaining at the apical membrane.

These different results in asymmetric segregation of the mother centriole may not confer blanket proliferative capacity. However, the asymmetric segregation of mother centrioles does seem to influence the fate of daughter cells within a cell type.

E. Midbody Remnants Can Influence Daughter Cell Fate and Epithelial Polarity

The cytokinetic abscission of the midbody, the connection between two daughter cells thought to occur unilaterally or bilaterally (Dionne et al., 2015). The regulation of abscission on either side of the midbody controls the release into extracellular space or directly inherited by one daughter cell. Once abscission has occurred, the post-abscission midbody is referred to as the midbody remnant. The released midbody remnant can be inherited by one of the daughter cells or neighbor cells through engulfment (Chai et al., 2012; Crowell et al., 2014; Dionne et al., 2017; Peterman et al., 2019). For a more detailed description of the regulation of unilateral or bilateral abscission see the section on cytokinesis. Proteomic, lipidomics, and transcriptomic approaches have revealed that the midbody remnant is enriched for certain lipids including a type of phosphatidylserine (PS), contains over 400 proteins and many mRNAs ((Addi et al., 2020; Arai et al., 2015; Atilla-Gokcumen et al., 2014; Skop et al., 2004), personal communication with Skop lab). The diversity of proteins within the midbody remnant and the varied stereotyped behavior in different model systems raises the question: what is the role of the midbody remnant? In this section, we will summarize what is known so far about midbody remnant in *C. elegans*, *Drosophila*, mammalian cell culture, and mammalian neuroepithelium.

a) *Midbody Remnant Handling and possible influences on cell fate or polarity in C. elegans*

Important polarity cues are established from stereotyped midbody remnant inheritance in *C. elegans*. *C. elegans* have a well-characterized invariant division pattern which allows each midbody remnant to be followed in the lineage. In *C. elegans* early embryo, there is stereotyped inheritance that influences the next cell division and polarity. The midbody remnant of the P0 division is internalized by the endomesodermal blastomere (EMS) and the midbody remnant helps rotate the spindle of the posterior cell for the next division, establishing dorsal-ventral polarity within the embryo (Singh and Pohl, 2014b). This first division and the following two divisions all occur with asymmetric spindle positioning that places the midbody remnant near the cell responsible for internalization (Ou et al., 2014). Later in *C. elegans* development, there is the division of the Q neuroblast. This stereotyped asymmetric division results in four divisions to produce three neurons and two apoptotic cells (Chai et al., 2012). All of the midbody remnants from these four divisions are released extracellularly and then engulfed by a stereotyped neighboring cell (Chai et al., 2012). This is the same cell responsible for clearing the apoptotic cells from the Q cell divisions. Midbody remnants are released into the intercellular space in the early embryo and later Q divisions and are cleared through apoptotic engulfment pathways (Chai et al., 2012; Fazeli et al., 2016; Ou et al., 2014). The Q division midbody remnants are marked for engulfment and degradation by externalized PS, a known “eat me” signal (Chai et al., 2012). Since Q cell divisions are meant to produce differentiated daughter neurons, the removal of midbody remnant through degradation supports a hypothesis that differentiating daughters get rid of the midbody remnant.

b) *Midbody Remnant Handling and Cell Fate Influences in Drosophila*

Drosophila have a unique requirement for the midbody remnant in cell identity and establishing polarity. In *Drosophila* germline stem cells, inheritance of the midbody ring in both male and female fly germlines is preferential to the daughter cell with the daughter centrosome (Salzmann et al., 2014). As mentioned in the previous section, the male germline stem cells inherited the mother centrosome, and the differentiated cell inherits the daughter centrosome (Yamashita et al., 2007). In female germline cells, the opposite is true.

Midbody remnants have been proposed to promote polarity and maintenance of individual cell characteristics. Cytokinesis remnants (RhoA and AuroaA) establish an apical pole that indicates where the first neurite will grow from (Pollarolo et al., 2011). Midbody remnants may help to set up polarity within the daughter cell. These data together suggest that midbody remnants are important for asymmetric segregation of factors to establish both cell identity and polarity in a cell type-dependent manner.

c) *Midbody Remnant Handling in Mammalian Cell Lines*

As implied by work from *C. elegans* and *Drosophila* midbody remnant engulfment has a primary role in differentiation phenotypes or polarity. Therefore, much of the work done in mammalian cell cultures has been centered around if the midbody remnant is engulfed and degraded. Multiple groups have now shown that cancer cells release midbody remnants and then proceed to engulf and accumulate midbody remnants at a higher rate compared to stem cells or other cell lines (Crowell et al., 2014; Dionne et al., 2017; Ettinger et al., 2011; Kuo et al., 2011; Peterman et al., 2019). Accumulation of midbodies in HeLa, US20, and human embryonic stem cells is linked to the inheritance of the older mother centrosome (Kuo et al., 2011). This pattern is different from the *Drosophila* germline, where the midbody remnant goes with the daughter centrosome (Salzmann et al., 2014). Interesting, the accumulation of engulfed midbody remnants in cancer cells lines is enabled by midbody remnants' ability to avoid the lysosome, perhaps by the membrane-bounded midbody remnant coating with actin patches (Peterman et al., 2019). Limited work has been done on the downstream effect of engulfing midbodies. At least in HeLa cells, engulfing the midbody remnants increases the transcriptional activity that promotes cell proliferation compared to HeLa cells without midbody remnants (Peterman et al., 2019). This is an exciting idea that midbody remnants could directly influence the ability of a cell to proliferate.

Two competing hypotheses have been proposed for how midbody remnants influence cell fate. Stemness of a cell is linked to either the release or accumulation of midbody remnants. As mentioned above, much of the work done in mammalian cell lines has been in immortal or cancerous cell lines, which confounds our interpretation of midbody remnants role in differentiation and proliferation. Cancer cells mainly proliferate;

however, tissue stem cells have well-controlled developmental time courses that balance both proliferation and differentiation. Therefore, it might not be surprising if there is more to the roles of midbody remnants than just proliferative capacity and this might be more important for establishing an epithelium, which is explored later in this section.

Interestingly, accumulation of midbody remnants in squamous cell carcinoma cell lines due to a reduction in autophagy of remnants does not cause an increase in proliferation (Dionne et al., 2017). However, there was an increase in invadopodia and ability to colonize in soft agar, which are all characteristics of invasive cancer (Dionne et al., 2017). Therefore, mammalian cell line studies indicate that midbody remnants behavior is not essential for maintaining proliferative capacity but may enhance proliferation and invasiveness of cancer cells.

Although there is no consensus for midbody inheritance conferring stemness or not, there are other examples of its importance. Midbody release or retention can influence differentiation potential in neural stem cell lines. When abscission is blocked using siRNA for endosomal sorting complex required for transport (ESCRT) - III accessory protein Alix (Apoptosis Linked Gene 2 interacting protein X), there was a decrease in midbody release (Ettinger et al., 2011). Additionally, when retinoic acid was used to induce neurite outgrowth in Alix knockdown cells, there were increased levels of differentiation accompanied by longer processes. The author's interpretation of these results supports a hypothesis that a proliferating cell able to respond to differentiation stimuli will release its midbody. This interpretation fails to consider the fact that abscission itself could be disrupted, promoting cell cycle exit, or disrupting the phagocytosis process of the remnant also influencing cell cycle exit. Overall, midbody remnant handling requires more investigation in which manipulations are independent of other abscission processes.

d) *Midbody Remnant Disposal and Positioning in Polarized Epithelia*

Midbody remnants are essential for establishing epithelial polarity in mammalian cell lines. When MDCK and Caco-2 cells are grown within extracellular matrix, a cyst-like structure will form with an apical membrane facing a fluid-filled lumen. To maintain this lumen structure, asymmetric cleavage furrowing, and proper spindle orientation must position the midbody at the apical membrane (Jaffe et al., 2008). Disruption of either of

these processes result in ectopic formation of lumens (Jaffe et al., 2008). Once abscission has occurred, the midbody remnants have been shown to stay at the apical membrane. If these remnants are displaced to the lateral membrane, then ectopic apical membrane formation would occur (Lujan et al., 2016). When midbody remnants were added to the basal side of a 2D-polarized monolayer of MDCK cells, there was re-localization of some apical membrane proteins but not all (Lujan et al., 2017). These remnants were not phagocytosed by the MDCK cells. Taken together these studies suggest, that the midbody is positioned during abscission at the apical membrane to release the remnant there to maintain the established polarity.

Midbody remnants have been implicated in enhancing primary cilia formation in MDCK cells. Bernabe-Rubio et al. reported that following abscission, midbody remnants move along the outside of the apical membrane of MDCK cells until the midbody remnant approaches the centrosome at the apex of the cell (Bernabe-Rubio et al., 2016). It has been reported, that the midbody remnant is surrounded by a special membrane patch and the midbody remnant must deliver a part of this membrane to the centrosome (Bernabé-Rubio et al., 2019). Once this interaction happens MDCK cells begin to grow out their primary cilium (Bernabe-Rubio et al., 2016; Bernabé-Rubio et al., 2019). Physically removing the midbody remnant from the surface of the cell prevented the majority of the MDCK cells (reduced percentage) from developing a primary cilium. Interestingly, this group also found through electron microscopy that a percentage of the “midbody remnants” may actually still be attached to the cell through a plasma membrane tether (Casares-Arias et al., 2019). This tether lacks microtubules but does contain the ESCRT protein Chmp4C. This tether may be a real part of abscission or it could be that the authors caught cells in the process of abscission. I think this will require additional research and would be important to determine if this was unique to MDCK cells. As will be discussed later Chmp4C regulates abscission duration through the abscission checkpoint. Knocking-down Chmp4C in MDCK cells reduced the number of midbody remnants with membrane tethers and the number of MDCK cells with a primary cilium. These data suggest that precise placement of the midbody remnant is important to the formation of the cilium. Interestingly, in another electron microscopy study using HeLa cells this membrane tether was not found (Crowell et al., 2014). It is possible that there are cell type differences. These experiments were all carried out in epithelium that is a single cell layer, it would be important to determine if these membrane tethers occur

in pseudostratified epithelium like the neuroepithelium since the formation of the primary cilia is an important signaling component for proper development.

There has been little work on how midbody remnants establish or maintain epithelial polarity in developing tissues. This is especially interesting in the developing brain where we and others have shown that midbodies align along the apical membrane (Dubreuil et al., 2007; Janisch et al., 2013). Following abscission, the remnants remain at the apical membrane or are released into the ventricle ((Dubreuil et al., 2007) **Chapter III**).

Additionally, we go on to show in Chapter III that more midbody remnants were found associated with younger apical membrane (E11.5) compared to older (E15.5).

Additionally, in E11.5 NSC cultures, we found remnants are more likely to be associated with proliferative divisions (**Chapter III**). These differences suggest developmental regulation of release or engulfment/degradation pathways.

The midbody remnant has been implicated in cell fate and establishment of polarity. While it is clear that there are cell-type differences, the midbody remnant is emerging as an important signaling component. The midbody remnant could be essential to be disposed of to keep stemness and prevent differentiation. More work is needed to understand the importance of the remnant during cortical development and to investigate the possibility that MBR serves to remove fate determinates or trash.

F. Length of the Cell Cycle May Control Types of Division (Neurogenic or Proliferative)

It has been previously reported that in mouse embryonic cortical neural progenitors, the cell cycle length increases over E11 to E18 from 8.1 hours to 18.4 hours (Takahashi et al., 1995). The change in duration due to development happens in two of the phases of the cell cycle: G1 and S. As development proceeds there is an increase in the duration of the cell cycle, and it is due to the increase in time spent in G1 (Takahashi et al., 1995). A recent study has shown that this overall timing increase is the result of more basal progenitor divisions (Arai et al., 2011). Basal progenitors have an extended time in G1 compared to apical progenitors (Arai et al., 2011). Another striking difference in length of the cell cycle was in S phase. Progenitor cells dividing that result in a neurogenic division have a significantly shorter S phase compared to progenitors

dividing to make proliferative daughters (Arai et al., 2011). A genome-wide screen comparing neurogenic neural progenitor cells versus proliferative neural progenitor cells showed a change in the regulation of DNA replication and repair mechanisms as well as cell cycle genes (Arai et al., 2011). Interestingly, no one gene seemed to be exclusively effecting this change. The longer S phase in early proliferative NSCs cells may be critical for these stem cells to maintain their genome for prevention of deleterious mutations.

Unlike G1 and S phase, change in the duration of M phase in NSCs appears to be consistent throughout development. Rather, extending the duration of mitosis can increase the number of neural progenitor cells that exit the cell cycle early (Feng and Walsh, 2004; Pilaz et al., 2016). The *Nde1* loss of function mouse model has microcephaly due to defects in spindle formation. Nde1 is a centrosome protein that directs the organization of gamma-tubulin, and loss of Nde1 increases odd number (3 and 5) of centrosomes per dividing cell. This causes spindle orientation defects, arrest in mitosis, and more cells exiting the cell cycle, resulting in an increase in neurons (DCX+) and a decrease in progenitors (Nestin+). The *Magoh* mutant extends mitosis duration but does not cause the cells to arrest (Pilaz et al., 2016). The haploinsufficient mutant causes microcephaly due to depletion of basal progenitors and neuronal apoptosis (Pilaz et al., 2016). The lengthening of mitosis to > 40 minutes leads to more apoptosis and more neurogenic divisions. Additionally, using pharmacological agents like the microtubule depolymerase, Nocodazole or STLC, which inhibits EG5-mediated centrosome separation, the phenotype in *Magoh* can be mimicked (Pilaz et al., 2016). After the treatment with Nocodazole, the cells exhibit no aneuploidy, normal cleavage planes, increased cell death, and slowed mitosis. This lengthening of mitosis resulted in more neurogenic asymmetric divisions and more symmetric neurogenic divisions (Pilaz et al., 2016). Lengthening mitosis over 40 minutes, independent of *Magoh*, causes increase P/N and N/N divisions as well as cell death (Pilaz et al., 2016). This combination of factors leads to fewer progenitors over time and a decrease in the ability to form new neurons. Thus, three independent methods of slowing mitosis results in the same outcome – more neurogenic divisions.

The work described above shows that daughter cell fate outcomes differ occur based on the duration of phases of the cell cycle. An example is the longer G1 in basal progenitor and shortening of S phase in NSCs as development progresses (Arai et al., 2011). Small

changes in mitosis can lead to significant developmental consequences in the brain through early cell cycle exit (Pilaz et al., 2016). Here we show that another aspect of the cell cycle, abscission, may be developmentally regulated and hypothesize that faster abscission can lead to significant developmental consequences in the brain (**Chapter III, Appendix II**).

IV. Polarization and Migration of Post-Mitotic Neurons

Newly born neurons are simultaneously polarizing, migrating, and have process outgrowth in order to achieve the complex structure of a mature neuron. The *in vivo* polarization for cortical neurons requires coordinated migration and polarization compared to neurons *in vitro* which undergo a process to re-polarize. It is important to keep in mind that neurons cultured *in vitro* most likely had already established polarity before being removed from the brain. When neurons are plated on coverslips, they undergo multiple stages. In stage 1 they send out actin-rich lamellipodia, by stage 2 the cell is now multipolar with dynamic processes. Then in stage 3 symmetry is broken, and an axon is specialized (Dotti et al., 1988). The following two stages involve the outgrowth of dendrites and maturation of the processes (Dotti et al., 1988).

There have been many proteins and factors identified that mediate neuron polarization (Barnes and Polleux, 2009). One protein that has been implicated in breaking the symmetry to transition from multipolar to polarized is, Shootin1. Shootin1 is transported to the growth cone of each growing neurite until symmetry is broken (Toriyama et al., 2006) After symmetry is broken, Shootin1 continues to accumulate in the growth cone of the axon. It is phosphorylated in the growth cone and interacts with L1CAM, and F-actin through Cortactin (Toriyama et al., 2013). Shootin1 is a part of the cellular machinery that transforms the force from F-actin treadmilling to outgrowth of the axon (Toriyama et al., 2013).

In vivo polarization occurs through a multi-step process with similarities to *in vitro* polarization (Polleux and Snider, 2010). First, the neuron adopts a bipolar morphology with a leading process directed towards the basal lamina and a trailing process directed towards the ventricle. The centrosome locates to the leading process to pull the soma forward while the trailing process is released. This movement allows the cell to rapidly

exit the proliferative zone (Gao et al., 2014; Noctor et al., 2004). Once the neuron has reached the SVZ/Intermediate zone the neuron becomes multipolar (Noctor et al., 2004). Interestingly, this multipolar state is very dynamic with retraction and outgrowth of processes similar to stage 2 neurons in culture. The neuron then resumes its bipolar state and migrates towards the cortical plate. Lastly, the leading process will form into the dendritic arbor as the trailing process extends during this migration to become the axon (Hatanaka and Murakami, 2002). Symmetry is broken *in vivo* through a range of factors including polarization cues from the surrounding neurons. These cues may be neurotrophins and the exact mechanism for extracellular cues is still not well understood. Many proteins play a role in neuron polarization like the Par3/6 complex and PI3 kinase, although their exact mechanisms of action remain unclear.

The molecular mechanisms that govern polarization and axon outgrowth are complex. Polarization and axon outgrowth require the remodeling of the cytoskeleton. Therefore, it is unsurprising that Kinesins play important roles in establishing and maintaining polarity. Kif20b facilitates axon outgrowth and polarization ((McNeely et al., 2017), **Chapter IV**) but this is differentially regulated across substrates (**Appendix V**). Microtubules in the *Kif20b* mutant neurons are not as compact as controls and there is more retraction of the growth cone during outgrowth ((McNeely et al., 2017), **Chapter IV**). Both of these findings suggest that Kif20b has an important microtubule bundling and stabilization role within axons. Additionally, we have found that the loss of Kinesin-6 family member Kif20b disrupts polarity protein Shootin1 localization. We hypothesize that Kif20b plays a role in maintaining the correct amount of microtubule stabilization to promote axon outgrowth but not allow for excess or unchecked growth.

1.3 Cytokinesis in a Developing Epithelium

The cell cycle is a well-controlled biological process in the mammalian brain. During the final steps of cell division called cytokinesis, the two cells are separating their connected membrane. The intercellular bridge is the last connection between the two daughter cells. Within this structure is the midbody, a dense microtubule structure that can be organized into two flanks and a central bulge. The last step in which the midbody, the connection between two daughter cells, is severed at one or both flanks is called abscission. In relation to cortical development, well-controlled abscission could

contribute to proper membrane inheritance, midbody inheritance, or duration of abscission itself could be a contributor to the fate or polarity of daughter cells.

I. Cytokinesis: the last step of cell division

Cytokinesis can be split into five parts: formation of the central spindle, specification of furrow plane, constriction of the furrow, midbody formation, and abscission. Abscission is both the process of removing microtubules and plasma scission as well as the final severing events. Experimentally, abscission can be measured from the formation of the midbody to the first microtubule disassembly at the constriction site. The localization of two proteins of interest in this dissertation are highlighted at each step of cytokinesis in the schematic below (**Figure 1-2**).

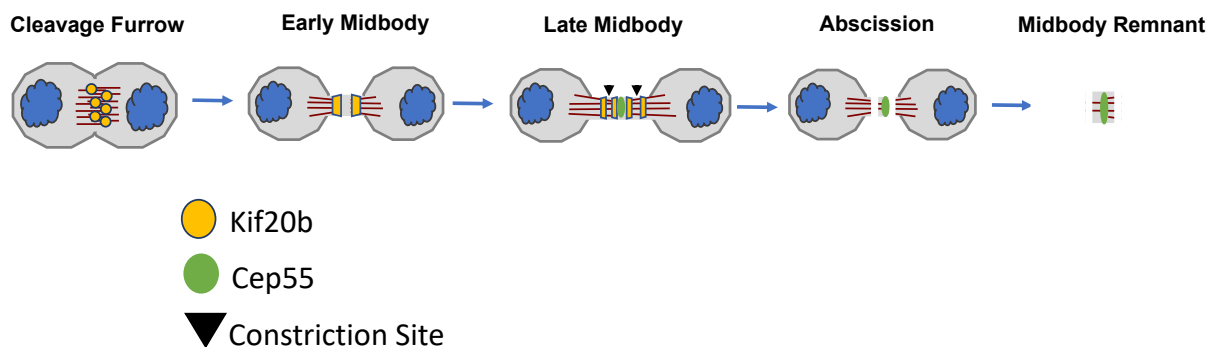


Figure 1- 2: Schematic of Kif20b and Cep55 localization during abscission. Kif20b is on the central spindle during cleavage furrowing and moves to either side of the central bulge during early midbody formation. Cep55 arrives later and distinguishes an early from late midbody. Kif20b is one either side of the constriction sites in a late midbody. Cep55 persists in the midbody remnant after abscission has completed.

The first step, the formation of the central spindle, requires multiple interdependent proteins for assembly. The central spindle is a microtubule structure that forms as the kinetochore microtubules are shortening to move the chromatin towards the poles. The microtubules that make up the central spindle are interpolar microtubules and emanate from opposite ends of the cell to form an antiparallel arrangement. There are three main requirements for central spindle assembly: PRC1, centralspindlin and chromosome passenger complex (Fededa and Gerlich, 2012). PRC1 (Protein Required for Cytokinesis) is a microtubule-bundling protein that is inhibited through phosphorylation

by CDK1 up until anaphase (Zhu et al., 2006). At the metaphase-anaphase transition, PRC1 is transported by Kif4 to the plus ends of the microtubules where PRC1 bundles the antiparallel microtubules (Zhu et al., 2006). Centralspindlin is a heterotetramer of MKLP1 and MgcRacGAP (Green et al., 2012). Centralspindlin recruitment to the central spindle is controlled in two ways. First by CDK1 phosphorylation of the motor head, which is removed at the onset of anaphase (Mishima et al., 2004). Second by Aurora B phosphorylation, which releases MKLP1 from the inhibitory protein 14-3-3 (Douglas et al., 2010). This allows for clustering of centralspindlin in the central spindle (Fededa and Gerlich, 2012). Aurora B is the kinase of the chromosomal passenger complex (CPC). Additionally, Survivin, Borealin, and INCENP are a part of the CPC. CPC is translocated from the centromeres to the central spindle during anaphase onset (Gruenberg and Stenmark, 2004). The translocation of the complex relies on the removal of CDK1 phosphorylation on INCENP (Hummer and Mayer, 2009). MKLP2, through direct interactions with Aurora B and the dephosphorylation of INCENP, allows for the targeting of the CPC to the central spindle (Gruenberg and Stenmark, 2004; Hummer and Mayer, 2009).

Specification of the furrow ingression, the second step, requires changes in the cell cortex as well as recruitment and sequestering of RhoA to a belt around the midzone. The furrow ingression can occur once the central spindle has been established between the separating chromosomes. The cell cortex at the poles undergoes polar relaxation to inhibit cleavage furrow formation at the poles; whereas the cell cortex at the furrow has increased stiffness. The establishment of RhoA, to the cell cortex at the equator, delineates the furrow ingression. RhoA is recruited to the cell cortex and activated by ECT2 (RhoA GEF) (Green et al., 2012). Sequestering of RhoA at the furrow occurs through this ECT2 interaction as well as dynamic astral microtubules and septin. Septin is a GTP-binding protein that can form actin filaments and possibly creates a barrier to help confine RhoA to the midzone (Normand and King, 2010).

In step three of cytokinesis, the actin-myosin ring at the cell cortex constricts the cleavage furrow through a not wholly understood mechanism (Green et al., 2012). Activated RhoA drives the formation of the actin-myosin ring through polymerization of unbranched actin filaments and myosin II activation. Actin polymerization occurs through the activation of formins, which are proteins that nucleate unbranched actin filaments.

Myosin II activity is prompted through Rho kinase (ROCK) phosphorylation of the myosin light chain. Anillin is a scaffolding protein within the ring, and it is believed to interact with myosin, F-actin, and septin through individual binding domains (Schiel and Prekeris, 2010). Once the ring has been established, the ingression of the cleavage furrow begins. The cleavage furrow stops when the intercellular bridge is approximately 1 μm thick (Green et al., 2012).

The fourth step of cytokinesis is the formation of the midbody within the intercellular bridge. The intercellular bridge contains compacted antiparallel microtubules and contains the midbody which has an electron-dense center. Components of the central spindle become a part of the midbody but separate into three different locations (Green et al., 2012). Kif4 and PRC1 remain associated with the central part of the midbody. Centralspindlin and ECT2 are released from the microtubules and become part of the midbody ring. The third area of localization is the midbody flank where MKLP1 and Aurora B can be found. Through centralspindlin recruitment of Cep55 to the central bulge, Cep55 establishes and maintains the midbody in vertebrate cells (Bastos and Barr, 2010; Zhao et al., 2006). *Drosophila* and *C. elegans* do not have Cep55 and MKLP1/Pavortiti has been shown to recruit ESCRTS (Lie-Jensen et al., 2019). When Cep55 is depleted in HeLa cells, the midbody forms but abscission is unable to complete in the majority of cells (Zhao et al., 2006). In a large percent of the cells that do not complete, midbody regression does occur and the cell becomes binucleate. There are around 400 identified midbody associated proteins including the previously mentioned cytokinesis proteins and all three kinesin-6 family members (Addi et al., 2020; Skop et al., 2004). With so many proteins at the midbody this reinforces the previously discussed idea that the midbody may be an important signaling organelle or important for disposal for proper abscission and cell fate.

The fifth and final step of cytokinesis, abscission, has been shown in HeLa cells to complete in G1 of the next cell cycle, happening up to hours after mitosis (Gershony et al., 2014). Abscission includes local disassembly of the cytoskeleton (microtubules and actin and septins) (see (Addi et al., 2018) for review) and the scission of the plasma membrane at sites on midbody flanks. The mechanism of membrane scission in the midbody is not entirely understood. However, there has been a recent consensus for the requirement of endosomal sorting complex required for transport (ESCRT) recruitment to

facilitate microtubule severing and membrane scission in mammalian cells. This model was based initially on ESCRT proteins' well-known role in viral budding where these proteins are responsible for the cleavage of the cellular membrane (Schiel and Prekeris, 2010). Microtubule severing happens concurrently with ESCRT mediated membrane scission. ESCRT-III protein charged multivesicular body protein (CHMP)1A recruits the ATPase, Spastin, to the constriction site to sever the microtubules (Connell et al., 2009; Yang et al., 2008). Spastin knockdown in cell lines causes persistent microtubule filled bridges and when control cells are treated with a microtubule depolymerizing drug after midbody establishment abscission proceeds normally (Connell et al., 2009; Guizetti et al., 2011). Taken together this suggests that microtubule removal or disassembly is a rate-limiting step in abscission.

Recently, extensive work has shown the requirement of ESCRTs is essential for efficient and timely abscission ((Christ et al., 2016; Elia et al., 2011; Goliand et al., 2014; Guizetti et al., 2011; Yang et al., 2008) For review (Stoten and Carlton, 2018)). Once the midbody is established and Cep55 is recruited to the late midbody, Cep55 independently recruits Alix and the ESCRT-I subunit TSG101 to the midbody (Christ et al., 2016). TSG101, in turn, recruits ESCRT- II, which recruits CHMP6 and then CHMP4B (Elia et al., 2011; Goliand et al., 2014). CHMP4B, ESCRT-III subunit, is recruited to a secondary position away from the center of the midbody (Elia et al., 2011). The mechanism for the formation of this second population of CHMP4B is still unknown and a significant question in the field. This secondary accumulation of CHMP4B is where microtubule disassembly, constriction site and the final membrane severing occurs. The constriction site contains 17nm helical filaments comprised of ESCRT-III proteins stemming from the midbody (Goliand et al., 2018; Guizetti et al., 2011). The ESCRT-III subunit ATP-ase VPS4 localizes to the constriction site at the time of abscission to mediate scission (Elia et al., 2011). This evidence supports the model that ESCRT-III subunits and accessory proteins mediate membrane scission, as they do in viral budding.

Abscission can happen on one or both sides of the midbody and regulation of this process is not well understood. Evidence from asymmetric spastin accumulation in the midbody suggests that recruitment of the abscission machinery is temporal and spatially regulated (Guizetti et al., 2011). Recently, reports from *Drosophila* germline and *C. elegans* embryos reported abscission on one flank and inheritance of the midbody by the

opposite daughter (Daniel et al., 2018; Ettinger et al., 2011; Gromley et al., 2005; Kuo et al., 2011; Salzman et al., 2014; Singh and Pohl, 2014b). However, the evidence is mounting towards a majority of abscission occurring bilaterally. This has now been reported to occur in HeLa cells, MDCK cells, *C.elegans* embryo, and NSCs ((Chai et al., 2012; Crowell et al., 2014; Gershony et al., 2017; Guizetti et al., 2011; Janisch et al., 2018; Konig et al., 2017; Lafaurie-Janvore et al., 2013), **Chapter II, Chapter III**). Additionally, one group has shown bilateral microtubule disassembly but a plasma membrane tether connecting the midbody remnant to the cell body of MDCK cells (Casares-Arias et al., 2019). This complicates our understanding of unilateral and bilateral abscission but highlights the need for ongoing work to elucidate the process of abscission. Here, we are the first to report that the majority of divisions of NSCs result in bilateral abscission as detected by microtubule disassembly (**Chapter III**). Interestingly, we do not know much about the coordination between the first and second event except for the recent evidence from *C. elegans* showing abscission happens randomly on either side of the midbody (Konig et al., 2017). In mammalian cells including NSCs the second abscission event usually happens within 90 minutes but more often within 15 minutes (Crowell et al., 2014; Gershony et al., 2017; Janisch et al., 2018) **Chapter III**). There needs to be more investigation into the regulation of both events. Despite this, some in the field currently believe that the midbody remnant is released extracellularly in across most cell types. This further supports the idea that the remnant is either a disposal method or signaling component as discussed earlier in this introduction.

II. Cytokinesis in an epithelium

Building and maintaining an epithelium requires precise coordination of events including cytokinesis. Proper cytokinesis within an epithelium has been shown to be essential for polarity and maintenance. Asymmetric cleavage furrowing and positioning of the midbody are both common features of epithelium to setup polarity within the tissue (Herszterg et al., 2014). Midbody placement within the epithelium has been explored in cyst structures and outlined in the previous section on midbody remnants. Another aspect to epithelium besides polarity of the tissue is the maintenance of the cell to cell barriers and connections. From the frog epithelium, it is hypothesized that vertebrate midbodies are connected to the adherens junctions (Higashi et al., 2016). This connection establishes tension on the cleavage furrow which is important for stabilization

of the furrow. As the furrow ingresses, neighboring daughter cells are pulled towards the furrow creating a new tri-cellular junction that flanks the midbody (Higashi et al., 2016). When adherens junctions have less tension, the furrow ingresses faster. Tension has also been implicated in the later step of cytokinesis, abscission, of cultured HeLa cells (Lafaurie-Janvore et al., 2013). In this case reduced tension, achieved through low density culturing, caused abscission duration to be increased. These data taken together would imply that precise positioning of the midbody and proper tension on the midbody and the cellular junctions regulates cytokinesis.

Interestingly, the neuroepithelium may be susceptible to malformations resulting from cytokinesis genes because of the unique structure of these cells. NSCs maintain a polarized structure during cell division that extends from the basal lamina to the ventricular surface. The nuclei migrate within the cell towards the ventricular surface where cleavage furrowing occurs asymmetrically to form the midbody at the apical membrane. The two daughter nuclei migrate away from the ventricular surface during abscission. The coordination between abscission and this migration is unknown. The midbody is located in an essential area for cell fate decisions because this is where candidate fate determinants like apical junctions, Notch/Numb, and centrosomes are segregated during cytokinesis (Dubreuil et al., 2007; Higashi et al., 2016; Kim et al., 2010; Paridaen and Huttner, 2014). The importance of cytokinesis to the neuroepithelium is evident from human and mouse mutations of genes (*Kif14*, *Citron Kinase*, *Cep55*, *SEPT7*, *MKLP2(Kif20a)* and *Kif20b*) associated with cytokinesis that cause forms of microcephaly (Bondeson et al., 2017; Di Cunto et al., 2000; Frosk et al., 2017; Janisch et al., 2013; Li et al., 2016; Little, 2019; Qiu et al., 2019). All of these proteins localize to the midbody and have varying roles during cytokinesis. The list of proteins to discuss was chosen based on human disease and phenotypes comparable to microcephaly mutants studied in the lab. The rest of this section will highlight how the loss of these proteins effects the neuroepithelium.

Cep55

A core midbody protein that is responsible for the establishment of the midbody, *Cep55*, has been linked to humans causing severe microcephaly (Bondeson et al., 2017; Frosk et al., 2017; Zhao et al., 2006). *Cep55* has been shown in cell lines to be required for

abscission to complete (Zhao et al., 2006). Only 6% of HeLa cells lacking Cep55 were able to complete abscission and more than 90% connected by an intracellular bridge for more than 7 hours (Zhao et al., 2006). This extreme cellular phenotype and the human disease makes Cep55 a prime protein to study the requirement of midbody proteins in neural development. We recently started to investigate a mouse mutant of Cep55 that has microcephaly. Interestingly, this mouse model of Cep55 microcephaly mimics many of the phenotypes observed in human patients: small brain, binucleate neurons and progenitors, and massive cell death (Little, 2019). However, the mouse mutant is born at Mendelian ratios and appears to have secondary neuromuscular atrophy that contributes to post-weaning lethality (Little, 2019). **In Appendix I**, we continue the characterization of the gross morphology and address some cellular mechanisms of the loss of Cep55. Briefly, we add to our growing body of evidence that the brain is more sensitive to defects in cytokinesis than other parts of the brain and while Cep55 phenotypes in culture are severe; cytokinesis can complete normally in the brain. Despite most of the cells being able to complete abscission, the cells that are unable to complete or complete slower than normal hinder the growth of the epithelium.

MKLP2 (Kif20a) and Kif20b

MKLP2 (Kif20a) and Kif20b are both members of the kinesin-6 family. We discuss this family of kinesins in more detail in the next section (section 1.4). Both MKPL2 and Kif20b localize to the midbody during cytokinesis. We have recently shown that Kif20b, a microtubule motor associated with a novel mouse microcephalic phenotype, regulates abscission duration in NSCs and HeLa cells ((Dwyer et al., 2011; Janisch et al., 2018; Janisch et al., 2013) **Chapter II, Chapter III**). We further describe the *Kif20b* mutant in the section on Kinesin-6 family members.

MKLP2 is important for furrow ingression and its role in abscission is unclear (Neef et al., 2003). MKLP2 knockdown in cell lines causes cells to fail to form a midbody and the cell subsequently undergoes furrow regression (Hill et al., 2000). In MKLP2 knockdown HeLa cells that were rescued with a phosphorylation-resistant MKLP2, abscission completed faster (Fung et al., 2017). This suggested that MKLP2 plays a role in the regulation of abscission duration. Recently, there has been a paper on a mouse mutant of MKLP2. The MKLP2 mutant mouse has decreased brain size, decreased

neurogenesis, no binucleate cells, and increase in apoptosis early in development (Geng et al., 2018). Interestingly, this paper did not look at any measurements of cytokinesis. They concluded that this neurogenic phenotype was separate from MKLP2's role in cytokinesis and was related to the asymmetric inheritance of MKLP2 in neural stem cells. Due to the overwhelming similarities in the phenotypes between the MKLP2 mutant and the *Kif20b* mutant we would hypothesize that defects in abscission are quite possible in this mutant.

Kif14

Kinesin Family Member 14 (Kif14) is a member of the Kinesin-3 super family and is a microtubule motor with a dynamic localization pattern during cytokinesis. Kif14 localizes to the central spindle and the midbody bulge during cytokinesis (Gruneberg et al., 2006). Kif14 localizes to the midbody through its interaction with PRC1 and is required to localize citron kinase. Kif14 depleted HeLa cells have increased binucleate cells suggesting furrow or midbody regression (Gruneberg et al., 2006). Additionally, citron kinase was not able to localize to the midbody in the absence of Kif14. These cellular phenotypes are similar to the human microcephaly caused by mutations in Kif14 (Moawia et al., 2017; Reilly et al., 2019). Patient fibroblasts lacking Kif14 do not have localization of either Kif14 or citron kinase, and had increased binucleate cells (Moawia et al., 2017). The mouse model of Kif14 has a dramatic reduction in brain size. This reduction is likely due to the increased cell death throughout development and the decrease in late cell proliferation (Fujikura et al., 2013). Although not shown the Kif14 mouse mutant most likely has increased binucleates from failed cytokinesis. The accumulation of binucleate progenitors and neurons is the likely cause of the cell death and diminished late proliferation.

Citron Kinase

Citron kinase localizes the cleavage furrow and the midbody during cytokinesis. As mentioned above Kif14 is responsible for targeting citron kinase to the midbody. Citron kinase is necessary for abscission to complete. HeLa and granule precursor cells lacking citron kinase successfully furrow but regress after midbody stage more than 50% of the time (Gai et al., 2011). Without citron kinase the midbody fails to be maintained with removal of essential proteins like PRC1 and delayed microtubule removal (Watanabe et

al., 2013a). Citron kinase, has also been linked to human and rodent brain malformations (Di Cunto et al., 2000; Harding et al., 2016; Li et al., 2016; Sarkisian et al., 2002; Shaheen et al., 2016). In neural progenitor cells derived from patient fibroblast, 25% of the cells failed cytokinesis and formed a binucleate resulting in an increase in the overall number of neural progenitor cells with multi-spindles (Li et al., 2016). Many of the neural progenitor cells that were able to complete did so with the length of cytokinesis significantly increased (Li et al., 2016). In the mouse mutant, the brain is significantly smaller with reduction in layer 5 neurons, increased apoptosis, and binucleate cells (Di Cunto et al., 2000). The loss of citron kinase causes double strand breaks in DNA which activates p53 apoptosis (Bianchi et al., 2017).

When citron kinase mutants are crossed with p53 null mice the brain size is rescued. There is however a large increase in multi-nucleated cells suggesting the brain normally tries to clear these cells that had previously failed cytokinesis. Interestingly, in the citron kinase single mutant the DNA damage was present in a majority of diploid stem cells and neurons (Bianchi et al., 2017). The authors suggest that citron kinase has a role separate from cytokinesis. However, it is possible that even in a diploid cell dysregulation in the previous cytokinesis could have caused DNA damage independently of failed cytokinesis and the formation of a binucleate. This is supported by the evidence from the human neural progenitor cells that have an increase in cytokinesis duration. The potential for small changes in cytokinesis to cause larger developmental phenotypes are often ignored in the literature. We will discuss the importance of considering the dynamics of cytokinesis in the epithelium later in this section and the discussion.

SEPT7

Septins are GTP-binding proteins that have been implicated in cytokinesis (Estey et al., 2010; Spiliotis et al., 2005). SEPT7 localizes to the plasma membrane and central spindle during furrowing and to the central bulge of the midbody during abscission in HeLa cells (Estey et al., 2010). Knockdown of SEPT7 in HeLa cells causes an increase in binucleate cells, due to increased furrow regression (Estey et al., 2010). Interestingly, when SEPT7 is knocked down in cell lines other septin family members have reduced expression (Kinoshita et al., 2002; Kremer et al., 2005). SEPT7 has been shown to interact in the midbody of Hek293 cells with Kif20a, another midbody protein that will be

discussed below (Qiu et al., 2019). Total loss of SEPT7 in the mouse causes failure in gastrulation, therefore a conditional mutant was developed to study its role in cytokinesis (Menon et al., 2014). Conditional loss of SEPT7 from the brain causes a small brain phenotype that is caused by early cell death and premature neurogenesis (Qiu et al., 2019). Despite cell line data to suggest cleavage furrow failure, no increase in binucleate cells was detected in the SEPT7 mouse mutant. Interestingly, when SEPT7 is lost in neural stem cells Kif20a is also lost from the midbody. No other cytokinesis parameters were investigated in this mouse mutant. It would be interesting to look at more cytokinesis parameters like midbody structure and abscission duration since SEPT7 interacts with Kif20b family member MKLP2/Kif20a.

The loss of these proteins (Kif14, Citron Kinase, Cep55, Sept7, MKLP2(Kif20a), and Kif20b) have varying levels of severity in cell lines but all of them have major consequences in the brain. This highlights the sensitivity of the brain to changes in cytokinesis and the important role cytokinesis plays in maintaining the epithelium during development.

III. Duration of abscission

Duration of abscission can vary based on cell type. In HeLa cells, we found the average duration for abscission is 68 minutes if you measure from the completion of the furrow ingression to the first abscission ((Janisch et al., 2018), **Chapter II**). In *C. elegans* early embryo, the time for abscission is much quicker at approximately 20 minutes (Green et al., 2013). In NS5, a neural stem cell line, in dissociated cultures, it took an average of 100 minutes from the establishment of the cleavage furrow to the first microtubule break (Ettinger et al., 2011). In Neuro2A, a neuroblastoma cancer cell line, the same event took twice as long. By contrast, when I analyzed abscission in intact explants of developing cortex the average duration for abscission in NSCs was 57 minutes at E11.5 and 47 minutes at E13.5 when abscission was measured from midbody formation to microtubule disassembly (**Chapter III**). Additionally, in the *Drosophila* male germline, there is highly regulated abscission timing suggesting the importance of this final step (Lenhart and DiNardo, 2015). The midbody is maintained through multiple cell cycles before abscission finally occurs. This coordinated division is necessary for the maintenance of discrete stem cell or differentiation characteristics within individual cells

(Lenhart and DiNardo, 2015). Perturbing abscission duration in either direction can be detrimental to the cell – causing cell cycle exit or apoptosis.

A. *Delayed and Failed Abscission*

The cell can delay abscission in order to fix problems, and then allow abscission to continue. The CPC is a part of a pathway known as the NoCut pathway in yeast and abscission checkpoint in mammals, triggers delay of abscission when chromatin in the bridge or nuclear envelope fails to reform (Mackay et al., 2010; Steigemann et al., 2009). Chromatin in the bridge or nuclear envelope reformation problems causes Aurora B to phosphorylate CHMP4C which binds in a complex with Abscission/NoCut Checkpoint Regulator (ANCHR) and VSP4 (Thoresen et al., 2014). This complex prevents VSP4 from re-localizing from the midbody bulge to the constriction site – preventing abscission (Thoresen et al., 2014). Under normal cell division, the phosphorylation decreases on CHMP4C at a regular rate allowing the complex to release VSP4 to the abscission site (Carlton et al., 2012; Thoresen et al., 2014). Additionally, the cell can delay abscission through a mechanism involving tension of the membranes. This tension is caused by the daughter cells pulling away from each other (Lafaurie-Janvore et al., 2013). Once the daughter cells stop moving, which releases the tension on the membrane, the authors suggest ESCRT-III proteins are recruited to the midbody, and abscission can take place. One kinase that interacts with the CPC, Unc-51-like kinase (ULK3), responds to lagging chromatin, nuclear pore defects, and high mechanical tension (Caballe et al., 2015). ULK3 phosphorylates CHMP4C keeping VPS4 at the midbody bulge and ESCRT-III subunits preventing them from forming their helical filaments necessary for membrane scission (Caballe et al., 2015). It is hypothesized that ULK3 phosphorylation can be reversed by a phosphatase dependent on the abscission checkpoint or resolution of lagging chromatin, nuclear pore defects, or tension.

If abscission does fail, one or both daughter cells can die, become binucleate or multinucleate which can lead to cell death, or form syncytia, where it reenters the cell cycle and continues to the next mitosis without separating. Abscission is not necessary for re-entry into the cell cycle, as seen in the *Drosophila* male germline (Lenhart and DiNardo, 2015). Additionally, we do not understand the effects of extending abscission has on the cells that are able to divide. Disruption of abscission has been mainly

measured by the number of cell deaths or bi-or multi-nucleated cells. One piece of evidence in a delayed abscission experiment showed a more differentiated phenotype in the cells that were able to complete abscission after a delay (Ettinger et al., 2011). These observations suggest delaying abscission does alter post-mitotic cell processes and fates.

B. Faster abscission

There has been less manipulations of the abscission pathway that cause faster abscission unlike delayed abscission which appears to be a more common defect. The mechanism for faster abscission and the resulting cellular consequences are not well understood. In this section, we will highlight the proteins when depleted are associated with faster abscission CHMP4C, ULK3, ANCHR, PRL-3, and Kif20b (Caballe et al., 2015; Carlton et al., 2012; Lujan et al., 2016; Thoresen et al., 2014) **Chapter III**). Three of these proteins (CHMP4C, ULK3, and ANCHR) are associated with the abscission checkpoint which is known to control abscission duration (reviewed in the previous section). Both Kif20b and PRL-3 have unknown links to abscission duration.

Depletion of abscission checkpoint components causes abscission to be faster. This might be unsurprisingly, since this complex is responsible for making sure chromatin is clear from the intracellular bridge and the nuclear envelope is reformed before abscission completes. When CHMP4C, ANCHR, or ULK3 are knocked down in HeLa cells they accelerate abscission between 15 to 30 minutes (Caballe et al., 2015; Carlton et al., 2012; Thoresen et al., 2014). Interestingly, HeLa cells depleted of CHMP4C or ULK3 can resolve the chromatin bridges quicker, which may be responsible for the increase in DNA damage seen in cells depleted of CHMP4C (Caballe et al., 2015; Carlton et al., 2012). Increased DNA damage in a cell type like NSCs which are responsible for producing many cell types would be more problematic therefore depleting CHMP4C, ULK3, or ANCHR from another cell type would be very informative.

Phosphatase of regenerating liver – 3 (PRL-3) is a phosphatase that is overexpressed in many cancer cells and has been implicated in establishing epithelial polarity (Lujan et al., 2016). Ectopic lumens form when PRL-3 is lost in 3D culture cyst-forming MDCK or Caco-2 cells. When PRL3 is lost in 2D dissociated culture, abscission is decreased in

these cells by 30 minutes (Lujan et al., 2016). Faster abscission was proposed to leave the midbody and the resulting remnants in the wrong location (not at the apical membrane) and promote ectopic lumen formation (Lujan et al., 2016). This suggests that the regulation of abscission timing and location is important for the establishment and maintenance of the epithelium.

We have evidence that depletion of Kif20b causes bundling defects in the midbodies of progenitors and axonal microtubules ((McNeely et al., 2017) **Chapter III, IV**). Additionally, in knockdown of Kif20b in HeLa cells we show decreased percent of midbodies with late ESCRT VPS4 suggesting a disruption in maturation (Janisch et al., 2018). The loss of Kif20b causes faster abscission on average by 18 minutes at E11.5 and 9 minutes at E13.5 in NSC cells (**Chapter III**). We hypothesize that Kif20b dysregulates the critical timing between ESCRT recruitment and microtubule compaction and disassembly. Further work to determine how these two elements occur when Kif20b is depleted remains to be done. Additionally, Kif20b could disrupt the abscission checkpoint like several other of the previous discussed proteins. The related Kinesin-6 family member Kif20a/MKLP2 was reported to act in the abscission checkpoint, although involving a tail sequence not shared by Kif20b (Fung et al., 2017). We discuss how the loss of Kif20b may causes faster abscission more in the discussion.

1.4 Kinesin-6 Family Member: Kif20b

Kif20b is a part of the kinesin-6 family of motor proteins and understudied compared to its other vertebrate family members, MKLP1 (Kif23) and MKLP2 (Kif20a). All three family members have independent functions and their compensatory capacity for each other is unknown.

I. What are the known functions of Kinesin motor proteins?

Kinesins are motor proteins that move along microtubules either in the minus or plus end direction. The function of kinesins is to move diverse cargo within the cell which includes anterograde axonal transport, dendritic transport, transport between ER and golgi, lysosomes transport and recycling of endosomes (Hirokawa and Noda, 2008). Additionally, kinesins function mitotically to organize the mitotic spindles and move the

spindle poles apart from each other using a sliding mechanism. Kinesins are identified from other motor proteins by a highly conserved 360 base pair globular domain that contains the catalytic pocket for the hydrolysis of ATP and the binding domain for microtubules (Miki et al., 2005). Kinesins are classified by their directionality, which is intrinsic based on the location of the motor within the protein (Hirokawa and Noda, 2008). The kinesins are further classified into 14 kinesin subfamilies by the homology of their motor domains. There are 45 mouse kinesin genes, 38 of which are in the brain (Hirokawa and Noda, 2008). Based on splice variant predictions there is believed to be approximately twice as many kinesin proteins as kinesin genes. The splice variants increase the differences in the tail domains that lead to the diversity of cargo selection.

II. Kinesin-6 Family members have cytokinetic and possible post-mitotic roles

The kinesin-6 family is composed of three members: MKLP1, MKLP2, and Kif20b. The identifying feature in the motor for this family is the insert in loop 6 of the catalytic core (Miki et al., 2005). All three members of the Kinesin-6 family are found in the midbody during cytokinesis; although their localization within the midbody varies temporally. Additionally, all three family members can be found in the ventricular zone of the brain (Dwyer lab unpublished *in situ* data). MKLP1 (Mitotic kinase-like protein 1, also known as Kif23) is essential for establishing the midbody (Zhu et al., 2005a). MKLP1 forms a heterotetrameric complex with MgcRacGAP to make centralspindlin. The complex consists of two molecules of MKLP1 and two molecules of MgcRacGAP (Green et al., 2012). Centralspindlin is an essential signaling component of the cleavage furrow. Once the furrow is complete and actomyosin ring is disassembled then, MKLP1 interacts directly with membrane-bound Arf6 (Green et al., 2012). This interaction holds the cleavage furrow in place, creating the intracellular bridge between the two cells known as the midbody (Green et al., 2012). MKLP2 (Mitotic kinase-like protein 2, also known as Kif20a) is required for Aurora B localization to the midbody (Gruneberg et al., 2004). Once Aurora B is at the midbody, it can phosphorylate MKLP1. MKLP1 recruits Cep55 that in turn recruits the ESCRT cascade leading to abscission of the membrane (Carlton et al., 2008; Morita et al., 2007; Zhao et al., 2006). Both of the family members play unique and significant regulatory roles in midbody formation, maintenance, and recruitment of abscission machinery.

MKLP2, outside its role in the midbody, has been implicated in cell fate of NSCs. Depletion of MKLP2 in the mouse embryo causes embryonic lethality and microcephaly (Geng et al., 2018). Interestingly, NSCs segregate MKLP2 symmetrically in symmetric proliferative divisions (P-P), and asymmetrically to the proliferative daughter in (P-N) division (Geng et al., 2018). This suggests that MKLP2 has a role in maintaining the proliferative capacity of a cell. NSCs depleted of MKLP2 in the mouse cortex have increased apoptosis compared to controls but no binucleate cells. Additionally, NSCs depleted of MKLP2 in culture have increased neurogenic symmetric divisions, supported by an early neurogenic phenotype in the cortex (Geng et al., 2018). Interestingly, the authors did not look for any cytokinesis phenotypes outside binucleates in the MKLP2 NSCs (addressed in previous section).

The non-mitotic roles of MKLP1 have emerged in neurons of *Drosophila* and rat. The MKLP1 *Drosophila* homolog Pavarotti has been shown, in neurons, to be necessary for inhibition of microtubule sliding that prevents overgrowth (del Castillo et al., 2015). When MKLP1 is lost from larvae, there is drastic axonal outgrowth throughout the larvae. In cultured rat sympathetic neurons, the depletion of MKLP1 leads to the thinning of dendrites. The mechanism is proposed to be due to a lack of microtubule transport into the dendrites (Lin et al., 2012; Yu et al., 2000). Interestingly, a knockdown of MKLP1 causes longer axons in cultured rat sympathetic neurons. In this case, the overgrowth was proposed to be caused by the loss of regulation of short microtubule fragments to the axon. The data for the *Drosophila* and rat axons is more convincing than the data regarding the dendrites, although the outgrowth mechanism may still be debated. It is important to keep in mind that this kinesin family's role in the cell may not be limited to cytokinesis, and a stronger post-mitotic influence is emerging.

III. The role of Kif20b in abscission of HeLa cells and Neural Stem Cells

Kif20b is a slow-moving plus-end directed motor protein with a role in cytokinesis and first discovered as a protein phosphorylated during mitosis (Westendorf et al., 1994). Kif20b has alternative names based on how the kinesin was isolated. These names are M phase phosphoprotein 1 (MPP1), and Kinesin-related protein interacting with PIN1 (KRMP1) (Abaza et al., 2003; Kamimoto et al., 2001; Kanehira et al., 2007). The gene

for *Kif20b* is located on chromosome 10 in humans and chromosome 19 in mouse (Abaza et al., 2003). *Kif20b* has an NH₂ terminal motor domain which gives its innate plus-end directed movement (Abaza et al., 2003). The alignment of *Kif20b*'s motor domain sequence with a conventional kinesin heavy chain showed that *Kif20b* has two large insertions in its motor domain. One insertion spans between alpha helix 2 and beta sheet 4 and the second spans between alpha helix 6 and beta sheet 9 (Abaza et al., 2003). Additional analysis of the secondary structure of *Kif20b* revealed that the central domain of *Kif20b* has four coiled-coiled regions that are alpha helices (Abaza et al., 2003).

Independent experiments define similar localization patterns of *Kif20b* at different times of the cell cycle (Abaza et al., 2003; Janisch et al., 2018; Janisch et al., 2013; Kanehira et al., 2007). *Kif20b* localizes to the nucleus during interphase, in prophase and metaphase it is in the cytoplasm, then in the midzone during anaphase, and once the midbody forms in telophase it appears on the flanks of the midbody closest to the dark zone ((Abaza et al., 2003; Janisch et al., 2018; Kamimoto et al., 2001; Kanehira et al., 2007) **Chapter II**). In late telophase, the localization changes, and it appears as two distinct dots further down the flanks near the constriction sites. *Kif20b* mRNA in mouse brain was in the ventricular zone with little to no detectable expression in post-mitotic layers at ages E14.5 and E16.5 (Janisch et al., 2013). *Kif20b* protein was detectable in E12.5 midbodies of apical progenitors (Janisch et al., 2013). At E14.5 midbodies presumed to belong to basal progenitors based on their position in the tissue also appear to have *Kif20b* (Janisch et al., 2013). This *in vivo* staining of midbodies agrees with the localization pattern of *Kif20b* seen in cultured cells.

The role of *Kif20b* in cytokinesis has been primarily characterized in cell lines up until recently. Knockdown of *Kif20b* results in lower growth rates due to increase multinucleated cells in bladder cancer and increased apoptosis in a variety of cell types (HCT116 cells, HeLa cells, NSC) (Abaza et al., 2003; Janisch et al., 2018; Janisch et al., 2013; Kanehira et al., 2007; Little and Dwyer, 2019). In HeLa cells, depletion of *Kif20b* delays cleavage furrowing and dysregulates abscission (Janisch et al., 2018) **Chapter II**). In NSCs, loss of *Kif20b* delays cleavage furrow in 25% of cells and abscission on average is faster (**Chapter III**). We further characterized the knockdown of *Kif20b* in HeLa cells and showed that there were a decreased mitotic index and perturbed

midbody maturation. Specifically, midbodies of cells lacking Kif20b had decreased VPS4 recruitment suggesting these midbodies have a late-stage maturation defect ((Janisch et al., 2018) **Chapter II**).

IV. Kif20b interactors

Kif20b has several candidate binding partners identified based on pull-down and interaction studies. Most of the protein interactions have not been validated which leaves much of Kif20b's role in the cell a mystery. Protein regulator of cytokinesis (PRC1) and Peptidyl-prolyl cis-trans isomerase NIMA-interacting 1 (PIN1) (Kamimoto et al., 2001; Kanehira et al., 2007) have been functionally confirmed through immuno-precipitation from cell culture. Kif20b was pulled out of an interactome study of the formin Diaphanous-3, (mDIA2) in HeLa cells. Evidence I found to support mDIA2 interaction and the possible role of mDIA2 in apoptotic response will be discussed in **Appendix IV** (Isogai et al., 2015). Additionally, more potential binding partners of Kif20b have been elucidated through an unbiased affinity purification-mass spectrometry analysis in interphase HeLa cells (Maliga et al., 2013). This analysis pulled out nuclear pore proteins, actin bundling protein and regulator of cytokinesis alpha-actinin-4 (Actn4), and interestingly a neuron polarization protein called Shootin1. I showed Shootin1 is decreased in the axons of *Kif20b* mutant neurons (McNeely et al., 2017). The role of Shootin1 in *Kif20b* mutant neurons will be further discussed in **Chapters IV and Appendix V**.

V. Mouse model of a loss of function mutation in Kif20b causes microcephaly

The mouse model for the loss of function mutation in *Kif20b*, named *magoo*, was found by Dr. Dwyer in a genetic screen using N-ethyl-N-nitrosourea (ENU) mutagen to look for mutants with thalamocortical axon guidance problems. The Dwyer Lab identified the causative mutation: the mutation occurs 13 base pairs upstream of exon 19 on chromosome 19. The mutation is a T to a G, which causes aberrant splicing 29 base pairs upstream of exon 19 (Janisch et al., 2013). This results in mRNA that is 29 base pairs longer in the mutant mouse. Although the mRNA is still present, it is reduced, and

there is no protein detectable. It is likely that the mRNA undergoes nonsense-mediated decay.

Before I joined the lab, initial characterization of the *Kif20b* mutant showed a smaller brain, microcephaly, and smaller body as well as enlarged ventricles (Dwyer et al., 2011; Janisch et al., 2013). Microcephaly, as defined in humans, is a reduced occipitofrontal head circumference of more than two standard deviations below the mean for age, sex, and ethnicity (Kaindl et al., 2010). The cortical thickness of the mutant brains from E12.5 to E18.5 are consistently smaller than control littermates (Janisch et al., 2013). Death occurs in the homozygous mutants either *in utero* or not long after birth from unknown causes. The heterozygous pups appear normal and are not distinguishable from their wild-type littermates (Janisch et al., 2013). Further characterization of the *Kif20b* mutant mouse revealed cortical lamination was intact. However, each layer was significantly thinner which suggests a loss of cells from the progenitor pool in addition to a loss of neurons (Janisch et al., 2013).

Therefore, I sought to address what could account for the loss of neurons in the *Kif20b* mutant brain. Through Jessica Little's graduate work, she found that the majority of the loss of progenitors and neurons could be accounted for by a combination of p53-mediated apoptosis (Little and Dwyer, 2019). Within this dissertation I was able to determine that additional loss of neurons is due to premature cell cycle exit of progenitors and with the help of Jessica Little we found that this premature cell cycle exit is p53-independent (**Appendix II**).

To determine what could cause early differentiation both previous lab members and I looked at potential cell fate determinants. Previously, the lab examined spindle pole and cleavage orientation. In the case of *Kif20b* mutant, there are normal cleavage angles and mitotic index (Janisch et al., 2013). Unlike cell lines, in the brain the loss of Kif20b did not cause binucleate cells. This is further supported by the lack of furrow or midbody regression seen in live imaging of NSCs (**Chapter III**). Since there doesn't appear to be difficulties in mitosis we next examined cytokinesis, where Kif20b localization becomes most evident. In the *Kif20b* mutant there are changes in midbody index compared to control. Midbody index tells us the percent of cells with a midbody. There was a decrease in the midbody index at E13.5 (# of midbodies/# of apical endfeet) of

progenitor cells in the *Kif20b* mutant mice compared to controls (Janisch et al., 2013). This decrease in midbodies can now be explained by my finding that *Kif20b* mutant NSCs on average abscising faster than controls (**Chapter III**).

Additionally, changes in the midbody are seen in the alignment to the apical membrane, and shape of the midbody as well as changes to the apical membrane (Janisch et al., 2013). The lab previously found there was an increase in the *Kif20b* mutant midbodies misaligned along the apical membrane. This altered midbody angle could influence the efficiency in which the cells can divide since the level of tension on the midbody would be altered. As mentioned previously, tension has been implicated as a regulator for abscission duration (Lafaurie-Janvore et al., 2013). The shape of the midbody in the *Kif20b* brain was wider than control midbodies (Janisch and Dwyer, 2016). The distribution of midbody widths is interesting since widths between 1.0 to 1.2 μ m are increased in the mutant brains compared to control and widths between 0.4 to 0.6 μ m is decreased in the mutant compared to control. This change in the distribution of midbody width could suggest problems with regulating the maturation of the midbody throughout the abscission process. Now based on my live data, we hypothesize we see wider midbodies because compaction and formation of the constriction site are happening at a faster rate compared to control cells. I investigated the inheritance of the apical endfoot and determined that apical endfoot asymmetry was caused by p53-mediated consequences and not associated with changes in cell fate (**Appendix II**).

1.5 Research Objectives

The field's investigations into cell fate determinants in the developing cerebral cortex have offered us a lot of possibilities, often with contradictory or inconclusive results. Here we strive to understand both the normal dynamics of a possible cell fate determinant, abscission, and focus on the effects of dysregulation of abscission in two novel microcephaly mutants caused by *Kif20b* or *Cep55* loss (**Chapter III and Appendix I, II**). The broad goals of this project were to characterize the dynamics of cytokinesis in NSCs both in the context of normal development, whether it differed at different stages of development, and in two mouse mutants.

In Chapter II we show that detailed analysis of the loss of Kif20b in HeLa cells reveals midbody maturation defects and dysregulated abscission. Importantly, this highlights the need for more work on “mild” cell line phenotypes since *in vivo*, these may lead to determinantal developmental consequences, like the loss of Kif20b (**Chapter III, IV**). We used the power of cell lines to try to determine if the expression pattern of interactor mDIA2 was changed when Kif20b was depleted. **In Appendix IV** we show preliminary data that mDIA2 is lost from the MB when Kif20b is depleted from HeLa cells. This suggests Kif20b may be necessary for re-localization of mDIA2 from the furrow membrane to the midbody microtubules or it may link the membrane to midbody microtubule’s via mDIA2. This regulation is a potential pathway for p53 activation in *Kif20b* mutant cells, based on work done in the Isogai lab.

In Chapter III we show that control NSCs have asymmetric and consistent cleavage furrowing, developmentally regulated abscission and midbody remnant disposal. A subset of NSCs without Kif20b take longer to furrow and NSCs on average undergo abscission faster. Additionally, more *Kif20b* mutant NSCs divide to produce neurons early in development sacrificing progenitors and contributing to the microcephaly independently of p53 (**Appendix II**). We also rule out the role of Kif20b in apical membrane inheritance and other general cell cycle parameters (**Appendix II**). We show evidence that midbody remnants influence are most likely local and/ or cell type specific (**Appendix III**).

In Appendix I we expand on previous evidence from the lab that the midbody protein, Cep55 is important for brain development. Specifically, we find ESCRT recruitment to the midbody is delayed in both mouse embryonic fibroblasts and neural stem cells from Cep55 mutant mice. I also found by live imaging in cortical slab explants that there is delayed abscission in NSCs of E13.5 Cep55 mutant brains. In the mutant, we also find increased midbody remnants at the apical membrane at E14.5 suggesting defects in plasma membrane scission or MBR disposal. We also find evidence for binucleate cells at the apical membrane, suggesting some abscission failure occurs without Cep55.

Tangential to the primary aim of this thesis we were able to explore the role of Kif20b in neuron polarization and axon outgrowth. **In Chapter IV**, we show that the Kif20b has cell cycle independent effects on neurons. The *Kif20b* mutant neurons have wider, shorter

axons. These axons have more dynamic microtubules and are wider. Interestingly, we show that the polarization protein, Shootin1 is reduced in the growth cones of the *Kif20b* axons. To better understand the relationship between *Kif20b* and polarization we grew the mutant neurons on the cell adhesion molecule L1 (L1CAM). L1CAM is an important transmembrane protein that connects Shootin1 with actin treadmilling necessary for axon outgrowth. We hypothesized the *Kif20b* mutant axons would be even shorter on L1CAM compared to normal growth conditions. Interestingly, *Kif20b* mutant neurons have axons that grow longer than controls on L1. In **Appendix V**, we explore this differential outgrowth phenotype and try to further describe *Kif20b*'s effect on axonal microtubules during polarization and axon outgrowth.

This work showed for the first-time cytokinesis happening live and quantitatively analyzed in the normal developing mouse cerebral cortex and in two mouse microcephalic mutants. We highlighted the developmental regulation involved in the duration of cytokinesis and the possible role of cytokinesis in cell fate determinants. Importantly, this work uncovered that mild cytokinesis defects in a cell line could translate to severe developmental consequences in the developing brain.

Chapter II: Kinesin-6 KIF20B is required for efficient cytokinetic furrowing and timely abscission in human cells

This chapter is published as K.M. Janisch*, K.C. McNeely*, J.M. Dardick, S.H. Lim, and N.D. Dwyer. 2018. Kinesin-6 KIF20B is required for efficient cytokinetic furrowing and timely abscission in human cells. *Mol Biol Cell*. 29:166-179.

*denotes co-first authorship

Abstract

Cytokinesis requires the cooperation of many cytoskeletal and membrane regulators. Most of the major players required for cytokinesis are known, but the temporal regulation and adaptations for different cell types are less understood. KIF20B (previously called MPHOSPH1 or MPP1) is a member of the Kinesin-6 family, which also includes the better-known members KIF23/MKLP1 and KIF20A/MKLP2. Previously, we showed that mouse *Kif20b* is involved in cerebral cortex growth and midbody organization of neural stem cells. Here, using siRNA-mediated knockdown of KIF20B in a human cell line and fixed and live imaging, we show that KIF20B has a cell-autonomous role in cytokinesis. KIF20B depletion affects the speed of both furrow ingression and abscission. It localizes to microtubules of the central spindle and midbody throughout cytokinesis, at sites distinct from the other Kinesin-6 family members. KIF20B is not required for midbody assembly, but may accelerate or coordinate midbody maturation. In particular, KIF20B appears to regulate late steps of maturation including anillin dispersal, ESCRT-III recruitment, and the formation of microtubule constriction sites.

Introduction

Cytokinesis is fundamentally important to building and renewing tissues, but it is still poorly understood. It consists of two sequential processes: cleavage furrow ingression, which takes minutes, and abscission, which can last more than an hour (for review see (Green et al., 2012) and (Mierzwa and Gerlich, 2014)). Moreover, cytokinesis has different spatial and temporal regulation in different cell types or at different times in development (Lenhart and DiNardo, 2015; Singh and Pohl, 2014b). While many of the major players of cytokinesis have been defined, how the temporal control of furrowing and abscission is regulated is not well understood. Furthermore, how abscission regulation influences tissue development is only beginning to be explored (Dionne et al., 2015).

After chromosome segregation, interpolar microtubules are bundled in an antiparallel manner to form the central spindle, which is involved in specifying and focusing the plane of cleavage. As the cleavage furrow ingresses to form a thin intercellular bridge, the central spindle microtubules are compacted into a dense structure called the midbody. The midbody serves as a platform to mediate the final severing event,

abscission. It contains over 150 proteins and lipids (Atilla-Gokcumen et al., 2014; Skop et al., 2004). During midbody assembly, these proteins are partitioned into distinct subdomains (Elia et al., 2011; Green et al., 2012; Hu et al., 2012). The midbody core or “dark zone” is at the center where microtubules of the two spindle halves overlap in an antiparallel arrangement and are surrounded by electron-dense material (Mullins and Biesele, 1977). PRC1 organizes the antiparallel microtubules in the central spindle and then localizes to the midbody core (Hu et al., 2012; Mollinari et al., 2002) Around the midbody core is a bulge that appears as a ring by light microscopy. The ring contains the scaffolding protein anillin. Tightly packed parallel microtubules emanate from either side of the midbody core and form the midbody flanks. The flanks are labelled by AuroraB kinase signal that terminates near the eventual abscission site(s). After midbody assembly, CEP55 is recruited to the midbody center where it helps form the bulge and scaffolds sequential recruitment of ESCRT-I and -III components on either side of the bulge (Lee et al., 2008; Morita et al., 2007; Zhao et al., 2006). As the time for abscission gets nearer, constriction sites (also called secondary ingressions) form on one or both sides of the midbody bulge. There the microtubules are even more tightly packed (Mullins and Biesele, 1977). How the constriction sites are positioned and formed is not understood, but ESCRT-III filaments and endosomes are thought to be involved (Elia et al., 2011; Guizetti et al., 2011; Schiel et al., 2012). Together the ESCRT disassembly factor VPS4 and the microtubule-depolymerizing enzyme spastin are thought to complete abscission by coordinating membrane scission and microtubule severing (Elia et al., 2011; Guizetti et al., 2011; Morita et al., 2007). In HeLa cells and MDCK cells, a second abscission occurs on the other flank to release the midbody (Elia et al., 2011; Guizetti et al., 2011). Other reports have observed abscission on only one side, and this may depend on cell type or daughter fates (Ettinger et al., 2011; Kuo et al., 2011).

Microtubule motors are crucial for mediating the cytoskeletal reorganizations that take place during cell division. The Kinesin-6 family members are thought to have roles in cytokinesis and cancer (Baron and Barr, 2015). The family is defined by homology in the motor domain; the stalks and tails are divergent (Dagenbach and Endow, 2004; Miki et al., 2005). They are distinguished by a long insertion in loop-6 of the motor domain, and a relatively long neck domain that may enable the two heads in a homodimer to bridge longer distances than adjacent tubulin binding sites. They homodimerize through their coiled-coil domains in the stalks. *C. elegans* has one member of this gene family, *zen-4*.

Drosophila has two members, *pavarotti* and *subito*. Vertebrates have three members of the Kinesin-6 family: KIF23/MKLP1, KIF20A/MKLP2, and KIF20B (previously called Mphosph1 or Mpp1). KIF23/MKLP1 partners with MgcRacGAP to promote central spindle assembly (Glotzer, 2005; Nishimura and Yonemura, 2006). Later, it localizes to the midbody bulge and is required for a stable midbody to form (Matuliene and Kuriyama, 2002; Zhu et al., 2005a; Zhu et al., 2005b). KIF20A/MKLP2 localizes to the midbody flanks, and is required to recruit AuroraB kinase there (Gruneberg et al., 2004; Neef et al., 2003; Zhu et al., 2005a). KIF20B apparently evolved in the vertebrate lineage to become structurally divergent, with an extraordinarily long stalk (~1000 amino acids) containing 3 hinges that may allow increased flexibility (Dagenbach and Endow, 2004; Kamimoto et al., 2001; Miki et al., 2005). In cell-free assays, KIF20B acted as a slow, plus-end directed microtubule motor, and was sufficient to slide and bundle microtubules (Abaza et al., 2003). When knocked down in human HCT116 cells, a subset of cells failed cytokinesis, and sometimes underwent apoptosis (Abaza et al., 2003). However, the role of KIF20B in cytokinesis is not known.

We previously isolated a *Kif20b* mouse mutant in a genetic screen for genes involved in cerebral cortex development (Dwyer et al., 2011; Janisch et al., 2013). The mutant embryos have small brains (microcephaly) with increased apoptosis. Mutant neurons have wider, more branched axons (McNeely et al., 2017). In the embryonic neural stem cells in mutant brains, no changes in mitotic indices or cleavage angles were evident, but abnormalities in cytokinetic midbodies were significant. Midbodies had altered shape and organization at the apical membrane (Janisch and Dwyer, 2016; Janisch et al., 2013). We hypothesized that defective or failed abscission in a subset of neural stem cells caused them to undergo apoptosis, thus depleting the progenitor pool, reducing neurogenesis, and leading to a small brain.

Motivated by a desire to understand mechanisms of abscission in polarized neural stem cells, but hindered by the dearth of data about KIF20B's role in cytokinesis, we set out to investigate it in a simpler more tractable system, to generate hypotheses which can then be tested in primary mouse neural cells and intact brain tissue. In the mutant brains, the observed phenotypes could be due to non cell-autonomous roles of KIF20B, or secondary effects from previous defective divisions. We chose the HeLa human cancer cell line because the cells proliferate as isolated cells, and have a flat morphology,

enabling easier imaging of cytokinesis and of the cytoskeleton. They are readily transfected, tolerant of live imaging, and many more antibodies are made against human proteins than mouse. Finally, since the majority of studies of abscission proteins have used HeLa cells, it is an essential baseline cell type for comparison.

Materials and Methods

Cell Culture

HeLa cells (human cervical carcinoma cells) were obtained from ATCC; we did not re-authenticate. HeLa cells were grown in 10 cm petri dishes with DMEM (Gibco, ThermoFisher Scientific, MA, USA) supplemented with 10% FBS (Atlanta Biologicals, GA, USA), 15 mM HEPES (Gibco, ThermoFisher Scientific, MA, USA), 1X glutamine (Gibco, ThermoFisher Scientific, MA, USA), 1X non-essential amino acids (Gibco, ThermoFisher Scientific, MA, USA) and 1X Penicillin/Streptomycin (Gibco, ThermoFisher Scientific, MA, USA). Cells were grown at 37 °C and 5% CO₂ until they reached ~70% confluency before subculturing for usage in experiments. Coverslips were examined for mycoplasma contamination monthly by DAPI staining of nuclei. For siRNA transfections, unsynchronized HeLa cells were harvested, counted and plated onto 22 mm diameter glass coverslips with a density of 50000 cells per coverslip, unless otherwise stated.

Transfection with GFP-KIF20B

GFP-KIF20B plasmid was provided by F. Pirollet (Abaza et al., 2003), and verified by sequencing. Cells were used when ~70% confluent and transfected using PolyJet transfection kit (SignaGen Laboratories®, MD, USA) according to the manufacturer's instructions. Cells were co-transfected with mCherry to allow for transfection efficiency. After 24 hours, cells were fixed with 4% PFA followed by ice-cold methanol prior to staining and imaging.

Transfection with siRNA

For knockdown experiments, we independently tested two custom-made small interfering RNAs (Invitrogen) previously reported to knock down human KIF20B (siRNA#1: 5'AAAGGACAGAGUCGUCUGAUUUU, siRNA#2: 5'AAUGGCAGUGAAACACCCUGGUU from (Abaza et al., 2003)). Since we observed that siRNA#2 depleted KIF23/MKLP1 as well as KIF20B, we discontinued use of

siRNA#2 and used siRNA#1 for most experiments. Additional siRNAs were purchased from Life Technologies/Thermo Fisher: s18420 (called siRNA#3) 5'GCAAGUUAAGAAUAUCGAtt; and s18421 (siRNA#4) 5'CAAACGUUUAGUUCAGCAtt. siRNAs #1, #3, and#4 caused similarly complete depletion of KIF20B to levels undetectable in 98-100% of midbodies at 24 hours post-transfection (Supplemental Figure 1, C and D), and caused increased multinucleate and multi-lobed cells (Supplemental Figure 1E). A standard negative control siRNA to firefly luciferase (siLUC) was designed by Invitrogen. Cells were transfected using Lipofectamine® RNAiMAX (Thermo Fisher) transfection reagent according to the manufacturer's instructions. The final concentrations of siRNA were 10 nM. Transfection efficiency was found to be 98-100% using fluorescently-tagged siRNA (Block-It from Invitrogen and siGlo, Dharmacon). Cells were either fixed 24 hours or 48 hours (with medium change) after transfection and analyzed by immunofluorescence staining. For live cell imaging, cells were plated at a density of 50,000 cells per chamber in a two-chamber coverglass (Nunc Lab-Tek, ThermoFisher Scientific, MA, USA) before transfection and imaged 22 – 24 hours after transfection.

Immunocytochemistry

The standard fixation for most antibodies used was 4% PFA/PBS for 2 min at room temperature, followed with -20 °C methanol for 10 min. Cells were then washed 3X with PBS to remove any residual methanol and stored at 4 °C until usage. For phospho-AURORA kinase B (pAURK) and spastin staining, cells were fixed with -20 °C methanol for 10 min followed by 3 washes with PBS. For staining for ANILLIN (ANLN) and alpha-ACTININ 4 (ACTN4), cells were fixed with 10% TCA in cytoskeleton buffer with sucrose (CBS; 10 mM MES pH 6.1, 138 mM KCl, 3 mM MgCl₂, 2 mM EGTA, 0.32 M sucrose). Shortly, 10% TCA in CBS was added to the cells and incubated on ice for 15 min. Cells were permeabilized with 0.2% Triton-X100, 50 mM glycine in PBS for 2 min on ice, then quenched with 50 mM glycine in PBS for 20 min.

Cells were blocked with 2% normal goat serum (NGS) in PBS with 0.1% Triton-X 100 (PBST) for 1 hour at room temperature. After 3 washes with PBS for 10 min each, primary antibodies diluted in blocking buffer were applied for 3 hours at room temperature. Appropriate secondary antibodies diluted in blocking buffer were applied after 3 washes with PBS for 5 min each and incubated for 30 min at room temperature in the dark. Cells were mounted with Fluoromount (Diagnostic BioSystems, CA, USA) after

a nuclear counterstain with DAPI (Fisher Scientific, PA, USA) and 2 washes with PBS for 10 min.

Antibodies

Primary antibodies used were as follows: mouse monoclonal DM1alpha (alpha-tubulin) (1:500) was from Abcam (MA, USA); rat anti-TUBA1A (clone YL ½) (1:750) was from Novus Biologicals (CO, USA); mouse polyclonal anti-CEP55 (1:200) was from Abnova (CA, USA); mouse anti-Aurora kinase B (AURKB) (1:300) was from BD Biosciences (MA, USA); rabbit anti-phospho-T232-Aurora kinase B (pAURKB) (1:200) was from Rockland (PA, USA); rabbit anti-KIF20A (A300-879A, 1:100) was from Bethyl Labs (TX, USA); goat anti-anillin (ANLN) (1:300); mouse monoclonal anti-ANLN (1:100), rabbit anti-MKLP1 (sc-867, 1:100), rabbit anti-PRC1 (1:50), mouse monoclonal anti-human-spastin (3G11/1, 1:50), and mouse anti-human-MPP1(KIF20B) (1:300) were from Santa Cruz (CA, USA); rabbit anti-mouse-Kif20b (1:500) was custom-made by Covance (NJ, USA; (Janisch et al., 2013)); rabbit anti-cleaved caspase 3 (CC3) (1:200) and rabbit anti-phosphohistone H3 (PH3, Alexa Fluor 647 conjugated) (1:400) were from Cell Signaling (MA, USA); rabbit anti-alpha-ACTININ4 (ACTN4) (1:250) was from Millipore (MA, USA); and rabbit anti-VPS4 (1:500) was from Sigma Aldrich (MO, USA). Both the monoclonal mouse anti-human MPP1(KIF20B) antibody (shown in Figures 1, 2, and Supplemental Figure 1) and the polyclonal rabbit anti-mouse-Kif20b (shown in Supplemental Figure 1B) were validated by verifying that the midbody staining was lost in *Kif20b* mutant mouse cells. All other primary antibodies were validated by verifying that the staining patterns matched multiple published reports. Secondary antibodies were goat or donkey polyclonal IgG (H+L) conjugated to Alexa fluorophores against according species and were used at 1:200 (Life technologies, NY, USA).

Imaging and data analysis

Fixed images were either collected with a Zeiss AxioVision ImagerZ1 widefield microscope with 40x/1.3 or 100x/1.25 Oil M27 APO objectives or a DeltaVision Elite with TrueLight deconvolution microscope with 60x/1.42 Oil Plan APO objective. For comparisons between siLUC and siKIF20B knockdown cells, exposure times were kept constant for each treatment and images were taken on the same day. For DeltaVision images, deconvolved maximum intensity projections of z-stacks are displayed unless

otherwise specified. For image analysis and data acquisition of images, we used Fiji/ImageJ (<http://imagej.net/Fiji/Downloads>).

Live cell imaging was done on an inverted Zeiss AxioObserver microscope equipped with a temperature and CO₂-controlled chamber set at 5% CO₂ and 37°C, multipoint acquisition and DefiniteFocus. Illumination and exposure times were kept to minimum practical levels. Images were acquired with an AxioCam Mrm camera and Zeiss Zen software. Cells in metaphase were chosen in brightfield based on their shape and chromatin appearance. siKIF20B cells were imaged first, followed by siLUC cells. Time 0 was the last frame when chromatin was aligned at the metaphase plate. Cells were unsynchronized. After each live imaging experiment, cells were immunostained for KIF20B and checked for expression; in each case 0/20 midbodies examined had detectable KIF20B.

Live imaging of furrow ingression was done by collecting brightfield images with a 63x oil objective. Image stacks with 0.75 μm step size were captured every minute. Furrow was considered completely ingressed when no further ingression could be observed using raw z-stacks or projections. In no case was furrow regression observed.

For abscission data:

Brightfield: Image stacks with 0.5μm step size were collected every 7.5 min with a 63x oil objective and differential interference contrast (DIC) for 4-6 hours. Abscission was scored in the z-plane where the midbody bulge was visible, and was defined as the separation of the midbody from one or both cells (i.e. movement of the bulge away from a cell, and connection no longer detectable). 25 siLUC cells and 30 siKIF20B cells were analyzed.

SiR-tubulin fluorescent imaging: Cells were treated with 100 nm Silicon-Rhodamine Tubulin (SiR-Tubulin) according to the manufacturer's instruction (Cytoskeleton Inc., CO, USA) at least 6 hours before imaging. Cells were confirmed to have bipolar spindles using the SiR-Tubulin. Cells with more than two spindles (observed in both control and depleted cultures) were not used for measurements. Image stacks with 1.0 μm step size were captured with a 20x objective and a Cy5 (far red) filter, and maximum intensity projections of selected planes were used for analysis. The first abscission was defined as the first microtubule break, with no visible fluorescence between the flank and the

bulge. The second abscission was defined as the last break of the microtubules allowing the release of the midbody remnant into the medium. SiR-Tubulin enabled the visualization of both abscission events. DIC images were blinded for analysis. Live cell images were collected and analyzed using Zen Blue software (Zeiss).

Other data analysis and statistics were done with Microsoft Excel, GraphPad Prism, and PAST. (http://palaeo-electronica.org/2001_1/past/issue1_01.htm). Unless otherwise indicated, p-values were calculated with two-tailed Student's t-test, and error bars are S.E.M.

Results

KIF20B protein localizes to microtubules in the central spindle and midbody throughout cytokinesis, in a pattern distinct from other Kinesin-6 family members

Before analyzing the specific role of KIF20B in cytokinesis in HeLa cells, we first sought to determine its detailed subcellular localization in relation to the microtubule cytoskeleton during cytokinesis. To do this we co-immunostained HeLa cells for endogenous KIF20B along with alpha-tubulin. KIF20B is a low abundance protein, but it is readily detected in dividing cells when concentrated in cytokinetic structures. In cells fixed in anaphase, KIF20B signal appears as puncta on the microtubules of the central spindle (**Figure 2-1A**). In cells with more deeply ingressed furrows, KIF20B is more concentrated in the center of the central spindle as a band (**Figure 2-1B**). In early midbodies, KIF20B signal is detected in two discs on either side of the midbody core or “dark zone” (arrowhead) (**Figure 2-1, C and D**). In late midbodies, KIF20B signal is more extended along the midbody flanks (**Figure 2-1E**). If microtubule constriction sites are visible, KIF20B surrounds them, in this case appearing as four distinct spots on the midbody (**Figure 2-1F**). In cells that appear to have undergone abscission (with a large gap in tubulin staining on one side of the midbody), KIF20B can be detected still surrounding the dark zone (arrowheads), and on both flanks on either side of the abscission site (**Figure 2-1, G – I**). In a few cases where a microtubule strand remained connecting the sister cells, they were decorated with dots of KIF20B (arrows in **Figure 2-1, G-G**). Overexpression of a GFP-tagged full-length KIF20B in cell lines or neurons usually causes cell death, as previously reported by our group and others (Abaza et al., 2003; McNeely et al., 2017). However, a small number of surviving cells expressing

GFP-KIF20B showed a similar localization as endogenous KIF20B detected by immunostaining, flanking the dark zone (**Figure 2-1, J – J''**). Together these data suggest that KIF20B first associates with central spindle microtubules starting in early anaphase, then accumulates at microtubule plus ends that coincide with the plane of furrow ingression, and finally remains concentrated at the narrowest portions of the midbody surrounding the dark zone and constriction sites throughout the abscission process.

To compare the subcellular localization of endogenous KIF20B with those of the related Kinesin-6 family members MKLP1/KIF23 and MKLP2/KIF20A, we performed double immunolabeling and imaged cells at four stages of cytokinesis: post anaphase pre-furrow, early furrow, early midbody, and late midbody (**Figure 2-2**). Interestingly, in cells that have segregated chromosomes but not yet begun furrow ingression (pre-furrow), KIF20B signal is widely distributed on the central spindle and mitotic spindle microtubules, while both MKLP1 and MKLP2 are enriched at the central spindle midzone (**Figure 2-2, Aa and Ba**). In early furrows, all three family members are accumulated at the central spindle midzone where microtubule plus-ends overlap (**Figure 2-2, Ab and Bb**). In the early midbody, MKLP1 is seen as a ring around the midbody core (**Figure 2-2Ac**), while MKLP2 and KIF20B are similarly localized on the inner flanks adjacent to the core, with KIF20B extending more widely than MKLP2 (**Figure 2-2Bc**). Late midbodies display this difference even more clearly. MKLP1 remains strictly at the midbody center (**Figure 2-2Ad**). KIF20B overlaps MKLP2 on the inner flanks, but shows additional enriched signal distally around the microtubule constriction sites (**Figure 2-2Bd**). These data show that KIF20B localizes differently than its other subfamily members, accumulating at the midzone slightly later in anaphase than either MKLP1 or MKLP2, and localizing more widely on the midbody flanks than MKLP2, surrounding the constriction sites. These data concur with our previous data in mouse cells showing that Kif20b protein localization overlapped with that of Aurora B kinase in the midbody flanks, but was more enriched on the outer flanks of Aurora B signal (Janisch *et al.*, 2013). In addition, these data support the notion that the three Kinesin-6 family members have different functions in abscission.

Knockdown of KIF20B increases multinucleate cells

To investigate the cell-autonomous requirement and primary role(s) of KIF20B in cell division, we depleted endogenous KIF20B from HeLa cells using small interfering RNA (siRNA) transfections. We used a previously published KIF20B-specific siRNA sequence (“siRNA1” from (Abaza et al., 2003), and confirmed that it depletes endogenous KIF20B to undetectable levels in 98% of HeLa cell midbodies by 24 hours post-transfection and did not deplete other Kinesin-6 family members (See Methods and **Supplemental Figure 2-1** for details). First, we compared general mitotic and cytokinesis parameters between asynchronous cells transfected with control siRNA (siLUC) or siKIF20B (siKIF), and fixed 24 or 48 hours after transfection. Depletion of KIF20B did not significantly change the mitotic index or midbody index, but only slightly reduced the fraction of mitotic cells in telophase detected at 48 hours (**Figure 2-3, A-C**). However, KIF20B depletion resulted in a 2.5-fold increase in the occurrence of multinucleated cells (with two or more clearly distinct nuclei) at 24 hours, and a striking increase in multi-lobed nuclei at 48 hours post-transfection (**Figure 2-3, D-H**). Two additional siRNAs targeting different KIF20B sequences also increased the rates of multinucleation and multi-lobed nuclei (**Supplemental Figure 2-1, D and E**). Multi-lobed nuclei are likely a later, secondary consequence of cytokinesis failure, fusion of two or more nuclei (Neumann et al., 2010). Lastly, KIF20B knockdown caused a small but significant increase in apoptosis at 24 hours (**Figure 2-3I**). Together these data support the conclusion that in dissociated human cells as well as in the developing mouse brain, KIF20B has a role in cytokinesis.

Furrow ingression is slower in KIF20B-depleted cells

Next, we sought to analyze cytokinesis in KIF20B-depleted cells in more detail. Analyses were done at 24 hours post-transfection of siRNA, since KIF20B was depleted and phenotypes were already observed. First, we examined the cleavage furrowing stage. In fixed cell images, we noticed that the central spindles of anaphase cells in the siKIF20B-treated cultures sometimes appeared disorganized, with non-parallel microtubule bundles or asymmetric gaps (**Figure 2-4, A and B**, arrowheads), but often appeared symmetric (**Figure 2-4A**, right cell, and **Supplemental Figure 2-2**). In blinded scoring, 7

of 18 (39%) siKIF20B-treated furrowing cells had discernible disorganization in their central spindles, while only 6 of 31 (19%) siLUC-treated furrowing cells did. While these sample sizes are too small and the microtubule spacing too variable during furrow ingression for statistical significance, these data suggest that KIF20B-depleted anaphase cells may have increased rates of irregularities in the central spindle. Together with the KIF20B localization on the central spindle microtubules shown in Figures 1 and 2, it seems plausible that KIF20B could help organize or stabilize microtubule bundles during anaphase to telophase.

Since the anaphase spindle regulates cleavage furrow positioning and ingression (Green et al., 2012), this notion prompted us to examine the kinetics of furrow ingression in live cell time-lapse imaging. By collecting images every one minute as control or KIF20B-depleted mitotic cells progressed through cleavage, we observed in each case that furrows appeared qualitatively normal, occurring only at the cell equator, ingressing steadily, and never regressing (**Figure 2-4, C and D**). However, there was a quantitative difference. The average total duration of furrow ingression from anaphase onset to completion was significantly increased in KIF20B-depleted cells, from 6.5 minutes to 8.4 minutes (**Figure 2-4E**). Plotting furrow width over time demonstrates that the onset of furrow ingression is similar, but ingression proceeds at a slower rate in siKIF-treated cells (**Figure 2-4F**). A smaller but similar reduction was seen in the rate of cell lengthening from pole-to-pole (**Figure 2-4G**). Together these data show that while KIF20B is not required for central spindle formation or furrow ingression, it may contribute to central spindle organization and promote rapid furrow ingression.

KIF20B loss alters midbody width but not subdomain structure

We previously showed that in embryonic mouse brains, loss of *Kif20b* disrupted the shapes and positioning of neural stem cell midbodies. Midbodies still formed at the apical membrane of the neuroepithelium, but were more often misaligned, and had an altered distribution of axis ratios, primarily due to increased width (Janisch and Dwyer, 2016; Janisch et al., 2013). To test whether this phenotype reflects a cell-autonomous primary requirement for KIF20B in abscission, and whether it occurs in cells not contained in a polarized epithelium, we measured the lengths and widths of midbodies of HeLa cells treated with control or KIF20B siRNA (**Figure 2-5A**). Indeed, we found that

siKIF20B-treated cells did have a significantly shifted distribution of midbody widths, but surprisingly there were more thin midbodies and fewer wide midbodies. This was observed with either tubulin or Aurora B kinase immunostaining (**Figure 2-5, B and C**). Midbodies also tended to be longer when KIF20B was depleted, but the shift was not statistically significant (**Figure 2-5D**). Together with our previously published midbody shape analyses in embryonic mouse brains, these data show that loss of KIF20B causes changes in the abscission stage of cytokinesis in a cell autonomous manner.

We hypothesized that KIF20B may regulate midbody shape directly or indirectly by binding microtubules or by localizing effectors to midbody microtubules. To further investigate midbody structure and protein recruitment when KIF20B is depleted, we took advantage of the wider variety of antibodies that work for immunofluorescence on human cells than on mouse cells. We tested whether the major subdomains of the midbody form when KIF20B is depleted, and whether several key regulators of cytokinesis are localized properly in the subdomains as well as in furrows (**Figure 2-6**). Protein Regulator of Cytokinesis 1 (PRC1), which is required for formation of the central spindle (Mollinari et al., 2002; Zhu et al., 2006) and was shown to interact with KIF20B (Kanehira et al., 2007), shows normal localization in KIF20B-depleted cells at the center of the central spindle in anaphase, and in the midbody in two discs in the dark zone, as well as the flanks. This pattern was not disrupted in KIF20B-depleted cells (**Figure 2-6, A-B**). The Kinesin-6 family member KIF23/MKLP1, required for midbody formation and abscission (Matuliene and Kuriyama, 2002; Zhu et al., 2005a) localizes normally to the central spindle and to the midbody center in KIF20B-depleted cells (**Figure 2-6, C-D**). Aurora B kinase (AURKB) localizes to the central spindle during furrowing, and on the flanks of the midbody in both control and siKIF20B-treated cells (**Figure 2-6, C-D**). Activated Aurora B kinase phosphorylated at Thr-232 (pAURKB), which was shown to regulate the abscission checkpoint (Carlton et al., 2012; Steigemann et al., 2009), localizes to the center of the midbody in both control and KIF20B-depleted cells (**Figure 2-6, E-F**). Anillin (ANLN), a scaffold that crosslinks filaments in the contractile furrow membrane, does not require KIF20B for recruitment. In both control and siKIF-treated cells, it localizes to the furrowing membrane, remains in the midbody as a ring around the central bulge at early stages, and later localizes to both the central bulge and constriction sites (**Figure 2-6G-H**). Alpha-actinin-4 (ACTN4), which crosslinks actin and regulates cytokinetic furrowing (Mukhina et al., 2007), was pulled down as a candidate

binding protein with KIF20B (Maliga et al., 2013). However, it appears indistinguishable in the furrows of KIF20B-depleted cells, and as expected, is not enriched in midbodies of control or KIF20B-depleted cells (**Figure 2-6, I-J**). These data demonstrate that KIF20B is not required for recruitment of several key proteins to the midbody, and moreover that when KIF20B is depleted, the primary midbody subdomains of central dark zone, bulge, and flanks are specified.

KIF20B depletion disrupts late midbody maturation

Since the higher proportion of thin and long midbodies in KIF20B-depleted cells suggested a delay in abscission (**Figure 2-5**), but the major midbody subdomains appear to assemble normally (**Figure 2-6**), we sought to further characterize the late stage midbodies. First, we quantified midbodies showing evidence of a late event, microtubule constriction sites. In fixed midbodies immunostained for tubulin, constriction sites appear as pinches or gaps in microtubule staining a few microns away from the central bulge, and are the presumed abscission sites (Guizetti et al., 2011; Hu et al., 2012). These constriction sites (also called secondary ingressions) may be visible on one or both sides of the midbody center (**Figure 2-7, A and B**). Interestingly, we found that in the KIF20B-depleted cells, a smaller percentage of midbodies had a detectable constriction site (**Figure 2-7C**). This suggests a defect in the structure or formation of constrictions. As a second marker of late midbodies, we analyzed the localization of CEP55, a key abscission regulator that accumulates in late midbodies, starting about 50-60 minutes after anaphase onset in HeLa cells (Guizetti *et al.*, 2011; (Bastos and Barr, 2010). It localizes to and maintains the structure of the central bulge of the midbody, and then recruits ESCRT proteins to mediate abscission (Lee et al., 2008; Zhao et al., 2006). Accordingly, we observed that in midbodies without constriction sites, CEP55 immunostaining signal appeared in two discs perpendicular to the microtubules inside the central dark zone (**Figure 2-7D, left**). In late midbodies with at least one microtubule constriction site, the CEP55 discs appeared closer together, usually still resolvable with deconvolution in most control cells, but less often in KIF20B-depleted cells (**Figure 2-7D, right**; arrowheads point to constriction sites). Interestingly, in KIF20B-depleted midbodies with at least one constriction, the CEP55 signal had a greater maximum intensity, though occupying the same area (**Figure 2-7, E and F**). Together, the decreased frequency of midbodies with constriction sites, and increased CEP55 intensity

in the midbodies that do have constrictions, suggest that KIF20B depletion causes a defect or delay in a late stage of midbody maturation, between CEP55 recruitment and the formation of constriction sites.

It is not well understood how late-stage midbodies form constriction sites in preparation for final abscission, but may involve both membrane constriction by ESCRT-III filament assembly and turnover, and localized microtubule severing by spastin (Connell et al., 2009; Elia et al., 2011; Guizetti et al., 2011; Mierzwa et al., 2017; Schiel et al., 2011). Spastin is recruited to late midbodies first to the central bulge and then to constriction sites (Gershony et al., 2017). This recruitment pattern of spastin does not appear to require KIF20B, as it was observed in most control and KIF20B-depleted midbodies (**Supplemental Figure 2-3**). To analyze ESCRT-III recruitment, we performed double immunostaining with anillin and VPS4, the most downstream component of the ESCRT-III machinery that mediates filament formation and turnover, and is enriched just prior to abscission (Elia et al., 2011; Mierzwa et al., 2017). It was shown that in late midbodies, anillin and ESCRT-III both localize to the midbody center and constriction sites, but that anillin dissipates and disappears as ESCRT-III accumulates (Renshaw et al., 2014). Accordingly, we observed by double immunostaining that midbodies variously showed enrichment of anillin only (early stage), both anillin and VPS4 (transitional), or VPS4 only (latest stage) (**Figure 2-8A**). Interestingly, we found that among KIF20B-depleted midbodies, almost twice as many had anillin enriched at the center bulge compared to control midbodies, and a higher percentage had anillin enrichment at constriction sites also (**Figure 2-8, B, C, and E**). However, the frequency of observations of VPS4 enrichment was reversed, with a smaller proportion of midbodies showing VPS4 at the center or constrictions when KIF20B was depleted (**Figure 2-8, B, C, and E**). Categorizing the midbodies by whether they had enriched anillin-only, VPS4-only, or both anillin and VPS4, we found that the population was shifted in the KIF20B-depleted cells to the earlier and transitional stage categories (**Figure 2-8, D and E**). The KIF20B-depleted midbodies were 50% more likely to be anillin-only enriched, more than twice as likely to be transitional, with both anillin and VPS4 enrichment, but only half as likely to be late stage VPS4-only. These data suggest that KIF20B is not required for VPS4 recruitment to the midbody bulge and constriction sites (nor presumably for upstream ESCRT-III components), but that its activity may enhance the speed or extent of VPS4 recruitment. Alternatively, KIF20B function may aid anillin dispersal. In any case, the

data support the notion that KIF20B functions to accelerate or coordinate late-stage midbody maturation processes.

KIF20B depletion disrupts abscission timing

Based on the late stage midbody defects we observed, we decided to directly test whether loss of KIF20B causes delays or failures in abscission, we performed live cell time-lapse imaging with siRNA-treated HeLa cells. First, the cell-permeable tubulin dye Silicon-Rhodamine Tubulin (SiR-tubulin) was used to label midbodies and monitor abscission (**Figure 2-9, A-D**). This far-red dye shows a more than 10-fold increase in fluorescence upon binding to polymerized microtubules (Lukinavicius et al., 2014). Figures 9A and B show example time-lapse images of abscission collected using wide-field microscopy with a 20x dry or 63x oil objective (**Figure 2-9, A and B**). In both cases, the first abscission (a1, white arrowhead) and second abscission (a2, yellow arrowhead) can be observed, and the midbody remnant can be followed for at least an hour after abscission (**Figure 2-9B**, thin arrow at 105 minutes). Interestingly, at the higher magnification, the severed midbody flanks can also still be resolved as coherent microtubule bundles more than an hour after the second abscission (**Figure 2-9B**, wide arrows at 105 minutes).

By imaging every 7.5 minutes, we found that control cells had a median time from anaphase onset to first abscission of 67.5 minutes (**Figure 2-9C**, black bars). This is similar to the timing observed previously in HeLa cells using both GFP-tubulin or photoactivatable dye transfer (Guizetti et al., 2011; Steigemann et al., 2009), suggesting that SiR-tubulin is a valid tool for abscission studies. Surprisingly, however, in KIF20B-depleted cells, the median time to first abscission was not significantly different from controls (**Figure 2-9C**, white bars). Since midbody inheritance or release has been proposed to influence daughter cell fate in stem cell divisions (Dubreuil et al., 2007; Ettinger et al., 2011; Kuo et al., 2011; Salzman et al., 2014), we also wanted to test whether KIF20B regulates the time between first and second abscissions. We found that the second abscission usually occurred within 15 minutes of the first abscission (~75% of the cells), in both siLUC and siKIF-treated cells (**Figure 2-9D**). This is similar to but slightly faster than what was reported using GFP-tubulin (Gershony et al., 2017; Guizetti et al., 2011). Interestingly, the cells that had the longest times to first abscission were not

the ones that had the longest times between first and second abscissions, suggesting they are independent events (data not shown).

The lack of a detectable change in abscission timing using SiR-tubulin imaging after KIF20B depletion was surprising, given the late midbody defects we had observed. SiR-tubulin is a derivative of the taxane docetaxel, which stabilizes microtubules, but it is much less toxic and does not arrest mitosis at the dosage we used (Lukinavicius et al., 2014). However, we hypothesized that SiR-tubulin might be slightly stabilizing microtubules and thereby rescuing the effect of loss of KIF20B. To test this hypothesis, we employed a different method of scoring abscission, differential interference contrast (DIC) imaging, without SiR-tubulin (**Figure 2-9E**). With this method, only the first abscission event could be discerned with confidence. The median time to first abscission in control siRNA cells was 67.5 minutes, the same as observed with SiR-tubulin (**Figure 2-9, C and F**, black arrows). Remarkably, however, we found that in siKIF20B-treated cells, abscission timing was significantly dysregulated, with a wider distribution of times, and a median increase of 15 minutes (**Figure 2-9F**, white bars, white arrow). Together, these live cell time-lapse imaging experiments show that KIF20B loss has a small but significant effect on the timing of abscission, and further suggest that KIF20B does so by stabilizing microtubules.

Discussion

With the major players required for cytokinesis largely identified, there is a growing need to understand the roles of proteins that regulate the temporal aspects of cytokinesis, or play specialized roles in different cell types. We have demonstrated here that KIF20B, a Kinesin-6 family member required for normal brain size, has cell autonomous roles in cytokinesis, temporally regulating both cytokinetic furrow ingression and abscission. We found that KIF20B localizes to microtubules of the central spindle and midbody throughout cytokinesis, particularly enriched near the midbody core and also around constriction sites, in patterns distinct from the other two Kinesin-6 family members. KIF20B depletion resulted in slower furrow ingression, and dysregulated abscission timing. Analyses of midbody structure and markers suggest that KIF20B is not required for midbody assembly or specification of subdomains, but may promote efficient midbody maturation and timely abscission. KIF20B may act in part by stabilizing

microtubules. In the context of our previous work, these data suggest that seemingly subtle defects in the midbody and temporal control of cytokinesis can have devastating consequences for brain development.

Midbody maturation is an evolving concept in the cytokinesis field, describing a series of events during an hour or more that prepare the intercellular bridge to be cut by the abscission machinery. It includes sequential recruitment of many proteins to the midbody bulge and their formation into rings, thinning of the midbody flanks, shedding of membrane, formation of constriction sites, and re-localization of some proteins (e.g., anillin, spastin, VPS4) to the constriction sites (Hu et al., 2012; Mierzwa and Gerlich, 2014; Renshaw et al., 2014). Our data suggest that KIF20B helps accelerate or coordinate midbody maturation. Its localization around the core of early midbodies and around the constriction sites of late midbodies suggests that it may aid maturation by keeping microtubules tightly packed or preventing them from sliding.

Multiple pieces of evidence suggest that KIF20B functions to organize microtubule bundles in cells by crosslinking. First, KIF20B is sufficient to crosslink microtubules in a cell-free assay (Abaza et al., 2003). Second, we previously showed that in axons of *Kif20b* mouse mutant neurons, microtubules are less tightly packed and more frequently invade growth cone filopodia, suggesting increased sliding (McNeely et al., 2017). Similarly, another Kinesin-6, pavarotti/MKLP1, inhibits microtubule sliding in *Drosophila* neurons (del Castillo et al., 2015). Third, here we showed that depletion of KIF20B caused increased disorganization in central spindle microtubules, and altered midbody widths. It could be that KIF20B helps bundle and anchor microtubules at the center of the midzone, and any irregularities in anaphase are compounded as the midbody forms and matures. Although KIF20B is not required for constriction sites to form, or for spastin localization to the constrictions, an attractive possibility is that KIF20B stabilizes microtubules in a particular arrangement to facilitate formation of constriction sites, or the activity of severing enzymes like spastin.

The finding that SiR-tubulin appears to rescue the abscission timing defect also supports the idea that KIF20B promotes efficient abscission by stabilizing microtubules. More work is needed to determine the utility and limitations of using SiR-tubulin to live image abscission. At a minimum, it provides a way to label endogenous microtubules in live cells with low background and without the need to transfect plasmids or inject labelled

protein. Of note, SiR-tubulin was recently used to label midbodies in a study of ESCRT recruitment during abscission in HeLa cells (Mierzwa *et al.*, 2017). However, careful comparisons of microtubule dynamics and the kinetics of cytokinesis measured with varying dosages of SiR-tubulin versus other tubulin reagents, such as GFP-tubulin, are important for the field.

The phenotypes caused by depletion of KIF20B from HeLa cells are subtle compared to those caused by depletion of other midbody proteins such as CEP55 or the other Kinesin-6 family members. HeLa cells depleted of KIF23/MKLP1 usually fail to assemble a proper midbody core, regress their furrow, and become binucleate (Matuliene and Kuriyama, 2002; Zhu *et al.*, 2005b). HeLa cells depleted of KIF20A/MKLP2 may either fail to complete furrow ingression (Kitagawa *et al.*, 2013; Neef *et al.*, 2003), or assemble a midbody but fail to complete abscission (Zhu *et al.*, 2005b). Knockdown of CEP55 causes cells to be stuck in abscission for hours, and manifests as a large increase in midbody index in fixed cell populations (Zhao *et al.*, 2006). But knockdown of KIF20B caused only a two-minute delay in furrowing and a 15-minute delay in abscission in our experiments, roughly 25% increases. This small effect size explains why we did not find an increased mitotic index or midbody index in fixed cells. This may also explain why KIF20B was not identified in high throughput RNAi screens for genes involved in cell division (Kittler *et al.*, 2004; Kittler *et al.*, 2007; Neumann *et al.*, 2010), or for motor protein knockdown phenotypes (Zhu *et al.*, 2005b). In retrospect, the small magnitude of KIF20B phenotypes probably did not meet the thresholds applied in those screens, but are only revealed upon focused quantitative analysis. Our genetic screen for developmental phenotypes, rather than a single-cell screen, revealed the importance of this Kinesin-6 (Dwyer *et al.*, 2011).

Our previous analyses showed that *Kif20b* is essential for normal brain size in the mouse, even though it is not absolutely required for cytokinesis. The *Kif20b* mutant embryos form most organs normally, and do grow a small brain. This demonstrates that some tissues do not require *Kif20b*, and that many neural stem cells divisions occur successfully without it. However, the mutant neural stem cells show abnormal midbody shapes and organization, and undergo increased apoptosis (Janisch *et al.*, 2013). What we do not yet know is whether the temporal changes in cytokinesis observed upon KIF20B loss in HeLa cells are increased in severity in neuroepithelial stem cells lacking

Kif20b, or whether the neural cells are simply much more sensitive to delays in cytokinesis. Polarized neuroepithelial stem cells are very tall and thin, and furrow ingression proceeds from the basal side to the apical. In addition, furrowing and abscission must be coordinated with the inheritance of cell fate determinants and apical membrane junctions. Interestingly, Kif20b may help link midbodies to the apical membrane (Janisch et al., 2013). These factors suggest that cytokinesis in the neuroepithelium is much more challenging than in a HeLa cell and requires both spatial and temporal precision (Dwyer et al., 2016; Johnson et al., 2017). Thus, small defects in cytokinesis could trigger apoptosis or premature differentiation, depleting the progenitor pool. HeLa cells, the most commonly used mammalian system to study cytokinesis, cannot fully model the cytokinesis mechanisms and phenotypes of developing tissues like the early brain.

Nevertheless, despite such limitations, the cell line work herein has generated valuable high-resolution data and hypotheses about KIF20B's functions to test in the developing brain. Future experiments will examine whether similar defects in midbody maturation and abscission occur in neural stem cells in culture and in intact brain explants, as well as how the timing of furrowing and abscission are coordinated with tissue polarity and daughter fates. This work underscores the need for more studies of cytokinesis in developing tissues in addition to isolated single cells. There may be many important players that regulate the timing or precision of cytokinesis that have not yet been identified from single cell screens. Mutations in these genes may be discovered as causing developmental or functional defects in animal models or human clinical diseases.

Acknowledgements

We thank Fabienne Pirollet for the GFP-KIF20B plasmid. We are grateful to Todd Stukenberg, Jim Casanova, Bettina Winckler, Jing Yu, Xiaowei Lu, members of their labs, and Jessica Little for advice and discussions. This work was supported by the National Institutes of Health (R01 NS076640 to NDD), an American Cancer Society seed grant (ACS-IRG-81-001-26 to NDD), and a Harrison Undergraduate Research Award to JMD.

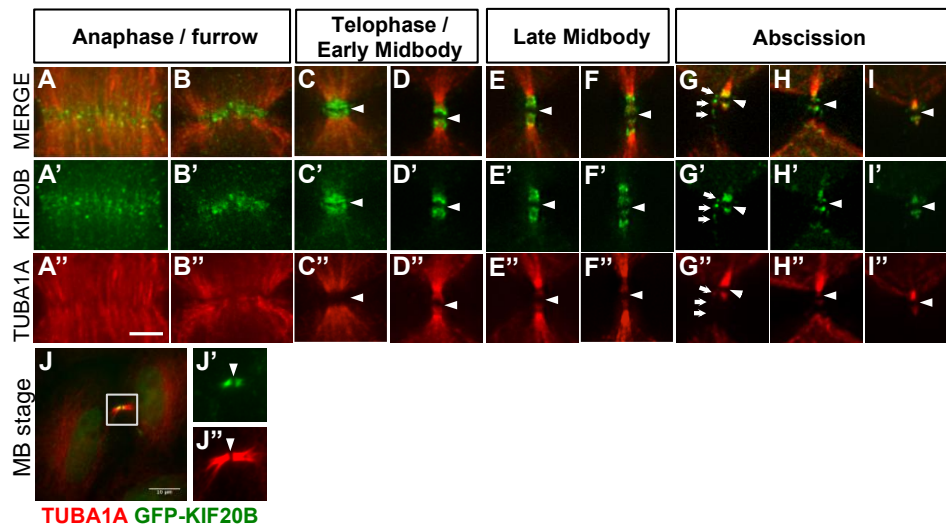


Figure 2-1: KIF20B localizes to the central spindle and midbody throughout cytokinesis in HeLa cells.

Panels **A-I** show immunofluorescence staining for endogenous KIF20B (green) and tubulin (red), at sequential phases of cytokinesis from anaphase furrowing (**A**) to post-abscission (**I**).

Arrowheads point to central dark zone in all pictures.

(A - B'') During anaphase, KIF20B starts to accumulate as speckles along the microtubules of the central spindle (**A'**), and in later furrows forming a dense band in the middle of the central spindle (**B'**).

(C - D'') In early midbodies, KIF20B accumulates on the inner flanks of the midbody surrounding the dark zone (arrowhead), forming a cap-like structure.

(E - F'') In late midbody stage, KIF20B spreads out on the midbody flanks surrounding the constriction sites, resulting in 4 distinct spots of KIF20B localization.

(G - I'') Near abscission in very thin midbodies, small spots of KIF20B can be seen still surrounding the central dark zone (arrowhead). The small arrows in the **G** panels point to KIF20B dots localizing along a strand of microtubules.

(J - J'') GFP-KIF20B expressed in HeLa cell shows the same localization within the midbody as detected by antibodies to KIF20B.

Scale bars represent 5 μm for **A** through **I'** and 10 μm for panel **J**.

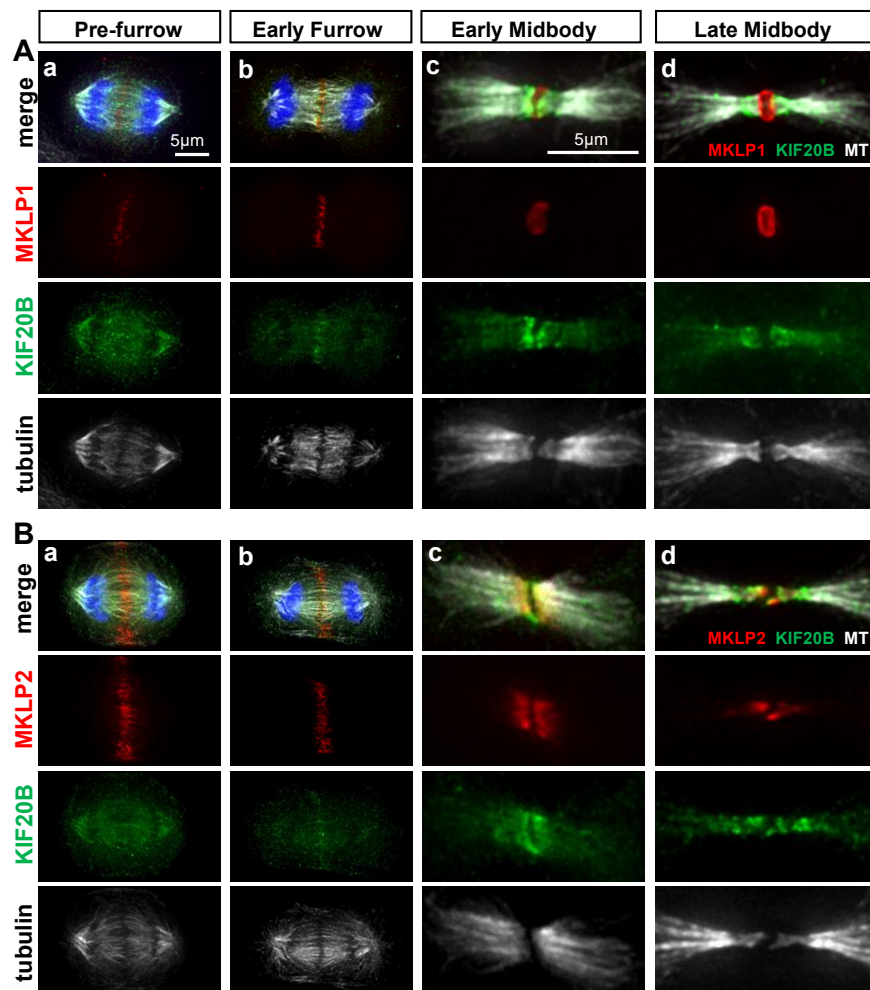


Figure 2-2: KIF20B protein shows overlapping but distinct localization from MKLP1/KIF23 and MKLP2/KIF20A during cytokinesis.

(A) Immunostaining HeLa cells for endogenous MKLP1 (red) and KIF20B (green) with alpha-tubulin (white) shows distinct localizations at pre-furrow (a) early furrow (b), early midbody (c), and late midbody (d) stages.

(B) Immunostaining for endogenous MKLP2 (red) and KIF20B (green) with alpha tubulin (white) shows substantial overlap in the early furrow (b) and early midbody (c) stages, but that KIF20B is more broadly distributed on the central spindle in the pre-furrow stage (a) and is enriched on the outer flanks of the constriction sites in the late midbody stage (d).

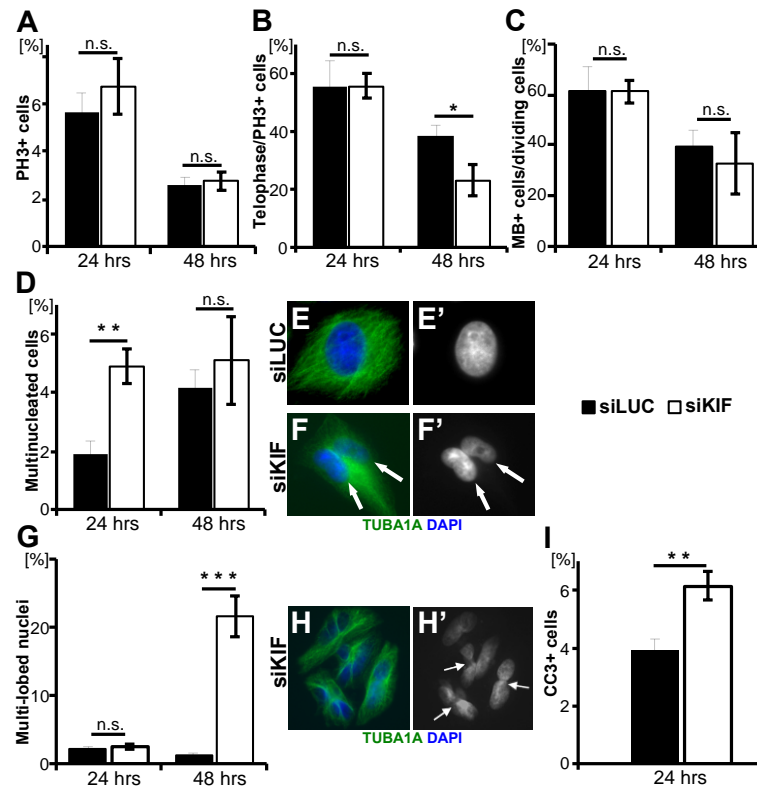


Figure 2-3: Cytokinesis defects in KIF20B-depleted asynchronous HeLa cell cultures.

(A) The average mitotic index was not altered by KIF20B depletion at 24 hours ($n = 5$ coverslips/treatment, siLUC = 1192 cells, siKIF = 1408 cells) or 48 hours post-transfection ($n = 7$ coverslips/treatment, siLUC = 1870 cells, siKIF = 2513 cells). Mitotic index was defined as the number of phospho-histone H3 positive (PH3⁺) cells divided by the total cell count by DAPI+ nuclei. PH3 immunostaining signal is strong in prophase, metaphase, and anaphase; weak in telophase; and absent in post-telophase late midbody stage cells.

(B) Average percentage of telophase cells out of mitotic cells (PH3⁺) was not changed at 24 hours but decreased at 48 hours post-transfection in siKIF knockdown cells ($p = 0.038$). Telophase was characterized by the presence of condensed chromatin. For 24 hours, $n = 5$ coverslips/treatment (siLUC = 67 cells; siKIF = 95 cells); for 48 hours post-transfection, $n = 7$ coverslips/treatment (siLUC = 49 cells; siKIF = 69 cells).

(C) The average percentage of midbody stage cells out of all dividing cells (PH3⁺ or PH3⁻ with a midbody) was not significantly different in siKIF-treated cells. At 24 hours, $n = 8$ coverslips/treatment, with 2556 total siLUC cells, and 3048 total siKIF cells; at 48 hours post-transfection, $n = 6$ coverslips/treatment, with 952 total siLUC cells, and 1176 total siKIF cells).

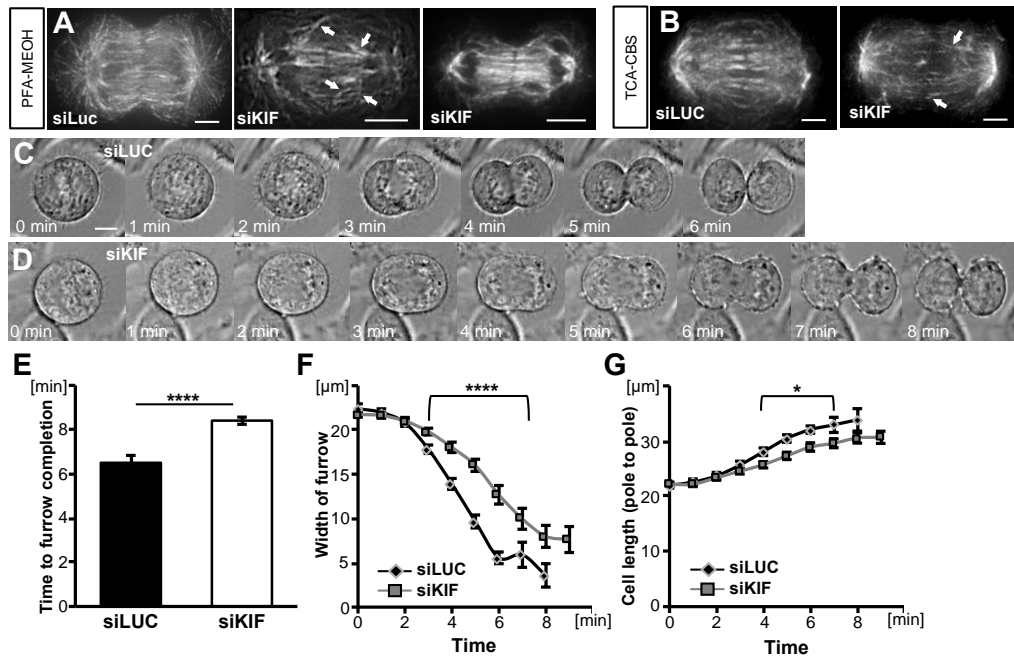


Figure 2-4: Cleavage furrow ingression is slower in KIF20B-depleted cells.

(A-B) Example images of central spindles of furrowing cells fixed with either PFA-MeOH (A) or TCA-CBS (B) and stained for alpha-tubulin (TUBA1A). Central spindles of some KIF20B-depleted cells appear to have irregularities in the angles or left-right symmetry of the microtubule bundles (arrowheads).

(C-D) Representative brightfield time-lapse live images of an siLUC-treated cell (C) that completed furrowing in 6 minutes, and an siKIF-treated cell (D) that completed furrowing in 8 minutes.

(E) Average total time from anaphase onset (chromosome segregation onset) to completion of cleavage furrowing ingression was increased in siKIF cells (**** $p = 3 \times 10^{-7}$).

(F) Furrow widths of siKIF cells decreased steadily but more slowly than those of siLUC cells (for points under bracket, **** $p = 3 \times 10^{-5}$).

(G) Cell lengths (pole to pole) of siKIF20B-treated cells also increased steadily but more slowly than in siLUC cells, (* $p \leq 0.05$). For E-G, $n_{\text{siLUC}} = 20$ cells, $n_{\text{siKIF}} = 24$ cells across 5 independent imaging sessions. $t = 0$ was the last time point before anaphase onset (chromosome segregation) was detectable. Scale bars represent $10 \mu\text{m}$.

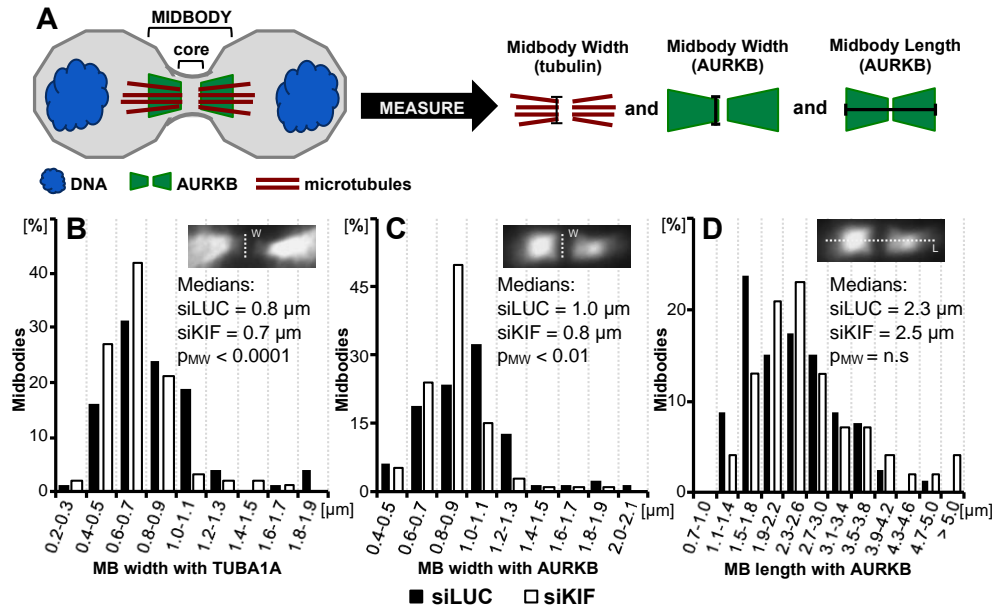


Figure 2-5: Midbodies tend to be thinner in KIF20B-depleted HeLa cells.

24 hours after transfection with control (siLUC) or KIF20B (siKIF) siRNA, cells were fixed and immunostained for α -TUBULIN (TUBA1A) and AURORA B kinase (AURKB). Midbodies were imaged and measured for width and length as shown in (A) and insets.

(A) Schematic of midbody (not to scale) and measurements. The midbody core “dark zone” contains dense overlapping microtubules, but does not stain with tubulin or Aurora B antibodies due to density. Midbody widths were measured adjacent to the dark zone by both tubulin and AURKB signal. Lengths were measured by AURKB signal only. The midbody “edge” was considered to be where no signal was detected.

(B and C) Plots of the distributions of midbody widths for KIF20B-depleted cells (siKIF, white bars) and controls (siLUC, black bars) show that KIF20B-depleted cells more often have thin midbodies when measured by TUBA1A or AURKB signal (medians: siLUC = 0.8 μm , siKIF = 0.7 μm , $p_{M-W} < 0.0001$, and distribution shape $p_{K-S} = 0.0205$; and siLUC = 1.0 μm , siKIF = 0.8 μm , $p_{M-W} < 0.01$, and distribution shape $p_{K-S} = 0.000419$, respectively).

(D) Median midbody length, as measured with AURKB signal, shows a trend to be increased in siKIF-treated cells, but does not reach statistical significance ($p_{M-W} = 0.28$; $p_{K-S} = 0.85$). p-values (p_{M-W}) for medians are calculated with Mann-Whitney U-test; p-values (p_{K-S}) for distribution shape are calculated with Kolmogorov-Smirnov test, n.s., not significant. $n_{\text{siLUC}} = 80$ midbodies; $n_{\text{siKIF}} = 100$ midbodies, from 3 independent siRNA transfections.

Figure 2-6: Midbody assembly appears normal in KIF20B-depleted cells.

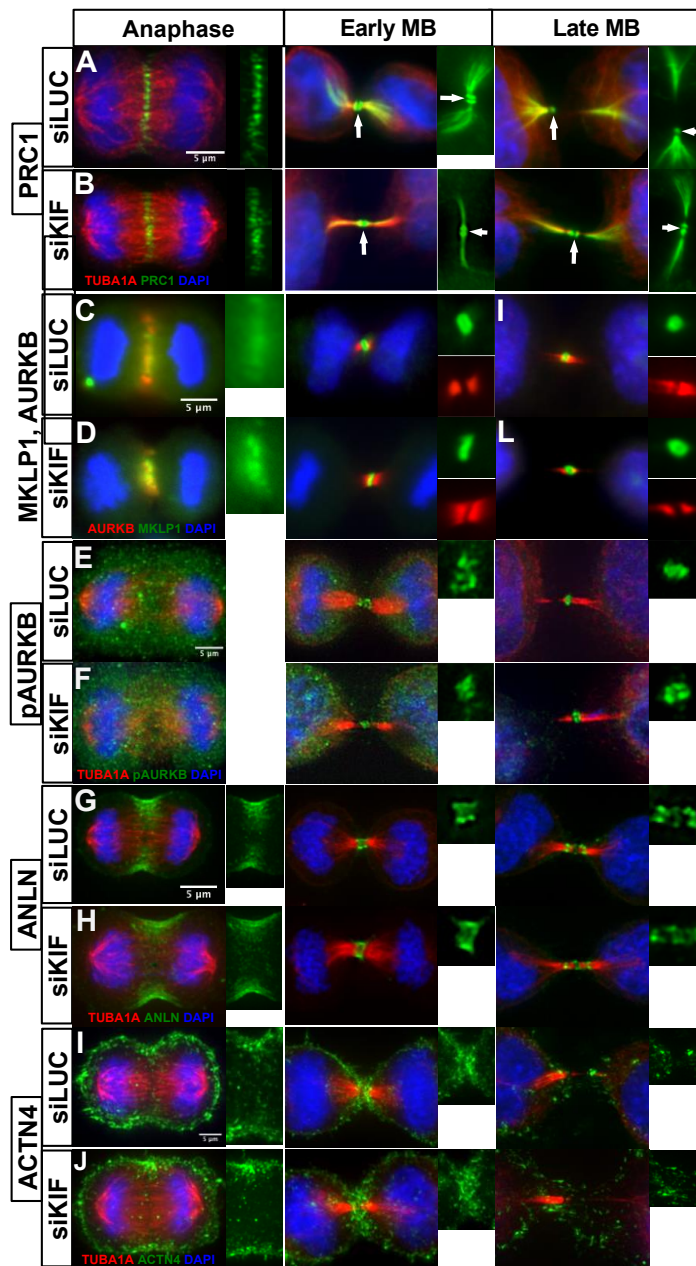


Figure 2-6: Midbody assembly appears normal in KIF20B-depleted cells. (Continued)

(A and B) PRC1 localizes to the central spindle in anaphase in both siLUC and siKIF cells. In early and late midbodies (MB), PRC1 lines the microtubules of the midbody flanks and extends into the cell on the microtubule network. It also forms two distinct discs around the core of the midbody (white arrow).

(C and D) MKLP1/KIF23 localizes to the central spindle in anaphase in siLUC and siKIF cells. In early and late midbodies, it is found in the center of the midbody (dark zone) in control or KIF20B depleted cells. By contrast, Aurora kinase B (AURKB) localizes to the flanks of the midbody in early and late stages in both siLUC and siKIF cells.

(E and F) Phospho-T232-Aurora B (pAURKB), representing “activated” Aurora B kinase, is diffusely localized during anaphase in both siLUC and siKIF cells. In early midbodies, pAURKB localizes to the center dark zone and inner flanks as a diffuse blob, but appears as a more compact disc in later midbodies, similar in siLUC and siKIF cells.

(G and H) Anillin (ANLN) localizes to the furrowing cell cortex during anaphase in siLUC and siKIF cells. In the early midbody stage, ANLN forms a wide ring around the center of the midbody. In late midbodies, ANLN can be found in the center of the midbody as well as at the constriction sites. These localizations were not disrupted in KIF20B-depleted cells.

(I and J) α -actinin-4 (ACTN4) is distributed on the entire cell cortex but clearly accumulates in the cleavage furrow during anaphase in both siLUC and siKIF cells. In early midbody stage, ACTN4 enriches in a half-circle shape at the edges of both daughter cells underneath the midbody. In the late midbody stage, there is no longer enrichment of ACTN4 around the midbody, in both siLUC and siKIF cells.

Images in panels A-B and E-J were taken with a DeltaVision deconvolution microscope, and those in C-D with a widefield microscope. At least 15 midbody-stage and 5 anaphase cells imaged for each marker and condition. Scale bars are 5 μ m for all images.

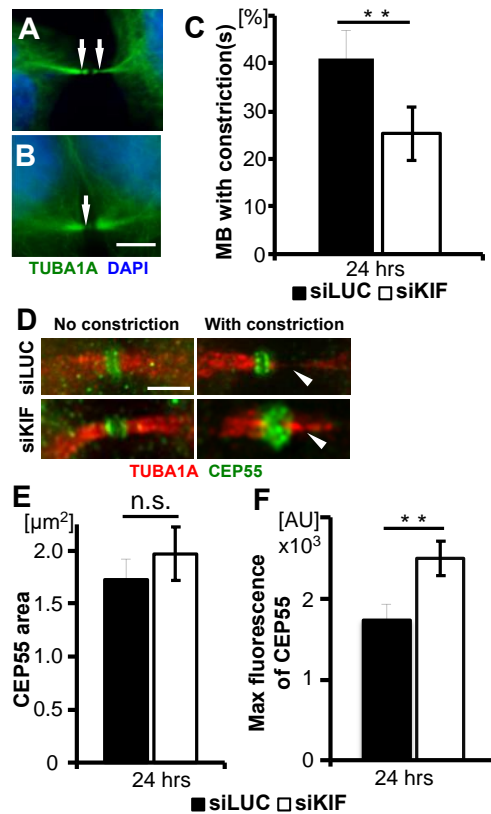


Figure 2-7: Midbodies of KIF20B-depleted cells show reduced frequency of constriction sites and increased CEP55 intensity.

(A and B) Representative widefield images of tubulin in midbodies with one or two constriction sites visible (arrows).

(C) The average percentage of midbodies having at least one visible constriction site was reduced in KIF20B-depleted cells at 24 hours post-transfection (**, $p = 0.01$, $n = 5$ experiments with 2 coverslips each).

(D) Representative deconvolved images of endogenous CEP55 localization to the midbody bulge in both siLUC and siKIF20B-treated cells. In midbodies without constriction sites, CEP55 appears in two distinct discs. In late midbodies having constriction sites (arrowheads), CEP55 is more dense but can still be resolved into two discs by deconvolution in control cells, but not in siKIF-treated cells.

(E) The average area of CEP55 signal in the core of late midbodies with constriction sites is not significantly different between siLUC- and siKIF-treated cells.

(F) The average maximum fluorescence intensity of CEP55 is significantly higher in late midbodies with constriction sites after KIF20B depletion. **, $p = .01$, $n = 26$ siLUC and 17 siKIF late midbodies.

p-values calculated with two-tailed Student's t-test, except in (C) paired t-test was used. Scale bars for A and B, 5 μm ; for D – K, 2.5 μm .

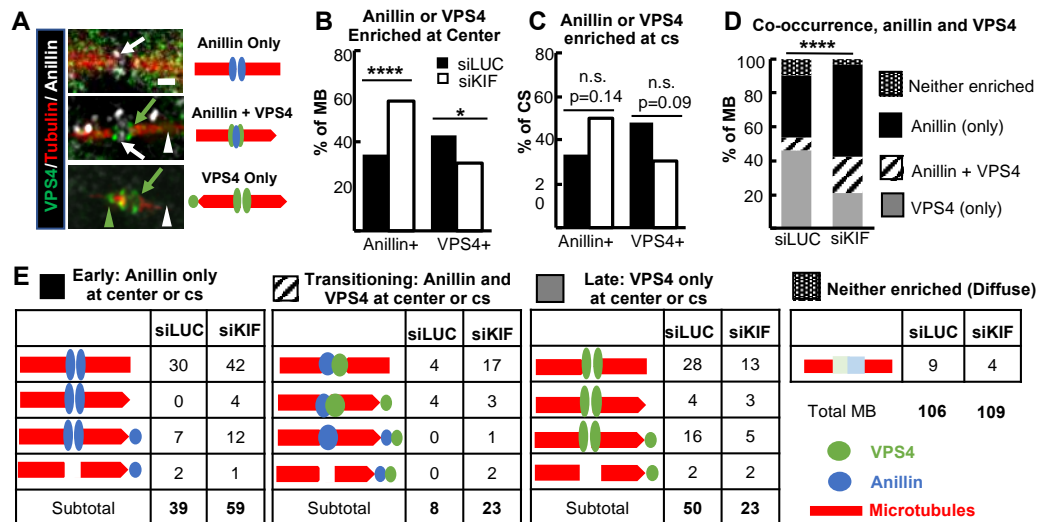


Figure 2-8: Pattern of anillin and VPS4 recruitment are consistent with late-stage maturation defect in KIF20B-depleted midbodies.

(A) Left, Example deconvolution images of endogenous VPS4 and anillin localization in representative midbodies of HeLa cells. Right, schematic representations of staining in images on left. Arrows point to the central bulge region, and arrowheads point to constriction sites. White, anillin; green, VPS4; red, tubulin. Scale bar, 1µm.

(B) The percentage of midbodies with anillin enriched in the center is increased, and the percentage with VPS4 enriched in the center is decreased. $n=106$ siLUC-treated cells, and 109 siKIF-treated cells from 2 coverslips each of 2 independent experiments.

(C) The percentage of constriction sites (cs) that have anillin enrichment was increased, while the percentage of constriction sites that have VPS4 enrichment was decreased, in KIF20B depleted midbodies, but did not reach statistical significance. $n=48$ siLUC constriction sites in 38 midbodies, and $n=46$ siKIF constriction sites in 34 midbodies.

(D) Bar plot of anillin and VPS4 co-occurrence in midbodies shows KIF20B-depleted midbodies are significantly shifted out of the latest-stage category (VPS4-only) and into the early (anillin only) and transitional (anillin plus VPS4) categories. $n=106$ siLUC-treated midbodies, 109 siKIF-treated midbodies.

(E) Detailed schematic representations and raw tallies of subcategories of anillin and VPS4 enrichment data plotted in bar graphs in B, C, and D. White space in microtubules symbolizes the central dark zone, and pointed ends symbolize constriction sites (cs). Anillin (blue) or VPS4 (green) enrichment was scored at midbody centers or constriction sites. *, $p < 0.05$; ****, $p < 0.0001$; n.s., not significant (Fisher's test for B and C, Chi-square test for D).

Figure 2-9: KIF20B depletion delays and dysregulates abscission.

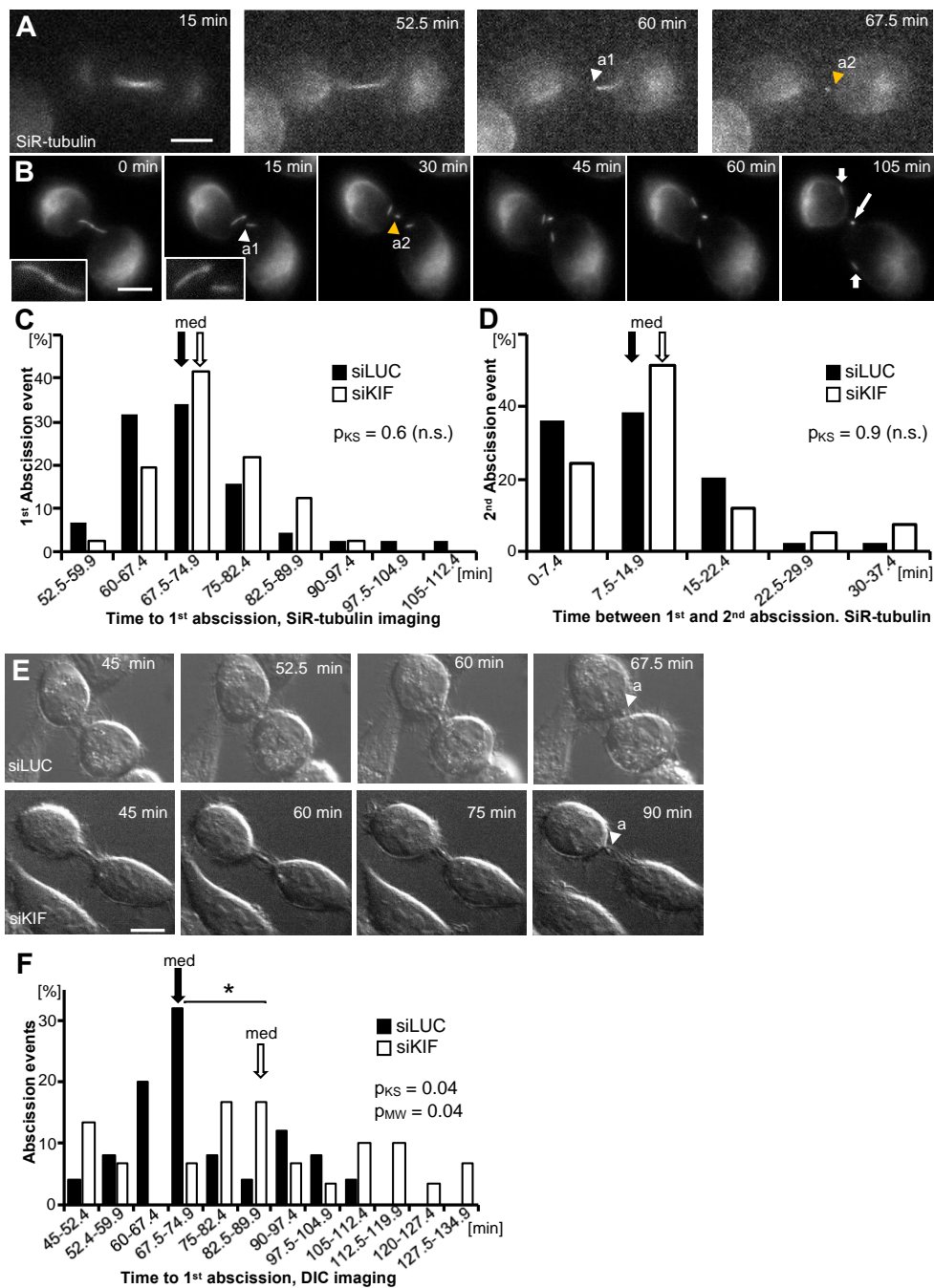


Figure 2-9: KIF20B depletion delays and dysregulates abscission. (Continued)

(A and B) Example widefield time-lapse imaging of abscission in a HeLa cell labeled with SiR-Tubulin at 20x (A) and 63x (B) (arrowhead a1: abscission 1, arrowhead a2: abscission 2, filled arrow: midbody flanks, open arrow: midbody remnant). Images captured every 7.5 minutes (A) and every 15 minutes (B). Insets in B are showing the intact midbody and the first abscission.

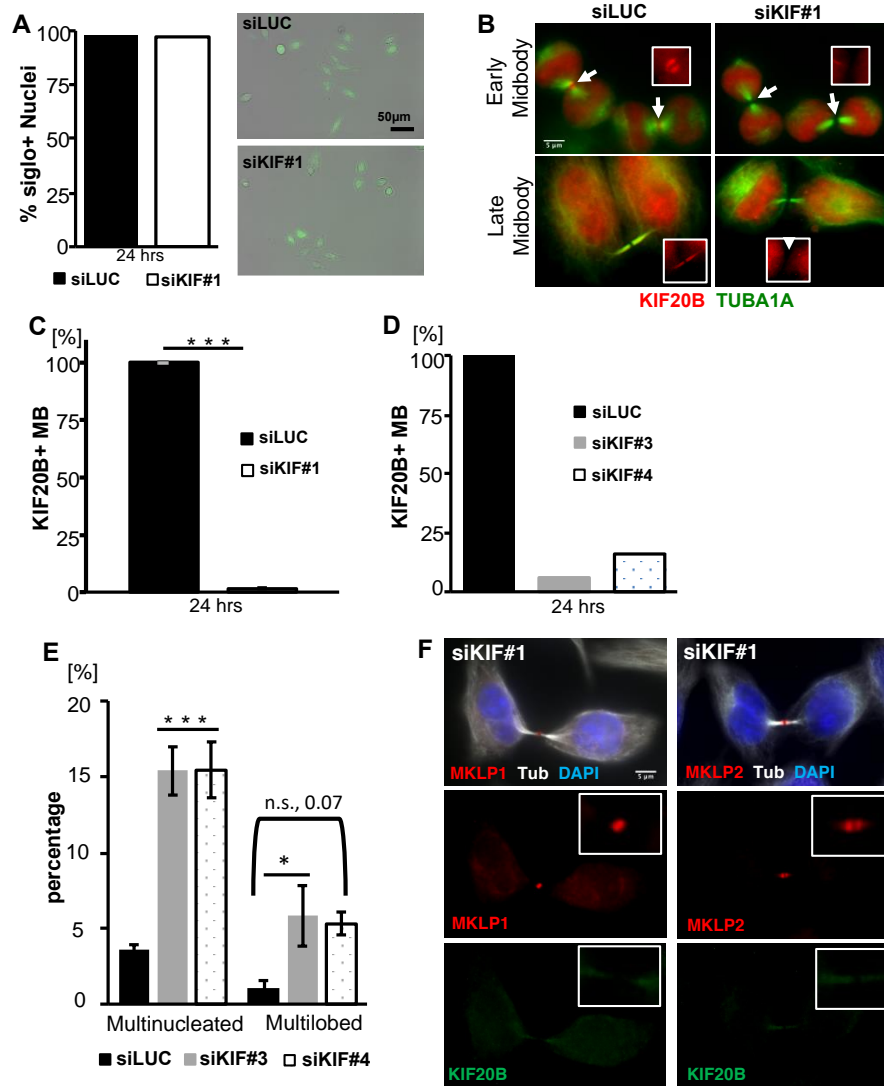
(C) Frequency distribution of time from anaphase to first abscission shows a similar median time (67.5 minutes, arrows, $p_{M-W} = 0.13$ and similar distribution shape ($p_{K-S} = 0.6$) for siLUC (black bars) and siKIF-treated cells (white bars) imaged and scored using SiR-tubulin. $n = 44$ siLUC cells and 41 siKIF20B cells from 4 experiments.

(D) The median time between first and second abscissions (arrows, 7.5 minutes, $p_{M-W} = 0.09$) imaged with SiR-tubulin was not different in KIF20B-depleted cells (siKIF) and controls (siLUC). The distributions were not significantly different between siLUC and siKIF-treated cells ($p_{K-S} = 0.9$). Sample is same as in C.

(E) Representative selected planes from time-lapse z-stack images of abscission using differential interference contrast (DIC) microscopy, captured every 7.5 minutes (arrowhead with "a" signifies abscission). Top: in this siLUC-treated cell, abscission was observed 67.5 minutes after anaphase onset. Bottom: in this siKIF-treated cell, abscission was observed 90 minutes after anaphase onset. The second abscission event was not discernible by DIC imaging.

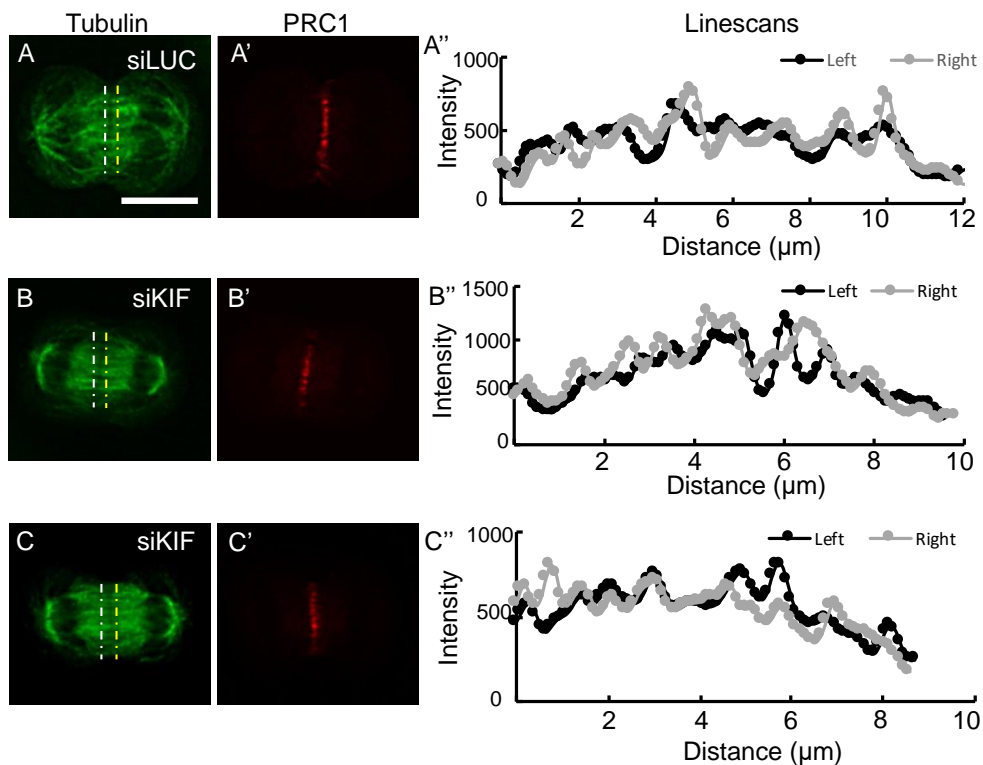
(F) Increased median time (67.5 versus 82.5 minutes) and altered distribution of time to abscission after KIF20B depletion, shown in frequency graph of time from anaphase to first abscission discerned using DIC time-lapse microscopy in siKIF- (white bars) compared to siLUC-treated cells (black bars). For distribution, $*p_{K-S} = 0.04$; for medians, $*p_{M-W} = 0.04$. $n = 25$ siLUC cells and 30 siKIF cells from 4 experiments.

K-S: Kolmogorov–Smirnov test, M-W: Mann-Whitney U-test. Scale bars, 10 μm .



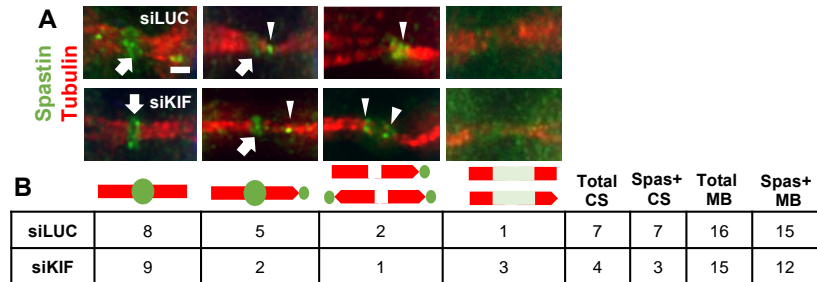
Supplemental Figure 2-1: Knockdown efficacy of siRNAs to human KIF20B.

(A) Transfection efficiency of both control siRNA to the Luciferase gene (siLUC) and siRNA to KIF20b (siKIF#1 from (Abaza *et al.*, 2003) was > 98% as indicated by siGlo transfection indicator (Dharmacon). n = 118 siLUC cells, 125 siKIF cells from 1 coverslip/treatment each. Scale bar, 50 μ m.



Supplemental Figure 2-2: Example deconvolution images of normally and abnormally organized central spindles.

Example deconvolution images of normally organized central spindles in siLUC- (A) or siKIF-treated (B, C) HeLa cells in anaphase/early furrowing. Images are single z-planes taken from the center of each cell. (A', B', C') show normal PRC1 localization at the midzone of central spindles in siLUC- and siKIF-treated HeLa cells. (A'', B'', C'') are linescans of tubulin signal from images A, B, and C, drawn perpendicular to the central spindle microtubule bundles on the left and right sides of the midzone (indicated by white and yellow dotted lines). Tubulin intensity peaks represent microtubule bundles that often show apparent symmetry on both halves of the central spindle. Scale bar 10 μ m.



Supplemental Figure 2-3: Spastin recruitment in the midbody does not require KIF20B.

(A) Example deconvolution images of endogenous spastin (green) localization in the midbodies of siLUC- (top) and siKIF-treated (bottom) HeLa cells also stained for tubulin (red). Localization can be seen in the central bulge (arrows) or at the constriction sites (arrowheads), or both, or spastin may be diffuse rather than enriched at any particular site (right-most panels).

(B) Schematic representations of spastin localization as seen in examples in (A), with tallies underneath of midbodies observed with each localization pattern, and subtotals for constriction sites (CS) or midbodies (MB).

**Chapter III:
Cytokinesis and post-abscission midbody
remnants are regulated during mammalian brain
development**

This chapter is in press at PNAS
McNeely, K.C. and Dwyer, N.D.

Abstract

Building a brain of the proper size and structure requires neural stem cells (NSCs) to divide with tight temporal and spatial control to produce different daughter cell types in proper numbers and sequence. Mammalian NSCs in the embryonic cortex must maintain their polarized epithelial structure as they undergo both early proliferative divisions and later neurogenic divisions. To do this they undergo a polarized form of cytokinesis at the apical membrane that is not well understood. Here we investigate whether polarized furrowing and abscission in mouse NSCs are regulated differently at earlier and later stages, and in a cytokinesis mutant, *Kif20b*. This mutant was previously shown to have microcephaly and elevated apoptosis of NSCs. We developed methods to live image furrow ingression and midbody abscission in NSCs within cortical explants. We find that polarized furrow ingression occurs at a steady rate and completes in ~15 minutes, at two different ages. However, ingression is slower in a subset of *Kif20b* mutant NSCs. Abscission is usually observed on both sides of the midbody, and takes 65-75 minutes to complete. Surprisingly, abscission is accelerated in the *Kif20b* mutant NSCs. Post-abscission midbody remnants are observed at the apical membranes of daughter cells, and are much more abundant in early stage cortices. After NSC divisions *in vitro*, midbody remnants are more often retained on the daughter cells of early proliferative divisions. Altogether, these results suggest that regulation of abscission timing and midbody remnants in embryonic NSCs may influence proper brain growth and structure.

Significance

In prenatal mammalian brains, billions of cells are produced by neural stem cell (NSC) divisions during a short developmental window. Small changes in divisions can result in abnormal brains, but the regulation is not well understood. Here we address whether cytokinesis—cleavage furrowing and abscission (intercellular bridge severing)—occur differently throughout development. We test whether cytokinesis is abnormal in a small-brained mouse mutant of a microtubule motor gene, *Kif20b*. We developed a method to live image NSCs undergoing cytokinesis in mouse brain explants. We found abscission remnants are more likely to remain on daughter cells at earlier ages. In *Kif20b* mutant

brains, abscission occurs faster. These surprising findings suggest that precise regulations of abscission processes are important during early brain development.

Introduction

To build a brain of the proper size and structure, neural stem cells (NSCs) must proliferate rapidly to produce billions of daughter cells in a short developmental time window, and generate different daughter cell types at specific times. NSCs are tall, thin cells that are highly polarized, extending radially to contact the pia on the basal side. Their apical membranes ("apical endfeet") are joined by junctions and form the walls of the lateral ventricles. Their nuclei move within them during the cell cycle, in a process called interkinetic nuclear migration. Nuclei move to the basal side for S-phase and to the apical membrane for M-phase and must carefully regulate the positioning of mitosis and cytokinesis (see **Figure 3-1B**). This nuclear movement creates a pseudostratified epithelium as NSCs proliferate. During early development, NSCs perform symmetric proliferative divisions to produce two NSC daughters and expand the stem cell pool. Later, NSCs increase neurogenic divisions, producing neuron daughters that differentiate, migrate basally, and never divide again (Bizzotto and Francis, 2015; Dwyer et al., 2016). Errors in these divisions can result in brains that are too small or have abnormal structure (Bizzotto and Francis, 2015; Jayaraman et al., 2018). How the NSCs accomplish these divisions and control the balance of proliferative and neurogenic daughter fates is a subject of intense study.

As they divide, the NSCs must faithfully segregate genomes and organelles to their daughters, and confer proper daughter fates, while maintaining their polarity and the integrity of the epithelium. To do this, NSCs undergo a polarized form of cytokinesis that is poorly understood: first, the furrow ingresses from basal to apical; then, abscission occurs at the apical membrane. Cleavage is near-perpendicular to the apical membrane (Noctor et al., 2008). While many studies have shown that disrupting the perpendicular cleavage plane can deplete the stem cell pool or disrupt cortical structure (Feng and Walsh, 2004; LaMonica et al., 2013; Postiglione et al., 2011; Yingling et al., 2008), the regulation of furrow ingression itself has not been thoroughly addressed.

The basic mechanisms of cytokinetic abscission have been established primarily from studies in single cell models (Green et al., 2012; Mierzwa and Gerlich, 2014). After chromosome segregation, the central spindle promotes cleavage furrow ingression and compacts its microtubules into a structure called the midbody, within the intercellular bridge. The center of the midbody microtubule bundle contains overlapping plus ends embedded in a dense matrix, which appears as a bulge on live imaging. The midbody contains over 450 proteins that assemble within the central bulge or on the lateral flanks of microtubule bundles that extend on each side of the central bulge (Addi et al., 2020; Hu et al., 2012; Mierzwa and Gerlich, 2014; Skop et al., 2004). This structure serves as a platform to mediate abscission, the process of severing the intercellular bridge. Abscission involves both microtubule disassembly and plasma membrane constriction by ESCRT-III filaments leading to scission of the midbody flanks (Connell et al., 2009; Guizetti et al., 2011). After abscission, the central bulge remains intact and is called the midbody remnant (MBR). Potentially, MBRs could transmit signals to neighboring cells by surface binding or internalization as "MBsomes" (Bernabe-Rubio et al., 2016; Crowell et al., 2014; Peterman et al., 2019). Evidence from developing worms and flies, as well as mammalian stem cell lines, suggests that temporal and spatial regulation of abscission can influence daughter cell polarity and fate (Chaigne et al., 2019; Dionne et al., 2015; Ettinger et al., 2011; Kuo et al., 2011; Lenhart and DiNardo, 2015; Pollarolo et al., 2011; Salzmann et al., 2014; Singh and Pohl, 2014b). It is unclear whether these simpler systems accurately model abscission dynamics in the developing brain, where polarized stem cells must alter the balance of proliferation and differentiation during development.

Previously, we showed that a loss-of-function mutation of the Kinesin-6 *Kif20b* in mice causes microcephaly, partly due to elevated apoptosis of NSCs (Dwyer et al., 2011; Janisch et al., 2013; Little and Dwyer, 2019). Kif20b protein shows a dynamic localization during cytokinesis that suggests it could play roles in furrow ingression or abscission. During the first part of cytokinesis, furrowing, Kif20b protein localizes to the central spindle (in anaphase). In the second part of cytokinesis, abscission, Kif20b is found first on the midbody flanks (in telophase), and later at the constriction sites where final scission will occur (in late telophase or G1) (**Figure 1E** and (Abaza et al., 2003; Gershony et al., 2014; Janisch et al., 2018; Janisch et al., 2013)). We showed that in HeLa cells, Kif20b depletion caused subtle disruptions of furrowing speed, midbody

maturation and abscission timing, but did not prevent abscission completion (Janisch et al., 2018). This raised the question of whether *Kif20b* loss causes more severe defects of cytokinesis in NSCs than in HeLa cells. In fixed brains of *Kif20b* mutants, we found no changes in the proportions or positions of mitotic or S-phase NSCs (Janisch et al., 2013). Cleavage furrow angles were not different than controls, and binucleate cells were not detected. However, the cortical NSCs did have a reduced midbody index and wider, disorganized midbodies. Together these data suggested that loss of *Kif20b* specifically causes defects in cytokinesis, and that regulation of cytokinesis in NSCs is critical for proper brain development.

Here we address two main questions: whether cytokinesis is differentially regulated in NSCs during early proliferative and later neurogenic stages of cortical development, and whether loss of *Kif20b* disrupts the kinetics of NSC furrowing or abscission. Since the durations of furrowing and abscission in cortical NSCs had not been measured before, we developed methods to quantitatively analyze these events in NSCs through live imaging in intact cortical explants, and compared different developmental stages. Using both live and fixed preparations, we find that abscission in NSCs usually occurs on each midbody flank sequentially, and that midbody remnants (MBRs) persist at the apical membrane. This is consistent with the idea that the MBR has the potential to induce or carry signals to daughter cells or neighbor cells post-abscission. Interestingly, MBRs are observed more often with proliferative divisions than neurogenic divisions. Furthermore, *Kif20b* appears to regulate both furrow ingression speed and abscission timing in cortical NSCs. Together these data add to a growing body of work showing that subtle alterations of abscission timing and MBR regulation can influence daughter fates and tissue development.

Materials and Methods

Mice

The animal protocol was approved by the UVA IACUC and the colonies maintained in accordance with NIH guidelines. The morning of the vaginal plug was considered E0.5. All embryos were harvested by cesarean section and littermate controls were used when possible. The *Kif20b*^{magoo} (*Kif20b*^{-/-}) mutant mouse was generated in an ENU screen (Dwyer et al., 2011). It carries a loss-of-function splice site mutation that reduces the

protein to undetectable levels (Janisch et al., 2013). The *Kif20b* mutant mouse was crossed with both the mT/mG reporter line (Jax stock #007576) and Sox2-Cre mice (JAX stock #008454) (Hayashi et al., 2002; Muzumdar et al., 2007) to produce mice that expressed plasma membrane-localized GFP.

Cortical slab explant culture for cleavage furrow and abscission live imaging

E11.5 or E13.5 embryos were removed from the uterus and dissected in cold 1x PBS. After decapitation, the skull was removed, and #5 forceps were used to pinch out the cortices. Each hemisphere was placed into a glass bottom dish (MatTek P35G-1.0-20-C) containing 50 nM silicone-rhodamine tubulin (SirTubulin) (Cytoskeleton CY-SC002) in Final Culture Medium (described below). The hemispheres were then trimmed to create flat cortical slabs, and flipped over so the apical surface faced the glass. Each dish was placed in a humidifying chamber and into a 37 °C incubator with 5% CO₂ overnight (Approximately 15 hours). The next day the cortices were removed from the incubator, and the 50nM Sir-Tubulin-containing medium was removed. Matrigel (Corning 356237) (1:3 dilution in Final Culture Medium) was added on top of the cortical slab. High vacuum grease (Fisher 14-635-5D) was placed on the edge of the glass bottom dish in four spots, and a coverslip (Fisher 12-545-100) was placed over the top of the cortical slab explant. Gentle pressure was applied to the coverslip at the spots where the vacuum grease was placed. The dish was put back into the incubator, and the Matrigel was allowed to solidify for 5 minutes. Final culture medium with 2% HEPES (Gibco 15630080) was added to the dish, and then imaging was performed. An Applied Precision (GE) DeltaVision with Truelight Deconvolution and softWorx suite 5.5 image acquisition software equipped with a heating plate and 40X objective (1.53 N.A.) was used for time-lapse image acquisition. Z-stacks of images approximately 10 µm deep (z- steps 0.4 µm) were taken every 15 minutes for abscission and every 3 minutes for cleavage furrowing for up to 6 hours. To minimize phototoxicity, the neutral density filter was set at 32% or lower and the exposure time was kept to a minimum (< 0.1 milliseconds per slice). The total cortical slab thickness varied by age (E11.5: ~150µm, E13.5: ~200µm). To confirm 50nM SiR-Tubulin treatment did not cause mitotic arrest, we fixed and stained for phospho-histone H3, a mitotic marker: we found no difference in the mitotic index after SiR-Tubulin treatment. Additionally, in time-lapse movies the cells that failed to complete furrowing or abscission was similar between genotypes and were excluded from analyses.

Cleavage furrow ingression and abscission analysis

Deconvolved full-z-stacks and maximum intensity projection images were analyzed using ImageJ. For cleavage furrowing, membrane-GFP cells were identified in mitosis by their characteristic round shape. Time zero was considered the last time point before furrowing began. The length and width of the cell were measured until furrow completion, considered complete when (1) there was no additional subsequent narrowing of the furrow tips and (2) the membrane between sister cells appeared continuous. For abscission, time zero was midbody formation as ascertained by SiR-Tubulin appearance (compact microtubule bundles). Abscission completion was scored as the time point when there was complete removal of microtubules on a midbody flank, ascertained when the SiR-tubulin signal intensity decreased to background level. Midbody membrane scission was shown to be temporally coincident with midbody flank microtubule disassembly by several previous publications using DIC or phase imaging of cell lines in 2-D dissociated cultures (Elia et al., 2011; Lafaurie-Janvone et al., 2013; Steigemann et al., 2009); but here, we cannot rule out the possibility that the midbody plasma membrane might remain connected for some period of time after the microtubules are gone. Still image stacks for 3-D renderings (**Figure 3-3A, B**) were acquired using longer exposure times and finer z-steps (0.2 μ m) on E13.5 cortical slabs incubated in higher concentration of SiR-Tubulin (200 nM). 3-D renderings were created in PerkinElmer Volocity 3D Image Analysis Software (access to Volocity kindly provided by Dr. Barry Hinton).

Immunohistochemistry on fixed cortical slabs

This method was previously described (Janisch and Dwyer, 2016). Briefly, the skulls were opened to reveal the cortices and the head was fixed for 20 minutes in 2% PFA for E11.5 and 4% PFA for E15.5. Cortical hemispheres were pinched off, placed in slide wells (Cat # 70366-12, 70366-13), and trimmed to flat pieces of neocortex (slabs) as outlined by the dashed line in **Figure 3-1A**. Total cortical slab thickness varied by age (E11.5: ~150 μ m, E15.5: ~400 μ m). The cortical slabs were briefly fixed again with PFA before immunostaining. After coverslipping, images were acquired using the 60x objective on the Applied Precision (GE) DeltaVision microscope.

Pair cell assay for NSC divisions

The pair cell assay for dissociated cortical NSC divisions was adapted from (Chau et al., 2015; Qian et al., 1998). E11.5 or E15.5 mouse embryos were removed from the uterus and placed in Hibernation Medium (Gibco Hibernate-E A12476-01), and cortices were dissected out. Meninges were removed from E15.5 cortices. The cortices were then placed into a 15 mL conical tube for dissociation. Papain from Worthington kit (Worthington Biochemical Corporation, LK003150) was added and cortices were placed on a rotator at 37 °C for 30 minutes (E11.5) or 45 minutes (E15.5). The cortices were then manually dissociated with a 1mL Rainin pipette followed by centrifugation at 4 °C at 1300 rpm for 10 minutes. The cell pellet was then washed with DMEM (Invitrogen 11960-051). The wash and centrifugation steps were repeated three times. After the final wash, the cells were resuspended in Final Culture Medium with a 1 mL Rainin pipette followed by a glass Pasteur pipette (resuspension volume varied by age and size of cortices). Final Culture Medium (made fresh on day of culture): 2 mL 100X Na-Pyruvate (Invitrogen 11360-070), 2 mL 200 nM L-glutamine (Gibco A2916801), and 4 mL 50X B-27 without Vitamin B (Gibco 12587010) per 200 mL of DMEM (Invitrogen 11960-051) were filtered through a 0.22 µm cellulose acetate membrane (BD Biosciences 302995). Once filtered, 100 µL of 100X N2 (Invitrogen Cat. No. 17502-048), 100 µL 100X N-acetyl-cysteine (Sigma Cat No A-9165), and 20 µL of 10 µg/mL bFGF (Invitrogen Cat. No. 13256-029) were added per 20 mL of medium. The cell suspensions sat at room temperature (20 °C) for 15 minutes to allow any cell clumps to settle to the bottom of the conical tube. Then, between 1 to 3 µL of cell suspension from the top of the tube were added to each well of the poly-L-lysine coated Terasaki plates (Fisher cat # 07-000-401) to get a very low density. The Terasaki plates were pretreated with 1mg/mL PLL for 30 minutes then rinsed with water and stored with 4mL of Base Culture Media at 4 °C until use. In the case of the NSC cultures, cells were plated at 50,000 cells per coverslip and cultured for 24 hours before fixation. The plates were placed in a humidifying chamber and into a 37 °C incubator with 5% CO₂ for 20 hours to allow one round of cell division. Afterward, the cells were fixed with 4% paraformaldehyde (PFA) for 2 minutes, followed by 5 minutes cold methanol (100% methanol at -20 °C) in -20 °C freezer. Immunostaining was followed as described below, except the plate was kept in a humidified chamber to prevent evaporation, and volumes of washes and antibodies were

adjusted. Images were acquired using a Zeiss AxioZoom Observer.Z1 with a 40x air objective.

Antibodies and immunofluorescence staining

Following fixation, cortical slabs or dissociated NSCs cultured on coverslips (Fisher Brand Microscope Coverglass 18Cir-1D Cat #: 12-545-84) were incubated for an hour at room temperature (20 °C) in blocking buffer (0.1% Triton-X, 2-5% Normal Goat Serum in PBS) and then overnight at 4 °C or for three hours at room temperature (20 °C) in the appropriate primary antibody solution (antibody diluted in blocking solution). After primary incubation, coverslips were rinsed in PBS (3 times every 10 minutes) or slabs were rinsed in PBS-triton once followed by two PBS rinses and then incubated at room temperature (20 °C) with appropriate secondary antibody solution (1:200 dilution) for 30 minutes (dissociated NSCs) or 45 minutes (cortical slabs) in the dark. Following final washes in PBS, coverslips were mounted onto glass slides with flurogel (Electron Microscopy Sciences 17985-10) or slabs were cover-slipped (22 x 22 #1 cover glass, Curtin Matheson Scientific Inc Cat #: 089-409) with Fluoromount (Vectashield, 4-1000). Antibodies used: chicken anti-Nestin (Aves Lab, NES), rabbit or mouse anti-Tubb3 (TUJ1, Abcam rabbit 52623, Biolegend mouse 801201), mouse anti-Citron kinase (CITK, BD Biosciences 611376), rabbit anti-Aurora B (AurKB, Abcam ab2254), mouse anti-Cep55 (Santa Cruz sc-377018), rabbit anti-Survivin (Cell Signaling Technology 2808). For F-actin visualization we used Phalloidin (ThermoFisher A12380).

Statistical analyses

Statistical analyses were performed with Excel (Microsoft) and GraphPad Prism. A statistician was consulted regarding the abscission duration analyses. T-test was used to compare averages for normal data. ANOVA was used for multiple comparisons in **Figure 3-5B**. Non-normal data was compared using Kolmogorov–Smirnov and Mann-Whitney tests. Categorical data was compared using Fisher’s and Chi square tests. The statistical tests used and p-values calculated in each graph are indicated in the corresponding figure legend. All error bars are standard error of the mean (s.e.m.).

Results

Furrowing and abscission kinetics of embryonic NSCs can be analyzed in intact cortical explants

To better understand cytokinesis events and kinetics of NSCs in their polarized epithelial structure, and to identify specific defects in cytokinesis mutants, we developed a method to live image both cytokinetic furrowing and abscission in intact cortical explants. Both furrowing and abscission occur near the apical membrane. Therefore, instead of cutting cross section slices, we dissect a flat "slab" of neocortex from membrane-GFP transgenic mice (**Figure 3-1A**), and culture it in a glass-bottom dish to view the apical membrane *en face*. The cultured cortical slabs, which are ~150 to 200 μm thick, are incubated with SiR-Tubulin (Silicon-Rhodamine-Tubulin), a cell-permeable dye which fluoresces in far red when it binds polymerized microtubules. Thus we can image fields containing many NSC apical endfeet. Cells in mitosis are rounded up with a bipolar spindle, making them easily detectable using membrane-GFP or SiR-Tubulin (**Figure 3-1B, C, D, subapical planes**). Midbodies form at the apical membrane (**Figure 3-1 B, C, D, apical planes**). Live time-lapse imaging of NSC cytokinesis can be done by collecting z-stacks of images at time points 3 minutes apart for single color imaging and 15 minutes apart for two-color imaging. These time intervals and short exposure times are both essential for maintaining the health of the NSCs. We live-imaged cytokinesis in both control and *Kif20b* mutant cortical explants at two ages.

Kif20b may facilitate furrow ingression in cortical NSCs

NSC cleavage furrowing controls the plane of division and positions the midbody at the apical membrane. Here, we set out to determine the kinetics of furrowing and if they change with developmental stage or loss of *Kif20b*. Mitotic cells are easy to identify near the apical membrane owing to their large, spherical shape. Cytokinesis begins with the cell elongating parallel to the apical membrane before the furrow initiates on the basal side, and ingresses asymmetrically towards the apical membrane. In control cells, furrow ingression proceeds smoothly, at a constant rate (**Figure 3-2Aa**). Under these conditions, the rate of furrow ingression for control NSCs is 0.4 $\mu\text{m}/\text{min}$ (**Figure 3-2B, E, black lines**) and takes ~15 minutes to complete (**Figure 3-2D, G, control**), at both

E11.5 (proliferative divisions) and E13.5 (neurogenic divisions). The elongation is also unchanged during development (**Figure 2C, F, black lines**). Most *Kif20b*^{-/-} NSCs behave like controls, and none show furrow regression (**Figure 2Ab**). However, a subset furrow abnormally, taking 24 minutes to complete (**Figure 2Ac, B, E, red lines**). This subset of slow cells causes the median time to furrow completion to be increased by 3 minutes in *Kif20b* mutant brains (**Figure 2D, G**). These data show that 1) furrowing kinetics do not significantly change between E11.5 and E13.5, and 2) *Kif20b* is not required for cleavage furrowing, but may help to ensure continuous rapid furrow ingression.

Abscission is accelerated in *Kif20b* mutants

It was unknown how long abscission takes following mitosis in cortical NSCs. Therefore, we analyzed the spatial and temporal dynamics of abscission in NSCs in the cortical explant system. Figure 3A shows a representative NSC at an early stage of abscission, with a wide pre-abscission midbody. A rotated image stack (X-Z view) illustrates how the midbody microtubule bundle bridges the two daughter cells across their cell junction. At later stages of abscission (**Figure 3-3B**), the midbody is narrower, and sometimes microtubule bundle thinning can be seen on one flank (open arrowhead). By live time-lapse, with two-color imaging of the membrane and microtubules, we were able to follow NSCs through abscission. Abscission involves both the disassembly of microtubules and scission of membrane on the midbody flanks. We cannot detect the midbody membrane, since the membrane-GFP label (myristoylated-GFP) does not enrich in the midbody. Therefore, we defined abscission completion as the time point when microtubules were disassembled on a midbody flank, ascertained when the SiR-tubulin signal intensity decreased to background level (**Figure 3-3C**). Microtubule thinning prior to complete disassembly was sometimes detected (**Figure 3-3C, 60'**).

The timing of abscission has been linked to daughter cell fates in fly germline stem cells and mouse embryonic stem cells (Chaigne et al., 2019; Lenhart and DiNardo, 2015). To ask if abscission duration changes as brain development proceeds, we measured the time from midbody formation to the first abscission at two different ages. At E11.5, when divisions are predominantly proliferative, we found that abscission duration ranged widely, from 15 to 120 minutes, with a mean of 57 minutes (**Figure 3-3D**). At E13.5,

when neurogenic divisions have increased, the range of durations was 15 to 105 minutes, and the mean 47 minutes (**Figure 3-3E**). A cumulative frequency plot shows a trend to faster abscission at E13.5 (**Figure 3-3F, solid lines**). These data suggest that abscission duration may decrease as development proceeds. However, we were not able to test this at a later age when divisions are primarily neurogenic, since the thicker cortical slab explants from older brains (>400um thick at E15.5) do not remain healthy in these cultures.

Based on our previous findings in fixed brains, that *Kif20b* mutant NSCs have abnormal midbody structure and increased apoptosis (Janisch et al., 2013; Little and Dwyer, 2019), we hypothesized that some *Kif20b* mutant NSCs have delayed or failed abscissions. To our surprise, in live imaging, every mutant NSC observed was able to complete abscission. Moreover, the average time from midbody formation to the first abscission was not delayed, but accelerated compared to controls, by 18 minutes at E11.5, and 9 minutes at E13.5 (**Figure 3-3D, E**). Comparing the cumulative frequency plots of *Kif20b* mutant abscissions at the two ages shows they almost overlie (**Figure 3-3F, dashed lines**), suggesting a loss of developmental regulation. Thus, *Kif20b* regulates the duration of abscission, particularly at E11.5 when symmetric proliferative divisions predominate.

Reports vary on whether abscission occurs on one midbody flank or both flanks. Studies in dissociated cells such as HeLa and MDCK showed that ESCRT-III recruitment occurs on both flanks followed by sequential, bilateral abscission (Elia et al., 2011; Guizetti et al., 2011). By contrast, unilateral abscission and midbody inheritance by one daughter cell was reported in the worm embryo (Singh and Pohl, 2014b), fly germline (Salzmann et al., 2014), and fly imaginal disc epithelium (Daniel et al., 2018). Furthermore, abscission duration and frequency of midbody release varied in different mammalian neural cell lines (Ettinger et al., 2011). These conflicting reports suggest that bilateral abscission may depend on cell type or developmental context. Therefore, we wanted to use our system of live imaging with SiR-tubulin to determine the frequency of cortical NSCs abscission on one or both midbody flanks, the relative timing, and if this varies with developmental stage or when *Kif20b* is absent. Interestingly, MBRs have been found in cerebrospinal fluid of early (E10.5) mouse embryos (Dubreuil et al., 2007), and it was suggested that bilateral abscission is important for symmetric fates in early

proliferative NSC divisions. Surprisingly, we detected bilateral abscission just as often in E13.5 divisions as E11.5 divisions, in at least 60% of the cases (**Figure 3-4A, B**). The two abscissions usually were captured in sequential images, but occasionally both took place within one time-lapse interval. The median time between the 1st and 2nd event was 30 minutes at E11.5 and 15 minutes at E13.5, with a maximum of 90 minutes (**Figure 3-4C, D**). *Kif20b* loss does not appear to alter the frequency of bilateral abscission (**Figure 3-4 A, B**), but it does significantly reduce the time between first and second abscissions in E11.5 NSCs (**Figure 3-4C**). In total, the mean time to complete bilateral abscissions was 23 minutes less in the *Kif20b* mutants at E11.5, and 13 minutes less at E13.5 (**Figure 3-4E, F, G**). Together these data suggest that bilateral abscission is common in NSCs of the early cortex, and that *Kif20b* does not regulate its frequency, but regulates the timing of its completion. These findings in the early mammalian neuroepithelium appear different from the unilateral abscission seen in fly larval epithelium (Daniel et al., 2018), but similar to observations of sequential bilateral abscission in HeLa and dissociated MDCK cells (Elia et al., 2011; Guizetti et al., 2011).

Midbody remnants are abundant in early cortex and associated with proliferative NSC divisions

Post-abscission midbody remnants (MBRs) have been shown to adhere to plasma membranes of daughter or neighbor cells, and may influence cell polarity or proliferation (Crowell et al., 2014; Lujan et al., 2016; Peterman et al., 2019). We wanted to ask whether MBRs of cortical NSCs remain on the apical membrane after abscission, and whether this changes across development. We could not follow post-abscission MBRs in live time-lapse imaging, due to the strong microtubule labeling throughout the tissue, so we used the same cortical slab explant preparation as described in Figure 1A, but fixed the cortical slabs for immunostaining. MBRs can be identified in fixed cortical slabs or dissociated NSCs by immunostaining for protein markers of the midbody central bulge and flanks. Pre-abscission midbodies have the central bulge (marked by Citron Kinase or Cep55) and two flanks (marked by Aurora Kinase B or Survivin). Post-abscission MBRs retain the central bulge, but have lost the flanks due to scission (**Figure 3-S1**). On the apical membranes of NSCs in cortical slabs, both pre-abscission midbodies (brackets) and post-abscission MBRs (arrowheads) are observed (**Figure 3-5A**). We quantified MBRs on the apical surface at three ages, when divisions progress from

primarily proliferative (E11.5) to mixed (E13.5) to primarily neurogenic (E15.5). Strikingly, ~4-fold more MBRs are observed on E11.5 and E13.5 cortices than E15.5 (**Figure 3-5B**). *Kif20b* loss does not alter the frequency of observed MBRs or the developmental difference. These data suggest that E15.5 brains alter their regulation of either MBR release or degradation, but that *Kif20b* is not required for this change.

To more precisely quantify MBR association with individual NSC divisions, we modified the established NSC “pair cell” assay (Qian et al., 1998). NSCs were plated as single cells at clonal density, and fixed the next day to assess whether MBRs are present on newly divided daughter pairs (**Figure 3-5C, D**). First, we found that with control NSCs, ~30% of E11.5 division pairs have a MBR, while only 5% of E15.5 division pairs do, an ~6-fold difference (**Figure 3-5E**). *Kif20b*^{-/-} divisions pairs showed a similar developmental difference. Then, to ask whether MBR were associated with particular daughter fate outcomes, we scored MBR presence in the different types of divisions of E11.5 NSCs. By co-labeling with NSC marker Nestin and neuron marker tubulin-beta-III (*Tubb3*), the division pairs were classified as proliferative symmetric (2 NSC daughters), neurogenic symmetric (2 neuron daughters), or asymmetric (**Figure 3-5F**). Interestingly, E11.5 division pairs that have an associated MBR are more likely to be proliferative symmetric (**Figure 3-5G, control**). In the *Kif20b* mutant, this association is no longer statistically significant; however, this may be precluded by a significant reduction in the percentage of divisions that are proliferative symmetric, compared to control NSCs (**Figure 3-5G, *Kif20*^{-/-} bars**). The reason for this is unknown, but does not seem to be due to a loss of MBRs. Together with the *in vivo* quantifications of MBRs, these data show that MBRs are more prevalent in the early cortex, and are more associated with early proliferative NSC divisions than later neurogenic divisions. Furthermore, *Kif20b* loss does not disrupt MBR production or prevalence in the early cortex.

Discussion

The polarized form of cytokinesis in embryonic cortical NSCs is poorly understood, but may influence the segregation of organelles and apical fate determinants to daughter cells as they make fate choices. Recent findings that mutations in *Kif20b* and other midbody genes cause microcephaly in humans and mice suggest that brain development is especially sensitive to defects in cytokinesis (Bondeson et al., 2017; Di

Cunto et al., 2000; Frosk et al., 2017; Janisch et al., 2013; Li et al., 2016; Moawia et al., 2017). To elucidate these issues, we developed methods to quantitatively analyze furrowing and abscission in NSCs of the developing cerebral cortex. Here we addressed 1) whether cytokinesis parameters differ as development proceeds from more proliferative to more neurogenic divisions, and 2) how the loss of kinesin Kif20b affects cytokinesis kinetics in the developing cortex. While furrow ingression kinetics do not change significantly with developmental stage, abscission processes in cortical NSCs do appear to be developmentally regulated. Midbody remnants are more prevalent on the apical membranes of early stage cortices, and are more associated with proliferative NSC divisions than neurogenic divisions. Kif20b loss did not disrupt this developmental regulation of MBRs. However, the loss of Kif20b resulted in accelerated abscission. In addition, *Kif20b* mutant NSCs make fewer symmetric proliferative divisions. In the context of emerging data in both the neurogenesis and cytokinesis fields, these data suggest that subtle changes in the kinetics of cytokinesis or in the handling of midbody remnants could influence NSC daughter fates.

Through live time-lapse experiments, we found that Kif20b loss causes subtle dysregulation of abscission timing in both HeLa cells (Janisch et al., 2018), and NSCs (this paper). In our previous analyses of fixed cell populations, we more frequently observed early-stage midbodies than late-stage mature midbodies in both *Kif20b* mutant NSCs and Kif20b-depleted HeLa cells (Janisch et al., 2018; Janisch et al., 2013; Little and Dwyer, 2019). Together these findings are consistent with the hypothesis that the late steps of abscission proceed more quickly in the absence of Kif20b. Exactly how Kif20b regulates abscission timing is not clear, but prior work suggests two main hypotheses. First, previous work by us and others shows that Kif20b can cross-link microtubules *in vitro* (Abaza et al., 2003), and helps bundle axonal microtubules in neurons (McNeely et al., 2017). Thus when Kif20b is absent, the reduced cross-linking of midbody microtubules could allow easier removal or disassembly at the abscission sites. Second, we previously identified a role for Kif20b in keeping NSC midbodies aligned with the apical membrane (Janisch et al., 2013; Little and Dwyer, 2019). Hypothetically, if Kif20b links midbody microtubules to apical junction proteins, it could mediate tension on the midbody, which has been shown to affect abscission timing in HeLa cells (Lafaurie-Janvore et al., 2013). Additional hypotheses, currently without evidence, are that Kif20b might localize an unidentified cargo that regulates timing of

ESCRT-III filament formation, or Kif20b could be part of the abscission checkpoint (Nahse et al., 2017; Petsalaki and Zachos, 2019). Interestingly, the related Kinesin-6 family member Kif20a/MKLP2 was reported to act in the abscission checkpoint, although involving a tail sequence not shared by Kif20b (Fung et al., 2017). Much more work is needed to understand how Kif20b and other mechanisms control midbody maturation and abscission timing in different cell types and developing tissues.

It is possible that altered abscission timing in NSCs could affect daughter fates or proliferation. Our data showed a trend for faster abscission at E13.5 than E11.5. Consistent with this, in an ES cell line, faster abscission was correlated with more differentiation and reduced potency (Chaigne et al., 2019). Interestingly, delayed abscission timing in the fly germline is important for maintaining stem cell fate (Lenhart and DiNardo, 2015). In HeLa cells, failed abscission causes persistent intercellular bridges, midbody regression/ binucleation, or cell death (Gromley et al., 2003), but faster abscission has no morphological or fate consequences (Carlton et al., 2012). Furthermore, *Kif20b* mutant NSCs at E11 display the same accelerated abscission as control E13 NSCs, and also have a significant reduction in proliferative symmetric divisions, about half the control percentage. This is accompanied by a concomitant increase in neurogenic divisions. It is tempting to speculate that the faster abscission in the *Kif20b* mutant contributes to the early loss in proliferative symmetric divisions, depleting the stem cell pool, and resulting in microcephaly. However, we cannot rule out some other role of *Kif20b* in promoting symmetric proliferative divisions.

In addition to loss of symmetric proliferative divisions, the *Kif20b* mutant brains have increased apoptosis that is mediated by p53 (Little and Dwyer, 2019). When the p53 knockout was crossed into the *Kif20b* mutant, the NSC apoptosis was prevented, and the microcephaly was partly but not fully rescued. Hence, the remaining microcephaly may be due to the loss of early symmetric proliferative divisions demonstrated here. Future work will determine if this fate change is also p53-dependent.

We found that the number of midbody remnants at the apical membrane is much higher in early stage cortices, even when normalized for number of divisions. The mechanism for this developmental difference is not known. But the correlation of MBR presence with proliferative symmetric fates is intriguing, because MBRs have been proposed to contain

fate determinants and to have signaling roles, either from the cell surface or being engulfed as MBSomes by daughter or neighbor cells (Crowell et al., 2014; Dubreuil et al., 2007; Peterman et al., 2019). An attractive hypothesis is that an early symmetric proliferative division of a cortical NSC would occur through bilateral abscission on both flanks, and release of the MBR extracellularly, whereas a later asymmetric neurogenic division could result from unilateral abscission on one flank and midbody inheritance by the other daughter, promoting asymmetric fates. However, our data argue against this possibility by showing bilateral abscission is observed with similar frequency at two different developmental time points. Another possible explanation for the difference in MBR persistence at early and late ages is that the disposal of MBRs is regulated differently by E15.5 NSCs. It is not known if NSCs have similar mechanisms for MBR engulfment and degradation as other cell types (Chai et al., 2012; Crowell et al., 2014), but differential regulation of these processes in early versus late-stage stem cells could alter the ability of MBRs to influence the polarity or fates of progeny. While Kif20b does not appear to regulate the persistence of MBRs, this assay may be used in future cytokinesis mutant analyses to discover the roles and regulation of MBRs. The composition and signaling capacity of MBRs in stem cells and other dividing cell types require further investigation.

In conclusion, subtle changes in early NSC abscission regulation could affect daughter cell fate choices that would have long-term consequences for global neurogenesis. In cortical NSCs, fate-signaling events at the apical membrane happen concurrently with abscission, and could be affected by abscission duration or midbody/MBR positioning. These include new apical junction building, notch signaling across it, centrosome docking, and ciliogenesis. As these events occur, the release of the MBR could serve to either remove fate determinants from daughter cells, or to transmit them to neighbor cells. Future studies in multiple stem cell types and developing tissue systems are needed to further elucidate how developmental regulation of cytokinesis contributes to stemness, differentiation, and building tissues and organs.

Acknowledgments

This work was supported by NIH (R01 NS076640 and R21 NS106162 to NDD) and the Robert R. Wagner Fellowship to KCM. We thank Jessica Neville Little, Xiaowei Lu,

Bettina Winckler, Ann Sutherland, Sarah Siegrist, Jung-Bum Shin, Maria Lehtinen, Anthony Lamantia and their labs for advice and discussion. We thank Michael Fleming for Figure 1E images.

Author Contributions

KCM conceptualized and performed experiments, curated data for Figures 1-5 and Figure S1, wrote the first draft, and edited the manuscript. NDD conceptualized and supervised experiments and data analyses, and edited the manuscript.

Figure 3-1: Imaging cytokinesis in neural stem cells of developing cortex

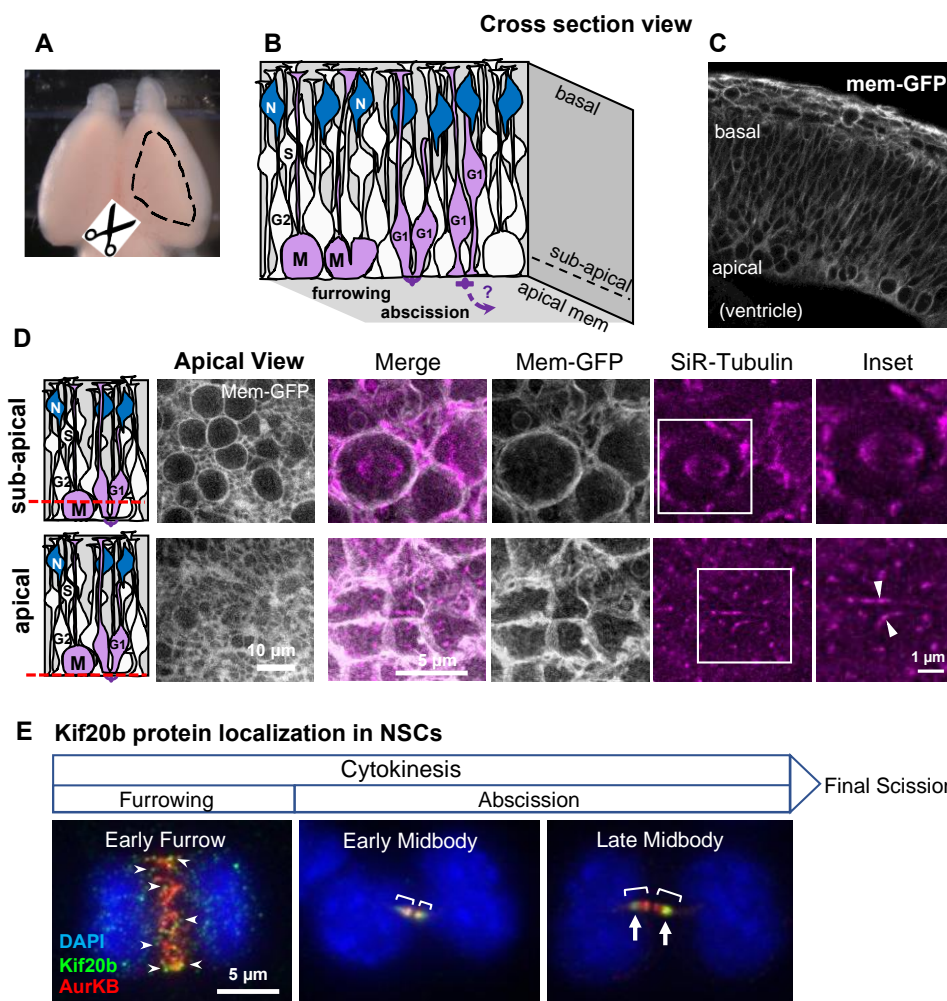


Figure 3-1: Imaging cytokinesis in neural stem cells of developing cortex

(A) Embryonic mouse brain with dashed outline showing area of cortex dissected for cortical slab preparation.

(B) Schematic of neural stem cells (NSCs) forming the pseudostratified epithelium of the developing cerebral cortex. NSCs undergo interkinetic nuclear migration. Their nuclei move basally for S-phase and apically for mitosis (M). Mitosis (M), furrowing, and abscission occur at the apical membrane. Abscission occurs during G1 phase. N, post-mitotic neurons.

(C) Cross section image of E12.5 mouse cortex expressing membrane-GFP shows the dense packing of NSCs in the epithelium. Round cells in mitosis can be seen close to the apical surface.

(D) Schematics and images of cortical slabs labeled with membrane-GFP and SiR-tubulin, viewing the apical membrane *en face*, at two different imaging planes (red dashed lines). *Top row* shows the sub-apical plane where the rounded mitotic cells with larger cell diameters and mitotic spindles are located. *Bottom row* shows the apical plane where apical endfeet and cell junctions are located, and where the midbody forms and abscission occurs. Arrowheads point to the central bulges of two different midbodies.

(E) Endogenous Kif20b immunostaining in dissociated fixed embryonic cortical mouse NSCs shows changes in Kif20b localization (green) at progressive stages of cytokinesis. A cell in the early furrowing stage shows many Kif20b puncta (arrowheads) on the central spindle, which is labeled by AuroraB kinase (red). A cell at early midbody stage of abscission shows Kif20b localized on the entire AuroraB-positive midbody flanks (brackets), but at late midbody stage Kif20b becomes enriched on the outer flanks (arrows), near the constriction sites. Furrowing starts during anaphase, and abscission progresses during telophase and completes with final scission in G1. Kif20b staining is undetectable in *Kif20b* mutant NSCs (Janisch et al., 2013).

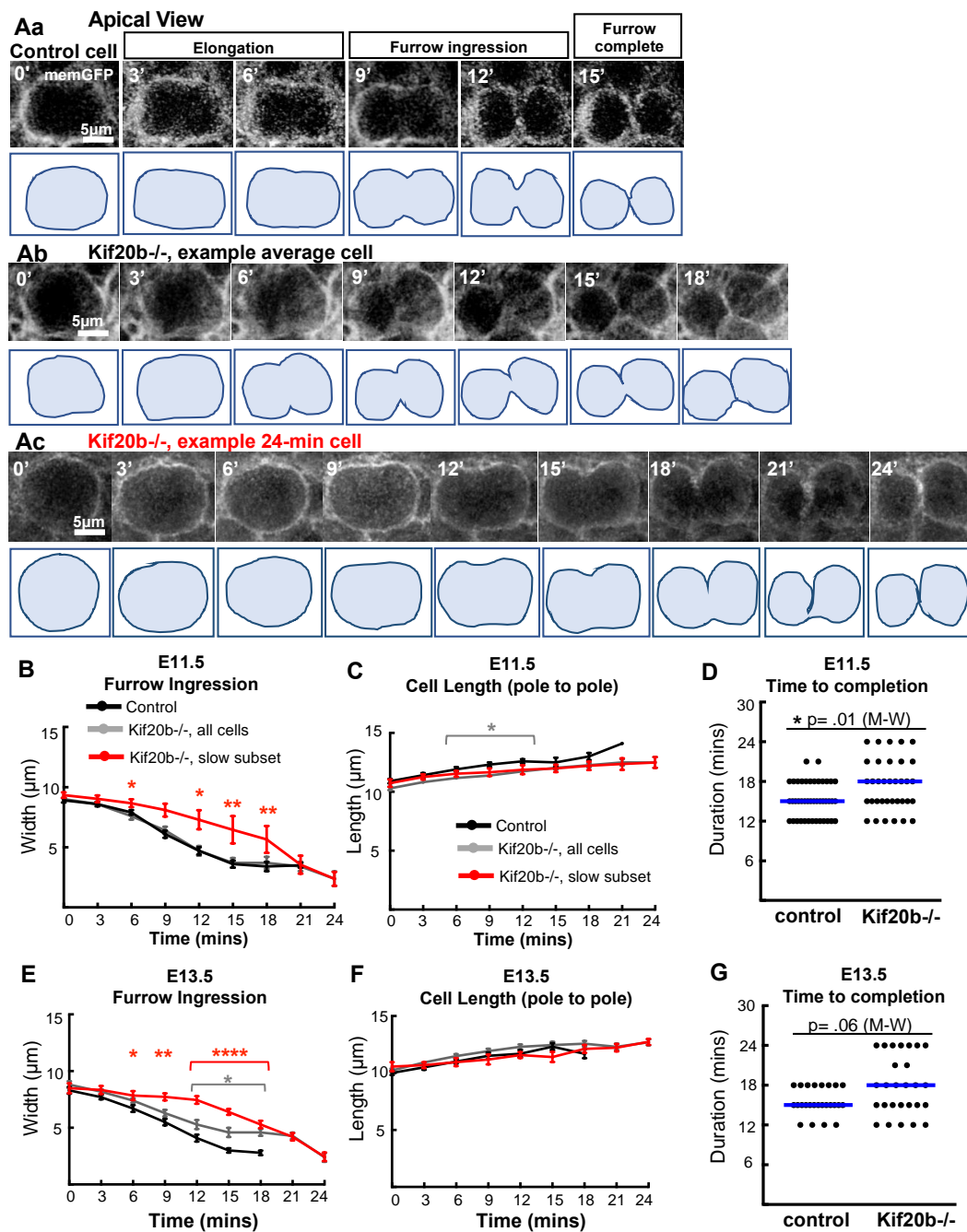
Figure 3-2: In *Kif20b* mutant brains, a subset of NSCs furrow more slowly

Figure 3-2: In *Kif20b* mutant brains, a subset of NSCs furrow more slowly

(Aa-Ac) Representative images and traced silhouettes of cytokinetic furrow ingression in one E13.5 control (Aa), one normally furrowing *Kif20b* mutant (-/-) NSC (Ab) and one abnormally slow furrowing mutant NSC (Ac). Furrowing was considered complete when no additional narrowing of furrow width occurred, and the membrane between sister cells appeared continuous.

(B, C, E, F) Furrow width and pole to pole length were plotted over time in E11.5 (B, C,) and E13.5 (E, F) control (black lines) and *Kif20b*^{-/-} (gray lines) cortical slab explants. Most *Kif20b*^{-/-} cells furrow at a similar rate to controls, but a subset (red lines) furrow more slowly and take 24 minutes to complete.

(D, G) Time to furrow completion was increased in E11.5 and E13.5 *Kif20b* mutant cortices, with a subset of NSCs taking 24 minutes to complete. Blue lines = medians.

n's for B-G: E11.5: n=43 control cells from 2 brains (1 +/- and 1 +/+); 35 total *Kif20b*^{-/-} cells from 2 brains, 5 *Kif20b*^{-/-} cells in slow subset (red line). E13.5: n=25 control cells (from 2 +/- and 1 +/+ brains); 27 total *Kif20b*^{-/-} cells from 3 brains, 7 *Kif20b*^{-/-} cells in slow subset (red line). For B, C, E, F: *p<.05, **p<.01, ****p<.0001 (Student's t-test). For D, G: p-values from Mann-Whitney (M-W) test.

Figure 3-3: Abscission is accelerated in *Kif20b* mutant cortex.

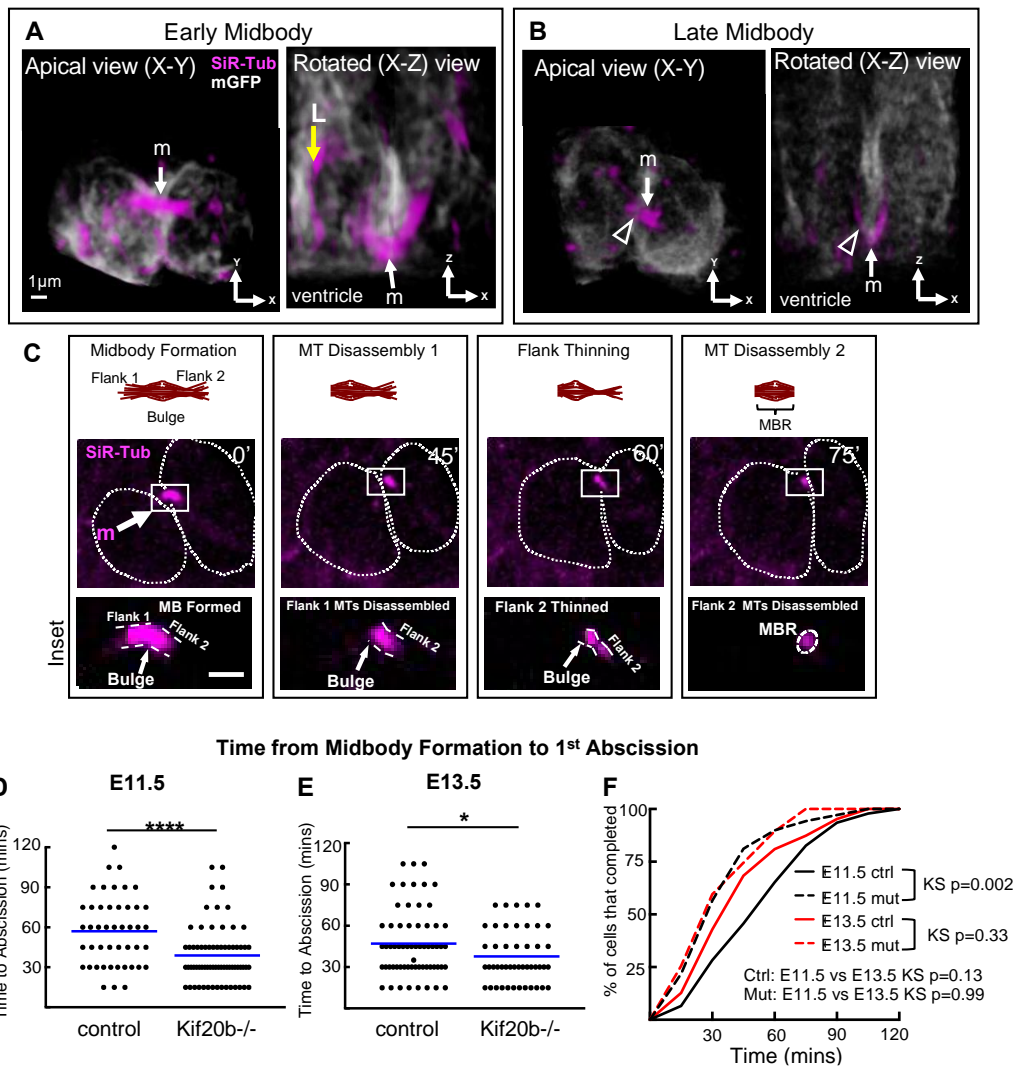


Figure 3-3: Abscission is accelerated in *Kif20b* mutant cortex.

(A, B) 3-D renderings of NSCs at early (A) or late (B) midbody stages labeled by membrane-GFP and SiR-tubulin, viewed from both the apical view (imaging plane) and rotated lateral view.

Midbodies (m, arrow) form at the apical membrane (ventricular surface). Late midbody has thinning on one flank (open arrowhead). L, longitudinal microtubule bundles.

(C) Schematic and images of time-lapse imaging of an NSC midbody undergoing abscission with central bulge and flanks indicated in insets. Distinct steps seen here are: midbody formation (m), microtubule disassembly on flank 1 (1st abscission), flank 2 thinning, and microtubule disassembly on flank 2 (2nd abscission). Dotted circular outlines show shape of sister cell plasma membranes at a subapical plane where cells are the widest.

(D, E) Time from midbody formation to 1st abscission is reduced in *Kif20b* ^{-/-} NSCs at both ages (E11.5 and E13.5). Blue lines show means.

(F) Cumulative frequency plots show E11.5 *Kif20b* ^{-/-} NSCs abscission timing curve is shifted to the left and has an altered shape.

For E11.5, n= 46 ^{+/+} cells (from 4 brains); 69 *Kif20b* ^{-/-} cells (4 brains). For E13.5, n= 63 ^{+/+} cells (5 brains); 47 ^{-/-} cells (3 brains). For D, E: * p<0.05, **** p<0.0001 (Student's T-test). Kolmogorov-Smirnov (KS) for F.

Figure 3-4: Sequential abscissions on both flanks are observed in most NSC divisions, and occur faster in *Kif20b*^{-/-} brains.

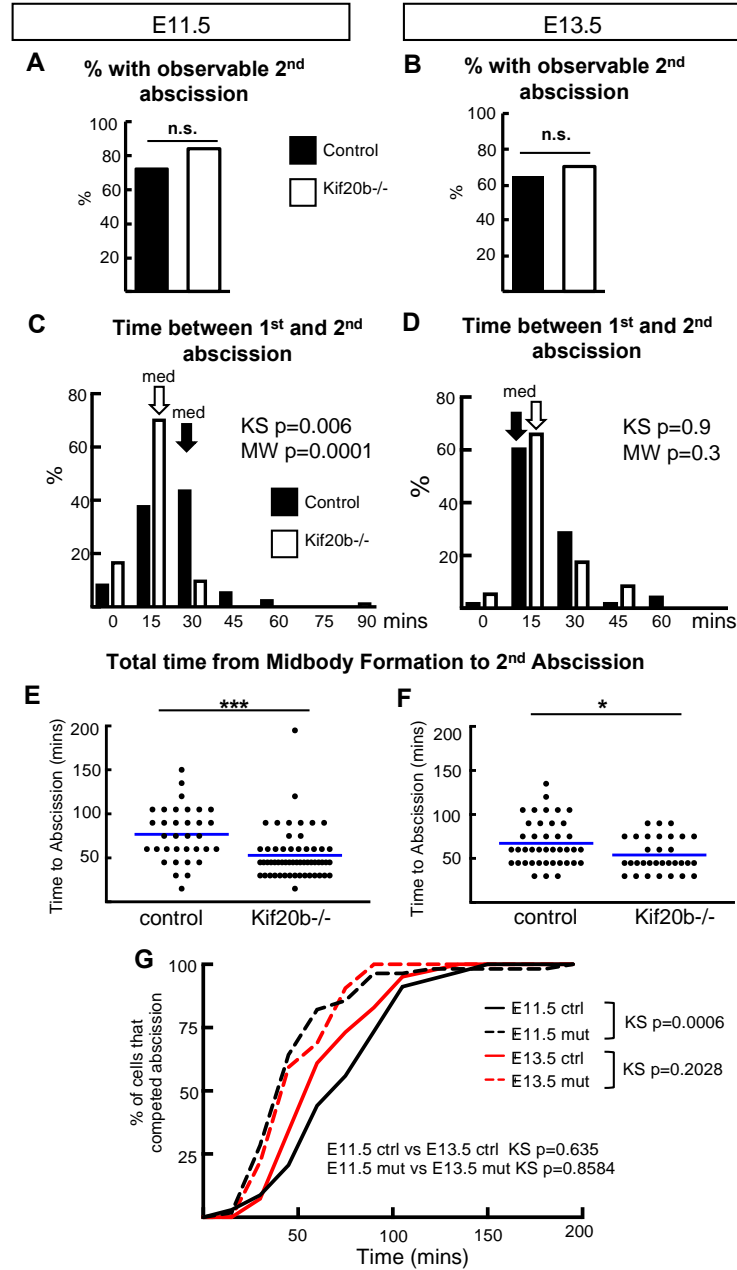


Figure 3-4: Sequential abscissions on both flanks are observed in most NSC divisions, and occur faster in *Kif20b* ^{-/-} brains.

(A, B) Using the same methods as in Figure 3, scoring abscission by the disassembly of SiR-tubulin on midbody flanks, the 2nd abscission on the other flank was observable in more than 60% of NSCs in E11.5 and E13.5 cortices, regardless of genotype.

(C, D) At E11.5, the 2nd abscission was usually detected within 30 minutes of the 1st abscission in control NSCs, but within 15 minutes in *Kif20b* ^{-/-} NSCs. At E13.5, the 2nd abscission was within 15 minutes in both control and mutant cells.

(E, F) The total time from midbody formation to completion of bilateral abscissions are reduced in *Kif20b* mutant NSCs at both ages. Blue lines show means.

(G) Cumulative frequency curves of total time to 2nd abscissions of E11.5 and E13.5 *Kif20b* ^{-/-} NSCs (dashed lines) are shifted to the left of control curves (solid lines).

For E11.5, n= 34 ^{+/+} (4 brains); 56 *Kif20b* ^{-/-} cells (4 brains). For E13.5, n= 41 ^{+/+} (5 brains); 32 ^{-/-} cells (3 brains).

For A, B: n.s., not significant (Fisher's Exact test). Kolmogorov-Smirnov (KS) and Mann-Whitney (MW) for C, D. KS for G. For E, F: *p<0.05, ***p<0.001 (Student's T-test).

Figure 3-5: Midbody remnants (MBR) are detected at the apical membrane, and correlated with early proliferative symmetric divisions.

(A) Schematic and three image-z-planes (Z1-Z3) of a field of apical membrane of a fixed E11.5 cortical slab show many NSC junctions (actin, white), a late furrow in planes Z1-2 (asterisks), pre-abscission midbodies (brackets, Z3''), and post-abscission midbody remnants (MBRs) in planes Z2-3 (arrowheads, Z3'''). AurKB labels pre-abscission midbody flanks. CitK labels both pre-abscission midbody central bulge and post-abscission MBRs.

(B) Many more MBRs are seen on E11.5 and E13.5 apical membranes than E15.5, normalized to either cell number or midbody number.

For E11.5, n= 4 control (3 +/- and 1 +/+); 4 *Kif20b*^{-/-} brains. For E13.5, n= 5 control (3 +/- and 2 +/+); 5 ^{-/-} brains. For E15.5, n= 3 control (1 +/- and 2 +/+); 4 ^{-/-} brains.

(C) Schematic of pair-cell assay.

(D) Pair of daughters of an E11.5 NSC division *in vitro*, with an associated MBR labeled by CitK (arrowhead).

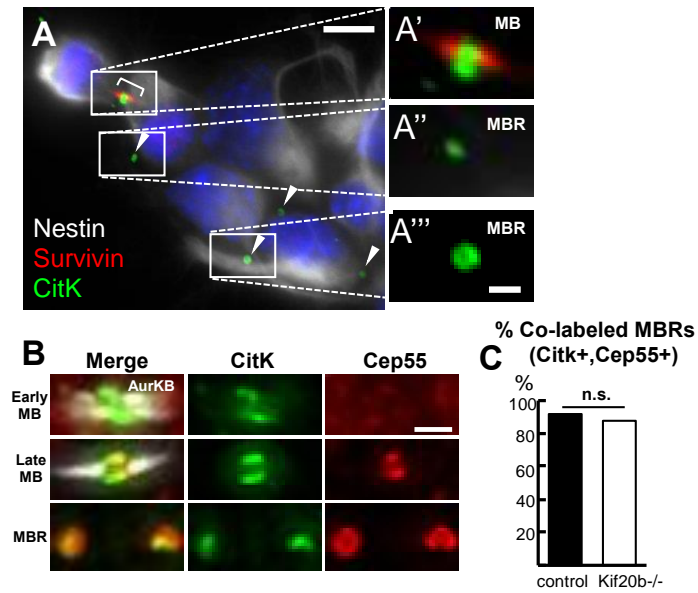
(E) E11.5 NSC division pairs are more likely to have a MBR present than E15.5 division pairs, in both control and *Kif20b*^{-/-} NSCs.

(F) Images of three division pairs of different fate types, each with a MBR detected (CitK+, arrowheads). P, progenitor (Nestin+, *Tubb3*⁻); N, neuron (Nestin+, *Tubb3*⁺). Note that newborn neurons still have Nestin protein inherited from the mother NSC during in the first day after division (Bott et al., 2019).

(G) The proportions of division types were compared in pairs with or without a MBR present. Control NSC division pairs with MBRs are more often proliferative symmetric (P-P). *Kif20b*^{-/-} NSCs have reduced proliferative symmetric divisions, with or without a MBR present.

For E11.5, n= 394 control (3 +/-, 2 +/+ brains); 272 *Kif20b*^{-/-} divisions (4 brains). For E15.5, n= 241 control (4 +/-, 1 +/+ brains); 280 *Kif20b*^{-/-} divisions (5 brains).

For B: * $p < 0.05$, ** $p < 0.01$, *** $p < 0.001$, **** $p < 0.0001$ (ANOVA). For E, G for individual category distributions: **** $p < 0.0001$, * $p < 0.05$ (Fisher's exact test). For G overall distributions: * $p < 0.05$ (Chi square test). n.s., not significant.



Supplemental Figure 3-1: NSC midbody remnants (MBRs) retain central bulge (marked by CitK or Cep55), but not midbody flanks (marked by Survivin or AurKB).

(A) Pre-abscission midbodies (bracket, MB) can be distinguished from post-abscission midbody remnants (arrowheads, MBRs) on NSCs. Dissociated E12.5 NSCs are identified by endogenous staining for Nestin. In pre-abscission midbodies, Citron kinase (CitK) appears as a ring within the central bulge (A'), while Survivin labels surrounding midbody flanks in a daughter pair still connected by a pre-abscission midbody (A'). CitK is also retained in post-abscission MBRs (A'', A''')(20, 54)).

(B) Images of dissociated E11.5 NSCs immunostained for endogenous CitK, Cep55, and AurKB show their distinct localizations at different midbody maturation stages. AurKB localizes to the flanks of early and late midbodies, but is mostly absent in post-abscission MBRs. CitK localizes as a ring in the central bulge of early and late midbodies as well as MBRs. Cep55 is absent in early midbodies, but accumulates in a ring at the midbody central bulge, but only at late stages, and remains in MBRs (16, 25, 55).

(C) MBRs of NSCs can be detected with either CitK or Cep55 immunostaining, as the vast majority of MBRs are labeled strongly by both markers.

Scalebars: 5 μ m in A; 1 μ m in A', A''', and B.

n= 61 control MBR (1 brain), 49 *Kif20b*^{-/-} MBR (1 brain) For C: n.s., not significant (Fisher's exact test).

**Chapter IV:
Mutation of Kinesin-6 *Kif20b* causes defects in
cortical neuron polarization and morphogenesis**

This chapter is published as McNeely, K.C*., Cupp, T.D*., Little, J.N., Janisch, K.M., Shrestha, A., and Dwyer, N.D. (2017). Mutation of Kinesin-6 *Kif20b* causes defects in cortical neuron polarization and morphogenesis. *Neural Dev* 12, 5.

*denotes co-first authorship

Abstract

How neurons change their cytoskeleton to adopt their complex polarized morphology is still not understood. Growing evidence suggests that proteins that help build microtubule structures during cell division are also involved in building and remodeling the complex cytoskeletons of neurons. Kif20b (previously called MPP1 or Mphosph1) is the most divergent member of the Kinesin-6 family of “mitotic” kinesins that also includes Kif23/MKLP1 and Kif20a/MKLP2. We previously isolated a loss-of-function mouse mutant of *Kif20b* and showed that it had a thalamocortical axon guidance defect and microcephaly. We demonstrate here, using the mouse mutant, that *Kif20b* is required for neuron morphogenesis in the embryonic neocortex. *In vivo* and *in vitro* cortical neurons were labeled and imaged to analyze various aspects of morphogenesis. Loss of *Kif20b* disrupts polarization as well as neurite outgrowth, branching and caliber. *In vivo*, mutant cortical neurons show defects in orientation, and have shorter thinner apical dendrites that branch closer to the cell body. *In vitro*, without external polarity cues, *Kif20b* mutant neurons show a strong polarization defect. This may be due in part to loss of the polarity protein Shootin1 from the axonal growth cone. Those mutant neurons that do succeed in polarizing have shorter axons with more branches, and longer minor neurites. These changes in shape are not due to alterations in cell fate or neuron layer type. Surprisingly, both axons and minor neurites of mutant neurons have increased widths and longer growth cone filopodia, which correlate with abnormal microtubule organization. Live analysis of axon extension shows that *Kif20b* mutant axons display more variable growth with increased retraction.

Conclusions: These results demonstrate that *Kif20b* is required cell-autonomously for proper morphogenesis of cortical pyramidal neurons. *Kif20b* regulates neuron polarization, and axon and dendrite branching, outgrowth, and caliber. Kif20b protein may act by bundling microtubules into tight arrays and by localizing effectors such as Shootin1. Thus it may help shape neurites, sustain consistent axon growth, and inhibit branching. This work advances our understanding of how neurons regulate their cytoskeleton to build their elaborate shapes. Finally, it suggests that neuronal connectivity defects may be present in some types of microcephaly.

Introduction

The function of the nervous system depends on neurons having a receiving end (dendrites) and a transmitting end (a single axon). A cortical pyramidal neuron grows a large apical dendrite at the apex of the cell body, several shorter basal dendrites, and a single axon from the base to connect to distant targets. Early polarization occurs soon after the neuron's birth, during the migratory phase through the intermediate zone. The newborn neuron first becomes multipolar with several short neurites, and then becomes bipolar with a leading process oriented outward in the direction of migration away from the ventricle. As it migrates, it extends an axon from the trailing end, but does not initiate dendrite growth until it finishes migrating.

Early polarization events can be modeled in dissociated cultures of embryonic hippocampal or cortical neurons (Dotti et al., 1988). During repolarization *in vitro*, the neurons first appear round and flat like a fibroblast (Stage 1, unpolarized). Within a day they begin to extend several undifferentiated neurites of about equal length (Stage 2, Multipolar). The growing neurites are full of microtubules, and they are tipped by actin-rich growth cones with lamellae and filopodia. In a stochastic manner, one of the neurites elongates rapidly to become the axon (Stage 3, Polarized). The remaining neurites become dendrites and remain shorter and thicker than the axon. This invaluable system has revealed many factors important for polarization (Lewis et al., 2013), but the cytoskeletal mechanisms underlying the development of complex neuronal morphology are still not well understood (Menon and Gupton, 2016; van Beuningen and Hoogenraad, 2016)

Various kinesin motor proteins are crucial for establishing or maintaining neuronal polarity and structure through their interactions with microtubules and cargoes (Hirokawa et al., 2010). The Kinesin-6 subfamily members are plus-end-directed microtubule motors known as "mitotic" kinesins for their roles in cytokinesis but some may have additional functions (Baron and Barr, 2015). Mammalian cells express three Kinesin-6 family members: Kif23/MKLP1, Kif20a/MKLP2, and Kif20b (formerly called mitotic phospho-protein 1, MPP1 or Mphosph1). RNAi of *Kif23* in cultured rat sympathetic neurons disrupted microtubule polarity of dendrites and resulted in longer axons and dendrites (Lin et al., 2012; Yu et al., 2000). Mutation of the *Drosophila Kif23* ortholog,

pavarotti (pav), caused excessive microtubule sliding, axon growth, and axon branching (del Castillo et al., 2015; Goldstein et al., 2005).

The third member of the mammalian Kinesin-6 subfamily, Kif20b, is less understood and has higher molecular weight and lower abundance than Kif23 or Kif20a. Interestingly, it has a two-fold longer stalk comprised of four coiled-coil domains linked by three hinges (Abaza et al., 2003; Kamimoto et al., 2001). In *in vitro* assays, Kif20b was sufficient to both slide and bundle microtubules in an ATP-dependent manner (Abaza et al., 2003). In a previous mouse ENU screen, we found a recessive, neonatal lethal mutant that displayed microcephaly and axon guidance defects in a subset of thalamocortical axons at embryonic day (E) 18.5 (Dwyer et al., 2011). Genetic mapping and a complementation test identified *Kif20b* as the mutant gene (Janisch et al., 2013). The point mutation in *Kif20b* causes an mRNA splicing error (Dwyer et al., 2011; Janisch et al., 2013), a consequent frameshift and premature termination codons, and reduces Kif20b protein to undetectable levels on immunoblots or cell staining (Janisch et al., 2013). Mutants show cytokinesis defects in neural stem cells of embryonic cortex. Cortical size and thickness is reduced in the *Kif20b* mutants due to decreased numbers of neurons and intermediate progenitors. Despite this, laminar organization and most axon tracts appear grossly normal at birth (Dwyer et al., 2011; Janisch et al., 2013).

Here, to explore *Kif20b* roles in neuronal development during corticogenesis, we took advantage of this genetic loss-of-function mutant. In *Kif20b* mutant brains, cortical pyramidal neurons have shorter, thinner, apical dendrites which branch closer to the cell body, extra axon branches, and are sometimes misoriented. To separate non-cell-autonomous effects, we pursued further analyses in dissociated neuron cultures. Surprisingly, when isolated from their normal brain environment, *Kif20b* mutant neurons show a strong polarization defect. This defect may be at least partly explained by a role for Kif20b in localizing the polarity protein Shootin1. The polarization defect is not due to cell fate changes and affected both deep and superficial layer types. Furthermore, the *Kif20b* mutant neurons that do successfully polarize have a variety of morphological changes including shorter, more branched axons and longer minor neurites. Mutant neurites are wider, and growth cone filopodia are longer with increased microtubule penetration. In live imaging, axons of *Kif20b* mutant neurons appear to pause less and retract more. These data indicate that Kif20b is important for polarization and

maintaining axon growth and preventing branching, and suggest that it acts both by localizing cargo and organizing microtubule bundles.

Materials and Methods

Cell Culture

To prepare for neuron culture and plating, 18 mm round coverslips were washed twice every 10 minutes with double-distilled, UV-irradiated water and treated in nitric acid overnight. Following three subsequent washes with double-distilled water, coverslips were placed in an oven at 160°C overnight to dry and sterilize. After allowing to cool the next day, each coverslip was treated with 200µL poly-L-lysine (PLL) solution (1µg/mL in borate buffer) and incubated overnight at 37°C. This was followed by double-distilled water washes (2 hour washes were done twice following three quick rinses) and application of neuron plating media (.5mL-1mL). Neuron plating media is filter-sterilized and consists of 500 mL Minimum Essential Medium (MEM) with glutamine, 5 mL Penicillin/Streptomycin, 15 mL 20% glucose, 5 mL Sodium Pyruvate, and 10% Fetal Bovine Serum. At E14.5, pregnant females were sacrificed and the embryos placed into cold HBSS mix (500 mL Hank's Balanced Salt Solution (HBSS) with 5 mL HEPES and 5 mL Penicillin/Streptomycin. Using fine forceps, pieces of cortex were collected and placed into a tube containing a 0.05% trypsin solution for 15 minutes in a 37 °C water bath. Following trypsin digestion, the resulting neuron pellets were rinsed 3 times every 5 minutes with HBSS mix and then treated with neuron plating medium during trituration. Appropriate volumes of the resulting solution of neuron plating medium and dissociated neurons were pipetted onto the PLL-coated coverslips to achieve a density of 50,000 cells/mL. Medium was switched from Neuron Plating Medium to Neurobasal and B27 (NB27) after three hours. 48 hours after being plated initially, the neurons were fixed in 2% Paraformaldehyde (PFA) for ten minutes and then in 2% PFA with 30% sucrose for 10 minutes. Finally, coverslips were rinsed in one time in Phosphate Buffer Saline (PBS) for 10 minutes three times and kept at 4 °C until ready for immunofluorescent staining.

Immunocytochemistry

Following dissociation, neuron plating, and fixation, coverslips were incubated for an hour at room temperature in blocking buffer (0.1% Triton-X, 2% Normal Goat Serum in mPBS) and then overnight at 4 °C or for 3hrs at room temperature in appropriate

primary antibody solution (antibody diluted in blocking solution). After primary incubation, coverslips were rinsed in PBS (3 times every 10 minutes) and then incubated at room temperature with appropriate secondary antibody solution (1:200 dilution) for 30 minutes in the dark. Following final washes in PBS, coverslips were mounted onto glass slides with Fluoromount.

Antibodies

Primary antibodies used were a rabbit or mouse monoclonal antibody against neuron-specific beta-III tubulin (Tuj1) at a dilution of 1:500 in blocking buffer (Covance clone 1-15-79 D71G9 and MMS-435P, Abcam ab52623), a rat polyclonal antibody against Ctip2 at a dilution of 1:500 (Abcam ab18465), mouse tubulin-alpha clone (DM1alpha) at a dilution of 1:500 (Thermo Scientific MS-581-PO), a mouse monoclonal antibody against Tau at a dilution of 1:200 (Millipore mab2370), a rabbit polyclonal antibody against DCX at a dilution of 1:1200 (Abcam, ab18723) and (green)-Phalloidin (Molecular Probes O7466) at a dilution of 1:50. Species-specific secondary antibodies were conjugated to Alexa fluorophores (Invitrogen) at a dilution of 1:200 in blocking buffer. Shootin1 antibody (1: 100, B627, raised against the first 456aa) was a gift from Tamar Sapir and Orly Reiner, Weizmann Institute (Sapir et al., 2013).

Multiple Kif20b antibodies have been verified for specificity by detecting signal in the midbodies of control dividing cells (HeLa and MEFs) and not in depleted or mutant cells. All of these antibodies were subsequently tried on mouse neurons. Published antibodies were kind gifts of Fabienne Pirollet (made to full length human KIF20B, (Abaza et al., 2003)) and Orly Reiner (made to 1002 to 1442 of Kif20b, (Sapir et al., 2013)). A commercially available monoclonal from Santa Cruz (raised against amino acids 1557-1675 of human KIF20B, catalog sc-515194) was tried. Both peptide anti-sera and purified antibodies to the N-terminal domain and C-terminal were also tried (Janisch et al., 2013). Multiple fixation conditions including TCA, PFA/MeOH, PFA only, permeabilized before fixing, and BRB80 then PFA were tried in combination with the previous mentioned antibodies. Due to large background to signal ratio no noticeable difference between control and *Kif20b* mutant neurons was detected with any of the antibodies or different fixation conditions.

Image acquisition and analysis

Fluorescent images were obtained on a Carl Zeiss widefield epi-fluorescence microscope via AxioVision camera and software. Low-magnification images for stage analyses were taken at 20x while High-magnification images for neuron measurements were taken at 40x or 100x. Image analysis was completed through ImageJ software. We used the NeuronJ software plugin to trace and measure axons and minor neurites. Axon branches were only counted if they were a minimum of 5 μ m. Neurite lengths were measured from the base of the process at the soma to the tip of the Tuj1 stain. Stage 3 neurons' minor neurites were measured in thickness at 0 μ m, 5 μ m, and 10 μ m from the edge of the soma. Stage 3 neurons' axons were measured in thickness at 0 μ m, 5 μ m, 10 μ m, and 25 μ m from the edge of the soma. For Figure 7D, images of tubulin in axons were captured using a Deltavision widefield microscope and then deconvolved. The intensity of tubulin staining was measured across the width of the axon at 5 μ m, 10 μ m, and 25 μ m using Zeiss Zen 2 lite imaging software profile tool.

Polarity Stage Analyses

Neurons were considered to be in Stage 1 if they extended broad lamellipodia with no clear, coalesced neurites. The neurites of Stage 2 neurons are all of similar length. A neuron was placed into the Stage 3 category when one neurite at least twice as long as the next longest neurite. Neuronal protrusions were considered to be neurites or neurite branches if they had significant microtubule invasion.

Measuring Growth Cones and Filopodia

The growth cone area was measured from the base of intense phalloidin-stained actin at the axon neck, around the growth cone tracing lamellipodial edges. The lamellipodial edge was considered to be where the filopodium becomes uniform in width (the filopodial base). We considered filopodia to be actin protrusions extending out of lamellipodia at growth cones. Filopodial extensions generally have brighter phalloidin staining than neighboring lamellipodial edges. Measurements were taken from the filopodia tip to its base, where the edges begin to splay apart and become lamelli.

Shootin1, DCX, and Tau Localization Measurements

Images of Shootin1 immunostaining were captured using the Zeiss AxioImagerZ1 Microscope with a 100x oil objective, and a constant 600 milliseconds exposure

time. Tau and DCX images were captured using the 40x objective on the Zeiss Observer Z1 microscope with AxioCam 506 mono camera. Exposure time was kept constant (DCX 300ms and Tau 200ms). Zeiss Zen 2 lite imaging software profile tool was used to measure intensity. Excel was used to compare individual cells line scans as well as create averages across genotypes for comparison.

RT-PCR

Mouse embryonic fibroblasts (from E14 mice) and mouse cortical neurons (4 DIV) were grown at a density of ~750000 cells/dish. RNA extraction of the harvested cells was done using the PureLink™ RNA Mini Kit from life technologies according to the manufacturer's handbook. RNA content in the samples was determined with a nano-drop spectrometer at 260 nm. 100 ng RNA were used in the reactions with the Invitrogen superscript III one-step RT-PCR kit. The PCR products were run on 3% ultrapure agarose with ethidium bromide at 95 V for 1 hour. Gels were visualized on a UV light box.

Primers (all 5' - 3'):

***Kif20b* exon 3-7:** FW: TGCTGAAAGACCCTCAAAGCATCCT,

RV: ACTGGACTGGTCACA ACTGTT CACG

***Kif20b* exon 17-19:** FW: GGTT CAGGCACTCAAGACATCAAGT,

RV: CGATACTTCTTGCAGCAGTCTCCAT

Beta-actin (*Actb* gene): FW: GATGACCCAGATCATGTTTGAGACC,

RV: TAATCTCCTTCTGCATCCTGTCAGC

Neuron electroporation

GFP-KIF20B constructs were electroporated into mouse cortical neurons. Shortly, neurons were dissociated from E14 mice cortices freed from meninges. After a cell count, the appropriate volume for one million neurons density was pipetted in eppendorf tubes and the neurons were spun down at 1.8 rpm for 10 min. The supernatant was carefully removed and the cells were re-suspended in 100 µl electroporation solution and 5 µg total plasmids were added (4 µg of *GFP-KIF20B* plasmid, 1 µg mCherry plasmid) and the suspension was mixed gently. The neurons were transferred carefully into an electroporation cuvette and electroporated with an Amaxa Electroporator following the instructions of the manufacturer for mouse cortical neurons (setting: O-005). Immediately after electroporation, 500 µl medium with serum was added to the cells and the suspension is carefully transferred into an eppendorf tube. 200 µl of cell suspension was

then plated on either glass bottom dishes or coverslips and plating medium is added to make up 1 ml. Medium was replaced after 3 hours with neuron growth medium with B27. Cells were grown at 37 °C, with 5% CO₂ until usage.

Dil Tracing

Lipophilic Dil (1,1'-Dioctadecyl-3,3',3'-Tetramethylindocarbocyanine Perchlorate) was used to stain neurons in E15.5 control and *Kif20b* mutant brains. Embryos were collected from pregnant heterozygote mothers at E15.5 and brains were dissected and fixed in 4% PFA for 2 days. A single small Dil crystal (Invitrogen, D-282) was then placed in the mid-lateral cortex of each hemisphere of each fixed brain using a needle pin. Brains were incubated at 37 °C in the dark for 3 days. Next, brains were cut in coronal sections at 100 µm on a Leica VT1000S vibratome and sections stained with DAPI (Invitrogen, D1306). Sections were mounted on slides with VectaShield (Vector Laboratories, H-1000) mounting medium. Z-stack images were taken of individual pyramidal neurons in the cortex at 40X on a Zeiss Axiomager.Z1 fluorescent microscope. Analysis of individual neurons was completed with ImageJ and NeuronJ by creating a maximum intensity projection of stacked images.

Golgi Staining

The Golgi method was used to stain neurons in E18.5 control and *Kif20b* mutant brains. Embryos were collected from pregnant heterozygote mothers at E18.5 and brains were dissected and rinsed with distilled water. The FD Rapid GolgiStain™ Kit (FD NeuroTechnologies, Inc., PK401) was used to stain whole brains, with the modification of placing brains in Solution A/B for 3 weeks instead of 2 at room temperature. Brains were next placed in Solution C for 1 week at 4 °C. Afterwards, brains were flash frozen on dry ice and stored at -80 °C until they were mounted in distilled water and cut on a Leica CM 3050S cryostat. Coronal sections were cut at 100 µm and mounted on slides with Solution C. The sections were allowed to dry for 3 days before completing the staining procedure with Solutions D and E as per instructions in the FD Rapid GolgiStain™ Kit. Slides were coverslipped with CytoSeal 60 (Thermo Scientific, 8310-4). Z-stack images were taken of individual pyramidal neurons in the cortex at 40X on a Zeiss Axiomager.Z1 microscope with Brightfield illumination. Neurons were also traced with Neurolucida Neuron Tracing Software (MBF Bioscience) for analysis. Analysis was

completed by combining results from NeuroLucida with results obtained from minimum intensity projection stacked images in ImageJ and NeuronJ.

Neuron Live Imaging

The neurons were allowed to grow at 5% CO₂ and 37°C for 45 to 54 hours in the incubator before imaging, and kept at 37°C and 5% CO₂ in the microscope controlled environmental chamber between time 0 and 6 hours. The microscope was a Zeiss AxioObserver with an inverted 20x objective, a motorized stage, and Definite Focus that allowed for multiple scenes within each chamber to be imaged. The camera was AxioCam Mrm and image analysis was done with Zeiss Zen software.

Results

Loss of *Kif20b* disrupts morphogenesis of pyramidal neurons in embryonic cortex

We examined individual neocortical neuron morphologies of control and *Kif20b* mutant cortices using Golgi-Cox staining at E18.5 (**Figure 4-1A, a-c**). Neonatal lethality precluded examination of fully developed neurons. Interestingly, *Kif20b* mutant neurons displayed several morphological differences compared to controls. The apical dendrites were ~ 30% shorter (**Figure 4-1B**) and had fewer terminal branches detectable. Furthermore, fewer neurites near the soma were detected, and some neurons appeared misoriented. One mutant neuron appeared to lie on its side with the apical dendrite curving up toward the pia (**Figure 4-1Ac, arrowhead**). The mutant neurons' apical dendrites appeared thinner; measurements showed they had the same width at their base, but then tapered more quickly and were thinner than controls (**Figure 4-1C**). To control for neuron size, and since *Drosophila pav* mutant neurons are abnormally large (Salzberg et al., 1994), we compared neuronal cell body sizes of control and *Kif20b* mutants. However, mutant neuron somas were the same size as controls (**Figure 4-1D**). Axons were not measured since Golgi staining did not reliably label them.

To test whether the neurite and orientation defects were detectable from early growth stages, we examined cortical neurons of E15.5 brains. Golgi-Cox staining does not label cortical neurons at this age, so retrograde dye-tracing was employed. In both control and mutant cortices, lateral dil crystal placements could retrogradely label pyramidal neurons

in the cortical plate, confirming that at least some mutant neurons had extended long axons (**Figure 4-1F, a-d**). However, the mutant cortical plate appeared disorganized, with fewer neurons labeled than in controls, and less than half of those oriented properly with apical dendrites perpendicular to the pial surface (12/31 mutant cells vs. 20/31 control cells), (**Figure 4-1Fa,c, 1G**). Mutant apical dendrites were only two thirds the normal height (**Figure 4-1H**). Strikingly, the mutant apical dendrites branched much closer to the cell body, at about one third the normal distance (**Figure 4-1Fb and d, arrowheads, and 1H**). Axons are not expected to branch much at this early age, but branching on proximal axons appeared increased among mutant neurons, with 5/15 mutant neurons having at least one detectable branch, versus only 3/22 control neurons detected with one branch each. Again, the average soma size was indistinguishable in mutants and controls (**Figure 4-1I**). Together, these analyses demonstrate that *Kif20b* is required for multiple aspects of normal neuron morphogenesis in the developing cortex, including polarity, branching, and dendrite width. The requirements for *Kif20b* could be cell-autonomous or non-autonomous. For example, the shortening of apical dendrites was proportional to the decrease in cortical thickness at both E15.5 and E18.5. By contrast, the shortened distance to the first branch point of the apical dendrites remained significant even after normalization to cortical thickness. Therefore, to sort out cell autonomous requirements for *Kif20b* in neuron growth from non-autonomous effects due to abnormal brain size and shape, we pursued further analyses on dissociated cortical neurons *in vitro*. This also enabled us to analyze more features of neuron shape.

***Kif20b* is required for normal polarization in dissociated cortical neurons**

To test for cell-autonomous roles of *Kif20b* in neuron morphogenesis, we first wanted to test expression of *Kif20b* in postmitotic neurons. Previously, we showed by *in situ* hybridization that *Kif20b* mRNA is expressed most strongly in the germinal zones of the embryonic brain and very weakly in neuronal layers. Also, Kif20b protein was readily detected in midbodies of dividing neural progenitors in control brains but undetectable in the *Kif20b* mutant progenitors (Janisch et al., 2013). Here, we first confirmed that *Kif20b* mRNA is expressed in postmitotic neurons by RT-PCR on cDNA from cortical neuron cultures (**Figure 4-2A**). Beta-actin was used as a control for the amount of template cDNA. *Kif20b* amplicons could barely be detected after 25 cycles of PCR from neuronal cDNA, but were clearly detected from mouse embryonic fibroblasts (MEFs). After 30

cycles, *Kif20b* bands were clear in neuron samples, and stronger in MEFs. This indicates that *Kif20b* mRNA is present but not abundant in neurons. As seen previously, the bands were more weakly amplified from mutant samples, and higher molecular weight for exons 17-19 primers, due to the mutation causing aberrant mRNA splicing at the exon 18-19 junction (Janisch et al., 2013). By contrast, the Kif20b protein band could not be detected in immunoblots of the cultured neuron lysates. This is not surprising given that even in control whole brain lysates, the Kif20b protein band is very thin, denoting low abundance (Janisch et al., 2013). Next we tried immunocytochemistry to detect the localization of endogenous Kif20b protein in dissociated neurons. However, the diffuse signal detected throughout control neurons was also seen in mutant neurons, indicating that this is background (**Figure 4-2B**). No specific signal was detected in control neurons over mutant neurons with any of several fixation conditions and independently-made polyclonal and monoclonal antibodies that were all verified for Kif20b reactivity ((Abaza et al., 2003; Janisch et al., 2013; Sapir et al., 2013); see Methods). To test where endogenous Kif20b protein would localize in neurons if we could detect it, we exogenously expressed GFP-tagged full-length human KIF20B, that localizes properly in dividing cells (Abaza et al., 2003). Though GFP-KIF20B overexpression caused death of many neurons, the small number of healthy neurons had numerous GFP puncta in the cell body, axons and minor neurites (**Figure 4-2C**). Some of these GFP puncta were motile and moved anterogradely (**Figure 4-2C' and 2C''**). A previous study showed that a tagged KIF20B motor head domain acted as a translocating motor that in mature cultured hippocampal neurons tended to accumulate in axons (Lipka et al., 2016). Together these data suggest that embryonic cortical neurons express Kif20b at low abundance, that the motor distributes through immature neurites by translocating on microtubules, and can accumulate in axons as the neuron matures.

Next we tested whether *Kif20b* is required for normal polarization of isolated cortical neurons *in vitro*. When embryonic cortical pyramidal neurons are dissociated and then cultured, they re-establish polarity by progressing through defined stages (**Figure 4-3A**). We observed that after two days *in vitro* (DIV), in control cultures 50% of the neurons were polarized (stage 3, with one neurite at least twice as long as the next longest neurite); but in *Kif20b* mutant cultures, only 23% were polarized (**Figure 4-3B**). Furthermore, 29% of control neurons were multipolar (stage 2), compared to 46% of

mutant neurons. These data suggest that loss of *Kif20b* disrupts the progression from multipolar to polarized. To test whether polarization was simply delayed, we examined cultures at 4 DIV. While both controls and *Kif20b* mutant cultures had more polarized neurons at 4 DIV, the mutants still had a significantly smaller proportion polarized than controls (**Figure 4-3C**). Finally, we confirmed that the *Kif20b* mutant neurons had a defect in axon specification and not simply axon growth by staining for the axon-enriched microtubule associated protein, tau1. Indeed, only about half as many mutant neurons had specified an axon as indicated by tau1-enrichment as controls did, confirming a polarization defect (**Figure 4-3D, E**). No cells with extra axons were observed. This robust polarization defect could be an exacerbated version of the disorganization and mis-orientation phenotype seen *in vivo* at E15.5 (**Figure 4-1Fc, G**).

Shootin1 is less enriched in growth cones of *Kif20b* mutant axons

The reduced ability of *Kif20b* mutant neurons to form an axon *in vitro* could be due to defective localization of a relevant cargo or binding partner. We hypothesized that the *Kif20b* polarization defect could be at least partly explained by a change in Shootin1 localization, based on previously published data. Shootin1 was shown to localize to axonal growth cones coincident with polarization, and afterward during rapid axon growth. Depletion of Shootin1 disrupted neuron polarization and axon extension *in vitro* (Toriyama et al., 2006) (Shimada et al., 2008). In addition, Shootin1 was found to immunoprecipitate with *Kif20b* from embryonic mouse brain lysates and human cell lines (Maliga et al., 2013; Sapir et al., 2013). Further, *Kif20b* knockdown caused de-localization of mCherry-Shootin1 (Sapir et al., 2013). To test whether genetic loss of *Kif20b* alters endogenous Shootin1 distribution in cortical neurons' axons, we compared the axonal distribution of Shootin1 in *Kif20b* mutant and control axons by measuring the intensity of anti-Shootin1 immunostaining from the tip of the growth cone into the axon shaft. All axons that were analyzed had similar length to control that as a potentially confounding factor. As expected in control polarized neurons, Shootin1 immunostaining showed enrichment in the axonal growth cones compared to the axon shaft, with a peak of signal in the growth cone (**Figure 4-4A, A'**). Interestingly, in *Kif20b* mutant polarized neurons, the Shootin1 signal was much weaker in the axonal growth cone (**Figure 4-4B, B'**). Averaging axonal line scans over many cells confirmed that the *Kif20b* mutant axons had a significant reduction in Shootin1 accumulation in the growth cone and distal axon

compared to control axons (**Figure 4-4C**). Interestingly, there was even a slight difference in Shootin1 intensity between heterozygous (+/-) and wild-type (+/+) control axons farther from the growth cone, suggesting a dosage effect of *Kif20b* on the amount of Shootin1 in the axon tip. Furthermore, a small amount of Shootin1 enrichment in the growth cone above the axonal level was still seen in *Kif20b* mutant cells, suggesting that another mechanism can still enrich it at the growth cone. To determine if the mislocalization was specific to Shootin1, we examined two other axonal proteins, Tau and DCX (doublecortin). Tau immunostaining had similar intensity throughout the axon in both control and mutant axons (**Figure 4-4D,E,F**). DCX immunostaining showed a normal high-distal localization (Fu et al., 2013) with similar intensity in the axons of both control and mutant neurons (**Figure 4-4D',E',G**). Thus *Kif20b* mutant neurons can localize DCX and Tau properly to the developing axon, but not Shootin1. These data are consistent with previously published work suggesting that *Kif20b* influences distribution of exogenous tagged Shootin1 in the axon (Sapir et al., 2013) but also that a myosin-based mechanism localizes Shootin (Toriyama et al., 2006). Thus, the reduction of Shootin1 enrichment in *Kif20b* mutant axonal growth cones may at least partly explain the neuron polarization defect.

Polarization and structure differences are not due to a shift in cell or layer fates

It was possible that the polarization defect and reduction in Shootin1 localization could be due to cell fate changes in the *Kif20b* mutant cultures. Indeed, cytokinesis mechanisms have been shown to play roles in daughter cell fate determination (Ettinger et al., 2011; Kuo et al., 2011; Singh and Pohl, 2014b), and we had previously demonstrated cytokinesis defects in the *Kif20b*^{-/-} embryonic cortex (Janisch et al., 2013). To rule out fate change as a cause of polarity loss, we compared the percentages of neurons (Tuj1⁺) and of layer 5/6 neurons (Ctip2⁺) in control and mutant cultures (**Figure 4-5A**). Both the percentage of neurons and of Ctip2⁺ neurons were not different (**Figure 4-5B, C**), indicating that the mix of cell types or neuronal layer types is not altered in *Kif20b* mutant cultures. To further control for this, Ctip2⁺ and Ctip2⁻ neurons were directly compared for polarization in control and mutant cultures. Both showed the same robust polarization defect (**Figure 4-5D, E**). These data strongly argue that *Kif20b* influences neuronal polarization and morphological development through a mechanism independent of cell fate and required by both deep and upper layer types.

***Kif20b* mutant neurons that do polarize have structural changes in both axons and minor neurites**

We hypothesized that if *Kif20b* helps establish polarity, then the mutant neurons that did polarize might have “weak” polarity, i.e., axons that are more dendrite-like (shorter and wider with more branches) and minor neurites (nascent dendrites) that are more axon-like (longer and thinner with fewer branches). Some observations are consistent with this idea (**Figure 4-6A-G**). First, the minor neurites of *Kif20b* mutant polarized neurons averaged 29% longer than controls, and the average number of minor neurites per cell was not different (**Figure 4-6B, C**). Furthermore, mutant axons were 14% shorter, but surprisingly had nearly twice as many collateral branches as control axons (**Figure 4-6E, F, G**). Thus, loss of *Kif20b* appears to cause minor neurites to be longer (more like axons) and axons to be shorter and more branched (more like dendrites). A previous study had found that RNAi of *Kif20b* in cultured hippocampal neurons caused reduced axon length, but did not note changes in dendrites or axon branching (Sapir et al., 2013).

Next we tested whether the weakened polarity characteristics of *Kif20b* mutant neurons alter axon and minor neurite width. In a mature pyramidal neuron, the axon is long and thin with constant caliber, while dendrites are shorter, wider, and more tapered. We had observed *in vivo* that *Kif20b* mutant pyramidal neurons had thinner apical dendrites (**Figure 4-1C**). Also, RNAi of the different Kinesin-6 family member *Kif23* in cultured sympathetic neurons had also caused dendrite thinning (Lin et al., 2012). Therefore we measured the widths of axons and minor neurites at given distances from the cell body, using neuronal (beta-III) tubulin staining (**Figure 4-7A**). Surprisingly, in culture, both the axons and minor neurites of *Kif20b* mutant neurons were significantly wider than controls (**Figure 4-7A-C**). At 10 microns from the soma, mutant axons averaged 21% wider than controls and mutant minor neurites were 24% wider. The increased widths appear to correlate with looser microtubule packing (**Figure 4-7A, insets**). To confirm this, the tubulin intensity was measured by linescans across the widths of the axons at 5 μ m, 10 μ m, and 25 μ m from the cell body. Interestingly, while control axons had compact tubulin intensity distributions with a clear peak, mutant axons had wider tubulin distributions with lower, irregular peaks (**Figure 7D**). Furthermore, the average total tubulin intensity at 25 μ m from the soma is significantly decreased in the mutant axons, suggesting that not only do microtubule bundles have more spaces between them, but

also that there is less tubulin in the axons at a given distance (**Figure 4-7E**). These data show that Kif20b not only supports axon specification in the cue-free *in vitro* environment, but also helps set up the structures of nascent axons and dendrites, possibly by regulating microtubule packing. Indeed, previous *in vitro* work showed that adding KIF20B protein to microtubules was sufficient to cause them to become crosslinked and bundled in an ATP-dependent manner (Abaza et al., 2003).

To confirm that the changes in branching and neurite width were not due to a change in neuron types in the Kif20b mutant cultures, we again controlled for this. Indeed, the foregoing findings held true when we controlled for neuron layer type: *Kif20b* mutant Ctip2⁺ neurons had increased axon branching, minor neurite length, and neurite width, compared to Ctip2⁺ control neurons (**Supplemental Figure 4-1**). Worth noting, Ctip2⁺ neurons did not differ significantly from Ctip2⁻ neurons by our measurements, and were affected similarly by Kif20b loss. This suggests that at least at early days *in vitro*, deep and upper layer pyramidal neurons develop similarly and both require Kif20b.

***Kif20b* mutant neurons have longer filopodia with increased microtubule invasion**

To address the possible mechanisms for increased minor neurite length and axon branching in *Kif20b* mutant neurons, we examined the structures of growth cones on both axons and nascent dendrites of polarized (Stage 3) neurons. Axons, axon branches, and minor neurites can all be tipped by growth cones, and their size and morphology varies (**Figure 4-8A**). There was no significant difference between control and *Kif20b* mutant growth cone areas, though axonal growth cones were at least a third larger than minor neurite growth cones in both controls and mutants (**Figure 4-8B**). *Kif20b* mutant growth cones also did not differ in the number of filopodia per growth cone, and had about 35% more filopodia on axonal than minor neurite growth cones, proportional to the larger area, just like controls (**Figure 4-8C**). Surprisingly however, *Kif20b* mutant filopodia were about 30% longer than control filopodia on both axons and minor neurites, with axonal growth cones having longer filopodia than minor neurite growth cones in both cases (**Figure 4-8D**).

All filopodia contain bundled actin, but when microtubules penetrate filopodia this may lead to stabilization of the filopodium, inducing a branch or growth cone extension (Gallo,

2013; Pacheco and Gallo, 2016). We hypothesized that longer filopodia could be due to increased microtubule invasion. We tested this by comparing the percentage of filopodia with detectable tubulin in control and mutant polarized neurons. Consistent with our hypothesis, the filopodia on *Kif20b* mutant growth cones were more likely to contain tubulin than control filopodia, suggesting increased microtubule invasion of the growth cone periphery (**Figure 4-8E, F**). Together with the above analyses, these data suggest that loss of *Kif20b* only partly blocks polarization, and the cells that do polarize have structural changes in both axons and minor neurites - length, branching, width, and filopodia length – suggestive of dysregulated microtubule packing or microtubule-actin interactions.

***Kif20b* mutant axons retract more and pause less than control axons**

The preceding experiments showed that dissociated cortical neurons from *Kif20b* mutant brains are less likely to have polarized after a few days *in vitro*, and if polarized, have shorter and more branched axons with less compact tubulin. This suggests the mutant neurons are ineffective at stabilizing the axonal cytoskeleton to sustain consistent and rapid axon growth. To test this idea, we compared axon growth of live control and *Kif20b* mutant neurons in a 6 hour period after 2 DIV (**Figure 4-9**). As expected, the change in axon length after 6 hours varied widely, with some axons having grown and some having retracted, ranging from +48 μm to -15 μm change in length (**Figure 4-9B**). To break this down, we categorized each axon as “grew” (length change at least +3 μm), “retracted” (at least -3 μm), or “paused” (within $\pm 2.9 \mu\text{m}$). Interestingly, in 6 hours, more mutant neurons retracted and fewer paused compared to controls, while about the same number grew (**Figure 4-9C**, Fisher’s exact test, $p=0.03$). Of the axons with positive growth, the average length increase was not significantly different (**Figure 4-9D**). However, of the axons that shrank, the average length decrease was significantly greater in the *Kif20b* mutant neurons compared to controls (**Figure 4-9D**). Since the distribution of length changes was wide, and our categorization was arbitrary, we analyzed the data in one additional way to confirm that mutant axons behaved differently. Taking the absolute values of length changes and plotting the distribution shows a shift to greater length changes in the mutants (**Figure 4-9E**). Together, these analyses suggest that the mutant axons have less consistent growth due to greater variability of length change. Loss of

Kif20b makes axons more likely to retract, and if they do, to retract more. Kif20b 's functions may normally act as a brake on axon retraction.

Discussion

The dramatic reorganization of the neuronal cytoskeleton during polarization and axon growth is an area of intense research. Recent work points to microtubule associated proteins being important downstream effectors of signaling cues that mediate neuronal polarization, axon guidance and branching (van Beuningen and Hoogenraad, 2016). While many kinesins have been shown to be important for intracellular transport in mature neurons, less is known about which kinesins are important for these early processes. Recent work in *Drosophila* or by mammalian knockdown approaches has suggested that mitotic kinesins are re-used in postmitotic neurons to organize microtubule arrays (del Castillo et al., 2015; Lin et al., 2012).

We report here for the first time through a specific genetic mutation that a Kinesin-6 family member, Kif20b, is required for neuronal morphogenesis in the mammalian brain. By *in vivo* and *in vitro* analyses, we find that loss of *Kif20b* disrupts development of cortical neurons, affecting polarization as well as neurite outgrowth, branching and caliber (see **Figure 4-10**). The morphological changes are not due to cell fate changes, and are seen in different layer types. Our results suggest that Kif20b acts to stabilize or bundle microtubules in neurites to allow polarization, sustain axon growth, keep neurites thin, and minimize branching. Kif20b may also tether Shootin1 in the growth cone, which helps to maintain the axon in a growth state. Analysis of live neurons suggests that Kif20b may normally act to limit axon retraction. Thus, Kif20b helps to organize microtubule arrays in neurites to shape the neuron, and can also act by localizing effector molecule partners.

Our analyses highlight the importance of studying neuronal morphogenesis both *in vivo* and *in vitro*, because phenotypes vary and provide different clues to gene function. While the *Kif20b* mutant neurons had a robust polarization defect *in vitro*, clearly most neurons *in vivo* polarized and made an axon. A neuron polarizing *in vitro* has perhaps a more difficult task than one polarizing *in vivo* because there are no directional cues, and the substrate is stiff and two-dimensional. However, the orientation defect in the *Kif20b*

mutant brains may reflect polarization defects in a subset of cells. Axon branching defects were seen both *in vivo* and *in vitro*, as well as effects on neurite width. *In vitro* we were able to analyze microstructures such as filopodia number and length. Previously, we reported that in the *Kif20b* mutant mouse brains, a subset of thalamocortical axons showed an axon guidance defect (Dwyer et al., 2011). Though the exact cause of the misrouting is still unclear, our new data analyzing individual neurons suggest that axon guidance defects could be secondary to axon outgrowth timing or abnormal branching.

The Kinesin-6 gene family appears to have expanded by duplication during evolution (Baron and Barr, 2015; Dagenbach and Endow, 2004). *C. elegans* has one Kinesin-6 gene, *zen-4*, orthologous to *Kif23*/MKLP1. *Drosophila* has two Kinesin-6 genes, *pavarotti* and *subito*. It may be that three members of this family are needed to build a more complex nervous system or larger neurons. While gene redundancy is often observed in neural development to ensure robustness (Menon and Gupton, 2016), this appears not to be the case for the mammalian Kinesin-6 family, since loss of *Kif20b* causes deleterious phenotypes in both cytokinesis and neuron development that are not compensated for by *Kif23* or *Kif20a* ((Janisch et al., 2013); this work). *Kif20b* must have some molecular function that the other two cannot substitute for. The family members are highly homologous in the motor domain, but the stalks and tails are completely divergent, enabling interactions with distinct binding partners and cargoes. The significance of the extra-long stalk of *Kif20b* is not known, but it may increase flexibility, or allow the motor to bind microtubules or other proteins at a greater distance apart.

This work substantially deepens the evidence that Kinesin-6 family members function in neuronal development. Previous RNAi data supported roles in mammalian neurons for *Kif23*/MKLP1 in microtubule organization and neurite growth (Lin et al., 2012). Knockdown or mutation of the *Drosophila Kif23* ortholog *Pav* caused increased microtubule sliding and excess axon branching (del Castillo et al., 2015). *Kif20b* knockdown was shown to decrease axon length and Shootin1 distribution (Sapir et al., 2013). Here we provide genetic evidence for a requirement for *Kif20b* in multiple aspects of mammalian neuron morphogenesis. *Kif20b* loss has morphological consequences throughout the cell, consistent with the appearance of exogenous GFP-KIF20B throughout the neurites. As the cell matures, *Kif20b* may accumulate at the axon tip due to axonal preference of the motor head as shown in (Lipka et al., 2016). The appearance

of looser microtubules in neurites and more microtubules in growth cone filopodia suggests Kif20b functions in microtubule crosslinking or packing organization in neurites. Indeed, the wider neurites are reminiscent of the wider midbodies we previously observed in dividing neural progenitors (Janisch et al., 2013). Both these phenotypes could be explained by loss of microtubule bundling activity of Kif20b that was demonstrated in biochemical assays (Abaza et al., 2003). A key process driving neuron polarization is likely to be local stabilization and bundling of parallel microtubules (van Beuningen and Hoogenraad, 2016; Witte et al., 2008). As the growth cone advances, microtubule bundling at the neck may be a crucial requirement for converting the growth cone into axonal structure (Tanaka and Kirschner, 1991). Thus, defective microtubule bundling could explain the mutant cells' difficulty forming the axon, regulating neurite width, and preventing axon retraction.

Interestingly, filopodia length and axon branching are linked mechanistically by microtubule invasion. This work provides one of the few known manipulations to increase the length of growth cone filopodia or increase microtubule penetration into them (Gallo, 2013; Pacheco and Gallo, 2016). Axonal branches are initiated as filopodia (Bastmeyer and O'Leary, 1996) and are dependent on filopodia formation (Dwivedy et al., 2007). Formation of axon branches correlates with localized splaying and breaking of microtubules (Lewis et al., 2013; Pacheco and Gallo, 2016). Thus, the increased axon branching and longer filopodia in *Kif20b* mutants could both be related to a loss of microtubule crosslinking or tight bundling.

Kif20b is likely to have functions beyond microtubule organization. For example, as a translocating motor protein, it can transport proteins or link them to microtubules. We have provided evidence that at least one endogenous polarity protein, Shootin1, requires Kif20b for enriched localization at the axon growth cone. The role of Shootin1 is proposed to reinforce the identity of the axon and keep it growing (Shimada et al., 2008; Toriyama et al., 2006). Kif20b may transport Shootin1 from the cell body to the growth cone, or it may help retain it at the growth cone after transport by other mechanisms (Toriyama et al., 2006). The high abundance of Shootin1 relative to Kif20b, as well as the remaining weak Shootin1 signal in *Kif20b* mutant axons support the notion of another transport mechanism. Shootin1 has also been shown to bind the actin cytoskeleton and mediate traction of the growth cone (Shimada et al., 2008). Thus

through Shootin1, Kif20b might link microtubules and actin. Importantly, there may not be one Kif20b function that explains all the phenotypes. There may well be as yet unidentified binding partners that Kif20b transports or tethers at different locations or times in development.

Conclusions

These analyses considerably advance our knowledge of post-mitotic roles of Kif20b in neuron polarization, branch inhibition, and axon growth. Kif20b may affect these processes by its activities in organizing microtubules and localizing effector proteins. Loss of Kif20b appears to have different consequences for mammalian neuron morphology than loss of the other Kinesin-6 family member Kif23. Understanding how different motor proteins and other microtubule associated proteins enable neurons to reorganize their cytoskeletons during early polarization, axon growth, and arborization is fundamental to knowing how the brain is wired and changes during learning. In addition, there are important implications for human health. Since the *Kif20b* mouse mutant is a novel model for human microcephaly, it is important to know that there could be defects in connectivity in addition to the small brain size in some cases of microcephaly. Finally, *KIF20B* is elevated in several cancers (Baron and Barr, 2015; Kanehira et al., 2007; Liu et al., 2014), and while that could be due to its role in cell division, our data suggest it could also be due to effects on cell motility and morphology that could enhance metastasis.

Authors' contributions

KM collected and analyzed axon length, Shootin1 localization, live imaging of axons, helped with the DCX localization, Tau localization and Tubulin intensity measurements, prepared figures, and helped write the manuscript. TC collected and analyzed polarization, minor neurite and axon morphology, and filopodia data. JN collected and analyzed *in vivo* data, performed RT-PCR, helped with the DCX localization, Tau localization and Tubulin intensity measurements. KJ performed RT-PCR. KJ and AS immunostained Kif20b on neurons and electroporated *GFP-KIF20B* in neurons. ND conceived the project, designed and supervised experiments, analyzed data, and wrote the manuscript. All authors read and approved the final manuscript.

Acknowledgements

We thank Luke Arnell for assistance with polarization and width quantification, Caitlin Cook for assistance with neuron tracing. Many thanks to Bettina Winckler, Kevin Pfister, Christopher Bott, Xiaowei Lu, Jing Yu, and Jung-Bum Shin for advice and discussions. We are grateful to Fabienne Pirollet, Naoyuki Inagaki, Tamar Sapir and Orly Reiner for antibodies and plasmids.

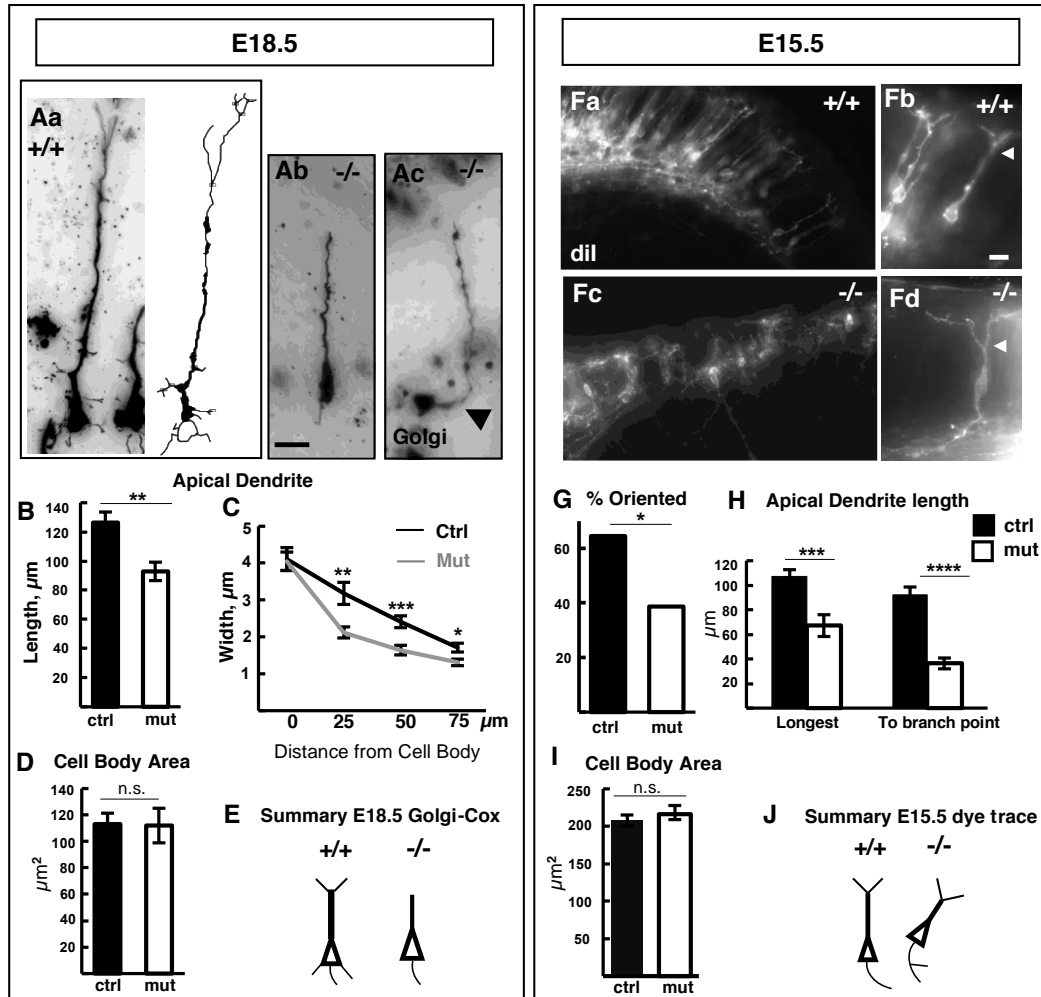


Figure 4-1. Cortical neurons show abnormal morphologies in *Kif20b*^{-/-} brains.

A. Example images of individual pyramidal neurons labeled by Golgi-Cox staining in *Kif20b* control (+/+), a) and mutant (-/-, b and c) E18.5 brains. An example projection of 3D-tracing is shown of a control neuron (a). Arrowhead in (c) points to proximal apical dendrite.

B. Apical dendrites of mutant pyramidal neurons were shorter.

C. Mutant neurons' apical dendrites tapered more quickly and remained thinner distally.

D. Average cell body area at E18.5 was the same in control and mutant brains.

E. Schematic summary of morphological differences of E18.5 mutant cortical neurons.

F. Examples of retrogradely labeled neurons in control (+/+, a and b) or *Kif20b* mutant (-/-, c and d) E15.5 cortical plate from lateral dil crystal placements. Arrowheads indicate first branch point of apical dendrite.

G. Fewer mutant neurons were properly oriented with apical dendrites within 10 degrees of perpendicular to the pia. n= 31 cells each from 4 control and 3 mutant brains, p=.04, Chi-squared test with n-1 correction.

H. *Kif20b* mutant neurons had shorter apical dendrites and shorter distance to first branch point. Distance to first branch point was still significant after normalization to cortical thickness.

I. Average cell body area at E15.5 was the same in control and mutant brains.

J. Schematic summary of findings from dil retrograde tracing in E15.5 cortices.

For E18.5, n= 26 control and 25 mutant neurons from 4 control (3 +/+, 1 +/-) and 3 mutant (-/-) brains. For E15.5, n= 30 control and 31 mutant neurons from 4 control (1 +/+, 3 +/-) and 3 mutant (-/-) brains.

Error bars are s.e.m. *, p \leq .05, ** p \leq .01, *** p< 0.001, **** p< 0.0001; student's t-test for all except panel G. Scale bars, 20 μm .

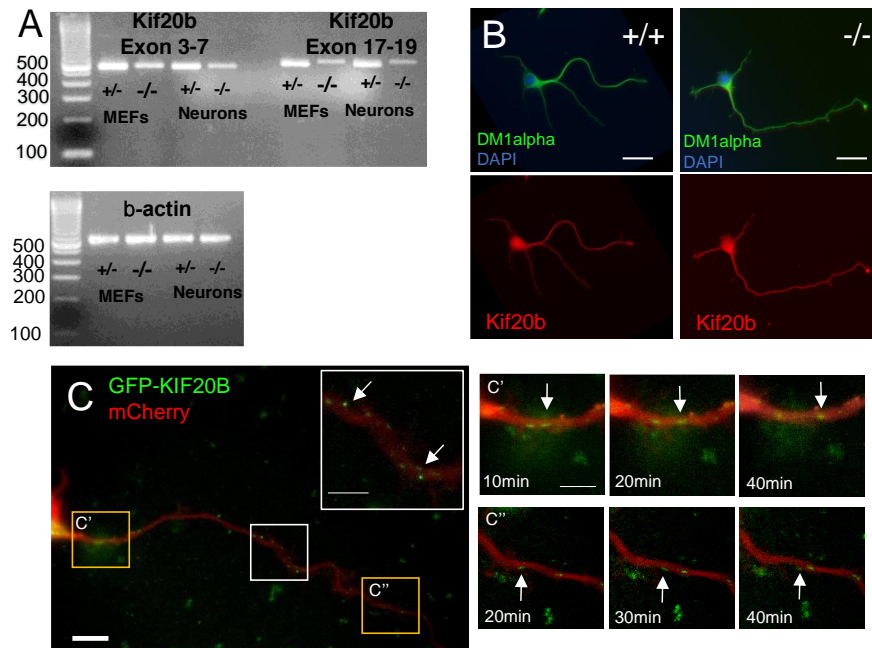


Figure 4-2. *Kif20b* expression and localization in cultured cortical neurons

A. RT-PCR detects *Kif20b* weakly in neuron culture lysates (E14.5 plus 4DIV) after 30 cycles. Bands are stronger in MEFs. Bands are weaker in mutant samples due to the splice mutation [14].

B. Immunocytochemistry for *Kif20b* does not detect signal in control neurons (+/+) above background seen in mutant (-/-) neurons. Images shown are of a polyclonal antibody to the full length protein [11], but are representative of staining appearance of five independent antibodies (see Methods). Scale bars, 20 μ m.

C. Plasmids encoding GFP-tagged human KIF20B and mCherry were electroporated into mouse cortical neurons and imaged live. GFP puncta were distributed throughout the neurites and axon (arrows, inset). C' and C'': Some GFP puncta moved anterogradely in the axon (arrows point to the same puncta at different time points). 10 μ m scale bar and 5 μ m in insets.

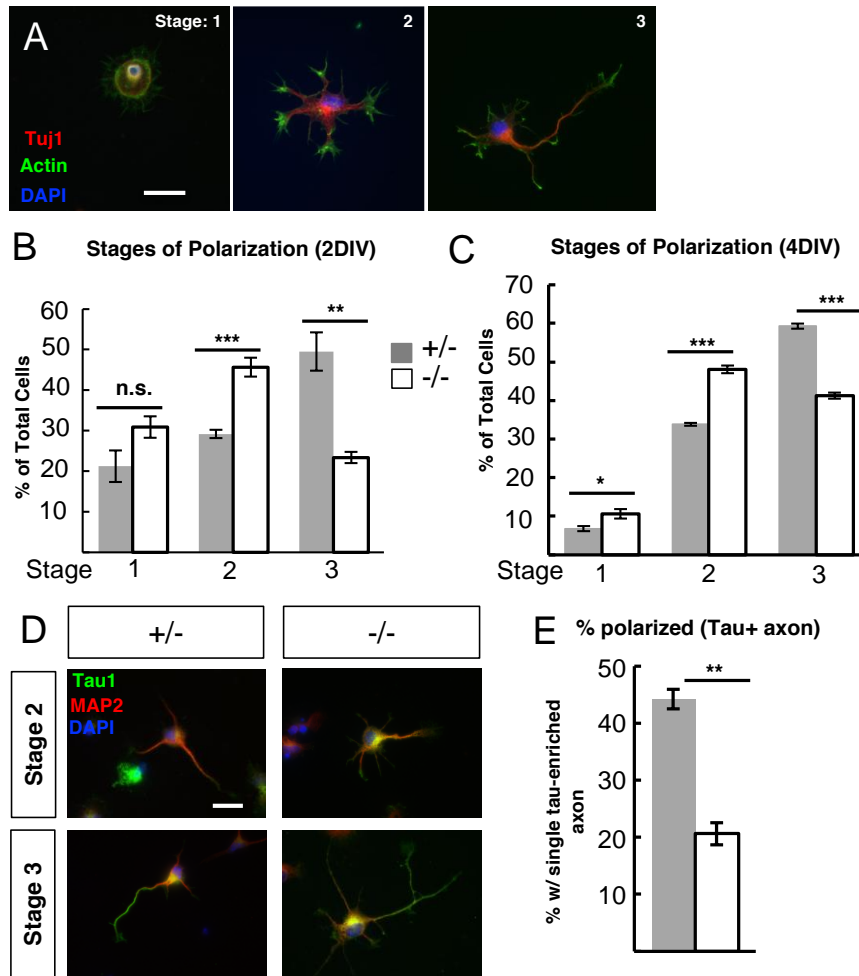


Figure 4-3. *Kif20b* mutant neurons are less polarized at 2 days or 4 days *in vitro*.

A. Representative images of dissociated E14.5 cortical neurons that are at Stage 1 (unpolarized), Stage 2 (multipolar), or Stage 3 (polarized; having one neurite at least twice as long as any other) after two days *in vitro*, and stained for neuron-specific beta-III tubulin (Tuj1, red), actin (phalloidin, green), and nuclei (DAPI, blue).

B. The average percentage (\pm s.e.m.) of neurons at each stage in cultures from control heterozygous (+/-, gray bars) or *Kif20b* mutant (-/-, white bars) cortices. Mutant cultures have fewer polarized neurons (stage 3) and more multipolar neurons (stage 2) compared to control heterozygous cultures. n = 6 control (+/-) and 6 mutant (-/-) coverslips from 3 independent experiments with 2258 total control and 1335 mutant cells scored.

C. After 4 days *in vitro* (4DIV), *Kif20b* mutant neurons are still less likely to be polarized. n = 4 control (+/-), n = 3 mutant (-/-) coverslips from 3 independent experiments; 827 control, 510 mutant neurons.

D. Representative images of dissociated cortical neurons stained for MAP2 and Tau1. Polarized neurons have a single, tau1-enriched neurite that is the axon.

E. The average percentage (\pm s.e.m.) of neurons with a single tau-enriched neurite (polarized) is decreased in *Kif20b* mutant cultures after 2 DIV. n = 3 control (+/-), 3 mutant (-/-) coverslips from 3 independent experiments; 615 control, 381 mutant neurons.

*, p < 0.05; **, p < 0.001; ***, p < 0.0001; n.s., not significant, t-test. Scale bars, 20 μ m.

Figure 4-4. Kif20b mutant axons have reduced enrichment of Shootin1 in the growth cone

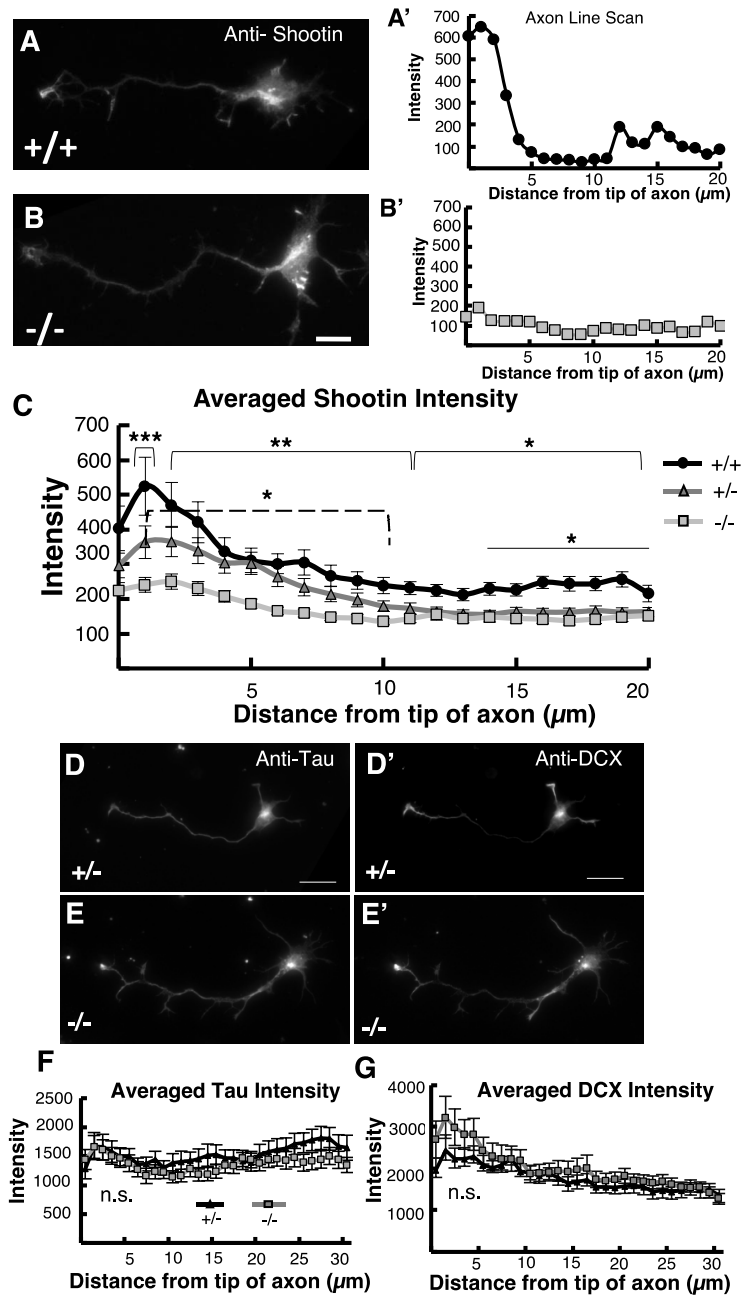


Figure 4-4. *Kif20b* mutant axons have reduced enrichment of Shootin1 in the growth cone.

A. Immunostaining for endogenous Shootin1 with anti-Shootin1 antibody [15] shows Shootin1 enriched in the axonal growth cone of a control (+/+) Stage 3 neuron.

A'. Linescan of Shootin1 staining intensity from image in A, starting from the tip of the axon and extending 20 μm shows a peak at the growth cone that flattens in the axon shaft.

B. Shootin1 immunostaining reveals Shootin1 in the soma of a polarized *Kif20b* mutant (-/-) neuron, but little enrichment in the distal axon.

B'. Linescan of Shootin1 staining intensity from image in B shows a severely reduced peak of Shootin1 at the tip of the mutant axon.

C. Averaged line scans of anti-Shootin1 signal intensity of 78 +/+, 101 +/-, and 100 -/- axons from 3 independent experiments show significantly bigger peaks in control axons than mutants. (+/+, black circles; +/-, gray triangles; -/-, light gray squares).

*, $p < 0.05$; **, $p < 0.01$; *** $p < 0.001$, t-test. Solid brackets compare wild-type (+/+) with mutant (-/-) for all points under each bracket. Dashed bracket compares heterozygous controls (+/-) with mutant (-/-) for all points under the bracket. Line compares +/+ with +/- for all points under the line.

D, E, and F. Tau immunostaining and axonal linescans reveal no significant difference in distribution or intensity between control and mutant neurons.

D', E', and G. DCX (doublecortin) immunostaining and axonal linescans show similar high distal distributions and intensities in control and mutant neurons. $n = 40$ +/- and 40 -/- cells both Tau and DCX linescans from two independent culture experiments (2 animals each, 2 coverslips from each animal).

Scale bar = 10 μm for A and B. Scale bar = 20 μm for D and E. F and G n.s., t-test

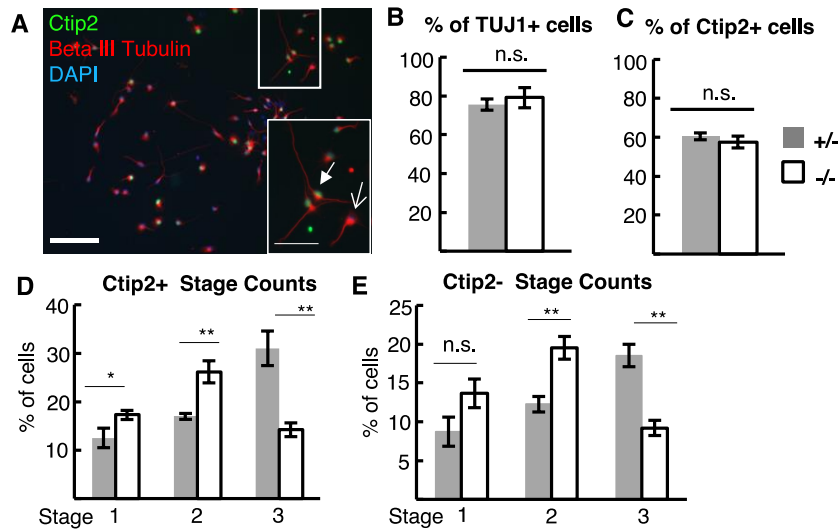


Figure 4-5. Morphological changes in *Kif20b* mutant neurons are not due to cell type changes

A. Representative field image of E14.5 cortical cells cultured for 2 days *in vitro*, immunostained for neuronal marker beta-III-tubulin (Tuj1, red), layer 5/6 marker Ctip2 (green) and nuclei (DAPI, blue). Filled arrow points to Ctip2⁺ neuron; open arrow to Ctip2⁻ neuron. Scale bars, 100 μm and 10 μm in inset.

B. The percentage of cells in control (+/-, gray bar) and mutant (-/-, white bar) cortical cultures expressing neuronal marker (TuJ1⁺) is not significantly different. n = 3 coverslips each with 1120 control cells and 769 mutant cells analyzed.

C. The percentage of neurons marked by Ctip2 does not differ in control and mutant cultures.

D and E. The average percentage (±s.e.m.) of Ctip2⁺ or Ctip2⁻ neurons at each stage in cultures from control heterozygous (+/-, gray bars) or *Kif20b* mutant (-/-, white bars) cortices. Mutant cultures have fewer polarized neurons (stage 3) and more multipolar neurons (stage 2) compared to control heterozygous cultures.

For C, D, and E n = 6 control (+/-) and 6 mutant (-/-) coverslips (2258 and 1335 neurons total, respectively).

Error bars are ±s.e.m.; *, p<0.05; **, p<0.01, n.s., not significant, t-test.

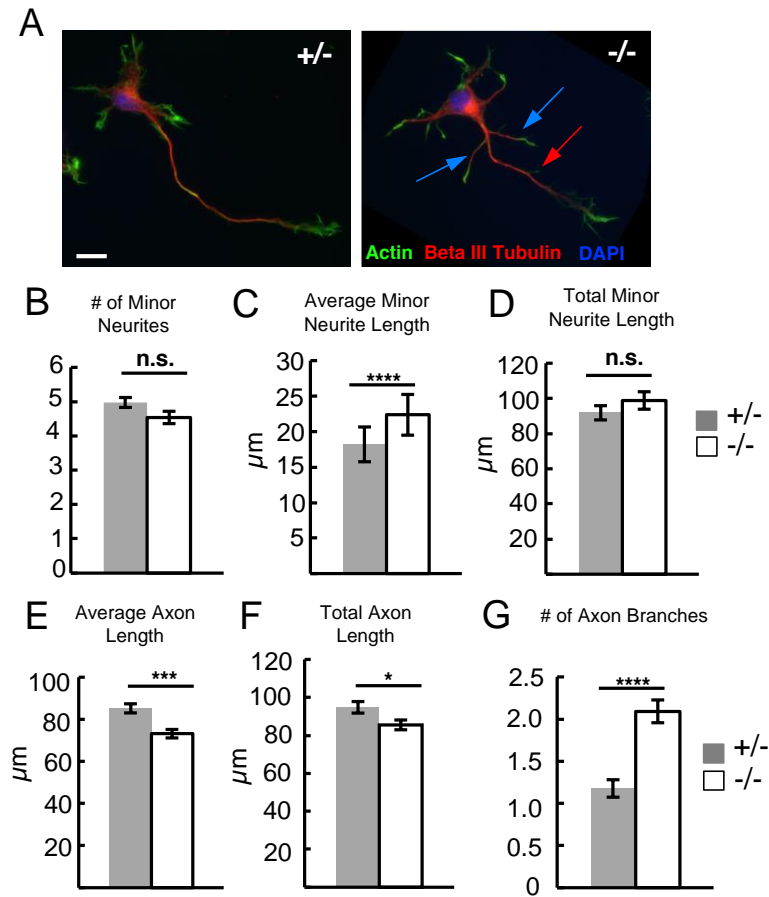


Figure 4-6. *Kif20b* mutant neurons that polarize have shorter axons, longer minor neurites, and more axon branches.

A. Representative images of control (+/-) and mutant (-/-) polarized (Stage 3) neurons from E14.5 cortical cultures after 2 DIV, stained with phalloidin (actin, green), anti-beta-III-tubulin (red), and DAPI (blue). Blue arrows indicate axon branches. Red arrow indicates branch with only actin. Scale bar, 10 μ m.

B. The average number of minor neurites (nascent dendrites) was slightly decreased in *Kif20b* mutant neurons (-/-, white bars), but was not statistically significant

C. Individual minor neurites of *Kif20b* mutant neurons (-/-, white bars) are longer on average than controls' at 2DIV. n = 323 +/-, 251 -/- minor neurites.

D. Summed dendritic length per cell is slightly increased in mutant neurons but is not statistically significant due to variable minor neurite number.

E. *Kif20b* mutant neurons (-/-, white bars) have shorter axons. n = 204 +/- and 260 -/- neurons.

F. Total axonal length including side branches was shorter in mutant neurons than controls. n = 202 +/- and 260 -/- neurons.

G. The average number of axon branches (containing tubulin) on mutant neurons was increased compared to controls.

All length measurements were made based on tubulin staining not actin signal.

For B, D, and G n = 79 +/-, 65 -/- neurons.

Error bars are \pm s.e.m. *, p < 0.05; ***, p < 0.001; ****, p < 10⁻⁶; n.s., not significant.

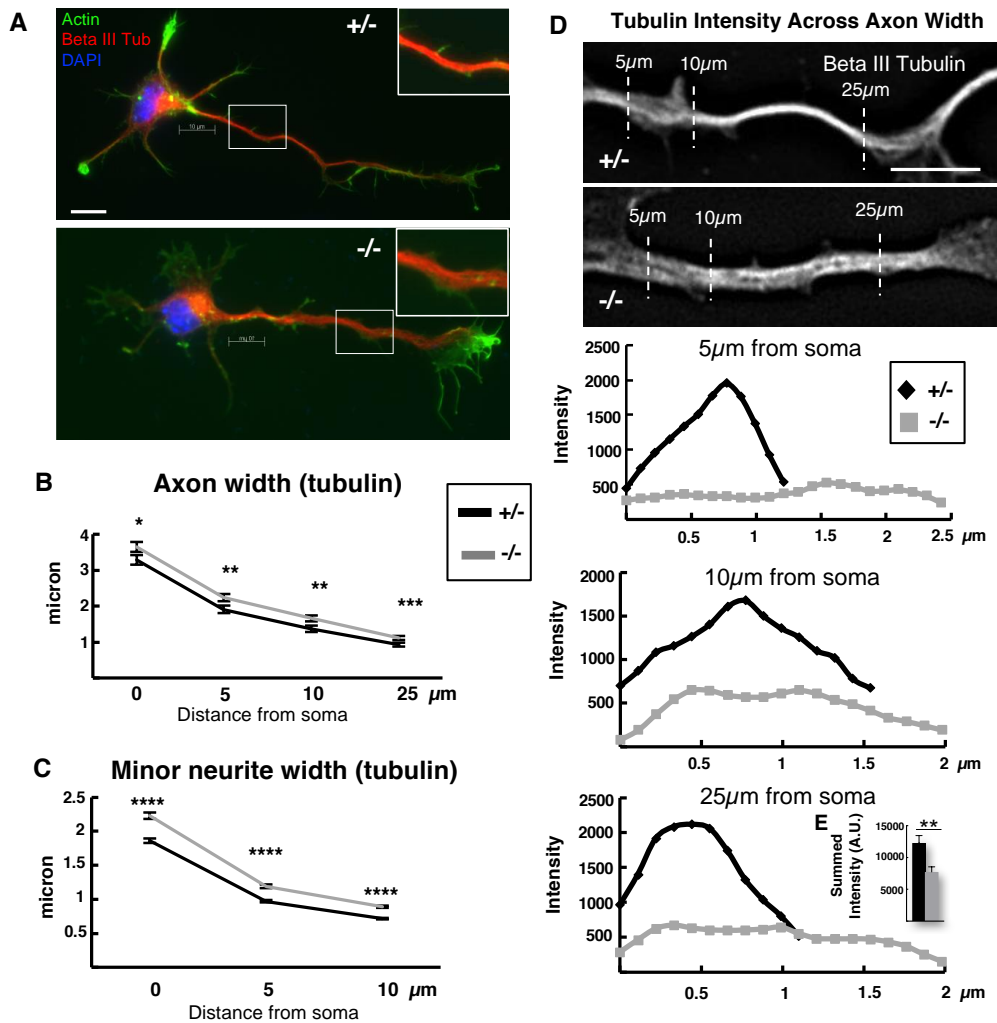


Figure 4-7. *Kif20b* mutant neurons have wider axons and minor neurites than controls.

A. Representative images of polarized control (+/-) and mutant (-/-) neurons cultured for two days and stained for actin (green), beta-III-tubulin (red) and nuclei (DAPI, blue). Insets show magnified axon segments for comparison.

B. Average width (\pm s.e.m.) of mutant axons (-/-, gray line) is greater than controls (+/-, black line) at each given distance from the edge of the soma. $n = 79$ +/- and 65 -/- axons.

C. Average width (\pm s.e.m.) of mutant minor neurites (gray line) is increased over controls (black line) at each given distance from the cell body. $n = 323$ +/- and 262 -/- minor neurites.

D. Representative images of and linescans across control (+/-) and mutant (-/-) axons stained for beta-III tubulin show that tubulin intensity was lower, more irregular, and more spread out in mutants than controls. Dotted lines represent where tubulin intensity linescans were taken.

E. Inset bar graph shows average total tubulin intensity summed across the width $25\mu\text{m}$ from the soma was significantly higher in mutant axons compared to controls. $n=15$ each +/- and -/- from 1 experiment.

*, $p < .05$; **, $p < .01$; ***, $p < .001$; ****, $p < 10^{-9}$. $10\mu\text{m}$ scale bars.

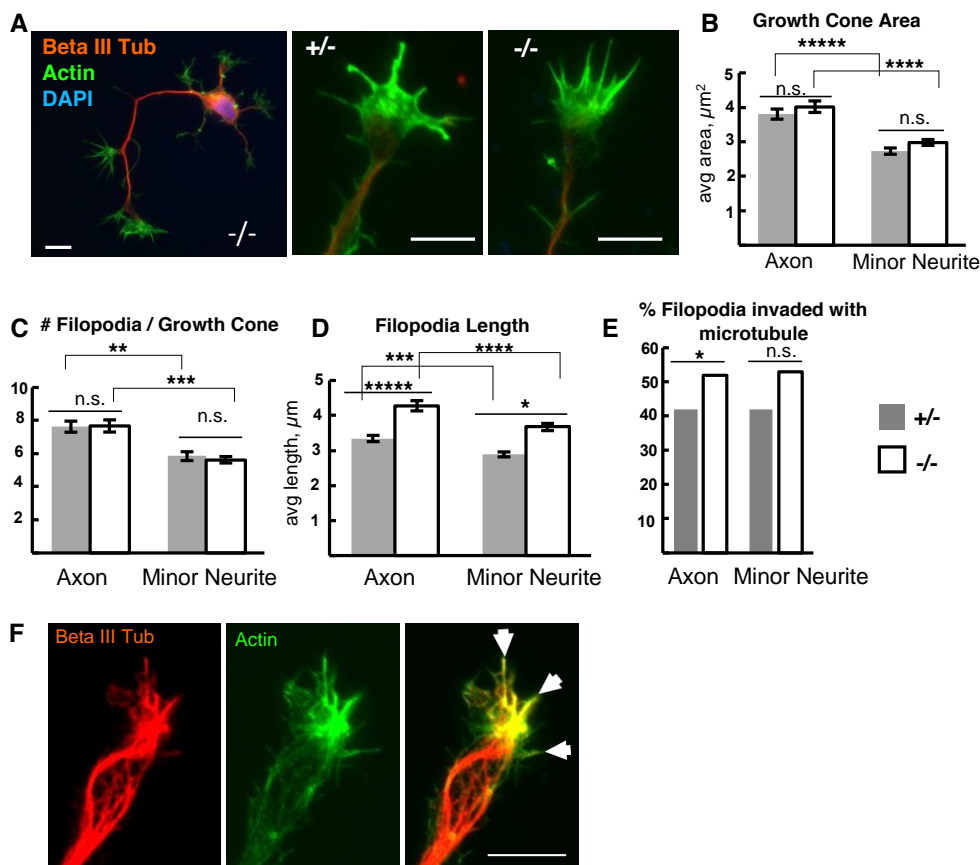


Figure 4-8. *Kif20b* mutant neurons' growth cones have longer filopodia

A. Representative images of control and *Kif20b* mutant growth cones of dissociated E14.5 cortical neurons cultured 2 DIV and immunostained to label neuronal tubulin (TuJ1, red), actin (phalloidin, green), and nuclei (DAPI, blue). Scale bars 10 μm.

B. The growth cones of axons are significantly larger in area than those of minor neurites, but similar in control (+/-, gray bars) and mutant (-/-, white bars) cells.

C. The average number of filopodia per growth cone did not differ significantly in *Kif20b* mutant neurons on either axons or minor neurites.

For B-C, n = 38 control (+/-) axonal and 54 minor neurite growth cones; mutant (-/-) n = 37 axonal and 49 nascent dendritic growth cones.

D. *Kif20b* mutant neurons have longer filopodia on both axonal and nascent dendritic growth cones. Axonal filopodia are slightly but significantly longer than dendritic filopodia regardless of genotype. n = 217 control and 308 mutant filopodia from 39 and 37 axonal growth cones, and n = 155 +/- and 134 -/- filopodia from 25 and 22 minor neurite growth cones respectively.

For A-D, error bars are ±s.e.m. *, p < 0.01; **, p < 10⁻³; ***, p < 10⁻⁵; ****, p < 10⁻⁶; *****, p < 10⁻⁸; n.s., not significant, t-test.

E. In *Kif20b* mutant neurons, a higher percentage of growth cone filopodia contain detectable microtubules than in controls, in both axons and minor neurites. n = 217 for +/- and 308 -/- filopodia on axonal growth cones and n = 155 +/- and 134 -/- filopodia on minor neurite growth cones. *, p < 0.05 Fisher's exact test.

F. Axonal growth cone labeled for actin (green) and tubulin (red). Arrowheads mark filopodia containing microtubules.

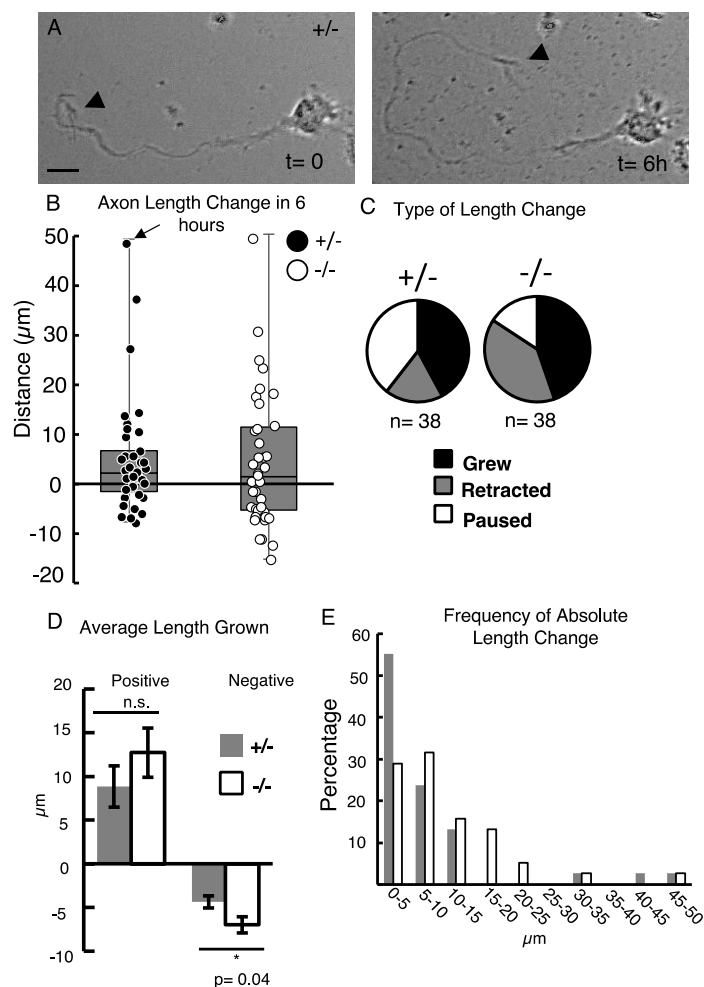


Figure 4-9. *Kif20b* mutant axons are more likely to retract and retract farther than controls

A. Example brightfield images of live 2 DIV cortical neuron imaged at time 0 hours and 6 hours. This neuron grew its axon 48 μm . Arrowheads point to growth cone. Scale bar, 10 μm .

B. Change in axon length after 6 hours for each individual neuron was plotted as a scatter plot, and the distribution as a box plot. The dot representing the axon imaged in A is marked by an arrow. $n = 38$ control (+/-, black dots) and 38 *Kif20b* mutant (-/-, white dots) neurons, imaged over 7 different experiments from 6 +/- embryos and 7 -/- embryos. Axons of similar starting lengths were chosen for imaging (averages 52 and 48 μm for +/- and -/-, respectively, p-value n.s.).

C. Mutant axons (-/-) were more likely to retract and less likely to pause than control axons (+/-) in six hours. The change in category distribution is significantly different by Fisher's exact test, $p = 0.03$. "Grew" signifies at least +3 μm length change; "Retracted", at least -3 μm ; "Paused", within $\pm 2.9 \mu\text{m}$ of starting length.

D. The average length retracted in 6 hours among axons that shrank was significantly increased in the *Kif20b*-/- neurons. The average length increase in 6 hours among axons that grew was not significantly different. Here, all above-zero changes were averaged for "positive" and all below-zero changes were averaged for "negative".

E. The absolute values of length changes were binned and plotted as a histogram to show greater length changes in *Kif20b* mutant axons (white bars) compared to heterozygous controls (black bars). The median was higher in the mutants (6.9 μm versus 4.4 μm , Mann-Whitney U-test $p = 0.04$).

*, $p < 0.05$; n.s., not significant, t-test.

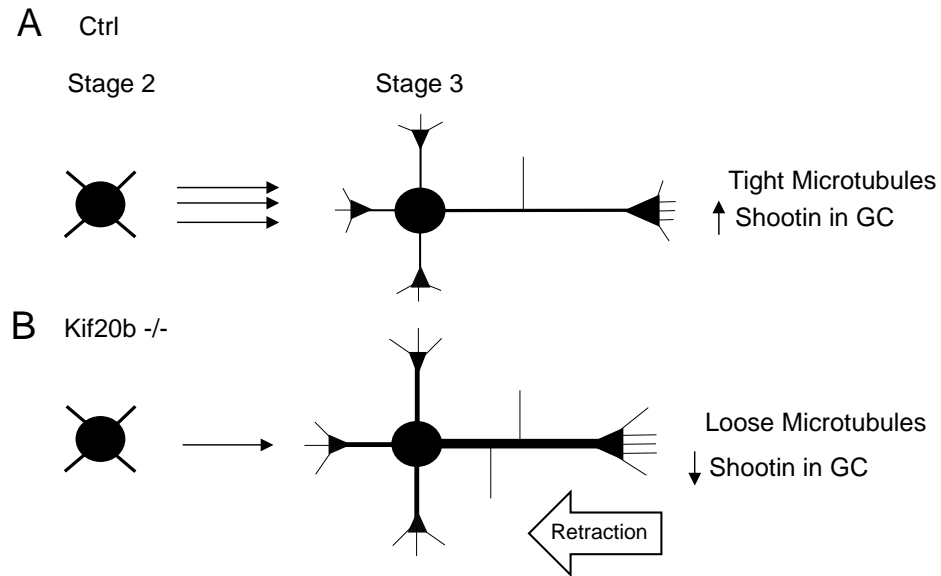
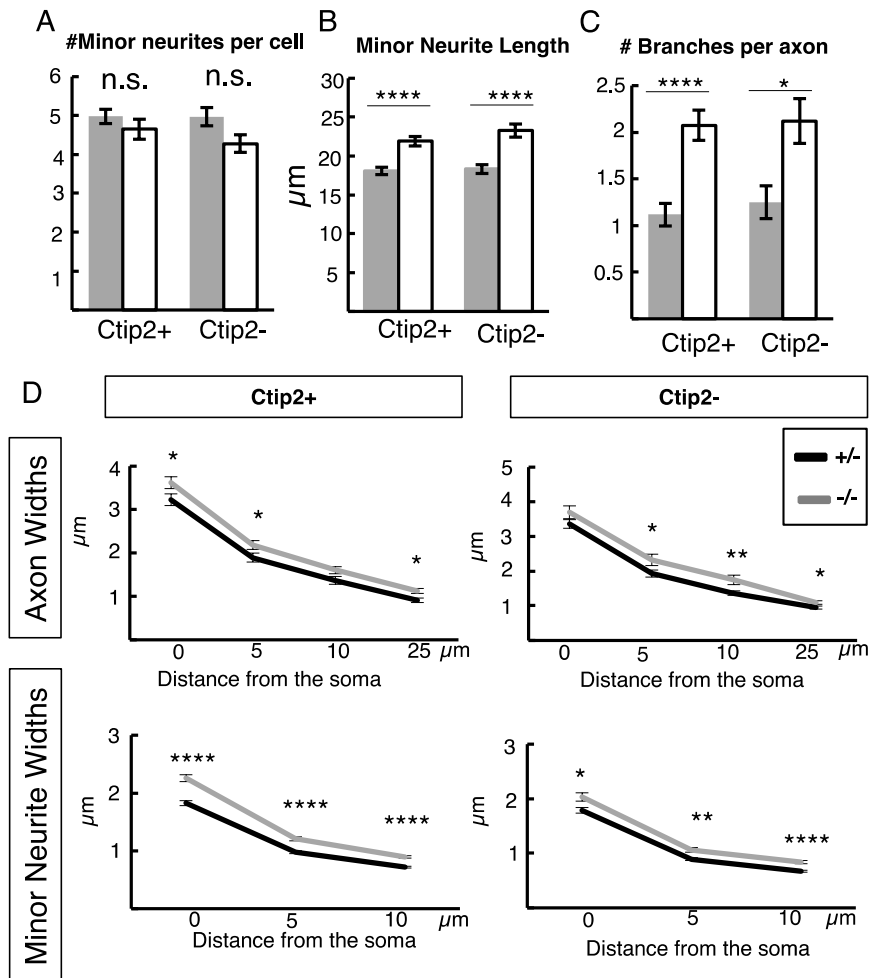


Figure 4-10. Summary of phenotypes of *Kif20b* mutant neurons seen in culture.

A. Normal cortical neurons transition from multipolar (Stage 2) to polarized with a single axon (stage 3) properly when *Kif20b* is present. *Kif20b* may organize or stabilize microtubule arrays in the axon and growth cone, keeping the axon thin and limiting its branching, and preventing microtubule invasion of filopodia. *Kif20b* may also tether Shootin1 at the microtubule plus ends in the axonal growth cone, which reinforces axonal growth. *Kif20b* may thereby enhance stability and inhibit axon retraction.

B. When *Kif20b* is absent, some neurons fail to transition from stage 2 to stage 3. Those that do polarize show a variety of phenotypes: longer minor neurites, shorter axons with extra branches, wider axons and minor neurites, and longer filopodia. Microtubules appear more loosely organized and extend into more filopodia. Shootin1 enrichment in the growth cone is severely reduced.



Supplemental Figure 4-1. Morphological abnormalities in *Kif20b* mutant cells are observed in both Ctip2⁺ and Ctip2⁻ neurons.

A. The average number of minor neurites is not different in *Kif20b* mutant cells (white bars) whether Ctip2⁺ or Ctip2⁻.

B. Minor neurites are longer on average in *Kif20b* mutant neurons (white bars) than in control neurons (gray bars), whether Ctip2⁺ or Ctip2⁻.

C. *Kif20b* mutant axons (white bars) have more branches than control neurons (gray bars) whether Ctip2⁺ or Ctip2⁻.

D. Axons and minor neurites of *Kif20b* mutant neurons are wider on average than controls, regardless of whether they are Ctip2⁺ or not. Measurements done using images of tubulin immunostaining at same exposure times. Ctip2⁺ neurons n= 43 +/- and 40 -/-. Ctip2⁻ neurons n= 36 +/- and 25 -/-. Error bars are \pm s.e.m; *, p<0.05; **, p<0.01, ***, p<0.001, **** p< 10⁻⁵, ***** p< 10⁻⁷; n.s., not significant, t-test.

Chapter V: Conclusions and Discussion

5.1 Overview

The development of the cerebral cortex requires elaborate and orchestrated events to form a correctly sized and structured epithelium. There is much about the development of the cerebral cortex that remains mysterious. Excitingly, in this dissertation, I was able to dissect the kinetics and possible mechanism of one aspect of these events, cytokinesis, the separation of two daughter cells. I characterized cytokinesis in the presence and absence of two different midbody proteins (Kif20b and Cep55). Despite finding subtle phenotypes in the *Kif20b* mutant, this dissertation establishes a reliable and novel *in vivo* method to dissect previously unknown cell division dynamics of neural stem cells (NSCs). This was evident when I found the loss of Kif20b or Cep55 alter abscission duration in different directions (**Chapter III, Appendix I**). Specifically, this work has uncovered varied roles of Kif20b in dividing cell lines (**Chapter II, Appendix IV**), NSCs (**Chapter III, Appendix II**), and post-mitotic neurons (**Chapter IV, Appendix V**). Neither Kif20b nor Cep55 are absolutely essential proteins for cytokinetic abscission completion in NSCs, but they are necessary for efficient cytokinesis and proper cerebral cortex development (**Chapter III, Appendix I**). Additionally, we were able to show that cytokinesis is developmentally regulated, and has the potential to influence cell fate, opening additional avenues of investigation.

More recently, there has been an understanding that proteins that were initially discovered to be important in cell division may have different roles in post-mitotic cells like neurons. This is particularly true for the Kinesin-6 family member, Kif20b. In this dissertation, we have shown that Kif20b is important for regulating the polarization and neurite outgrowth of neurons as well as the balance between microtubule stability and instability (**Chapter IV, Appendix V**).

This dissertation has advanced our understanding of NSC cell division, specifically cytokinesis, in proper cerebral cortex development. This discussion synthesizes the previous chapters and the following appendices. It focuses on the exciting conclusions and the potential future directions of these projects. In addition, all chapters and appendices have additional findings and future directions.

5.2 Role of abscission duration and midbody remnants in cell fate and cortical development

During cortical development, neural stem cells need to produce the correct cell types in a particular order to build the brain. As outlined in the introduction (**Chapter I**), cell fate determinants and maintenance of the epithelium during development are both active fields of study. Before this work, there was limited understanding of cytokinesis within epithelia, especially within the brain. Using live imaging of cortical slabs at E11.5 and E13.5, we were able to dissect the kinetics of both steps of cytokinesis: cleavage furrowing and abscission. We found that cleavage furrowing takes, on average, 15 minutes to complete and is asymmetric, steady, and not developmentally regulated between E11.5 and E13.5 in NSCs (**Chapter III**). Abscission appears to be developmentally regulated between E11 and E13.5 and mostly bilateral when using microtubule disassembly as a readout (**Chapter III**). The average time to the first abscission is 57 minutes for E11.5 and 47 minutes for E13.5 (**Chapter III**). Considering there is more than 60% bilateral abscission, which differed from our initial hypothesis, we were intrigued by the fate of the post-abscission midbody remnants left behind.

Midbody remnants could be produced by bilateral microtubule scission, but whether they remain tethered to plasma membrane or are free to float away is unknown. Therefore, we wanted to determine where midbody remnants localize after NSC abscission in the brain. We found suggestive evidence that midbody remnants could have a role in cell fate (**Chapter III, Appendix II**). We find midbody remnants associated with the apical membrane at E11.5, E13.5, and E15.5. Interestingly, there were 75% more midbody remnants associated with the apical membrane of younger NSCs (E11.5) compared to older NSCs (E15.5). At E13.5 there is an intermediate phenotype with more remnants on the apical surface compared to E15.5 and less compared E11.5. When using the pair-cell assay at E11.5, we showed a correlation between proliferative symmetric divisions and remnants (**Chapter III, Appendix II**). *In vivo* experiments were unable to determine the precise location (internal versus external) of the midbody remnants to the NSCs. However, we find that HeLa midbody remnants are taken up by NSCs in culture, suggesting there is a potential for them to be phagocytosed *in vivo* (**Appendix III**). How midbody remnants could influence cell fates or polarization remains an open question. There is much work to be done on how midbody remnants interact with NSCs (external

or internal signaling) and what components of the midbody remnant are important (specific proteins or RNAs). Overall, we can conclude that NSCs have subtle developmental changes in abscission dynamics that could contribute to cell fate decisions that are essential for proper brain growth.

5.3 Midbody proteins, Kif20b and Cep55, reveal essential cytokinetic regulation in brain development

To dissect the roles of midbody proteins in efficient abscission and to dissect the role of abscission in cortical development, we focused on two proteins, Kif20b and Cep55. The loss of Kif20b and Cep55 has been associated with microcephaly in mice, and Cep55 has a known role in a human brain malformation ((Bondeson et al., 2017; Dwyer et al., 2011; Frosk et al., 2017; Janisch et al., 2013; Little, 2019), **Appendix I**). Kif20b and Cep55 appear to have evolved in vertebrates and have separate localization patterns and functions within the midbody (**Chapters II-III, Appendix I-II**, (Abaza et al., 2003; Bastos and Barr, 2010; Janisch et al., 2018; Little, 2019; Zhao et al., 2006)). Kif20b is a plus-end directed microtubule motor that binds and bundles microtubules (Abaza et al., 2003). It localizes to the central spindle and then re-localizes to the midbody flanks (**Chapter II**, (Janisch et al., 2018)). We were able to show that when Kif20b is lost in HeLa cells, cleavage furrowing and abscission are abnormal, microtubules in the central spindle are abnormal, there is a defect in midbody maturation based on the shape of the midbody and uncoordinated ESCRT recruitment (**Chapter II**, (Janisch et al., 2018)). In testing whether Kif20b mediates localization of any midbody proteins, the only protein that we have found so far that fails to localize correctly in Kif20b-depleted cells is mDIA2, a formin with reported Kif20b and p53 interactions, and both actin and microtubule-binding (**Appendix IV**, (Bartolini et al., 2008; Isogai et al., 2015; Miki et al., 2009; Watanabe et al., 2008)). Cep55 is a protein that localizes in late-stage midbodies to the central bulge through interaction with MKLP1 and ubiquitin (Said Halidi et al., 2019; Zhao et al., 2006). Cep55, in mammalian cells, is responsible for the efficient recruitment of ESCRT proteins, which is essential for the completion of cytokinesis. When Cep55 was knocked-down in HeLa cells, more than 90% of the cells failed to complete abscission (Zhao et al., 2006). We will discuss the role of Kif20b in NSC division first, and then Cep55.

Kif20b in NSC division

In previous papers, the lab has characterized the role of Kif20b in fixed NSCs midbodies both *in vivo* and *in vitro*, as well as knockdown HeLa cells (Janisch et al., 2018; Janisch et al., 2013; Little and Dwyer, 2019). However, we still had questions about Kif20b's role in abscission, specifically in the abscission of NSCs. To interrogate the role of Kif20b in NSCs, I used live imaging and immunostaining of cortical slabs. I found in NSCs lacking Kif20b, cleavage furrowing is normal in the majority of cells but takes longer in a subset, abscission is faster on average, midbody remnants are apparently unaffected, and there is an increase in neurogenic symmetric divisions, which is p53 independent (**Chapter III, Appendix II**). Since abscission completes faster, and apical junctions form just basal to the midbody, we first hypothesized that apical junctions would be impaired in formation or segregation. We found that NSC apical membrane was asymmetrically inherited to the daughter cells in the *Kif20b* mutants, but this due to p53-dependent mechanisms (**Appendix II**). Having ruled out a defect in apical membrane segregation, we next hypothesized that faster abscission in the *Kif20b* mutants cause this early neurogenic phenotype. This is consistent with the developmental evidence we have that abscission is faster at E13.5 compared to E11.5 cell divisions (**Chapter III**). This hypothesis still requires more experiments to prove causation but is an intriguing line of investigation.

The loss of Kif20b also disrupts other aspects of cortical development, including neuron polarization and axon outgrowth ((McNeely et al., 2017), **Chapter IV**). *Kif20b* mutant neurons cultured *in vitro* on poly-L-Lysine have difficulty polarizing and growing out axons, and have reduced localization of the polarization protein Shootin1. When *Kif20b* mutant neurons are grown on L1CAM, axon outgrowth surpasses control, and polarization is rescued. Based on *Kif20b* mutant neurons growth on the substrates L1CAM and Laminin, we hypothesize that Kif20b's role is to mediate a balance between microtubule stability and instability is essential for efficient polarization and controlled axon outgrowth (**Appendix V**).

Cep55 in NSC division

Next, we will discuss Cep55's role in abscission and cortical development. As previously discussed, the loss of Cep55 causes lethal microcephaly in both humans and mice

((Bondeson et al., 2017; Frosk et al., 2017; Little, 2019), **Appendix I**). Interestingly, the midbodies of NSCs and MEFs lacking Cep55 are mostly structurally normal when we measured the length and width using AuroraB and Tubulin (**Appendix I**). This is surprising because Cep55 was proposed to have a role in organizing and stabilizing the central bulge (Bastos and Barr, 2010; Zhao et al., 2006). We were expecting to see an accumulation of wider and possibly longer midbodies, in the mutant, which would indicate defects in midbody maturation and delayed abscission. Additionally, there has been one report in HeLa cells that the dark zone, the central bulge of the midbody that is often not penetrable by antibodies, is lost when Cep55 is knocked-down, suggesting Cep55 is important for maintaining the organization within this electron-dense core (Zhao et al., 2006). However, we found that the dark zone was still present using AuroraB in Cep55 mutant MEFs and NSCs (**Appendix 1**). Cep55 is also thought to be necessary for the recruitment of ESCRT components to the central bulge. I found in both mutant MEFs and NSCs that ESCRTs recruitment to the central bulge is perturbed but not completely lost. This finding is surprising because the dogma in the field would suggest that without Cep55, no ESCRT recruitment to the midbody could occur in mammalian cells. These data suggest that Cep55 is not necessary for maintaining the structure of the midbody, and ESCRTs can be recruited independently of Cep55. ESCRTs could be recruited through MKLP1, as has been shown in invertebrates (Lie-Jensen et al., 2019). In our live NSC movies, using SiR-Tubulin to observe microtubule disassembly, we find that the majority of NSCs can complete abscission (**Appendix I**). However, abscission is delayed on average by 16 minutes, and there is some percentage of failure based on the increase in the number of tripolar spindles (**Appendix I**).

Cep55 has been clinically called a ciliopathy and has been shown by one group to localize to centrosomes (Bondeson et al., 2017; Fabbro et al., 2005). Therefore, we wanted to investigate if our mouse mutant shared any of the characteristic phenotypes of a ciliopathy, like an accumulation of fluid in organs and changes in cilia number and shape. We found previously that the mouse mutants do not have polycystic kidneys (Little, 2019). In this thesis, we decided to continue investigating the cilia and looked at the structure of NSC cilia. I found in *Cep55* mutants, the percentage of ciliated NSCs is similar to controls, but there was a significant increase in multiciliated cells, most of the multiciliated cells had two cilia, and rarely 3 cilia (**Appendix I**). The multiciliated cells are

most likely a result of the increased binucleate NSCs in the *Cep55* mutants. In both the single and multiciliated cells, the cilia length was correlated with apical endfoot size at E14.5 (**Appendix I**). We hypothesize that the longer cilia are a result of an extended G1 due to abscission defects or binucleate cells. However, we have not been able to show changes in G1 length at this point. Interestingly, certain defects in the apical membrane of *Cep55* mutants, including endfoot number and size, and cilia structure are more severe at E14.5 compared to E12.5, which is surprising because of the elevated apoptosis at both ages (**Appendix I**, (Little, 2019)). By contrast, the midbody remnants, which have a more profound accumulation at the apical membrane at E12.5 in *Cep55* mutants compared to E14.5. *Cep55*'s role or importance in different types of NSC divisions remains a big question. There is a lot left to investigate in this mutant, but we can conclude that *Cep55* is necessary for efficient NSC abscission and proper brain growth.

Kif20b and *Cep55* have differing abscission duration and midbody remnant disposal phenotypes (**Table 5-1**). However, these mutants both emphasize the idea that 1) cell line data is not always predictive of developmental or tissue level consequences, and 2) efficient and temporally and spatially precise abscission in NSCs is essential for proper brain growth. On the first point, *Kif20b* knockdown HeLa cells had mild cell phenotypes but devastating consequences to the brain, whereas *Cep55* knockdown HeLa cells had catastrophic consequences that would suggest no viable embryo, yet both human and mouse mutations show initial embryo growth despite large deficits in brain growth. Secondly, NSCs seem to be more susceptible to defects in abscission than other tissues due to the structural abnormalities observed in the brain. Both *Kif20b* and *Cep55* are expressed in many other tissues, but gross phenotyping in both mutants suggest these tissues are at least morphologically normal. Thus, *Kif20b* and *Cep55* may have specific functions in NSCs not necessary for other cell types. Another possibility is that NSCs are more prone to exit the cell cycle or die after an abnormal cell division. This would protect the brain from large numbers of abnormal neurons. Neurons are long-lived cells and rarely replaceable (except in the few instances of adult neurogenesis); therefore, neurons must be protected, and cannot tolerate binucleation or disrupted polarity. Together these findings suggest that efficient and precisely controlled abscission is vital for proper brain growth.

	Furrowing	Abscission	Midbody Remnants	Midbody Alignment	Midbody Structure	Fate
Control Early vs. late	No difference (E11 vs. E13)	Faster at E13 compared to E11	Developmentally regulated (E11 and E13 are similar, both E11 and E13 are different from E15)			
<i>Kif20b</i> mutant vs. control	Similar	Faster than controls at E11.5 and E13.5	Similar	Misaligned	Wider	Early neurogenesis
<i>Cep55</i> mutant vs. control	Not tested	Slower than controls at E13.5	More per cell at E12 and E14. More per midbody at E12	Aligned	Shorter	No change in fate at E12.5. Should re-try in <i>Cep55/p53</i> double

Table 5-1: Comparison between *Kif20b* and *Cep55* mutant phenotypes.

5.4 Microtubule function of *Kif20b* may explain abscission and axon outgrowth phenotypes.

Kif20b is a plus-end directed microtubule motor that can bind and bundle microtubules (Abaza et al., 2003; McNeely et al., 2017). Besides microtubules, there is limited evidence for other cargos of *Kif20b* like *Shootin1* and *mDia2* ((Sapir et al., 2013), **Appendix IV**). Evidence presented in Chapters II, III, and IV suggests that while *Kif20b* may have other cargo, its known role is microtubule bundling and organization. We have shown that *Kif20b* localizes to the central spindle and midbody microtubules during cytokinesis (**Chapter II**, (Janisch et al., 2018)). Without *Kif20b* in HeLa cells, the central spindle microtubules are more disorganized. Midbodies of *Kif20b* mutant NSCs are wider (Janisch et al., 2013). Both results suggest defects in the organization and bundling of microtubules in cytokinesis. The microtubules in the axon of neurons without *Kif20b* are spaced further apart, further supporting this important role in microtubule bundling (**Chapter IV**, (McNeely et al., 2017)).

We hypothesized that disruption in the structure of both midbodies and neurons would have implications on cellular function. Therefore, we examined key midbody and axonal proteins in midbodies and neurons. Surprisingly, we found that most protein localization was normal, and only a few midbody and axonal proteins were disrupted when *Kif20b* was depleted (**Chapter II, IV**, (Janisch et al., 2018; McNeely et al., 2017)). Specifically, *mDIA2* and *ESCRT* proteins in the midbody of HeLa cells (**Appendix IV** (Janisch et al.,

2018)). In the axon, Shootin1 has reduced localization to the growth cone. The loss or reduction in localization suggests defects in the recruitment or underlying structural defects preventing localization. Kif20b might be important as a motor to localize these proteins, sequester, or even tether them at a specific location, or their mislocalization could be a secondary defect of the disorganized and wider microtubules. *Kif20b* mutant neurons grown on a substrate that promotes axon bundling, like L1CAM or Laminin, no longer have an axonal bundling defect, but Shootin1 localization is not restored (**Appendix V**). Our evidence from neurons suggests that rescuing the structure of axons is not sufficient for Shootin1 to localize to the axonal growth cone. Therefore, Kif20b or its cargo most likely contributes to the sequestering or localization of Shootin1.

5.5 Future Directions: Where can we go from here?

Questions remain with linking neural stem cell abscission duration with cell death and cell fate changes. These open questions involve better elucidating Kif20b and Cep55 roles in cell division and neurons as well as biological questions involving the roles of cytokinesis in building the brain.

I. Identifying Kif20b binding partners and cellular function

There are gaps in our knowledge of Kif20b's role from cytokinesis to post-mitotically. We still do not know Kif20b's primary molecular role in cytokinesis, even though multiple groups, including us, have described Kif20b's localization to the midbody. We have found that Kif20b is important in microtubule bundling and organization, but we do not know all of Kif20b's binding partners. Determining the binding partners for Kif20b could be important for elucidating roles outside of abscission or better understanding of abscission. Kif20b has been linked to proteins through immunoprecipitation and mass spectrometry studies. These candidate binding partners are involved in nuclear pore formation, neuron polarization, and cytokinesis ((Kamimoto et al., 2001; Kanehira et al., 2007; Maliga et al., 2013; Sapir et al., 2013), **Table 2**).

We have preliminary evidence for some of these binding partners. PIN1, PRC1, and ACTN4 did not have changes in localization, suggesting their interaction with Kif20b is not due to Kif20b's function as a motor. We found that PIN1 has increased nuclear to

cytoplasmic ratio in Kif20b knockdown HeLa cells suggesting Kif20b might have a role at the nuclear pore (Dwyer Lab Unpublished Data). In this thesis, we focus on Shootin1 and mDIA2 (**Chapter IV, Appendix IV, Appendix V**). We have evidence that the localization of these proteins is disrupted with the loss of Kif20b, suggesting these candidates could be direct binding partners of Kif20b. We have tried to look for Shootin1 in the midbody of HeLa cells but the staining with antibodies from the Orly Reiner Lab was inconsistent (Dwyer Lab Unpublished Data). It might be interesting to use the Proteintech Shootin1 antibody made to the human protein and look for Shootin1 localization in the midbodies of HeLa and NSCs. A potential new candidate from RNAseq is Arl3, which may be regulated directly or indirectly by Kif20b. The ciliary protein Arl3 is decreased in the RNAseq of Kif20b and Kif20b/p53 double mutants (Little, 2019). We have preliminary evidence that cilia are present, but the number is reduced in the *Kif20b* mutant (Janisch and Dwyer, 2016). This raises questions about Kif20b having a role in the cilium either in the basal body or shaft.

Candidate Binding Partner	Cellular Localization	Evidence of interaction	Data from Dwyer Lab
PIN1	Midbody Ring, nucleolus, cytoplasm	Immunoprecipitation (Kamimoto et al., 2001)	Localization in the midbody was not disturbed in knockdown HeLa cells. Increase in Nuclear/Cytoplasmic ratio in knockdown HeLa cells (unpublished)
PRC1	Midbody Ring	Immunoprecipitation (Kanehira et al., 2007)	Localization not disrupted in Kif20b knockdown HeLa cells (Janisch et al., 2018)
Shootin1	Axon growth cones and possibly midbodies	Pulldown, Mass Spec, and co-IP (Maliga et al., 2013; Sapir et al., 2013)	Reduced localization in <i>Kif20b</i> mutant axon growth cones (Chapter IV (McNeely et al., 2017))
ACTN4	Adherens junctions	Pulldown and Mass Spec (Maliga et al., 2013)	Localization not disrupted in Kif20b knockdown HeLa cells (Janisch et al., 2018)
NUP153	Nuclear Pore Component	Pulldown and Mass Spec (Maliga et al., 2013)	-
mDIA2	Cleavage Furrow and Midbody inner flanks	Mass Spec (Isogai et al., 2015)	Reduced localization in cleavage furrow and midbody (Appendix IV)
Arl3	Cilia	Reduced mRNA in RNAseq of Kif20b ^{-/-} cortex (Little, 2019)	Have not found a working antibody for cortical slabs or MEFs (unpublished)

Table 5-2: Candidate protein interactions of Kif20b that are of the most interest.

In addition to Table 5-2, there are other importins, cdks, and condensins that have been proposed as candidate interactors (Maliga et al., 2013). To find additional candidates or confirm these untested candidates, we could express a tagged-Kif20b to pull down unknown targets from NSC and neurons and then identify those targets with mass

spectrometry. Previously, all of the candidates have been determined from HeLa cells or yeast two-hybrid screen. Therefore, it would be useful for our lab to determine interactions that may be cell type specific.

A difficulty with studying Kif20b has been the fact that we currently do not have a working antibody that detects Kif20b protein in mouse cell IF or IHC. To continue the exciting work on Kif20b's role in NSC midbodies and neurons, we have outlined in Chapters II-Chapters IV and Appendix II, V, it would help to have either a new antibody or a knockin mouse to detect Kif20b localization. This would provide us with a valuable tool to determine how Kif20b functions during the cell cycle within NSCs and post-mitotically within neurons.

II. Identify any post-mitotic role of Cep55.

With more and more cell cycle proteins linked to post-mitotic functions, it is worth investigating Cep55 in neurons. Although we see low RNA expression in the neuronal layer at E14.5 based on Genepaint *in situs*, there could still be a functional role in neurons. In the case of Kif20b, *in situs* showed little expression in the neuronal layer, but we have gone on to show that Kif20b has roles in post-mitotic neurons (**Chapter IV, Appendix V** (Janisch et al., 2013; McNeely et al., 2017)).

It is possible post-mitotic consequences in *Cep55* mutant neurons could be the result of defects from disrupted abscission, which is just as exciting. To address this question, we can plate *Cep55* mutant E14.5 neurons, and then analyze polarization, binucleation of neurons, and axon outgrowth. We have evidence that 25% of neurons are binucleate at E15.5 (Little, 2019). We could speculate that binucleate cells would have difficulty polarizing, migrating, or with process outgrowth. Additionally, neurons may be influenced by post-abscission midbody remnants that may be attached to a daughter cell after incomplete abscission. We currently have evidence that microtubule disassembly is delayed, but no evidence regarding plasma membrane scission. If we had a knock-in *Cep55* mouse, we might be able to determine whether and where *Cep55* localizes within neurons. Since knock-ins can be challenging to make, we could try to culture neurons for several days and then use western blot from the isolate to determine if *Cep55* protein is expressed. Additionally, we could knock-down *Cep55* from wild-type neurons to assess

if Cep55 is necessary once polarization and axon outgrowth has been initiated. This would help to answer if any defects in the neurons were secondary to cytokinesis defects or primary phenotype from a role in the neurons.

III. What are the cellular consequences of faster abscission?

The loss of Kif20b is the first mouse mutant with documented faster abscission. There is limited data from cell lines of other causes of faster abscission, but most of the identified proteins are a part of the abscission checkpoint (Chmp4C, UKL3, ANCHR). The abscission checkpoint responds to DNA replication stress, chromatin in the intracellular bridge, high membrane tension, and nuclear pore defects (Nahse et al., 2017). The abscission checkpoint is controlled by active AuroraB acting upstream of Chmp4C, UKL3, and ANCHR to prevent VPS4 from being released to the constriction site, therefore preventing abscission. Faster abscission caused by defects in the abscission checkpoint release VPS4 to the constriction site earlier than normal. The consequence in the case of Chmp4C is an increase in DNA damage in the daughter cells. In the case of loss of Kif20b or PRL-3, abscission is faster, but there is no known role in the abscission checkpoint, the answer is less clear. Additionally, it is possible that the abscission checkpoint is sensitive to and can respond to midbody maturation defects. There is much work to be done on the causes of faster abscission.

There is minimal understanding of the cellular consequences of faster abscission. We can speculate that cell death and cell fate changes are downstream consequences of faster abscission in the *Kif20b* mutant, but we do not know if they are primary or secondary effects of this process. The related Kinesin-6 family member, MKLP2/Kif20A, interacts with the abscission checkpoint preventing abscission (Fung et al., 2017). While we do not believe the domain responsible for this interaction is in the Kif20b protein, it suggests that the Kinesin-6 family may have key regulatory roles within the abscission checkpoint.

DNA damage could be a consequence of accelerated abscission or of disabling the abscission checkpoint. When the abscission checkpoint is disrupted, and abscission proceeds before chromatin can be cleared from the bridge as in the case of knockdown of Chmp4C in HeLa cells, DNA damage will accumulate over time, causing cell death

and possibly forcing the stem cell to exit the cell cycle rather than trying to reenter. In *Kif20b* mutant brains, we did not see an increase in γ H2aX in the nuclei of NSCs (Little, 2019). However, we have suggestive evidence of DNA damage from RNAseq of the *Kif20b* mutants because DNA repair genes were upregulated (Little, 2019). This suggests that the DNA damage may be subtle or cleared quickly by p53-dependent apoptosis. To try and answer this question, we could perform western blots for the DNA damage proteins that were upregulated from the RNAseq.

The abscission checkpoint being disrupted could also account for the ESCRT recruitment defects we see in the *Kif20b* knockdown HeLa cells. I found that in fixed, unsynchronized HeLa cells without *Kif20b*, fewer midbodies were observed VPS4 accumulation at the central bulge and the constriction site, whereas Anillin is more often detected at the central bulge and constriction sites (Chapter II, (Janisch et al., 2018)). This could mean that the midbody maturation that occurs between Anillin recruitment and abscission happens on a faster time scale. It could also be a symptom of AuroraB dysregulation. The abscission checkpoint is necessary for VPS4 to be kept at the central bulge before being released to the constriction site. Without a normal functioning pathway, VPS4 might be recruited less often to the central bulge and go immediately to the constriction site where abscission occurs. Another hypothesis is that *Kif20b* is responsible for the sequestering of the abscission checkpoint proteins in the dark zone. Since *Kif20b* does move to the constriction site, it would be informative to determine if this is coincidental with VPS4 movement. Therefore, without *Kif20b* present, VPS4 could be released to the constriction site too early. Overall, how the cell responds to faster midbody maturation versus disruption of the abscission checkpoint could be different and result in different phenotypes.

Unlike the PRL-3 knockdown in cysts, we do not see ectopic midbody position in the *Kif20b* mutants but we do see misaligned midbodies to the apical membrane. While we have not observed lagging chromatin in *Kif20b* depleted HeLa cells, we have evidence from RNA sequencing of the *Kif20b* mutants that DNA damage genes are upregulated (Little, 2019). It is essential to compare different causes of faster abscission to eliminate potential protein specific phenotypes versus hallmarks of faster abscission. While we are unable to link faster abscission with cellular defects directly, the *Kif20b* mutant does have fewer neurons produced due to early neurogenesis and cell death ((Janisch et al.,

2013; Little and Dwyer, 2019) **Appendix II**). It is tempting to speculate that faster abscission could be driving these cellular consequences whether directly or indirectly. Recently, duration of abscission has been linked to stemness in mouse embryonic stem cells. These embryonic stem cells were forced to exit pluripotency through a media change. The exit from pluripotency significantly decreased the duration of abscission in these stem cells (Chaigne et al., 2019). Together these data support abscission timing driving cell cycle exit in stem cells, indicating faster abscission may be as detrimental to development as abscission delay.

To address the cell-autonomous consequences of altered abscission, we can use the MADM mice to examine clone size and differentiation in *Kif20b* mutants. By live imaging single cells for abscission duration, then looking at clonal formation, we can determine if the cells that abscise faster are more likely to differentiate or die.

IV. Additional live imaging can elucidate more about the dynamics of NSC abscission.

We have learned a lot from analyzing abscission in neural stem cells at E11.5 and E13.5 using the cortical slab culture method with a membrane-gfp and SiR-Tubulin. However, it would be beneficial to add a later age to confirm our hypothesis that abscission is developmentally regulated. The later age has presented many problems with imaging in the past due to the thickness of the tissue. Therefore, trying to image abscission in slice culture at a later age may be more feasible. As we have learned more, we have more questions about abscission. To address some of these questions, we need different fluorescent markers or other imaging techniques to better answer as outlined below.

a. Timing of nuclear basal migration compared to abscission.

Abscission was shown to complete in G1-phase of the next cell cycle in HeLa and NSC cells ((Gershony et al., 2014; Little, 2019), **Appendix II**). Within G1, the nuclei of neural stem cells begin to migrate basally towards the basal lamina. However, we do not understand the temporal relationship between nuclear envelope reformation, movement of the nuclei basally, and abscission. From cell lines, we know that the nuclear envelope reformation is coordinated with abscission timing (Mackay et al., 2010). We have a

sense from cortical development that the movement of the nuclei is a coordinated event that is essential for the cell cycle of other stem cells to proceed normally. Therefore, it would be interesting to know the temporal relationship between these three critical events. To elucidate this question, we would need live cell markers for nuclei, cell membrane, and the midbody to mark abscission. We would want the cell membrane label to be sporadic to track the thin basal process during all parts of the cell cycle. Additionally, we would need to image the cortex using cross-sections rather than slabs. Together we would be able to determine when within G1 abscission occurs and how long before abscission do nuclei begin to migrate away from the apical membrane.

b. Determine regulation of unilateral and bilateral abscission in NSCs

There is very little known about the dynamics between the first and second abscission. We know from our work in NSCs and in HeLa cells that microtubule severing happens on average 15 minutes after the first (**Chapter II, III**, (Janisch et al., 2018)). This is similar to what has been seen in dissociated MDCK and HeLa cells (Gershony et al., 2017; Guizetti et al., 2011). Previously, microtubules and plasma membrane scission have been shown to be coincident (Steigemann et al., 2009). This suggests that these events are highly coordinated. Recently, one pre-print suggested that plasma membrane scission may be unilateral, but microtubule scission may be bilateral in MDCK cells in an epithelial monolayer, and thus midbody remnants remain tethered by the plasma membrane connection (Casares-Arias et al., 2019). This presents a unique opportunity to try to determine what is happening in NSCs. To address this, we need to image abscission with shorter time intervals and to image with both a microtubule marker and plasma membrane marker that is specific for the midbody. Currently, we do not have the tools to make a mouse with a specific plasma membrane marker for the midbody. With more work on midbody proteins and organization, I am hopeful that in the future, we will be able to find something unique enough about the plasma membrane in midbodies to use as both a pre- and post-abscission marker. An option to mark the post-abscission plasma membrane would be the use of phosphatidylserine, which flips to be exposed extracellularly post-abscission (marked by Annexin V) (Arai et al., 2015). While this does not allow us to see both pre and post-abscission membranes, it does indicate when at least the first abscission is complete. When a membrane marker that is usable for both

pre and post-abscission does become available, we would be able to answer these questions more thoroughly about unilateral and bilateral abscission in NSCs.

c. Apical endfoot junction formation during cytokinesis

During midbody formation, ZO-1 junctions form around the midbody. As discussed in the introduction, apical endfoot inheritance is a controversial cell fate determinant. Not only do we not have a clear understanding of the role junctional proteins play in cell fate, but we do not know the dynamics in which they reestablish during cytokinesis. From our work, we have evidence that apical endfoot size is not altered due to cell fate but rather as a result of cell death in the *Kif20b* mutants. Is junctional formation an event coincidental with abscission, or does it happen before or after abscission? To better understand this, a mouse with an apical membrane marker like ZO-1 fluorescently tagged along with a microtubule marker would be able to expand on this line of inquiry. A mouse is currently commercially available through Jackson Laboratories that expressed RFP-tagged ZO-1. This mouse used in combination with SiR-Tubulin in our live cortical slab preparation could answer questions regarding the junctional formation during cytokinesis. Additionally, ZO-1 endfeet of newly born neurons and IPs would need to be removed from the apical membrane making this a possible neurogenic readout as discussed further in the next section.

The ZO-1 mouse could also help us address the significance of the misaligned midbodies in the *Kif20b* mutant. I could not distinguish misaligned midbodies at the apical membrane with the membrane-GFP because there was no clear marker for the apical membrane. With ZO-1 marking the apical membrane, I would be able to determine how misaligned midbodies form *in vivo* and if the misaligned midbodies abscised faster than aligned midbodies. We do not have a clear understanding of how the misaligned midbodies form and if they abscise faster than aligned midbodies.

We only looked at zona occludin -1 (ZO-1) and F-actin at the apical membrane in this thesis. It would be interesting to look at other junctional proteins like Beta-catenin to determine if junctions are fully reformed post-abscission. Additionally, we could look for cell fate markers like Notch at the apical membrane to determine if there are changes in

distribution that may reflect early neurogenesis that we see in the *Kif20b* mutants (**Appendix II**).

d. Test the hypothesis that NSC abscission duration influences cell fate

A question that has lingered throughout this dissertation is how can we directly connect abscission duration with cell fate outcomes. This is a question that is both exciting as it is daunting. The ideal experiment would include a neuronal-specific protein that localizes to the apical endfoot and turns on within 15 minutes of abscission. This should give us enough temporal resolution to follow the endfoot from formation during cytokinesis to completion of fate decision. At this time, there are fluorescently tagged neuronal-specific proteins, but their temporal component and localization within the apical endfoot are uncertain. One such protein is DCX, and a mouse is commercially available from the Jackson Laboratory (DsRed-DCX Mouse). We could cross this mouse with our GFP-Membrane mouse to outline the daughter endfeet and use SiR-Tubulin to mark midbodies. The experiment would be similar to what we did in Chapter III. The hope would be that the fluorescently labeled DCX would be visible in the apical endfoot within a time frame that is detectable in our current live imaging paradigm. The above ZO-1 experiment may be beneficial if we can see the endfoot being removed from the apical membrane, but again, the coordination between endfoot removal and abscission is unknown.

Dissociated cell culture can offer more opportunities to try to correlate cell fate with abscission duration. Dissociated cortical progenitors from the DCX-DsRed mouse could be plated and incubated with SiR-Tubulin. Traditionally, confocal imaging of single cells would not be practical for abscission timing because of the low rates of NSCs within the cell cycle (Ki67+ cells) at any given time (~12%, **Appendix II**). Therefore, using the Operetta confocal system would be ideal. This would allow us to image an entire 6-well dish at high resolution over many hours in a temperature and CO₂ regulated environment. This would allow us to measure the time to abscission, wait for DCX to turn on, and have confidence as to which pair of daughter cells came from which progenitor. We also have the ideal experiment in which we can perturb abscission in two different directions by imaging NSCs from the *Kif20b* and *Cep55* mutant. This would allow us to correlate abscission duration with different daughter cell fates (death, progenitor (DCX-),

neuron (DCX+)). These proposed experiments would begin to establish cell fate and death outcomes of control NSCs and in the context of abscission mutants.

e. Midbody proteins and microcephaly

Multiple midbody proteins, when lost in the brain, cause varying severities of microcephaly (Kif20b, Cep55, SEPT7, Kif20a, Kif14, Citron Kinase) (Bondeson et al., 2017; Di Cunto et al., 2000; Frosk et al., 2017; Janisch et al., 2013; Li et al., 2016; Little, 2019; Qiu et al., 2019). Currently, we have imaged mouse mutants of Kif20b and Cep55 and found differing abscission and brain phenotypes (**Chapter III, Appendix I**).

Determining if any of these other proteins have consequences for abscission duration helps us to answer bigger picture questions regarding abscission duration and development: Does perturbing abscission in one direction or another have separate or different consequences? Does perturbing abscission in either direction have a cell fate consequence? One significant phenotypic difference between microcephaly mutants with faster abscission compared to other cytokinesis mutants is the lack of binucleate cells and other secondary phenotypes related to changes in nuclear content. Even though faster and longer abscission both have different cellular phenotypes, the common phenotype between them is cell death. Therefore, are the cell death mechanisms the same regardless of abscission duration or is a specific response to downstream consequences.

The simplest way to start interrogating the link between midbody proteins and microcephaly is to analyze cytokinesis phenotypes in fixed tissue. We would want to follow up with the live imaging of these mutants as well. In fixed cortical slabs, we could measure the midbody index (midbodies/apical endfoot). The direction the midbody index changes would give us an indication if abscission is likely to be delayed (increased midbody index) or faster (decreased midbody index). By following up on the fixed data with live imaging of each of these mutants (Kif20a, SEPT7, Kif14, Citron Kinase), we could classify known phenotypes as resulting from defects in cleavage furrowing or abscission. Since all of these mutants produce embryos, a percentage of cell divisions must complete normally. Therefore, perturbations to different aspects of cytokinesis may be subtle. Kif14, Citron Kinase, and SEPT7 all localize to the central spindle than relocated to the central bulge or what will become the midbody remnant. It would be

interesting to look at the midbody remnant distribution in these mutants. Kif20a, like Kif20b, is located on the flanks of the midbody but in a different pattern (Janisch et al., 2018). Comparing these family members could reveal interesting similarities and differences in their roles. Despite these proteins (Kif20a, Kif14, Sept7, Citron Kinase) all being midbody proteins, little work has been done to explore their roles further within the context of NSC divisions and cortical brain development.

f. Determine why abscission is happening faster in Kif20b mutants

Exactly how the loss of Kif20b causes abscission to occur faster remains unknown. We speculate that faster abscission may have to do with looser microtubule bundling, but Kif20b or its cargo could have an unknown role. Some possibilities include 1.) rapid ESCRT recruitment, or Spastin activity, 2.) abscission checkpoint absent or weakened, or 3.) tubulin disassembly is faster, but the membrane is still intact for some time. To address these different possibilities, we would need several experiments as outlined below. 1.) To determine if faster ESCRT recruitment or microtubule disassembly is occurring, we would need live ESCRT, or Spastin constructs to image their recruitment to the midbody. 2.) To analyze the abscission checkpoint, we would need to live image the dynamics of phospho-AuroraB in NSCs. Earlier activation would suggest that the abscission checkpoint is being cleared earlier on and allowing for faster abscission (Petsalaki et al., 2011). 3.) To address the separation of microtubule and membrane scission, we would need to be able to resolve the membrane scission from the microtubule disassembly. To attempt these experiments, we would need to mark the midbody membrane in addition to the microtubules specifically. As previously discussed, Annexin V would be the most useful tool to identify post-abscission midbodies. Adding this marker to our current live imaging conditions would allow us to measure plasma membrane scission in relation to microtubule disassembly. Based on cell line data, we know membrane scission and microtubule scission are happening coincidentally and rely on ESCRT dynamics (Green et al., 2012; Guizetti et al., 2011; Schiel and Prekeris, 2010; Steigemann et al., 2009), but we do not know how they can be separated and the consequences of separating these processes. The above-proposed experiments may begin to answer these questions in cortical NSCs.

g. Test the hypothesis that midbody remnants have a function in the cerebral cortex

Midbody remnant biology is an exciting area of research because of the uncertain role midbody remnants play in the proliferation and fate decisions of stem cells. We have previously shown that midbody remnants appear to be developmentally regulated since there are more present at the apical membrane early in development compared to later in development (**Chapter III**). However, we do not know if midbody remnants are phagocytosed or released into the CSF differently at different ages or how signaling from the midbody remnant can occur. Additionally, we have only looked at NSCs and not IPs. IPs do not have the same polarity to their divisions and are surrounded by migrating neurons, and the cell bodies of NSCs. It is reasonable to speculate that midbody remnant release or engulfment in IPs may be different from NSCs. It would be more challenging to study IP midbody remnants because of the dense SVZ. However, we could try to look for midbody remnants in the SVZ using the MKLP1-GFP mouse. We would be able to count the number of midbody remnants in an area, but we might not be able to determine if the midbody remnants are engulfed or on the surface of the cell.

We need to determine if the midbody remnants are only on the surface of the NSCs or if they are internalized. If they are internalized, how are the midbody remnants phagocytosed? And what cells are doing the phagocytosis – it could be NSCs or microglia. Do midbody remnants persist in the cytoplasm by avoiding lysosomes? Are they immediately degraded? If midbody remnants are only ever on the surface of the cell, are they attached by a plasma membrane tether, adhesion, or receptor? Once this plasma membrane has completed scission, do the remnants get swept away in the CSF? What is the composition of the midbody remnant of NSCs (proteins, RNAs, ribosomes, microtubules, actin)? Do the contents change based on development, and how different are these remnants compared to CHO or HELA or MDCK where proteomes, lipidomes, and RNA sequencing are being actively performed? The list of questions is long, but we have tools available to start answering them.

To better study the composition and activity of midbody remnants, we need to isolate them more efficiently. We could try to FACS sort midbody remnants from the CSF or cultured NSCs from MKLP1-GFP mice (recently done in HeLa cells, (Addi et al., 2020)).

Once isolated, midbody remnants could be sent for proteomics, lipidomics, and RNA sequencing and compare with existing literature from cell lines. One way to test the direct role of midbody remnants is to isolate midbodies from older embryonic age and “feed” them to NSCs in culture or cultured cortical slabs that are younger and vice versa. We would then test for changes in the type of cells produced in these divisions. Similar experiments have been performed for CSF, and the results are striking that the developmental age of the CSF can alter the output of NSCs (Chau et al., 2015). Midbody remnants may act on cells from the apical membrane to affect polarity, spindle orientation, or even ciliogenesis, as suggested in other cell types (Bernabe-Rubio et al., 2016; Pollarolo et al., 2011; Singh and Pohl, 2014a). Therefore, we should look for changes in polarity in NSC cultures, as well as changes in spindle orientation and the number of cilia on slabs “fed” with additional midbody remnants.

To isolate midbodies from the CSF might prove to be difficult if they are adhered to the apical surface. One group has suggested they can disrupt the interaction between the midbody remnant and the surface of the HeLa cell using EDTA (Addi et al., 2020; Crowell et al., 2014). If this holds true for NSCs, we may need to wash cultures or brains with EDTA to release the midbody remnants and then do the FACS sorting. I have previously tried to wash midbody remnants off of cortical slabs with EDTA and did not have success. This is worth repeating using the new methods outlined by the Echard lab (Addi et al., 2020).

Ultimately, we would want to create an imaging paradigm where midbody remnants are observable over long periods. Ideally, we would want to image them being engulfed at the apical membrane or floating away into the CSF. We also want to determine which cell type is responsible for the engulfment of midbody remnants, NSCs, or microglia. We could do this by crossing the MKLP1-GFP mouse with the MTMG mouse (Tomato or GFP targeted to the membrane). This would give us a red plasma membrane and a green midbody bulge/remnant. To separate intact midbodies from midbody remnants, we would use SiR-Tubulin. For separating internalized from external midbody remnants, we would use a live lysosome marker or using fixed MKLP1-GFP cortical slabs stained for a lysosome marker to determine if remnants are being degraded. With the MKLP1-GFP mouse, we could stain for NSC and microglia markers to determine which cells at the apical membrane are most associated with the midbody remnants. It is possible that

as more microglia migrate to the cerebral cortex, they become a part of the clearance mechanism of the midbody remnants driving the decrease in remnants that we see at E15.5. These proposed experiments would begin to address the behavior of midbody remnants at the apical membrane.

Appendix I: Neural stem cell abscission in the absence of Cep55

Abstract

Proper brain growth involves elaborate coordination between neural stem cells to produce billions of neurons during the correct developmental window. When defects arise in these events brain malformations can occur. In the case of human disease, a lethal mutation in Cep55 causes a severe brain malformation. Cep55 is a midbody protein and in cell lines has been shown to be essential for cytokinesis. Here, we investigate the loss of Cep55 in a mouse mutant. This allows us to dissect Cep55's role in abscission within the context of brain growth. We hypothesize that Cep55 is important for maintaining regulated cytokinesis but is not essential for cytokinesis to complete in the mammalian brain. In this appendix, we found that Cep55 mutant brains have structural defects at the apical membrane and disruption in regulation of neural stem cell midbody remnant disposal and delays in neural stem cell abscission.

Results

Mutations in abscission proteins can elucidate critical roles for this cellular process in the development of the neuronal epithelium. We previously described normal abscission in the developing cortex and the role of midbody protein Kif20b in abscission (**Chapters II, III, Appendix II**). In this appendix, we will focus on the role of another midbody protein, Cep55. Cep55 is considered the master regulator of abscission, as discussed previously in the introduction. In numerous cell line papers, Cep55 is essential for the recruitment of ESCRT proteins to the midbody and the completion of abscission (Carlton et al., 2008; Morita et al., 2007; Zhao et al., 2006). Cep55 arrives after the establishment of the midbody and is only visible in late midbodies of neural stem cells (NSCs) and mouse embryonic fibroblasts (MEFs) (Bastos and Barr, 2010; Little, 2019; Zhao et al., 2006). Recently, cases of severe brain malformations in humans have been linked to mutations in Cep55 (Bondeson et al., 2017; Frosk et al., 2017).

We have obtained a mouse mutant for Cep55 from the Canadian Mouse Mutant Repository. This mouse mutant is missing 601 base pairs from the *Cep55* gene, removing all of exon 6. Exon 6 of Cep55 encodes for the binding site to MKLP, which is

responsible for the localization to the midbody. This large deletion results in severe microcephaly and is lethal by weaning age (Little, 2019). Truncated mRNA is detectable in the *Cep55* mutant but no detectable Cep55 protein in the midbodies of *Cep55* mutant MEFs and NSCs (Little, 2019). The *Cep55* mutant has elevated cell death as early as embryonic day 12.5 (E12.5), increased binucleate cells at E15.5, and decreased neuron production. We hypothesize that cell death, binucleates, and loss of neurons are consequences of disruption in the late stages of cytokinesis. In this appendix, we further explore the *Cep55* mutant by analyzing gross morphology, the structure of the apical membrane, and molecular mechanisms of abscission.

Gross Morphology of the *Cep55* Mutants

Cep55 mutants have normal eye size

We have already shown that the overall brain of *Cep55* mutants is smaller at post-natal day 0 with cortical thickness reduced as early as E12.5 (Little, 2019). To determine if other structures derived from the diencephalon are reduced in size in the *Cep55* mutants, we decided to look at the eye. Part of our motivation to look at the eye is due to the striking no eye or significantly reduced eye size in the *Kif20b* mutant, another abscission mutant (Dwyer et al., 2011; Janisch et al., 2013). Additionally, there is evidence from zebrafish that the loss of Cep55 causes increased cell death in the eye and reduction in retina size (Jeffery et al., 2015; Yanagi et al., 2019). Previously, we found no elevated cell death in the retina at E10.5 or noticeable gross anatomical differences in the mouse *Cep55* mutants (Little, 2019). To quantitatively address this, we measured the length and the width of the eye both within the head and removed from the head at post-natal day 1 (**Figure App 1-1A, A'**). The diameter of the eye was not different between control and *Cep55* mutant mice at post-natal day 1 when measured out of the head, although there was a trend for the *Cep55* mutant to be slightly smaller (**Figure App 1-1B**). Importantly, when the diameter was normalized to the size of the head, there was no difference between control and *Cep55* mutants eye size, suggesting any subtle decrease in size is due to the smaller head size (**Figure App 1-1C**). The loss of Cep55 seems to be more detrimental to the mammalian brain than other parts of the body. What role Cep55 has in forebrain NSCs that is unique from other neural stem cell

types such as in the retina, is an intriguing question and one that is still under active study.

Cep55 mutants have normal cell cycle exit at E12.5

Defects in neurogenesis can also arise from the loss of NSCs due to cell death and premature cell cycle exit, which decreases the output potential of these stem cells. Previously, we found that the *Cep55* mutants have decreased production in neurons most likely caused by the high levels of cell death through-out development (Little, 2019). We have seen both the cell death and early cell cycle exit in another abscission mutant, *Kif20b*, which is described in more detail in Chapter III and Appendix II. To measure cell cycle exit *in vivo*, we injected BrdU into pregnant dams at E11.5. We sacrificed the dams at E12.5. Brains were collected, fixed, and then sectioned on the cryostat. Antigen retrieval was used on the sections before immunostaining for BrdU and Beta-III tubulin (neuronal marker). Cells that were in S-phase at the time of BrdU injection should have incorporated BrdU into their DNA. Therefore, any cell that had BrdU in the nucleus and Beta-III tubulin staining was marked as exiting the cell cycle (**Figure App 1-2A**). In the *Cep55* mutants, there was no change in cell cycle exit, and the thin neuronal layer or preplate at E12.5 was not different in thickness proportional to the cortical thickness (**Figure App 1-2B, C**). One reason we might not be able to detect early cell cycle exit is the massive cell death that occurs in the cortex by E10.5. This experiment would be worth repeating in the *Cep55/p53* double mutants before completing ruling out cell cycle exit as a contributor to the microcephaly. Although, we can say with confidence that the reduction in neuron production is primarily due to cell death in the *Cep55* mutants.

Structure of the Apical Membrane

There is a decrease in the number of apical endfeet and increased midbody index at later developmental time points.

Cytokinesis happens at the apical membrane; therefore, we wanted to determine if the loss of *Cep55* disrupts this membrane. We found a decrease in the number of E14.5 apical endfeet in the *Cep55* mutant but no change in endfoot number at E12.5 (**Figure**

App 1-3A, C, F). The decrease in endfoot number is likely due to the large endfeet present at the apical membrane and cell death. The hypothesis is that the large endfeet are binucleate neural stem cells, which would accumulate over development as cytokinesis fails. The E14.5 mitotic index at the apical membrane was not altered, most likely owing to Cep55's specific role in late cytokinesis (**Figure App 1-3A, D**). There was a significant increase in the E14.5 apical midbody index and a trend for an increase at E12.5, suggesting that cytokinesis could be delayed (**Figure App 1-3 B, E, G**).

Surprisingly, we found that the structure of the *Cep55* mutant midbodies in the apical membrane had structural changes that were different from cell culture. The midbodies were shorter and had no change in width (**Figure App 1-4 A-C**). Interestingly, we found 2.4% of *Cep55* mutant midbodies (6 of 249) were tripartite compared to 0.41% of control midbodies (1 of 246). This suggests that NCS with odd number of centrosomes are able to divide and form a midbody in the *Cep55* mutant. We also looked at the midbody structure in MEFs, and there was no striking change (**Figure App 1-4 D-F**). These data suggest that without Cep55, NSC midbodies have a slight structural abnormality, and the slow accumulation of cytokinetic errors may lead to cell death and binucleate cell accumulation.

Cep55 mutants have increased midbody remnants at the apical membrane

Cep55 localizes to the midbody bulge of late midbodies and persists in the midbody remnant once abscission is complete (Little, 2019; Zhao et al., 2006). Therefore, we investigated whether midbody remnant association with the apical membrane was disrupted. There is a significant increase in midbody remnants per midbody at E12.5 but only a trend at E14.5 (**Figure App 1-5 A, B**). To have a better sense of the number of midbody remnants persisting at the apical membrane, we looked at midbody remnant/endfoot. There is a drastic increase in the number of midbody remnants per endfoot at E12.5 and E14.5 in the *Cep55* mutants (**Figure App 1-5C**). These data suggest that disposal mechanisms for midbody remnants are disturbed in *Cep55* mutants. Of interest is that the developmental regulation of midbody disposal still seems to be intact in the *Cep55* mutants because there is a decrease in the number of midbody remnants at the apical membrane between E12.5 and E14.5 (**Figure App 1-5C**). How Cep55 influences the disposal of midbody remnants remains a mystery. Cep55 may be a crucial part of engulfment of midbody remnants, or there are fewer bilateral

abscissions in the *Cep55* mutant brains tethering the remnants to the apical membrane. We need further investigation of the role *Cep55* plays in the midbody remnant and the remnants association with the apical membrane.

Cep55 mutant NSCs have defects in cilia shape

Cep55 is named centrosome protein of 55 kilodaltons and has been found in the centrosomes of HeLa cells (Fabbro et al., 2005). Our lab and others have looked for *Cep55* in centrosomes of HeLa cells, MEFs and NSCs and have not found localization (unpublished Dwyer lab, (Zhao et al., 2006)). Papers on the human-associated diseases have suggested this mutation could be classified as a ciliopathy based on indications like cystic kidneys (Bondeson et al., 2017; Frosk et al., 2017). Therefore, we wanted to investigate ciliogenesis during *Cep55* mutant NSC cell division. The cilium is positioned at the apical side of the NSC so it can sense extracellular signals like sonic-hedgehog within the ventricle. Before M-phase, the cilia needs to be disassembled to allow the centrosomes to be used for the formation of spindle poles (Farkas and Huttner, 2008). Therefore, cilia disassembly and assembly is an active part of the cell cycle and development and maintenance of the epithelium. We hypothesize that cilia formation and structure are intact in the *Cep55* mutants. To investigate cilia in the developing cerebral cortex, we used cortical slab preparations to visualize the apical membrane and stained for cilia protein ARL13b (Proteintech Rabbit 17711-1-AP 1:100). The apical membrane of the *Cep55* mutant looked indistinguishable from controls in coronal sections suggesting there is no gross defect in ciliogenesis (**Figure App 1-6A**).

To determine if each cilium was associated with one endfoot, we turned to the cortical slab preparation (**Figure App 1-6B**). We first measured the number of apical endfeet that had a cilium at both E12.5 and E14.5. There was a slight decrease in the percent of endfeet with a cilium in the *Cep55* mutants at E12.5 (**Figure App 1-6C**). Additionally, there is a trend at both E12.5 and E14.5 for there to be more endfeet with multiple cilia (**Figure App 1-6D**). Having multiple cilia is often a sign of binucleate cells because there is an abnormal number of centrosomes. We can also measure the cilia length at both E12.5 and E14.5. There is a wide distribution of cilia length in the controls at E12.5 and E14.5 (**Figure App 1-6E, black bars**). The median at E14.5 was significantly increased, the *Cep55* mutant median is 1.3 μ m and the median in control cilia is 1.1 μ m, a 18%

increase, suggesting that more cilia are longer in the E14.5 *Cep55* mutants (**Figure App 1-6E, white bars**). Since we saw large apical endfeet at E14.5, we wanted to know if the length of the cilium was correlated with apical endfoot size. We found single and multi-ciliated cells endfoot size was correlated with cilia length at E14.5 in the *Cep55* mutants (**Figure App 1-7A, B**). These correlations support a hypothesis that an increase in cilia length may be a secondary phenotype to perturbed cell cycle length due to defects in abscission or increased DNA content. Increase in cilia may also be promoted by increased midbody remnants on the surface of the apical membrane. As mentioned in the introduction midbody remnants have been proposed to give membrane to the centrosome and this is essential for cilia outgrowth in MDCK cells (Bernabé-Rubio et al., 2019). It is possible having disturbed midbody remnant disposal could cause an increase in midbody remnants available to promote ciliogenesis.

Molecular Mechanisms of Abscission

ESCRT recruitment is reduced but not absent in Cep55 mutant MEFs and NSCs

Cep55 recruits ESCRTs in a stereotyped fashion, and this has been well documented in cell lines (Morita et al., 2007). Since ESCRTs are essential for abscission in mammalian cells, we hypothesized that recruitment would still occur without *Cep55*. We chose to look at two of the direct proteins recruited by *Cep55*: TSG101 and ALIX. TSG101 and ALIX midbody localization are both decreased in MEFs and NSC cultures (**Figure App 1-8A-D**). We also looked at a downstream target *Chmp2a* in MEFs (antibody did not work well in NSCs), which was decreased but not as significantly as TSG101 and ALIX. Another measurement of midbody maturation, or abscission progression, is the formation of constriction sites. Constriction sites are where ESCRT proteins re-localize to promote membrane scission and the removal of microtubules allowing abscission to occur. In the *Cep55* mutant, there is no difference in the percentage of MEFs with a constriction site compared to the controls. A midbody that has both a constriction site and localized ESCRT is decreased in the *Cep55* mutant. These data indicate that constriction sites form independently of *Cep55* recruitment of TSG101 and ALIX. We did not measure constriction sites in the NSC cultures, but it could be done since the NSCs were stained with both Aurora B and Tubulin. The question that remains is what recruits the ESCRT instead of *Cep55*. The most obvious candidate is MKLP1/Kif23, which is

responsible for recruiting Cep55 to the midbody central bulge, and believed to be what recruits the ESCRTs in non-mammalian cells (Lie-Jensen et al., 2019; Zhao et al., 2006). Evidence from RNAseq of the *Cep55* mutant shows no upregulation of MKLP1 mRNA, but it could still recruit ESCRTs in place of Cep55. In support of alternative pathways for ESCRT recruitment outside of Cep55 or MKLP1, is evident when you knockdown those proteins in mammalian cells or fly cells, respectively, and some low level of recruitment of ESCRTs persist. In knockdown of Cep55 in HeLa cells, ALIX recruitment is reduced to 10% of midbodies from almost 50% in controls and VPS4 recruitment was reduced to 3% compared to almost 40% in controls (Morita et al., 2007). The reduction in ALIX in *Cep55* mutant MEFs is not quite as severe as in Cep55 knockdown HeLa cells, the reduction is by 80% in HeLa cells and 60% in MEFs. In *Drosophila*, *D.mel2* cells, when MKLP1/Pav was knocked down there was a significant reduction in recruitment as measured by intensity of ALIX (Lie-Jensen et al., 2019).

Abscission kinetics of Cep55 mutant NSCs are perturbed

Using siRNA knockdown, Zhao et al 06 found that more than 90% of Cep55-depleted HeLa cells failed to complete abscission (Zhao et al., 2006). This does not appear to be the case in this *Cep55^{em1(IMPC)Tcp}* mutant with a deletion of 602 base pairs which encompasses the entire exon 6, or there would be early embryonic lethality. Abscission must be successful in the majority of cells. However, we have evidence from the increased midbody index at the apical membrane and the reduced recruitment of ESCRTs and the increased midbody remnants at the apical membrane that abscission may be delayed. Therefore, we wanted to investigate the dynamics of abscission in E13.5 NSCs. To do this, we used the same methodology outlined in Chapter III for imaging NSCs live within cortical slabs, that is membrane-gfp and SiR-tubulin to label microtubules, and using microtubule disassembly to score abscission timing.

The first noticeable difference between control and *Cep55* mutant NSCs were the tripolar spindles in 9% (6 out of 66 NSCs observed in mitosis) of the *Cep55* mutant NSCs (**Figure App 1-9A**). These likely resulted from failed cell divisions in the previous cell cycle causing supernumerary centrosomes and a tripolar mitotic spindle. Of these 6 NSCs, four went on to form a tripartite midbody and have microtubule disassembly taking anywhere from 15 minutes to 315 minutes from midbody formation, one moved off

the screen, and one regressed. Regression was defined as a furrow began to descend apically but was not completed, no midbody was formed, and the furrow disappeared.

Of the NSCs that had bipolar spindles, 3 *Cep55* mutant NSCs regressed compared to 0 in the controls. Two of the NSCs never formed a midbody and only had observable membrane regression after partial furrow ingression. One of the NSCs tried to form a midbody and had both membrane regression and microtubule disassembly. This early membrane regression was slightly surprising because *Cep55* is not essential for midbody formation in cell lines; instead is essential in the maintenance of the midbody. While this regression only occurred 4.5% of the NSCs, it is an indication of what might be taking place in previous divisions to cause 9% tripolar cells (**Figure App 1-9B**). It would be interesting to compare this to a later age since the number of these NSCs with increased nuclear content, and an odd number of centrosomes should increase.

The vast majority (93%) of *Cep55* mutant NSCs were bipolar and able to complete abscission. These mutant NSCs, on average, have a slight but significant delay to the first abscission (delay of 16.5 minutes, **Figure App 1-10B**). Eighty percent of both control and *Cep55* mutants have observable second abscissions (**Figure App 1-10D**). The time to second abscission is increased in the *Cep55* mutants, and is significant (**Figure App 1-10C**). The cumulative frequency plots emphasize the delayed abscission kinetics in the *Cep55* mutant NSCs (**Figure App 1-10 E, F**). Interestingly, the time between the first and second abscission in the *Cep55* mutant was 15 minutes faster than controls (**Figure 1-10 G**). We hypothesize that abscission machinery is able to assemble on both midbody flanks concurrently, allowing the second abscission to complete closer to the first in the case of the *Cep55* mutants.

Overall, the phenotypes observed in the live movies are mild compared to the cell line knockdown experiments. However, these results make sense within the context of the *Cep55* mutant brain. Small changes to NSC proliferation over time can compound to cause massive amounts of binucleate cells and cell death, contributing to the small brain phenotype. Many questions remain about *Cep55*'s role in NSC abscission. 1.) Do *Cep55* mutant cells that take longer to abscise or regress go on to die? During these movies, there was no detectable cell death because it is likely a process turned on hours after the cell has completed the defective cell division. Being able to image longer with a cell

death marker could help to answer this question. 2.) Is membrane scission uncoupled from microtubule disassembly in *Cep55* mutants? These movies measure microtubule disassembly as a readout for abscission. It is possible that membrane severing is uncoupled from microtubule severing, and membrane scission is delayed even further in *Cep55* mutants. One possibility is that microtubule severing completes after a delay, whereas membrane scission only completes on one side, leading to increased midbody remnants at the apical membrane, as discussed previously. Having a specific marker for the midbody plasma membrane would be helpful for better characterizing membrane scission and the limited regression we did observe.

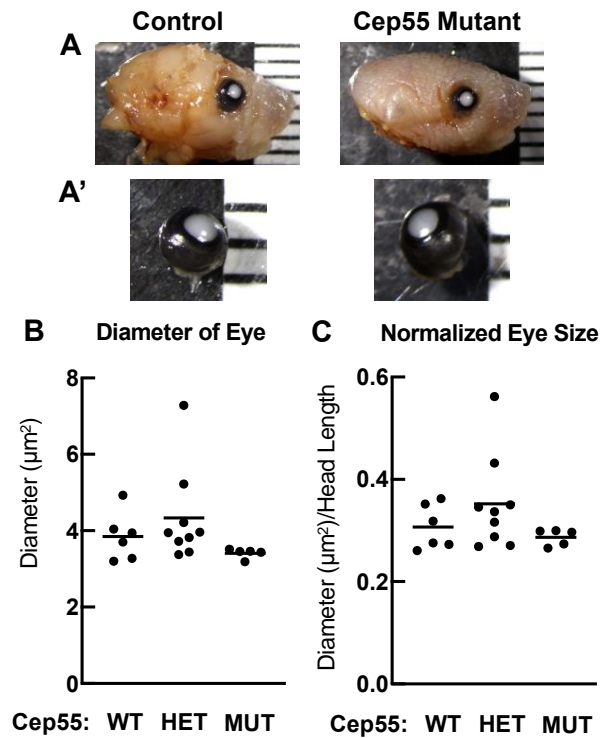


Figure App 1-1: Cep55 mutant eyes are similar in size to controls

(A-A') Examples of post natal day 1 Control and Cep55 mutant eyes in the head (A) and removed (A') from the head. (B) Measurements of the eyes removed from the head show a trend for Cep55 mutants to be slightly smaller but there is no significant difference. (C) Normalizing the diameter to the length of the head showed no change between control and Cep55 mutants. WT n= 6, Het n=9, Cep55 mutant n=5 B-E: ANOVA: n.s.

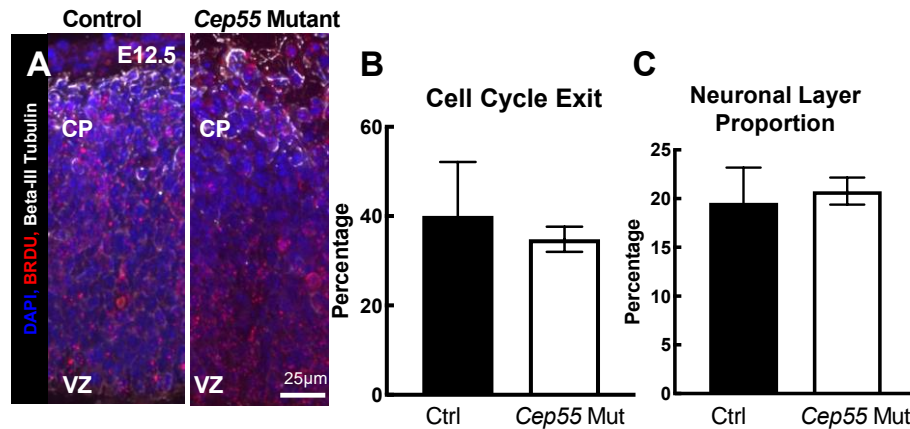


Figure App 1-2: *Cep55* mutants have a normal proportion of NSCs exiting the cell cycle at E12.5

(A) Example E12.5 cortical sections injected with Brdu 12 hours before sacrifice then fixed and immunostained for Brdu and Beta III tubulin.

(B) There is no change in cell cycle exit (BrdU+Beta III tubulin+/ Brdu+ cells)

(C) The thickness of the neuronal layer to the cortex is not different in the *Cep55* mutants. B, C N= 3 controls and 3 *Cep55* mutants. T-test for B,C

There is no difference in the number of Brdu+ Beta-III Tubulin + cells/ Brdu+ cells between control and mutant suggesting that cell cycle exit is similar in control and mutant brains. This translates to a similar amount of neurons produced at E12.5.

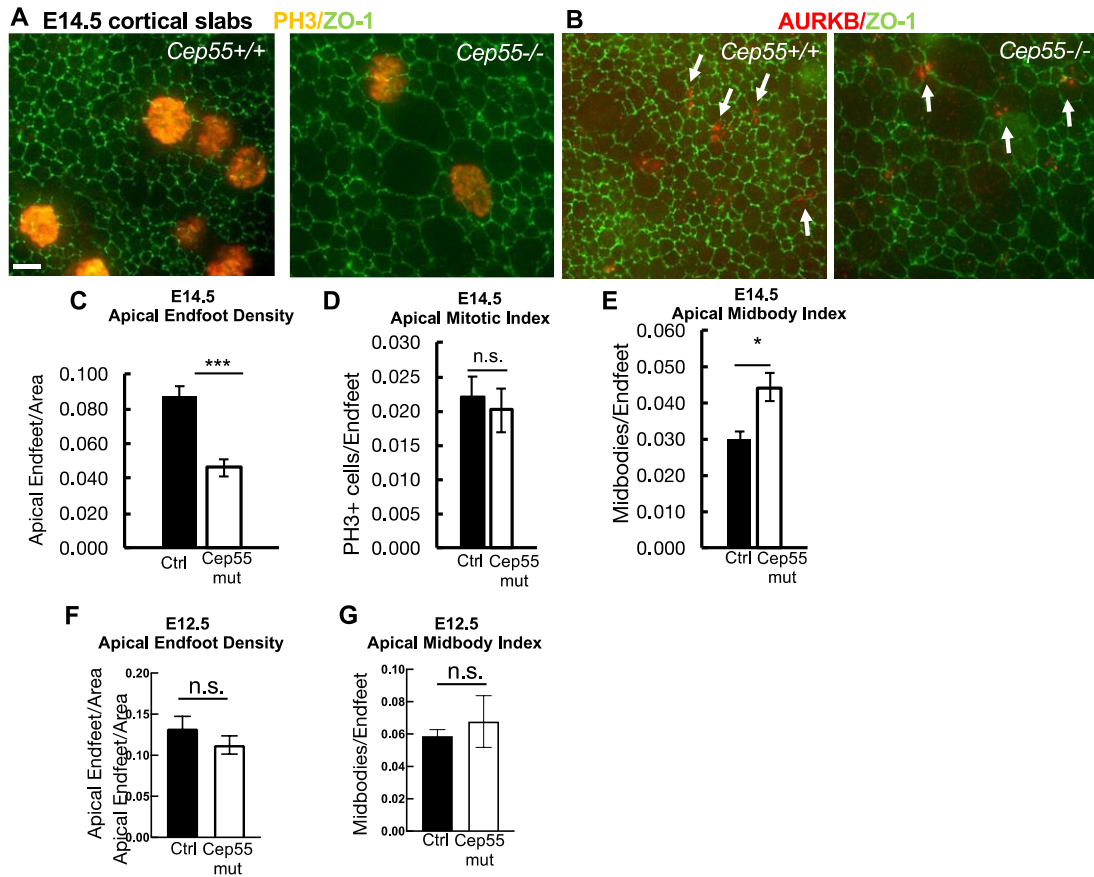


Figure App 1-3: Cep55 mutation results in an increased midbody index in apical NSCs
(A-B) E14.5 cortical slabs were immunostained for Zona-occluden-1 (Zo-1, apical junctions), PH3 (mitotic cells), and AuroraB (midbodies). **(C)** There is a significant decrease in the number of endfeet in the E14.5 Cep55 mutant. **(D)** There is no change in the number of mitotic cells per endfoot, **(E)** but there is an increase in midbodies per endfeet suggesting defects in cytokinesis at E14.5. **(F)** There is no change in the apical endfoot density or apical midbody index **(G)** at E12.5. N for C = 6 slabs, 6 brains wild type, 7 slabs, 6 brains Cep55 mutant N for D = 4 slabs, 4 brains wildtype and 5 slabs, 6 brains Cep55 mutant. N for E = 5 slabs, 5 brains wild type and 5 slabs, 5 brains Cep55 mutant. N for F and G = 4 slabs, 4 brains for both control and Cep55 mutant. Scale bars: A: 2 μ m; n.s., not significant, * $p < 0.05$; ** $p < 0.01$; *** $p < 0.001$. C-G: t-test.

Figure App 1-4: Cep55 mutant midbodies are shorter in NSCs and thinner in MEFs

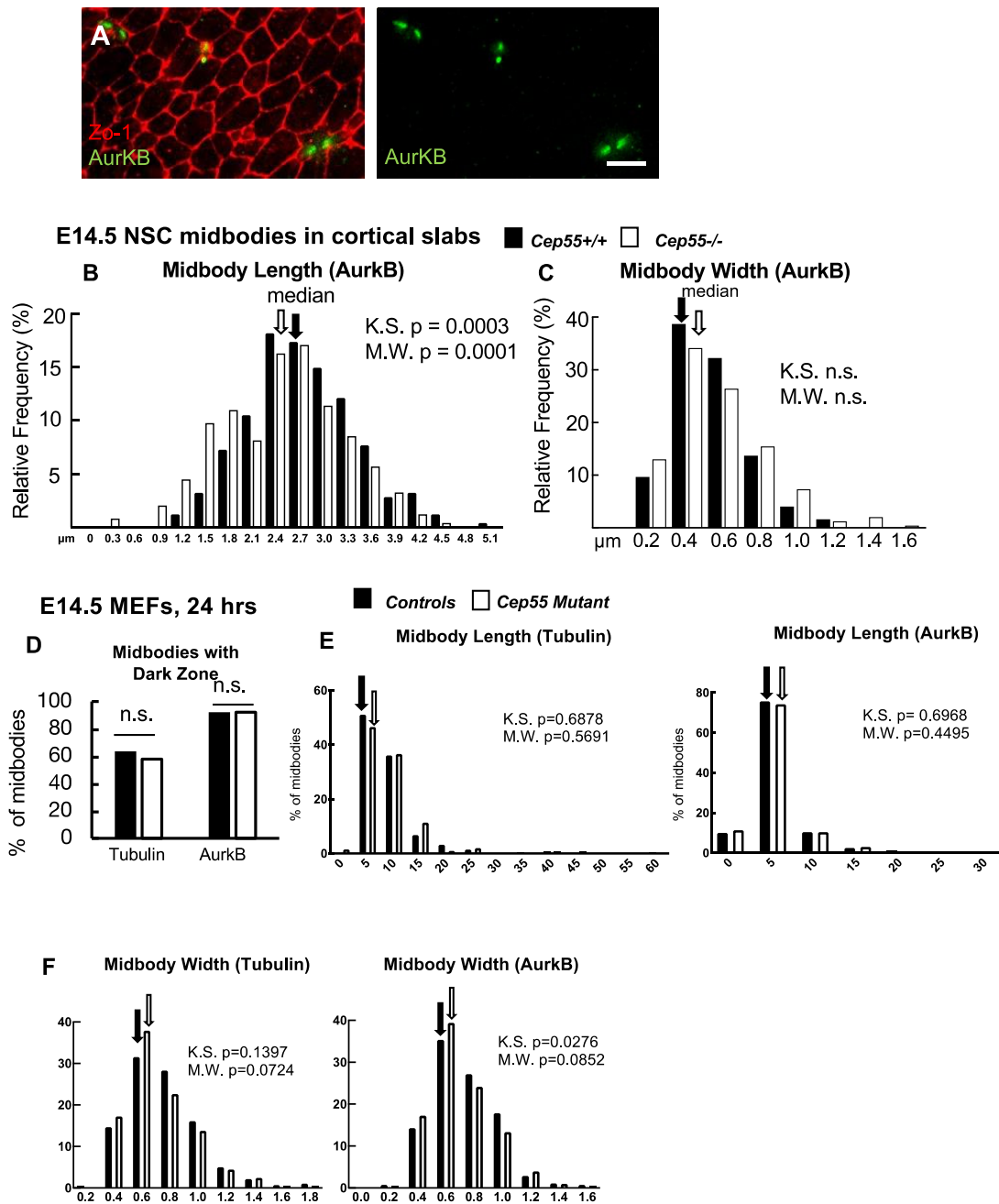


Figure App 1-4: Cep55 mutant midbodies are shorter in NSCs and thinner in MEFs

(A) Representative images of E14.5 cortical slab immunostained for Zo-1 (apical junctions_ and AurKB (midbody flanks). Scalebar 5 μ m. **(B-C)** NSC midbodies in E14.5 Cep55 mutant cortical slabs are shorter **(B)**, but have normal width **(C)**. Length and width determined by Aurora kinase B (AurKB) immunolabeling. Medians: A: Cep55+/+ 2.71; Cep55 mutant 2.48 μ m. B: both 0.51 μ m. For images, see Figure 6. **(D)** Midbodies in E14.5 Cep55 mutant mouse embryonic fibroblast (MEF) cells cultured for 24 hrs have a detectable dark zone (defined as absence of immunostaining) in a similar percentage of midbodies as control cells. **(E-F)** Midbodies in E14.5 Cep55 mutant mouse embryonic fibroblast (MEF) cells cultured for 24 hrs have normal length distribution **(E)**, but the width is slightly shifted towards thinner as determined by AurKB immunolabeling **(F)**. Medians: E (Tubulin) control 7.46; Cep55 Mutant 7.874 (AurKB) control 3.923; Cep55 Mutant 4.414. (F) (Tubulin) Control 0.733; Cep55 Mutant 0.66; (AurKB) Control 0.692; Cep55 Mutant 0.665. For images, see Figure 8. N for (B-C) = 248 control and 246 mutant midbodies; for (D) = 402 control and 366 mutant midbodies; for (E-F) = 280 control and 202 mutant midbodies. n.s., not significant, * $p < 0.05$. K.S., Kolmogorov-Smirnov test; M.W., Mann-Whitney test. C-E, t-test.

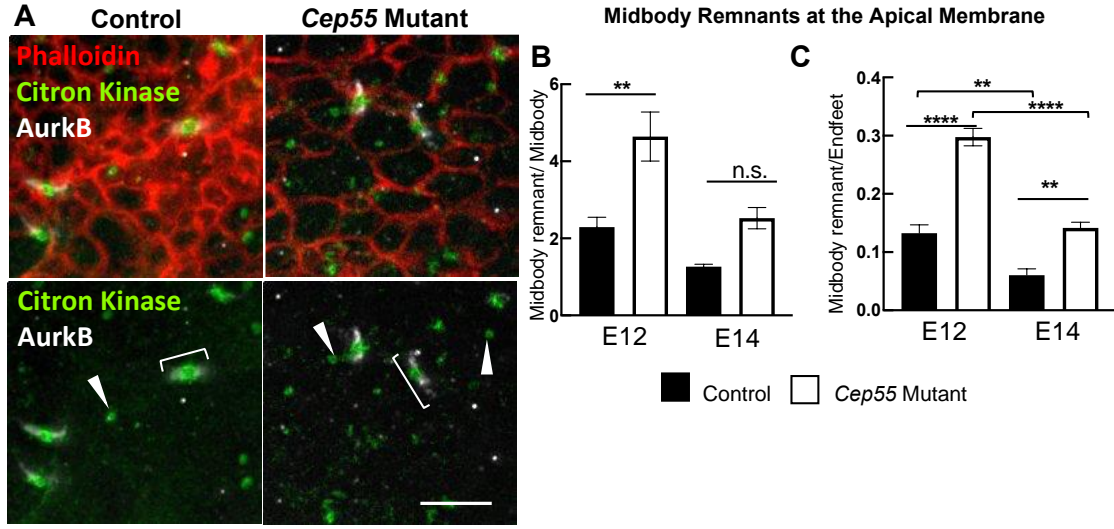


Figure App 1-5: Midbody Remnants are increased at the apical membrane in Cep55 mutants
(A) E14 slabs immunostained for apical membrane (actin, phalloidin), AurkB (midbody flanks) and citron kinase (midbody buldge/midbody remnant). **(B)** Midbody remnants per midbody is increased at E12 in the Cep55 mutants. **(C)** At E12 and E14 there is increased midbody remnants per apical endfeet. E12 and E14 n = 4 slabs for control and Cep55 mutant. Controls for E12 are all Hets. Controls for E14 2 Hets, 2 WT.
 *p<0.05, **p<0.01, ***p<0.001, ****p<0.0001, n.s. not significant B, C ANOVA Scale bar is 5µm.

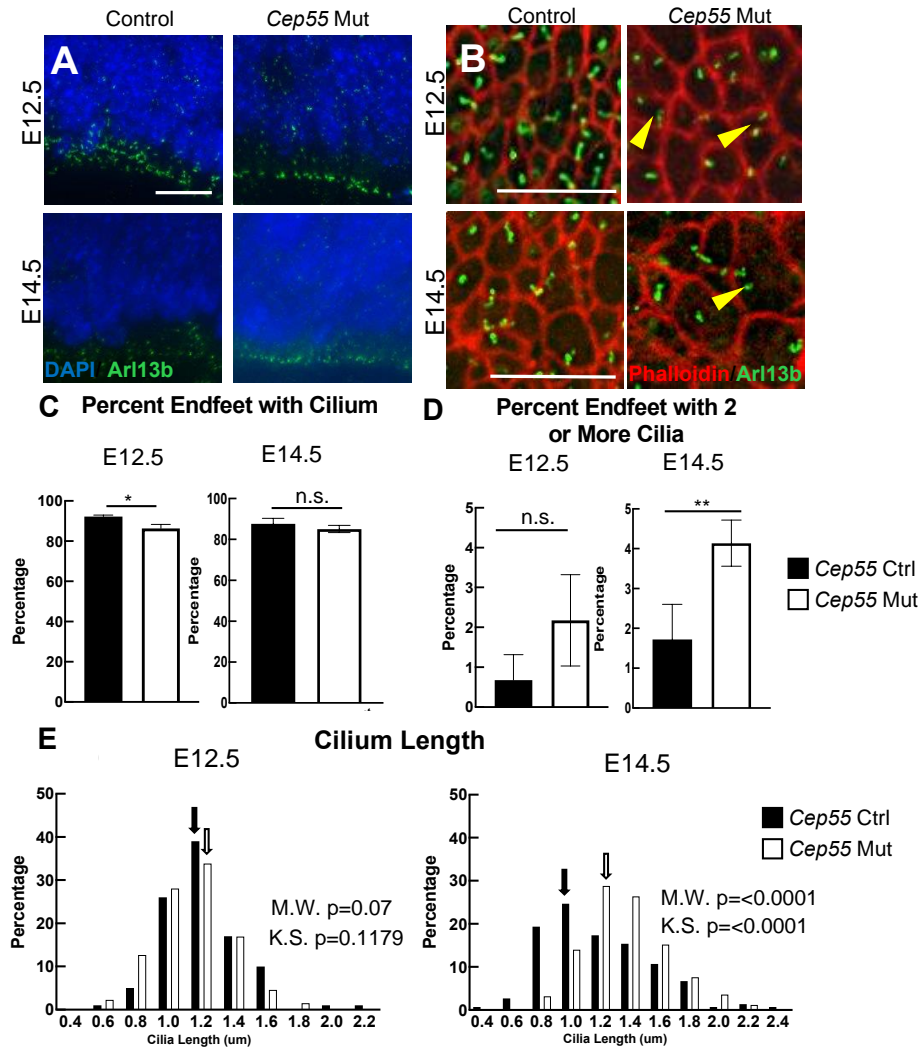


Figure App 1-6: Increase in multiciliated NSCs and longer cilia at later developmental stage

(A) Cortical sections immunostained with DAPI and cilia marker Arl13b. (B) Cortical slabs immunostained with Phalloidin (actin, endfoot marker) and Arl13b (cilia). Most endfeet contain a single cilium but some endfeet have multiple cilia (yellow arrows). (C) Quantification of cilia containing apical endfeet at E12.5 and E14.5. (D) Quantification of apical endfeet with 2 or more cilia at E12.5 and E14.5. (E) The distribution of cilia length was similar between control and *Cep55* mutant at E12.5 and significantly shifted to be longer at E14.5. N= endfeet For E12.5, n=2470 control (2 brains (1 WT, 1 Het)) and 3477 *Cep55* mutant (5 brains). For E14.5, n=2292 control (1 WT, 2 Het brains) and 2270 *Cep55* mutant (5 brains). * not significant, * p < 0.05; ** p < 0.01: Fisher's exact test in C and D; Kolmogorov-Smirnov (K.S.) and Mann-Whitney (M.W.) tests for E. Scale bars, 10 μm.

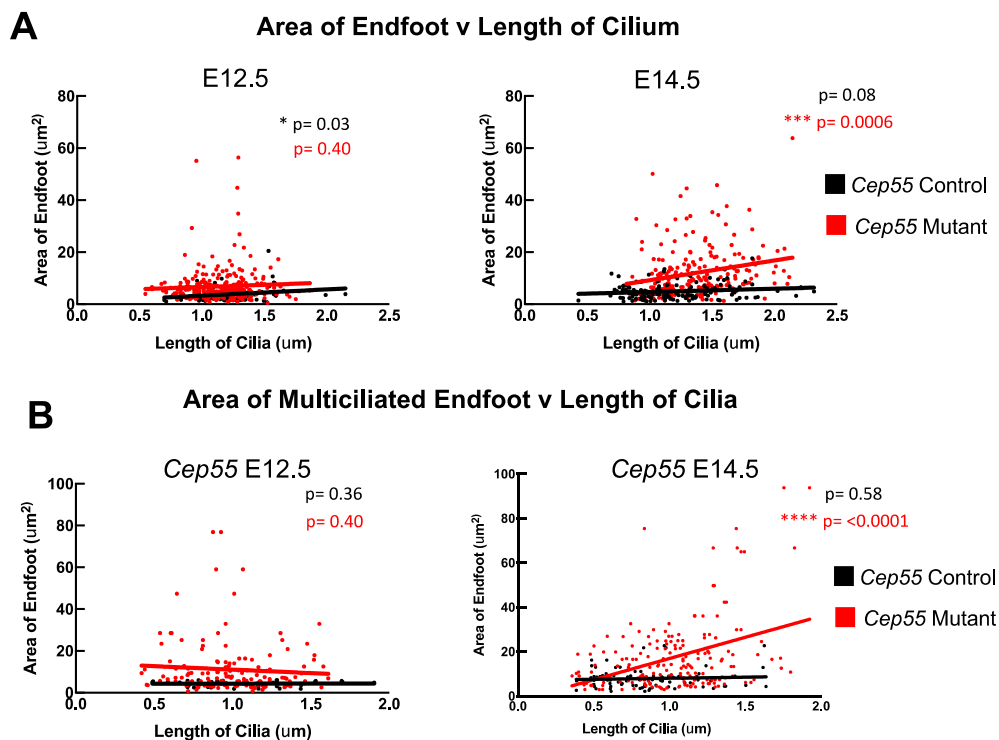


Figure App 1-7: Cilium length is correlated with endfoot size in *Cep55* Mutants during later developmental stages

(A) Correlation analysis shows that area of apical endfoot is correlated in controls during early development but not later development. Additionally, mutant endfoot size is greatly correlated with cilium length at E14.5

(B) Correlation analysis of the multiciliated endfeet shows a strong positive correlation between endfoot size and cilium length. This is consistent with a binucleate cell that would have a larger cell size, longer cell cycle, and longer cilium.

N= endfeet For E12.5, n =2470 control (2 brains (1 WT, 1 Het)) and 3477 *Cep55* mutant (5 brains). For E14.5, n=2292 control (1 WT, 2 Het brains) and 2270 *Cep55* mutant (5 brains). * not significant, * $p < 0.05$; ** $p < 0.01$; *** $p < 0.001$; **** $p < 0.0001$: Pearson Correlation test for A,B.

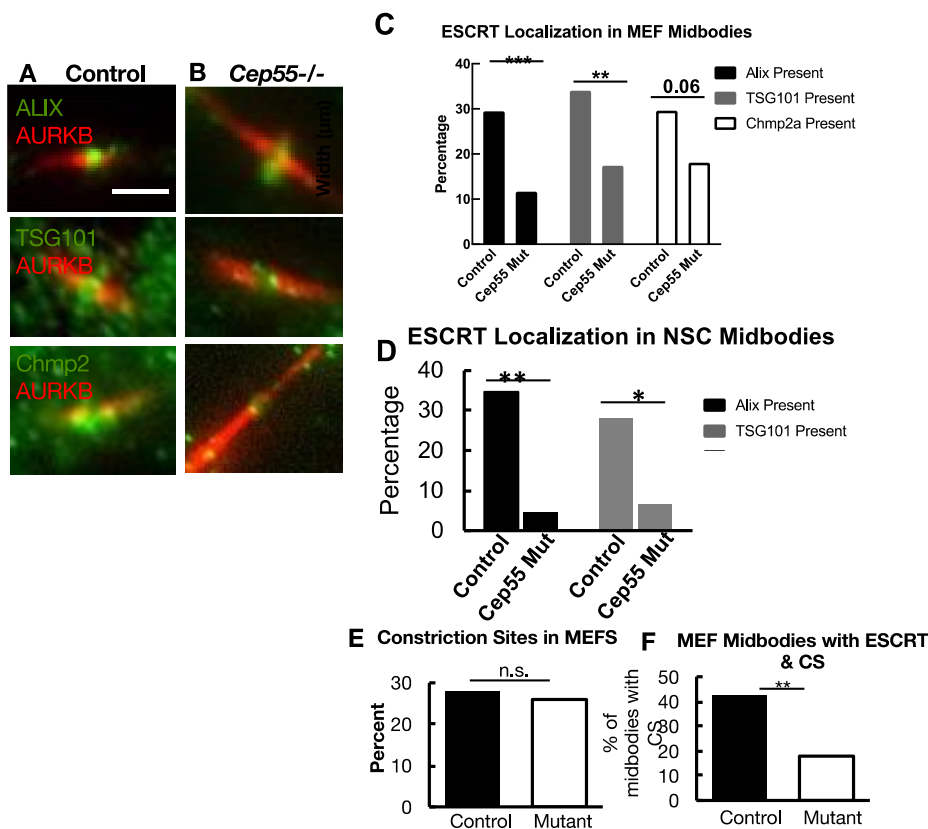
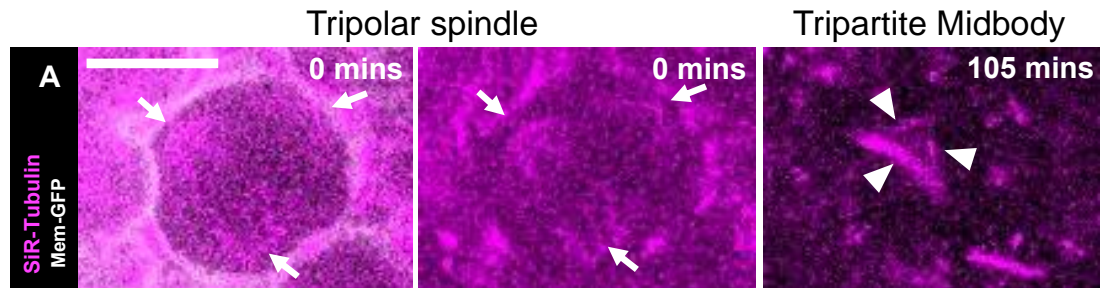


Figure App 1-8 : Cep55 mutant MEFs and NSCs have delayed ESCRT recruitment

(A) Immunofluorescent labeling of AurKB (midbody) and ESCRT components Alix, TSG101, and Chmp2a on E14.5 mouse embryonic fibroblasts. **(B)** Alix, TSG101, and Chmp2a are recruited to the midbody in the absence of Cep55. Quantification reveals a significant decrease in the percentage of midbodies with ESCRTs in Cep55 mutant **(C)** MEFs and **(D)** NSCs. MEFs: Alix: control n=153 Cep55 mutant n= 129 (4 animals, 4 coverslips, 3 experiments) ; Tsg101: control n= 141 Cep55 mutant n= 132 (4 animals, 4 coverslips, 3 experiments); Chmp2a: control n=108 Cep55 mutant n= 105 (3 animals, 3 coverslips, 3 experiments) NSCs: Alix: control n= 49 (3 animals, 3 coverslips) Cep55 mutant n= 46 (2 animals, 3 coverslips) TSG101: control n= 32 (2 animals, 2 coverslips) Cep55 mutant n= 45 (3 animals, 3 coverslips) **(E)** Cep55 mutant MEFs had a similar number of constriction sites as control MEFs. Constriction sites detected by alpha - Tubulin staining. N= 402 control, 355 Cep55 mutant (5 animals, 11 coverslips, 3 experiments) **(F)** The number of midbodies with an ESCRT and a constriction site (CS) out of the number of midbodies with a CS is decreased in the Cep55 mutant. N (midbodies with constriction sites) = 110 control, 95 Cep55 mutant, (5 animals, 11 coverslips, 3 experiments. Scale bars: A: 2 μ m; n.s., not significant, * p < 0.05; ** p < 0.01; *** p < 0.001; **** p < 0.0001. C-F: Fisher's exact test; I: t-test. MEFs were passaged 1-2 times before the time points indicated.



B % Tripolar spindles

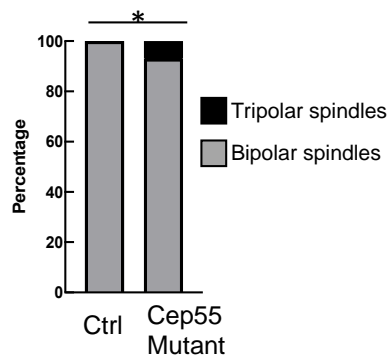


Figure App 1-9 Cep55 mutant NSCs have tripolar spindles and tripartite midbodies.

(A) Cep55 mutant NSC with tripolar spindle marked by SiR-Tubulin. Membrane GFP shows the large endfoot size of this cell. This tripolar cell goes on to form a tripolar midbody at 105 minutes. Arrows point to spindles. Arrowheads point to midbody "flanks". (B) There is increase in tripolar spindles in the *Cep55* mutant. G: Control= 71 and Cep55 mutant = 86 Fisher's Exact. n.s. not significant * $p < 0.05$, ** $p < 0.01$ Scale Bar, 10 μ m.

Figure App 1-10: Cep55 mutant cells have a delay in microtubule disassembly

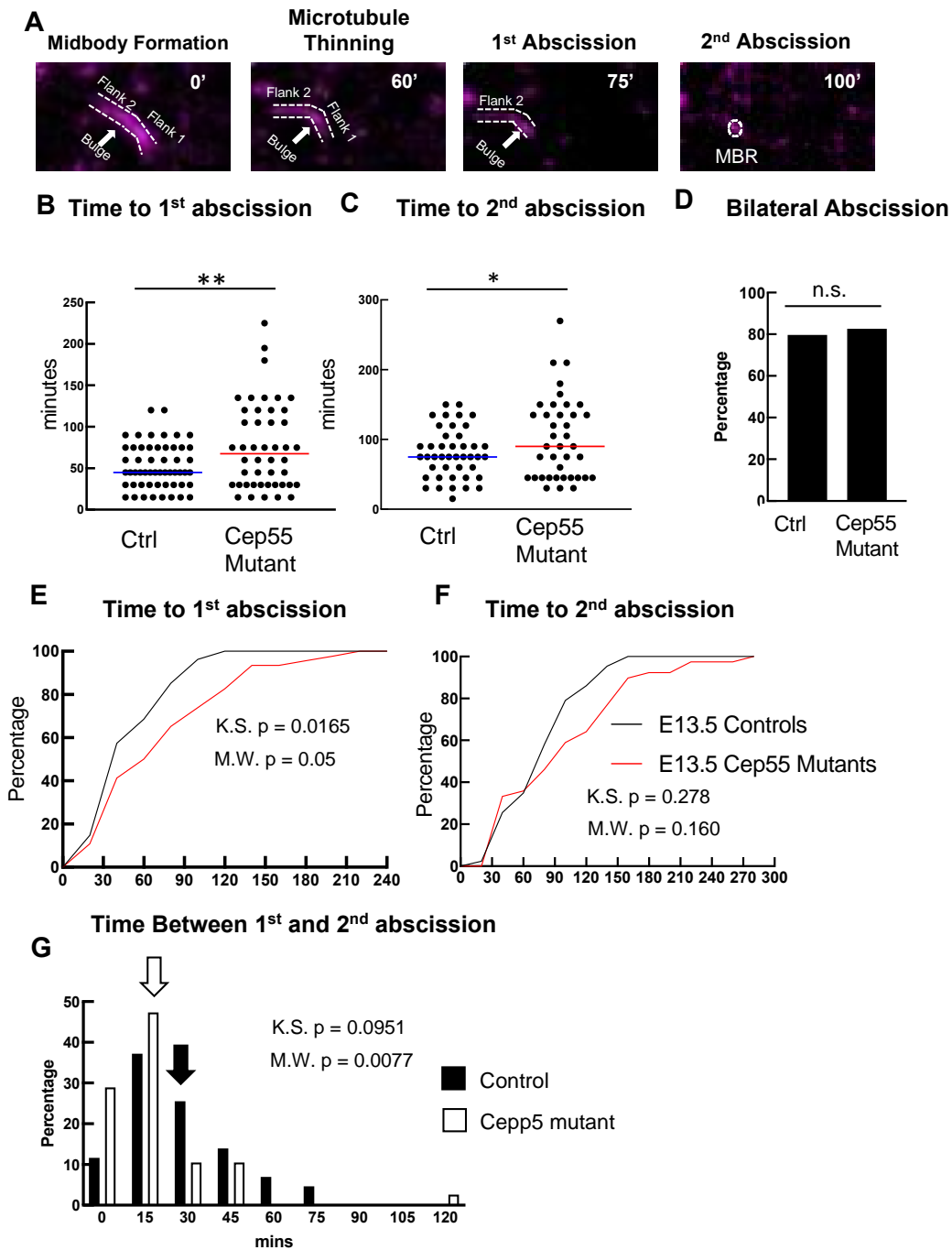


Figure App 1-10: Cep55 mutant cells have a delay in microtubule disassembly

(A) Time-lapse imaging of an NSC midbody undergoing abscission with central bulge and flanks indicated in insets. Distinct steps seen here are: midbody formation, flank 1 thinning, microtubule disassembly on flank 1 (1st abscission), and microtubule disassembly on flank 2 (2nd abscission). After the second microtubule disassembly the midbody remnant (MBR) is left at the apical membrane. Time to abscission was measured from midbody formation to 1st microtubule disassembly **(B)** and 2nd microtubule disassembly **(C)** in embryonic day 13.5 cortical slabs. Microtubules were visualized by SiR-Tubulin. **(D)** There is no change in the percentage of detectable bilateral abscissions in the Cep55 mutant. Cumulative frequency plots for the 1st abscission **(E)** and the 2nd abscission **(F)** show the delay in abscission duration in Cep55 mutants. **(G)** The time between the first and second abscission is shifted to the left indicating the second abscission event may occur faster than in controls. N: A,C: Control= 54, Cep55 Mutant= 46; B,E,F: Control=43,Cep55 mutant= 39.. A, B: T-test. C Fisher's Exact. n.s. not significant *p<0.05, **p<0.01

Appendix II: *Kif20b* mutant NSCs undergo premature neurogenesis

Within this appendix, we focus on experiments to further explore different aspects of cell fate both in relation to *Kif20b* and during normal development. As previously described in the introduction (**Chapter I**) there, are many cell fate determinants in the literature and some that are still controversial. Here we investigated whether the *Kif20b* mutants have excessive early neurogenesis or not, and the possible mechanism. We found that the *Kif20b* mutants have some premature NSC cell cycle exit and thereby extra early neurogenesis. NSC daughter cell that exits the cell cycle after division becomes a neuron and cannot re-enter the cell cycle. This loss of neural stem cells by early neuron production is in addition to the previously shown apoptosis in *Kif20b* mutant NSCs. We found that the excess cell cycle exit is not dependent on p53. This could explain the incomplete rescue of brain size in the double *Kif20b;p53* mutant mouse which blocked the apoptosis through the loss of p53 (Little and Dwyer, 2019). Finally, to try to address why excess early neurogenesis occurs, we investigated the overall cell cycle parameters of *Kif20b* mutants and the apical endfeet symmetry in *in vivo* slabs of both *Kif20b* and *Kif20b/p53* mutants.

*Are more neurons being produced in the *Kif20b* mutant?*

Normally during development cell fate outcomes are stochastic, but as development progresses the probability of certain fates changes. During early development the probability of having a progenitor-progenitor division is higher than having a neuron-neuron division. This changes during later development when neuron-neuron divisions are more likely. In Chapter III, by using the pair-cell assay to determine the daughter cell fates of individual NSC divisions (**Figure 3-5**), we noticed that *Kif20b* mutant NSCs had fewer proliferative symmetric divisions resulting in two progenitor daughters, and more neurogenic divisions with two postmitotic neuron daughters, regardless of midbody remnant association. To directly test whether *Kif20b* mutant NSCs have different division fate outcomes, we quantified the daughter fates of individual NSC divisions again using the dissociated pair-cell assay (**Figure App 2-1A-D**). We find that *Kif20b* mutant NSCs from E11.5 brains have a significant increase in neurogenic symmetric divisions

compared to controls, 61% versus 42% (**Figure App 2-1A**). The increase in neuron production comes at the expense of fewer proliferative symmetric divisions (17% versus 38%). NSCs from older (E15.5) control brains have more neurogenic and fewer proliferative divisions, as expected (**Figure App 2-1B**, control, and **Figure App 2-1C**). However, *Kif20b* mutants do not show this profound developmental shift: they always have a majority of neurogenic symmetric divisions, i.e., the E11 NSCs behave as if they are older, like E15 NSCs (**Figure App 2-1D**). These data suggest that *Kif20b*'s function helps bias early NSC divisions to produce two NSC daughters.

In the *Kif20b* mutant brains at E14.5, there are fewer intermediate (Tbr2+) progenitors (IPs) than in control brains, but by E18.5, there is no longer a significant difference (Janisch et al., 2013). The early reduction of IPs *in vivo* prompted us to ask what the contributions of IPs are to neuron-neuron divisions in the E15.5 pair cell experiments. We wanted to confirm that the neurogenesis happening *in vitro* at E15.5 was not influenced by a bias towards IPs in the cultures. Therefore, we immunostained for Tbr2+ cells in E15.5 cultures. There is a slight increase in Tbr2+ progenitors in the *Kif20b* mutant cultures, however they only amount to 7 to 9% of the cells (**Figure App 2-1E, F**). Therefore, this tiny increase in IPs cannot account for the 50% increase in neuron-neuron daughter pairs being produced in the *Kif20b* mutant cultures.

These data led to the idea that *Kif20b* mutant NSCs have some premature neurogenesis (early excess cell cycle exit). To test this *in vivo*, we measured the width of the neuronal layer at E12.5 in control and mutant cortices, when the earliest neuronal layer (preplate) is thin. Indeed, we find a small but highly significant increase in the proportional thickness of the neuronal layer of *Kif20b* mutant cortices over controls' (**Figure App 2-1G, H**). This change in thickness is not due to decreased neuron density (**Figure App 2-1I**). These results suggest that in early *Kif20b* mutant cortices, some daughters of NSC divisions prematurely exit the cell cycle to become postmitotic neurons, depleting the early pool of NSCs, contributing to the smaller brain size at birth.

The lab previously showed that a small percentage of NSCs in *Kif20b* mutant cortices undergo apoptosis, and that this is p53-dependent (Little and Dwyer, 2019). We further showed that p53 accumulates in the nucleus of *Kif20b* mutant NSCs at the late midbody stage. Therefore, we hypothesized that the increase in symmetric neurogenic divisions

(both daughters exiting the cell cycle) could also result from p53 activation. To test this, we assayed division types in *Kif20b*; *p53* double mutant NSCs. We modified the previous pair-cell assay by feeding BrdU to NSC cultures at plating so that NSCs that divided in the dish could be identified as pairs of BrdU+ cells (**Figure App 2-2A**). Surprisingly, the increase in symmetric neurogenic divisions caused by loss of *Kif20b* is not prevented by p53 knockout (*Kif20b*; *p53* double mutants, **Figure App 2-2B**). Both the *Kif20b* mutant and *Kif20b*; *p53* double mutant had a 45% increase in neurogenic divisions. Cell cycle exit (BrdU+Tubb3+ cells /BrdU+ cells) was increased in NSCs double mutant for *Kif20b* and p53, but not p53 alone (**Figure App 2-2C**). To determine if the early cell cycle exit is occurring *in vivo*, we used an *in vivo* BrdU assay in the *Kif20b*; *p53* mouse line. We injected 20mL of 10mg/mL BrdU into dams of *Kif20b*; *p53* at E11.5 and collected the embryonic brains the next day at E12.5. Brains were fixed in PFA and cryo-sectioned, as previously described (Janisch et al., 2013). Frozen cryo-sections were immunostained with BrdU, TUBB3, Tbr2 after citrate antigen retrieval was performed. There was a lot of overlap between the TUBB3 and Tbr2 immunostaining, in agreement with other papers showing that IPs can express Tubb3 (Englund et al., 2005). Therefore, for this analysis, cells were counted as either TUBB3+ or TUBB3- and BrdU+ or BrdU-. We found a 40% Increase in TUJ1+ BrdU+ out of total BrdU+ cells in the *Kif20b*; *p53* double mutants as well as *Kif20b* single mutants, showing that there is early cell cycle exit *in vivo* as well as *in vitro*, and confirming that it does not occur through p53 activation (**Figure App 2-2E**). Thus, our data show that early NSCs in the *Kif20b* mutant mouse are depleted due to both p53-dependent apoptosis (Janisch et al., 2013; Little and Dwyer, 2019) and p53-independent cell cycle exit (this appendix). More studies are needed to determine the nature of the p53-independent pathway, and whether and how these pathways are activated by defects in midbody structure or abscission timing.

Recent progress in cell lines has elucidated a few of the signaling molecules that activate p53-mediated cell cycle arrest following mitotic delay, but cleavage furrowing and abscission delay was not addressed (Lambrus et al., 2016; Meitinger et al., 2016). Furthermore, cortical NSC daughters appear to respond differently: p53 is not required for cell cycle exit (neurogenesis) following mitotic delay, but p53 does mediate apoptosis in some cells instead (Pilaz et al., 2016). This echoes the findings above in *Kif20b* mutant NSCs, but we found no evidence for delayed or defective mitosis in the *Kif20b* mutant (Janisch et al., 2013; Little and Dwyer, 2019). Since cell cycle exit is a normal

developmental event for the neuronal daughters of NSCs, a non-p53 pathway may be primed to mediate it.

Gross Cell cycle parameters are relatively unperturbed in Kif20b mutants.

Early neurogenesis could be the result of changes to many cell fate determinants, including cell cycle length. We have found in Chapter III that abscission is faster in the *Kif20b* mutants. However, we do not know how abscission duration effects the timing of G1, which is when abscission occurs (Gershony et al., 2014). Therefore, we wanted to characterize the general cell cycle parameters within these NSC cultures. Within the cultures made from E12.5 cortices, there are proportionally fewer neurons and more NSCs in the *Kif20b* mutant compared to control (**Figure App 2-3A**). This result is in line with our previous findings that stem cells are being lost early on, and both daughter cells are likely to exit the cell cycle to become neurons. However, it is not what we would expect based on **Figure App 2-1G**. It is possible that in culture *Kif20b* mutant neurons are not able to survive and this could contribute to the loss of neurons in culture. The loss of stem cells ultimately reduces the number of neurons that can be born over time. Interestingly, the proportion of NSCs that are cycling in culture is similar (**Figure App 2-3B**). Again, this is in line with our observations of NSCs within the cortex. To determine if G1 phase, when abscission occurs, is also altered, we looked at the percent of cells with Cyclin D1 and Ki67. Cyclin D1 is required for the cell to progress through the G1/S-phase checkpoint. If we find elevated Cyclin D1 in the NSCs, that could signify G1 delay or arrest. We found that there were more cells with Cyclin D1, Ki67, or both compared to controls (**Figure App 2-3C**). But this is reflective of more NSCs in the culture since when it is normalized to the number of cells dividing, there is no longer a significant difference (**Figure App 2-3D**). However, it is close to significance, suggesting there might be a small increase in NSCs in G1. Finally, to determine if S-phase can begin in progenitors before abscission occurs, we treated cells with BrdU for an hour, then washed it out and fixed the cells. BrdU in the nucleus marks all the cells in S-phase. We did not find any cells connected by a midbody in S-phase, supporting the previously published data that abscission happens in G1 before S-phase begins (**Figure App 2-3E**). Overall, these data show that the loss of *Kif20b* does not grossly change the cell cycle, and would argue against the lengthening of G1 as a possible cell fate mechanism for the early excess neurogenesis phenotype.

Increased asymmetry in daughter apical endfeet sizes in Kif20b mutants appears to be due to apoptosis

Another possible cell fate determinant is asymmetric inheritance of the apical membrane. Since Kif20b is a midbody protein, and we have evidence that midbody structure and organization is disrupted in the *Kif20b* mutants, we decided to investigate the apical membrane. The apical junctions surrounds the midbody during cytokinesis (**Figure App 2-4A**). A new apical junction has to form between the two daughter cells as they are undergoing cytokinesis, in a process that is not well understood. We know from studies in the frog epithelium that this process is dynamic and happens during cytokinesis (Higashi et al., 2016). Apical membrane inheritance has been implicated in cell fate decisions in the cortex (reviewed in **Chapter I**). To try to determine if apical membrane inheritance is significant developmentally and if the loss Kif20b is essential for this process, we analyzed the apical endfeet of NSCs from E11.5 and E15.5 control and *Kif20b* mutant slabs. Cortical slabs were prepared as previously described in a methods paper published by the lab and in the methods of Chapter III (Janisch and Dwyer, 2016). Cortical slabs were stained with AuroraB kinase to mark the midbody and Zona-occludin -1 (ZO-1) to mark the apical junctions. We will refer to each polygon of ZO-1 staining as an individual apical endfoot of an NSC.

An NSC apical endfoot undergoing abscission (that is, with a midbody present) can be open or closed (**Figure App 2-4A**). An open endfoot contains an early, wide midbody. A closed endfoot marks the formation of a new junction between the two daughter cell endfeet, and the midbody is thinner and closer to abscission at this point. We can count the number of open endfeet in a specific area and measure the size of these endfeet. We find that there is no difference between the number of open endfeet between E11.5 and E15.5 for either control or *Kif20b* mutant (**Figure App 2-4B**). Interestingly there is an increase in the size of the open endfeet at E11.5 in the *Kif20b* mutants and a decrease in size in the *Kif20b* mutants at E15.5 (**Figure App 2-4C**). We wanted to know if this change in size remained once the apical endfoot closed, and a new apical junction was established. The closed endfeet in controls are larger at E15.5 compared to E11.5, which is not surprising since it has been previously reported that endfeet size does change over development (Nishizawa et al., 2007). The average *Kif20b* mutant closed

endfoot area (total area of the two sister endfeet) is much larger at E11.5 compared to E15.5 (**Figure App 2-4D**). This result is suggestive of a developmental difference or even a reflection of the cell death happening at E11.5 in the *Kif20b* mutants. The endfeet may expand to take up space that is left by apoptotic cells. To try to determine if the endfeet size could be related to cell fate or merely a secondary effect of cell death, we measured the daughter endfeet of a closed endfoot separately. The asymmetry between daughter endfeet has been suggested to both promote neurogenesis and influence apical progenitor detachment from the apical surface (Konno et al., 2008; Kosodo et al., 2004). In the *Kif20b* mutant, we currently do not have evidence that apical progenitors prematurely detach from the apical membrane to become non-surface progenitors (Janisch et al., 2013). In control NSCs, the ratio of daughter endfeet asymmetry (large endfoot/closed endfoot) was similar between E11.5 and E15.5 (**Figure App 2-4E**). This suggests there is not developmental regulation in endfeet size. In the *Kif20b* mutants, there is increased asymmetry at E11.5 compared to control at E11.5 and *Kif20b* mutant at E15.5 (**Figure App 2-4E**). These data suggest that the asymmetry is caused by *Kif20b*'s role at E11.5 or a secondary effect.

We know that at E11.5, there is increased cell death in the *Kif20b* mutants compared to E15.5. Therefore, we wanted to determine if the apical endfoot asymmetry at early developmental time points was dependent or independent of apoptosis and p53. We use E13.5 *Kif20b*; *p53* cortical slabs, in which apoptosis is prevented, and analyzed them as above. We found an increase in the number of open endfeet in the *Kif20b* mutant and *Kif20b*^{-/-}; *p53*^{-/-} (**Figure App 2-5A**). These data support the observation that there are increased proportion of early midbodies in the *Kif20b* mutant brains, and this phenotype is persistent when apoptosis is blocked (Janisch et al., 2013; Little and Dwyer, 2019). Open endfoot size is similar in all three of the genotypes (**Figure App 2-5B**). Interestingly, the closed endfoot size is increased in both the *Kif20b* mutant and *Kif20b*^{-/-}; *p53*^{-/-} (**Figure App 2-5C**). The ratio of asymmetry (large endfoot/closed endfoot) shows that the loss of p53 rescues the apical endfoot asymmetry (**Figure App 2-5D**). Therefore, our evidence supports the hypothesis that asymmetry is not influencing cell fate and appears to be a consequence of cell death in the *Kif20b* mutant.

Conclusion

Despite investigating possible causes of the excess early neurogenesis in the *Kif20b* mutants -- cell cycle changes, and apical membrane inheritance-- we are left without an explanation. *Kif20b* may have a role in or at the nucleus that influences cell fate. However, based on evidence provided in this thesis, our current hypothesis is that abscission duration itself may alter cell fate in a p53-independent pathway. To explore this hypothesis further, we would need to be able to make abscission faster independently of *Kif20b*. It is possible to do this through knockdown of *Chmp4C* (Carlton et al., 2012). While *Chmp4C* is essential for other processes besides abscission, using shRNA to knockdown in the cortex should be able to provide us with a number of cells exiting the cell cycle. Additionally, in the discussion, we propose imaging other known midbody mutants for abscission defects. If one of these mouse mutants also has faster abscission, we could use this to compare to the *Kif20b* mutant phenotype to determine if there are specific characteristics of faster abscission in NSC. Overall, these experiments could provide evidence that early neurogenesis is a result of an abscission defect and not due to a separate function of *Kif20b*.

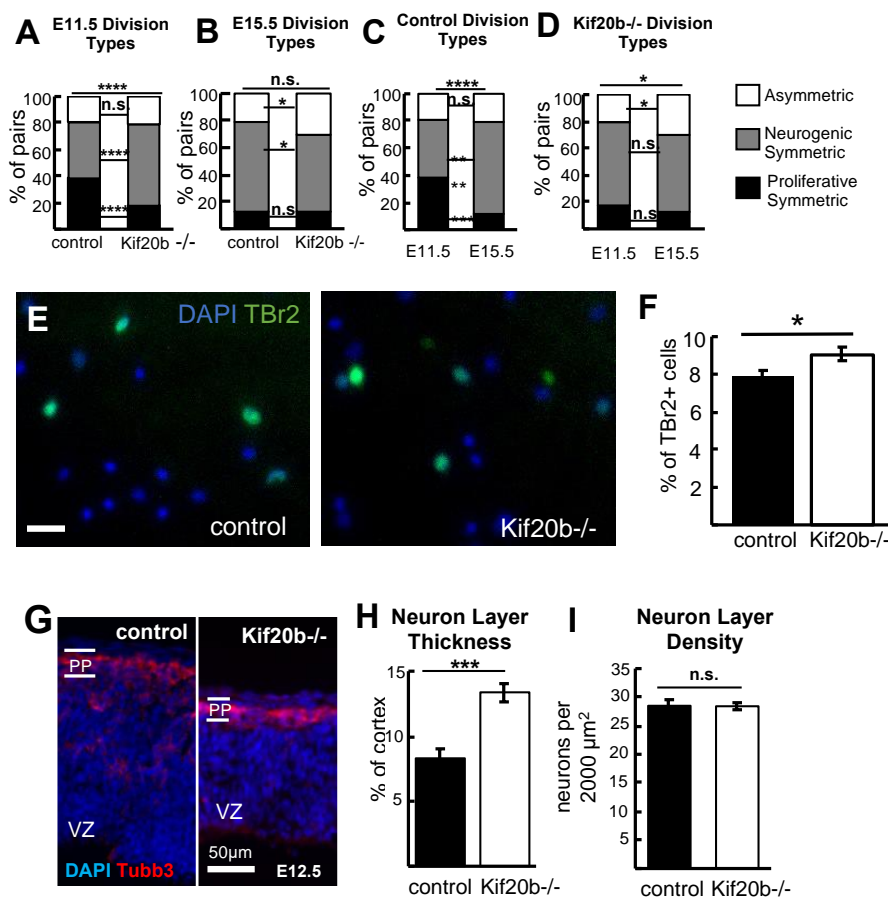


Figure App 2-1: *Kif20b* mutant brains show reduced proliferative symmetric divisions and increased neuron daughters in early corticogenesis

(A, B) *Kif20b*^{-/-} NSCs have less than half as many proliferative symmetric divisions as controls at E11.5, with a concomitant increase in neurogenic symmetric divisions. E15.5 *Kif20b*^{-/-} NSCs show similar percentage as control. (C, D) Comparing the proportions of division types in the pair-cell assay between E11.5 and E15.5 NSCs (using the same data set as in A, B) shows that control NSCs have ~4-fold more proliferative symmetric divisions at E11.5 than E15.5, while *Kif20b* mutant NSCs have the same proportion of proliferative divisions at both ages. For E11.5, n= 394 control (3 +/- and 2 +/+ brains); 272 *Kif20b*^{-/-} divisions (4 brains). For E15.5, n= 241 control (4 +/- and 1 +/+ brains); 280 *Kif20b*^{-/-} divisions (5 brains). (E) TBr2 (green) progenitors in an E15 NSC culture. (F) Increase in the percentage of TBrR progenitors born after one cell division in culture in the *Kif20b* mutants. Control n= 3 brains, 6 coverslips. Mutant, n=4 brains, 8 coverslips Scale bar 20 µm. (G) Sections of control and *Kif20b*^{-/-} E12.5 brains stained for Tubb3 show the nascent neuron layer (preplate, pp) above the NSC nuclei (ventricular zone, vz). The neurons were born from NSC divisions at E11.5. (H, I) The preplate is proportionally thicker in E12.5 *Kif20b*^{-/-} cortices, but density is similar. N= 6 control (+/+), 5 mutant (-/-) brains. χ^2 and Fisher's exact test in A-D. T-test in F, H, I.

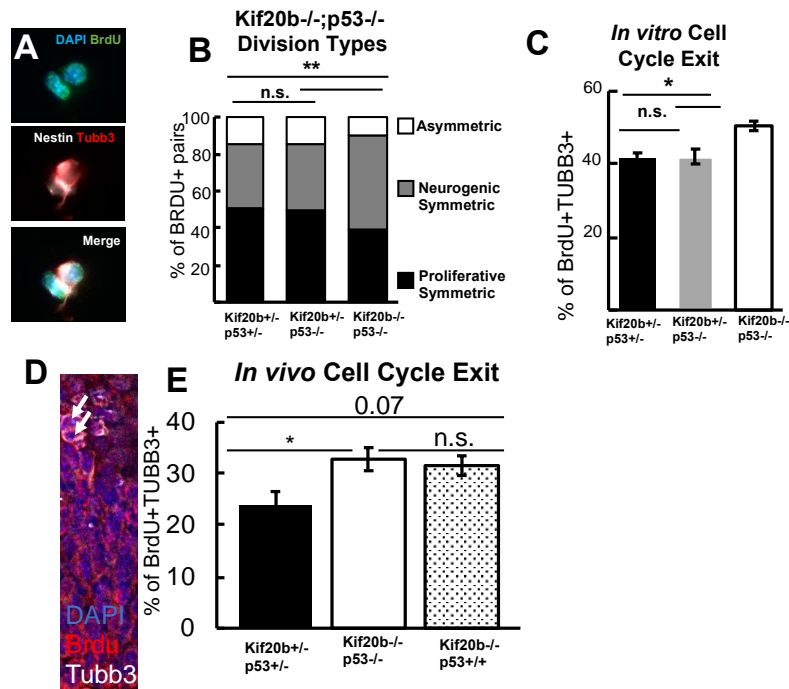


Figure App 2-2: The increased neuronal fate of *Kif20b* mutant NSC daughters during early cortical development is not p53-dependent

(A) Higher density dissociated NSC cultures from E12.5 cortices were treated with Bromodeoxy-Uridine (BrdU) one day before fixation to identify NSC divisions. BrdU+ daughter pairs were classified as one of the three different division types using Nestin (white) and Tubb3 (red).

(B) The increased proportion of neurogenic symmetric divisions was still observed when the *Kif20b* mutant was combined with p53 knockout (*Kif20b*^{-/-}; *p53*^{-/-}), but was not seen in controls: double heterozygotes (*Kif20b*^{+/-}; *p53*^{+/-}) or p53 single mutants (*Kif20b*^{+/-}; *p53*^{-/-}). N=276 control (*Kif20b*^{+/-}; *p53*^{+/-}) division pairs (3 brains), 228 p53 single mutant (*Kif20b*^{+/-}; *p53*^{-/-}) division pairs (3 brains), and 270 double mutant (*Kif20b*^{-/-}; *p53*^{-/-}) division pairs (5 brains).

(C) Cell cycle exit among the daughters of NSC division pairs was scored as daughters that were BrdU+, Tubb3+. The increased cell cycle exit in *Kif20b*^{-/-} daughters is not dependent on p53 function. n= 613 control (*Kif20b*^{+/-}; *p53*^{+/-}) daughter cells; 689 p53 single mutant daughters (*Kif20b*^{+/-}; *p53*^{-/-}); and 593 double mutant daughter cells (*Kif20b*^{-/-}; *p53*^{-/-}).

(D) Dams were injected with BrdU at E11.5 and then embryos were collected 24 hours later at E12.5. Cortical sections were stained with BrdU and Tubb3. **(E)** There was increase in cell cycle exit in the double mutants and single *Kif20b* mutants compared to controls. n= 5 control (*Kif20b*^{+/-}; *p53*^{+/-}) brains, 4 double mutant (*Kif20b*^{-/-}; *p53*^{-/-}) brains, and 4 *Kif20b* single mutant (*Kif20b*^{-/-}; *p53*^{+/-}) brains. **** p<0.0001, *** p<0.001, ** p<0.01, * p<0.05, n.s. not significant; c² for populations in A, B, D, E, and Fisher's exact test for individual groups in A and B. Scale bar, 10µm.

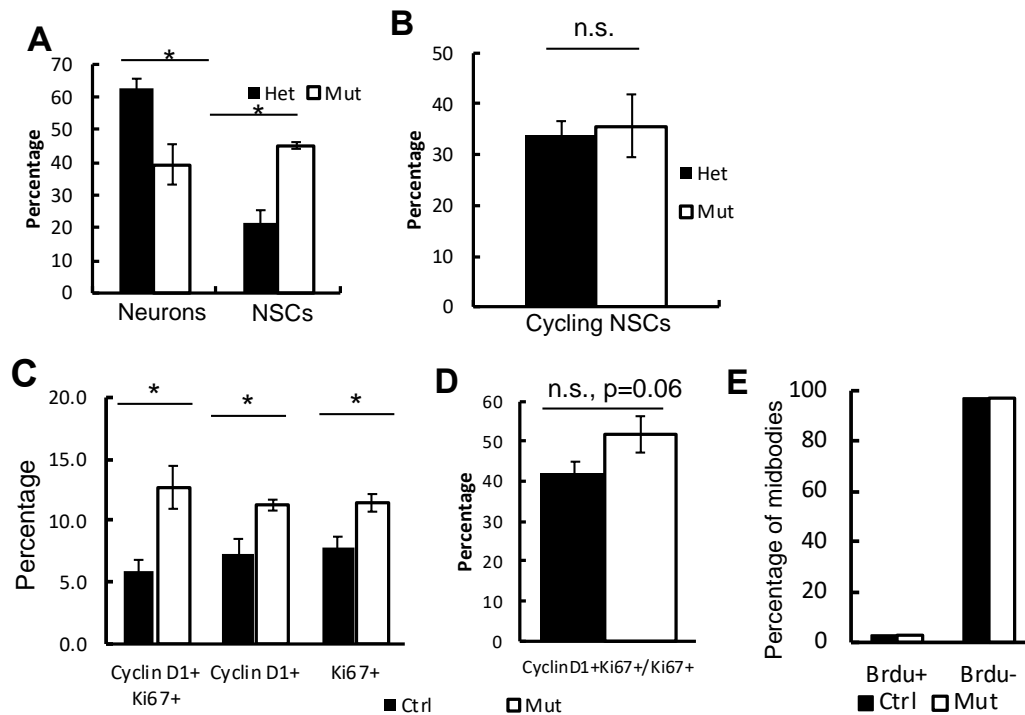


Figure App 2-3: *KIF20B* mutant cultures have increased NSCs and NSCs have a normal cell cycle

(A) There are less neurons and more progenitors in the *Kif20b*^{-/-} cultures. (Neuron: Nestin⁺/TUJ1⁺, Progenitor: Nestin). **(B)** Of the cells that are progenitors the same percentage are dividing based on Ki67 staining. 3 hets, 4 coverslips, 2 mutants, 3 coverslips. **(C)** There are more cyclinD1⁺ cells in the mutant cultures. **(D)** There is a trend for more cyclinD1⁺ progenitors. 3 Muts (5 coverslips) 3 ctrls (1 WT, 2Hets, 6 coverslips). **(E)** There is no difference in the number of Brdu⁺ midbodies between ctrl and mutant. Majority of cells with a midbody are not in S phase. 2 ctrls, 2 mutants ctr n = 98, mut n=103 T-test (A-D) * p<0.05, n.s. not significant

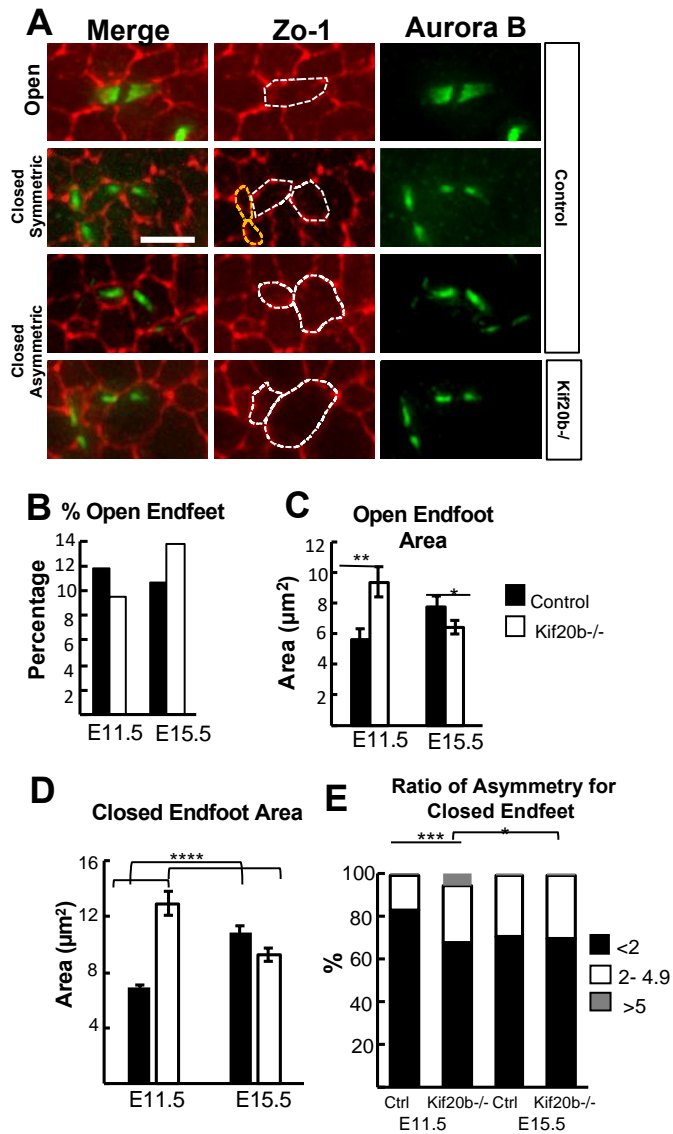
Figure 2-4: *Kif20b* mutant endfeet are more asymmetric at E11.5 than E15.5

Figure App 2-4: *Kif20b* mutant endfeet are more asymmetric at E11.5 then E15.5

(A) Max projection images of apical endfeet (ZO-1) and midbody (Aurora B) from E13.5 *Kif20b;p53* slabs. White or yellow dotted outline marks the endfoot. An endfoot can be open in early midbody stages. Once the endfoot has formed a new junction the size of the endfeet can vary as seen between the white and yellow dotted endfeet in the closed symmetric image. The endfeet can be equally sized and are grouped as closed symmetric or the two daughter endfeet can be different sizes which is closed asymmetric. Scale bar, 5 μ m.

(B) There is no difference in the number of open endfeet between control and *Kif20b* mutant at either E11.5 or E15.5. **(C)** *Kif20b* mutant open endfeet have a larger area at E11.5 compared to E15.5. **(D)** Closed endfeet are larger in the *Kif20b* mutant at E11.5 but not at E15.5. Control closed endfeet increase in size between E11.5 and E15.5. Closed endfeet are measured as total area of both endfeet. **(E)** Ratio of asymmetry for closed endfeet. The ratio is: larger endfoot area/ smaller endfoot area. Open endfeet: E11.5: ctrl n=23 mut n=19, E15.5: ctrl n=28, mut n=28 Closed endfeet: E11.5: Control n = 172 Mutant n = 180 E15.5: control n = 228 mutant n = 175 B,C ANOVA, D Chi-square * p<0.05, **p<0.01, *** p<0.001, ****p<0.0001 n.s not significant

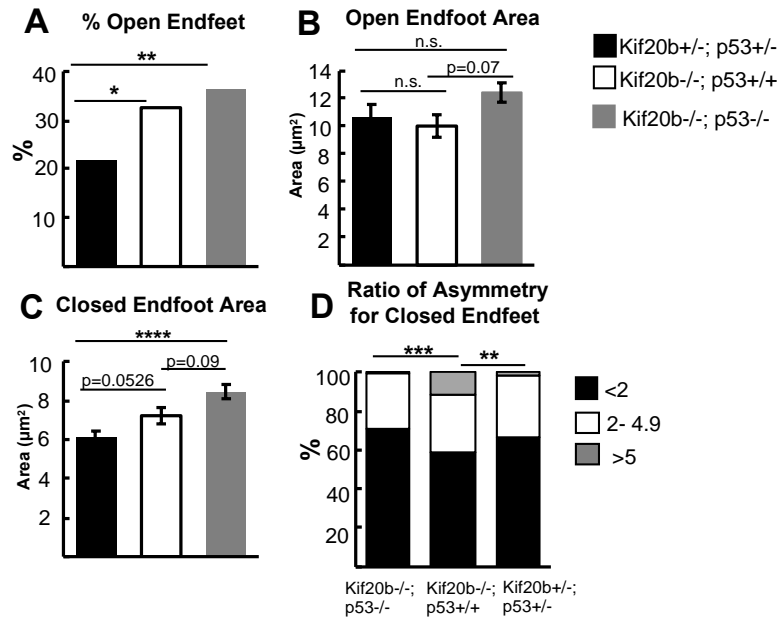


Figure App 2-5: Apical endfoot asymmetry is a consequence of cell death in the *Kif20b* mutants

(A) The % of open endfeet is increased in the apical membrane of E13.5 *Kif20b*^{-/-} and *Kif20b*^{-/-};*p53*^{-/-} brains, Fishers exact, *Kif20b*^{+/-};*p53*^{+/-}, n=181, *Kif20b*^{-/-};*p53*^{+/-} n=178, *Kif20b*^{-/-};*p53*^{-/-} n= 231. **(B)** The size of the open endfeet are not significantly different in any of the genotypes. *Kif20b*^{+/-};*p53*^{+/-}, n = 40, *Kif20b*^{-/-};*p53*^{+/-} n=58 *Kif20b*^{-/-};*p53*^{-/-} n= 84. **(C)** *Kif20b*^{-/-};*p53*^{-/-} and *Kif20b*^{-/-};*p53*^{+/-} closed endfeet are larger than control. Closed endfeet are measured as total area of both endfeet. **(D)** There is an increase in apical endfeet that have an endfoot that is five times larger than the sister in the *Kif20b* mutants. The ratio is: larger endfoot area/ smaller endfoot area. D *Kif20b*^{+/-};*p53*^{+/-} n=168 from 4 brains, *Kif20b*^{-/-};*p53*^{+/-} n= 143 from 4 brains, *Kif20b*^{-/-}, *p53*^{-/-} n= 147 from 4 brains B,G Fishers, C-F ANOVA, G Chi-square * p<0.05, **p<0.01, *** p<0.001, ****p<0.0001 n.s not significant

Appendix III: HeLa midbody remnants do not influence cell fates of NSCs or neuron polarization

Cell line studies have shown that midbody remnants can be engulfed and accumulated within the cytoplasm (Crowell et al., 2014; Ettinger et al., 2011; Kuo et al., 2011). As previously discussed, midbody remnants can influence both cell fate and polarization in a cell-type specific manner (Ettinger et al., 2011; Kuo et al., 2011; Lujan et al., 2016; Pollarolo et al., 2011; Salzmann et al., 2014; Singh and Pohl, 2014a). We have shown that midbody remnants are associated with the apical membrane of the cerebral cortex, and the number of midbody remnants can be altered in abscission mutants (**Chapter III, Appendix I**). However, it is difficult to determine if these midbody remnants are within the cytoplasm or attached to the apical surface of neural stem cells (NSCs). Therefore, we wanted to ascertain if cultured NSCs or neurons could engulf midbodies and if this would change cell fate or polarization phenotypes. Midbody remnants are challenging to obtain from mouse embryonic brains. Therefore, we opted to use midbody remnants from cultured MKLP-GFP HeLa cells. The midbody remnants collected from these cultures would be GFP positive making them easy to identify.

Neurons or NSCs in culture were fed midbody remnants from HeLa cells. We can characterize the association of the HeLa midbody remnants with the neuron or NSC as being inside the cell or internalized, not associated, outside the cell, or partially internalized (**Figure App 3-1A**). There is no preference in the NSC cultures between neurons and NSCs for being associated with a HeLa midbody remnant (**Figure App 3-1B**). Even separating the data based on the location of the midbody remnant, there is no difference between NSCs and neurons. Additionally, in a neuron only culture, we found no correlation between the midbody remnant association and neuron polarization stages (**Figure App 3-1C**). We discovered that Kif20b status does not seem to influence midbody remnant association or engulfment, which is in line with our previous findings at the apical membrane (**Chapter III, Figure App 3-5**). Midbody remnants were collected with or without EDTA; a calcium chelator thought to inhibit the binding of midbody remnants to the membrane (Crowell et al., 2014). We found that this did not prevent the association of HeLa midbody remnants with NSCs or neurons (**Figure App 3-1D**). Overall, we learned that *in vitro* NSCs and neurons can associate or engulf HeLa cell

midbody remnants, but these remnants do not alter fates of NSCs or influence polarization of neurons.

To perform this feeding experiment, we used cultured NSCs or neurons. Culturing of E12.5 NSCs and E14.5 neurons was done as previously described (**Chapter III, IV**). Midbody remnants are difficult to obtain in large quantities from the cortex or neural NSC cultures. Therefore, MKLP-GFP HeLa cells were used to collect midbody remnants. All midbody remnant isolation was done in Ahna Skop's lab by Randall Dahn at the University of Wisconsin Madison. The remnants were shipped overnight to the Dwyer lab, where we stored them in the 4°C for up to 2 weeks. NSCs and neurons were cultured for 24 hours at 37°C before 400µl of media was removed. Then 50µl of midbodies or other media components were added to each well of cells. The plate was given a swirl and placed back in the 37°C incubator for 24 hours. The cells were fixed at 48 hours with PFA-MeOH. The cell membrane was labeled with WGA (wheat germ agglutinin 647, Invitrogen Cat # W32466), and the remnants were identifiable by staining with a GFP antibody post-fixation. Cells were permeabilized and stained with GFP (Aves Lab Cat # gfp-1020) and TUJ1 (neuronal tubulin, Biolegend Cat# 801201 or Abcam 52623). Images were taken using the Deltavision oil 60x objective with a 0.2µm z step. We decided the remnant location was inside or outside the cell based on the z-position of the remnant relative to the membrane marker (WGA). All cell fate and stage counts were done by analyzing 20x images from a Zeiss AxioImager.

Despite the mostly negative results, this project still has the potential to move forward. It would be worth trying the feeding assay with freshly isolated HeLa (or another cell type) remnants. RNA or other essential components of the midbody could be degraded in shipping and lag time before feeding. Additionally, finding a way to isolate midbody remnants from mouse cerebral spinal fluid and repeating the feeding experiments would be very informative. A new FACS based sorting method in HELA cells was recently released as a preprint, and this could be useful for isolating midbody remnants from the cerebral spinal fluid (Addi et al., 2020). The cerebral spinal fluid could be collected from MKLP1-GFP embryos and using FACS isolate the GFP+ midbody remnants. Midbody remnants may have RNAs or proteins that are cell- type specific. Therefore, it would be informative for the field to collect the proteomes of midbody remnants from not only different cell types but different developmental ages. It is especially motivating to look at

different developmental ages within the brain since we have evidence that midbody remnant disposal is developmentally regulated (**Chapter III**).

With the ability to sort midbody remnants efficiently from cerebral spinal fluid, we could repeat the feeding assays. We could feed midbody remnants from older brains to younger NSCs or slabs to determine if these midbody remnants could change cell fate properties. It has been previously shown that cerebral spinal fluid from different ages can alter the cell fate of neural stem cells (Chau et al., 2015). It would be exciting to determine if the midbody remnant could be an essential driver of these fate changes.

Engulfment of midbody remnants has been explored in cancer cell lines but not in NSCs. It would be interesting to determine if NSCs engulf midbody remnants *in vivo* in a phagocytic process, as previously described (Chai et al., 2012; Crowell et al., 2014). And once the midbody remnants are engulfed, are they able to avoid lysosomes using actin patches as described in HeLa cells (Peterman et al., 2019). These experiments would help the field determine what the universal properties of midbody remnants are and what is unique to cell culture, cancer cell lines, or *in vivo* tissue.

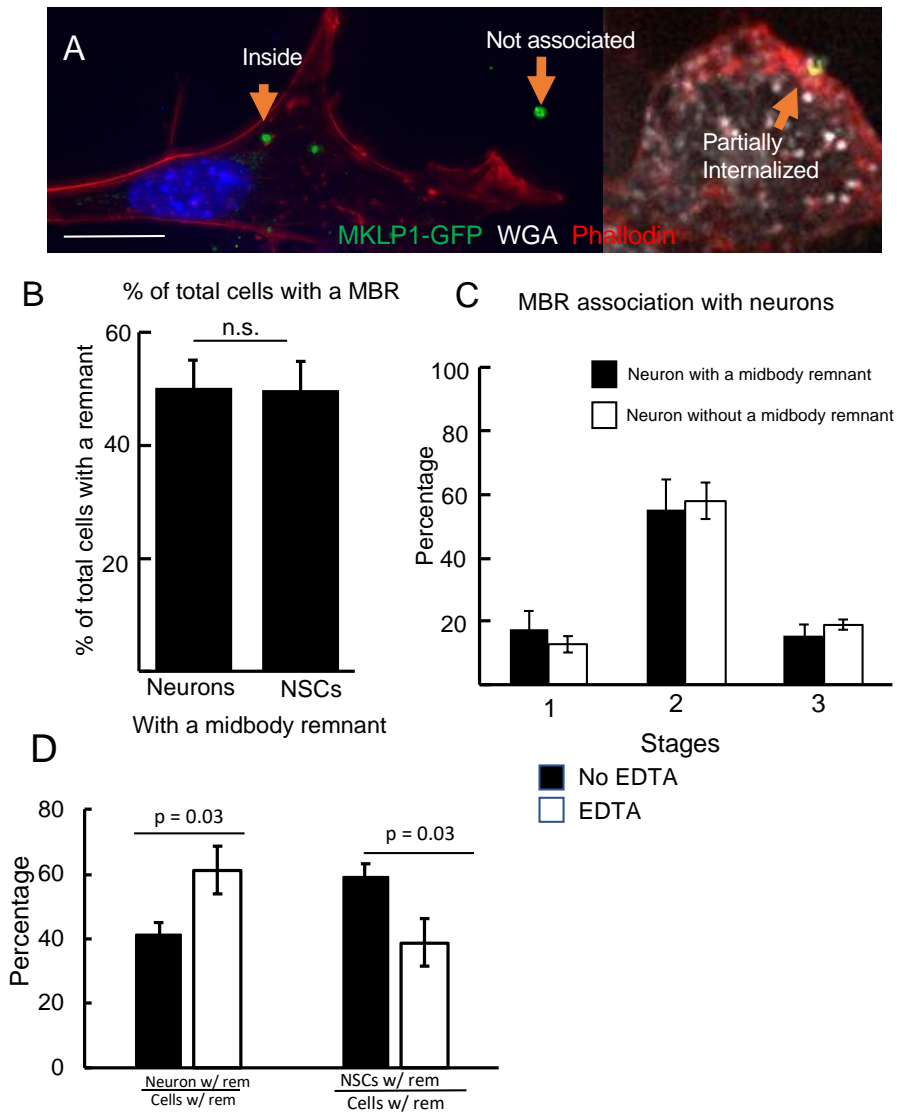


Figure App 3-1: HeLa cell remnants do not offer cell fate or polarization cues to cultured neural stem cells

(A) Example images of neural stem cells (NSCs) immunostained for actin, wheat germ agglutinin (WGA), and GFP (MKLP1+ HeLa Midbody Remnants (MBR)). Arrows are pointing to MBRs. NSCs can engulf HeLa midbody remnants. **(B)** In NSC cultures MBRs from HeLa cells are associated with both neurons and progenitors equally. N= 11 coverslips **(C)** In neuron cultures midbody remnant association does not alter polarization. N=5 coverslips **(D)** Midbody remnants collected with or without EDTA are able to be associated with a neuron or an NSC. No EDTA n = coverslips = 6, EDTA n = coverslips = 5. B-D T-test., n.s., not significant Scale bar 10 μ m.

Appendix IV: Diaphanous- 3 (mDIA2) midbody localization is reduced in Kif20b knockdown HeLa cells

Diaphanous-3 (gene: *Diaph3*, protein: mDIA2) a formin, nucleates actin filaments to establish a scaffold for the contractile ring during cleavage furrowing and can shuttle between the nucleus and the cytoplasm (Miki et al., 2009; Watanabe et al., 2008). Additionally, mDIA2 has a separate function from traditional formin activity in which it can stabilize microtubules (Bartolini et al., 2008). mDIA2 localizes to the furrow during cleavage furrowing and then re-localizes to the midbody. When mDIA2 is depleted in cell lines, the contractile ring is unstable, causing furrow regression and increased binucleate cells (Watanabe et al., 2008). mDIA2 interacts with anillin in the cleavage furrow most likely stabilizing the furrow during ingression (Watanabe et al., 2010). mDIA2 has a microtubule-binding site in the C-terminus of the protein that is essential for the localization of mDIA2 to the midbody (Watanabe et al., 2010). Unfortunately, we do not know much about the role of mDIA2 in the midbody. We can hypothesize, that stabilizing microtubules within the midbody could be essential for proper recruitment of other midbody proteins and efficient abscission.

mDIA2 is expressed throughout the body and is essential for proper embryonic development. Two separate groups have developed mDIA2 knockout mice. Both groups found that mutant mDIA2 mice appear in Mendelian ratios up until embryonic day 10.5 (E10.5) (Damiani et al., 2016; Watanabe et al., 2013b). After E10.5, there was substantial death of the embryos. Of particular interest to us, mDIA2 mRNA is found diffusely in the brain at E10.5 and was more confined to neural stem cells (NSCs) and intermediate progenitors by E13.5 (Damiani et al., 2016). The depletion of mDIA2 in the brain through a floxed allele using EMX1-cre causes embryonic lethality and microcephaly. Embryos appear normal until E10.5 but most die before birth. Damiani et al. proposed that without mDIA2, there is a defect in the spindle assembly checkpoint allowing neural stem cells with mis-segregated chromatin to proceed into anaphase (Damiani et al., 2016). However, they did not examine cytokinesis or abscission at all. This mis-segregation of DNA leads to a 7-fold increase in aneuploid cells within the brain. These NSCs eventually exit the cell cycle or undergo apoptosis, reducing the proliferative capacity causing microcephaly.

An interactome study using affinity purification and mass spectrometry identified mDIA2 potential binding partners. It was confirmed through pull-downs and coimmunoprecipitation experiments that Kif20b and p53 are binding partners of mDIA2 (Isogai et al., 2015). mDIA2 and FBXO3 were found to increase the transcriptional activity of p53 (Isogai et al., 2015). This interaction was of interest to us because we want to investigate how depletion of Kif20b can activate p53. Separately, we found mDIA2 mRNA was upregulated in RNA sequencing comparing the double mutant Kif20b; p53 to single p53 mutant (Little, 2019). These data suggested to us that the loss of Kif20b influences mRNA levels of mDIA2. Therefore, we wanted to see how this altered the expression and localization of mDIA2 in the cell.

Based on these data, we hypothesized that mDIA2 would be increased in the midbody and able to activate p53 upon microtubule dysregulation or faster abscission. To determine if mDIA2 was increased in Kif20b depleted HeLa cells, antibodies from Proteintech (Cat 14342-1-AP, 1:100), and N-term and C-term antisera from (Watanabe et al., 2008) (1:50) were obtained. The HeLa cultures were fixed with methanol only (-20°C methanol for 10 minutes). Initially, images were taken on the Zeiss and the percentage of midbodies with and without mDIA2 were determined. We found 75% of random midbodies has mDIA2 on control coverslips suggesting mDIA2 is present for most of the abscission process. In the siKif midbodies, there was less than 25% with mDIA2 localization. To get better resolution, we imaged cells in anaphase and midbody stage with the same exposure time on the Deltavision and then drew line scans along the furrow or through the midbody. The line scans were drawn on the center z-plane for furrow analysis and the collapsed stack for the midbody analysis. Surprisingly, we found that in HeLa cells, all three siRNAs to Kif20b caused a loss of mDIA2 localization in both the cleavage furrow and the midbody when we used the Proteintech antibody (**Figure App 4-1A-D**). However, there appeared to be increased mDIA2 staining in the cytoplasm of the siKif20b HeLa cells (**Figure App 4-1E-F**). To test this, we drew a line across the middle z-plane of the cell. We found an overall increase in the intensity of mDIA2 in the cell, but there was clear mislocalization from the furrow and the midbody (**Figure App 4-1E-F**). For the N-term and C-term antisera from Watanabe lab, there was less of a definite conclusion. There was an increase in the background staining and disagreement between these two antisera (**Figure App 4-2A**). In control HeLa cells, for

both N-term and C-term antibody, the expected two peaks for mDIA2 localization at the dark zone were not detectable (**Figure App 4-2B, C**). Instead, the line drawn across the midbody looked flat. For the C-term antiserum, there appeared to be a decrease in the antibody staining in the midbody, but for the N-term antiserum, there was no difference. It is important to note that both of these antibodies were made ten years prior and were the serum, not the purified antibodies used in the original paper (Watanabe et al., 2008). Since the expected peak in the control cells were not present in the line scans, it is hard to make any conclusions from these antibodies.

We tried all three of these antibodies on neural stem cell cultures that were fixed with methanol. There was inconsistent staining, but we were able to find a few control cells with localization (less than 10 out of 50 cells across three different antibodies, examples in **Figure App 4-3**). Unfortunately, the failure of these reagents to reliably stain mDia2 in mouse cells or tissue make it challenging to determine if this mislocalization of mDIA2 from the midbody to the cytoplasm happens within dividing NSCs in the brain. Due to the inconsistency in the staining, I did not try these antibodies on Kif20b mutant proteins, MEFs, or slabs.

The RNA sequencing data combined with the antibody staining of mDia2 mislocalization in Kif20b-depleted HeLa cell midbodies help begin to piece together how Kif20b and mDIA2 may be a part of the p53 axis that activates cell death in response to abscission defects. We now hypothesize mDIA2 is unable to localize to the midbody during cytokinesis without Kif20b, therefore, increasing its shuttling into the nucleus and activation of p53. Kif20b may bring mDIA2 to the midbody or be responsible for sequestering it at the midbody. Alternatively, it is possible that without Kif20b, the microtubules are too loose in the midbody to adequately provide the scaffolding for mDIA2 to relocate from the cytoplasm and the furrow to the midbody (indirect effect). To test this hypothesis, we measured the nuclear to cytoplasmic ratio of mDia2 signal intensity in early and late telophase cells (**Figure App 4-4**). We found that there was no significant increase in the nuclear localization of mDIA2 in HeLa cells that were knockdown for Kif20b. This finding is evidence against our hypothesis, but it is important to note that HeLa cells do not have a normal p53 response. Therefore, mDIA2 nuclear localization could be disrupted.

This project is exciting and deserves further exploration. To further explore the role of mDIA2 in cytokinesis, we would want to have an inducible knockdown of mDIA2 in cell lines and perform synchronization of the culture. By making sure all the cells are in the same part of the cell cycle, we would be able to knockdown mDIA2 only after furrowing is complete. We would avoid any of the known defects the loss of mDIA2 causes in cleavage furrowing and be able to focus on the late cytokinetic role. It would be interesting to see if mDIA2 loss had any effect on abscission and if the result would be similar to Kif20b, dysregulated/faster abscission. We have access to gfp-mDIA2 HeLa cells that we can use to knockdown Kif20b in and more definitively determine if mDIA2 accumulates in the nucleus of cells in cytokinesis. We also have a stable short hairpin-mDIA2 HeLa cell line, which could be immunostained for Kif20b to see if mDIA2 is required for Kif20b recruitment to the midbody or at the midbody.

We have not entirely ruled out that mDIA2 might be triggering the activation of p53 and cell death in neural stem cells. We need an antibody that reliably works in neural stem cells to co-label with p53. HeLa cells do not have normal p53 activation; therefore, shuttling to the nucleus could be disrupted in HeLa cells but active in a cell type with normal p53 response. We could ask specifically in cells with p53 activation if the localization of mDIA2 increased in the nucleus. Averaging the nuclear to cytoplasmic ratio may miss the subtlety of the Kif20b phenotype since many of the neural stem cells do not activate p53 and subsequently undergo cell death. This experiment could be done in mouse embryonic fibroblasts from the Kif20b mutant mouse or knockdown in 3T3 cells. It would be worth determining if the antibodies we currently have work on MEFs or 3T3 cells before pursuing this experiment too far.

Figure App 4-1: Knock-down of Kif20b disrupts mDIA2 localization in the midbody and cleavage furrow

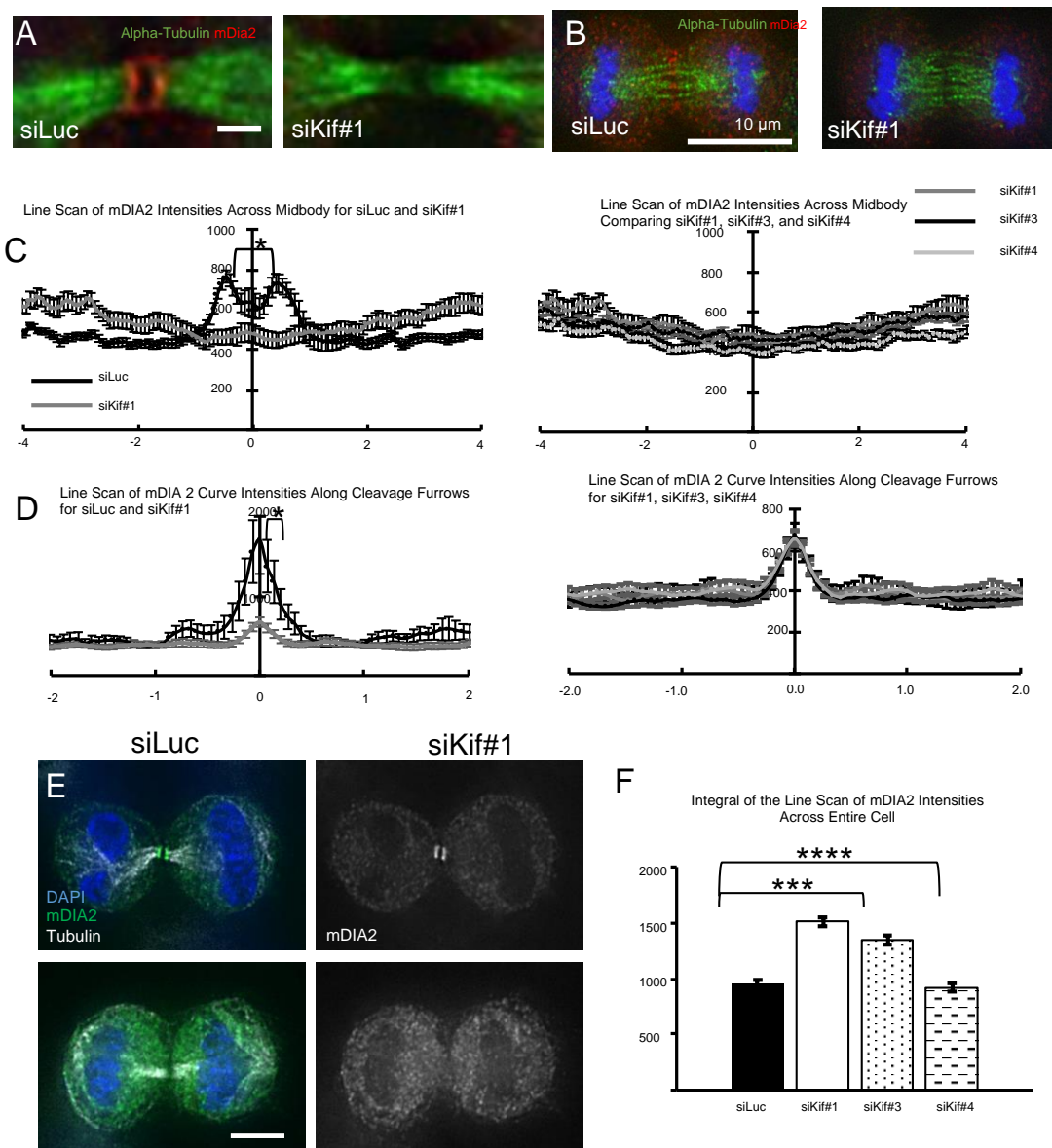


Figure App 4-1: Knock-down of Kif20b disrupts mDIA2 localization in the midbody and cleavage furrow

(A) Representative images of PROTEINTECH mDIA2 in the midbody and **(B)** cleavage furrow. HeLa cells were transfected with siRNA and then allowed to grow for 24hrs before fixation with cold MEOH for 10mins. Then immunostaining was done with DM1alpha at 1:500 and mDIA from Proteintech at 1:100. Images were then taken using the DV 60x and 1.6x mag.

(C) Line scans of mDIA2 intensity averages across (2 experiments, 4 cs per siRNA (2 cs per experiment), siLuc=64, siKif#1=44, siKif#3=49, siKif#4=50) midbodies. Significance also found on the sides of the dark zones. Line scans were drawn on the max projection.

(D) Line scans of mDIA2 curve intensity average along cleavage furrows (From the same coverslips as midbody pictures, 2 linescans per cell, n here is cell, siLuc=16, siKif#1=12, siKif#3=12, siKif#4=12) in anaphase cells. Both sides of the furrow were measured and included as an individual n. Line scans were drawn on the center z plane.

(E) Representative images of the center z-plane of the cell. Line scans were drawn across the entire cell at the center zplane in late anaphase to early telophase, and **(F)** area under the curve calculated from it to give estimate of the sum mDIA2 levels throughout the cell. Line scans were drawn on the center z plane. *P<0.05 ****P<0.0001

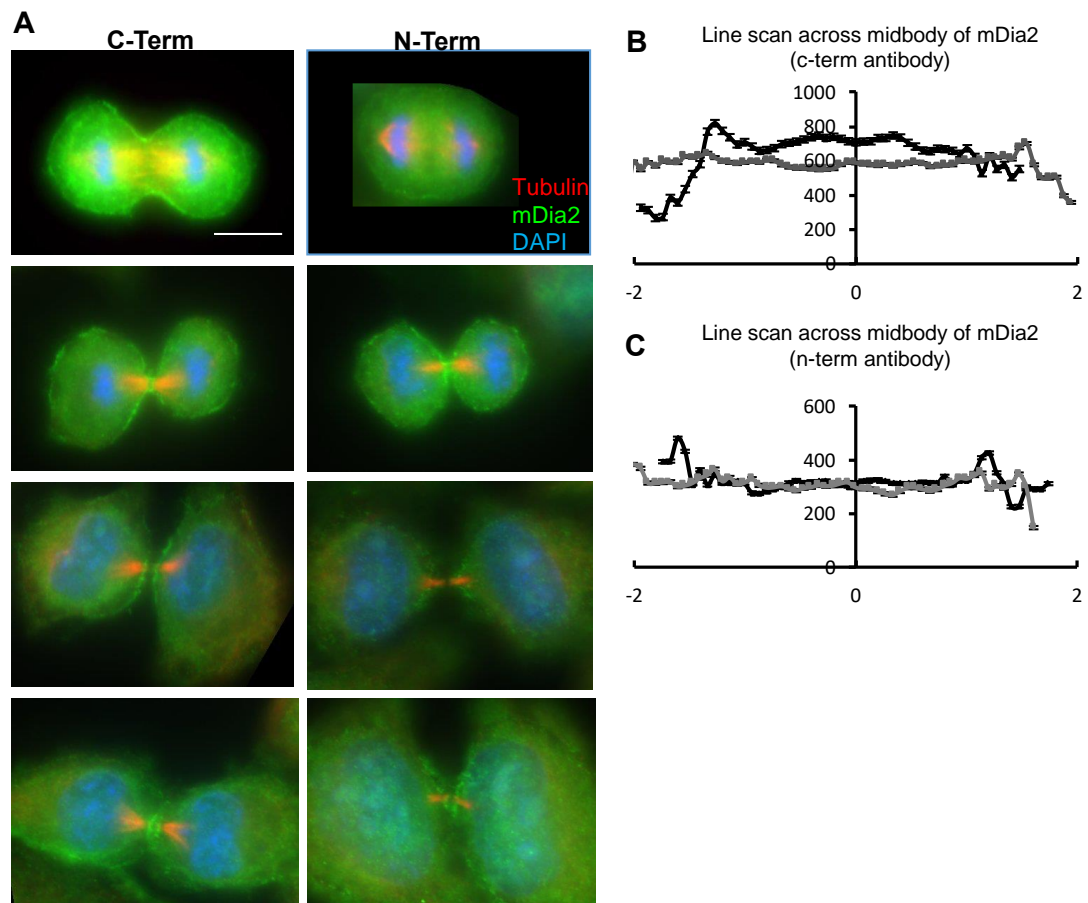


Figure App 4-2: Serum antibodies for mDIA2 are not as specific as Proteintech antibody

(A) Representative images of C term and N term serum antibody from Wanatabe et al. 2008 paper in the midbody of HeLa cells

(B) C-term serum antibody shows no midbody peak but an over all reduction of mDia2 at the midbody of HeLa cells.

(C) N-term serum antibody shows no difference between siLuc and siKif20b HeLa cells

Midbodies: C term antibody siLuc n= 21 siKif20 n=21, N term antibody siLuc n=19, siKif20b n=19

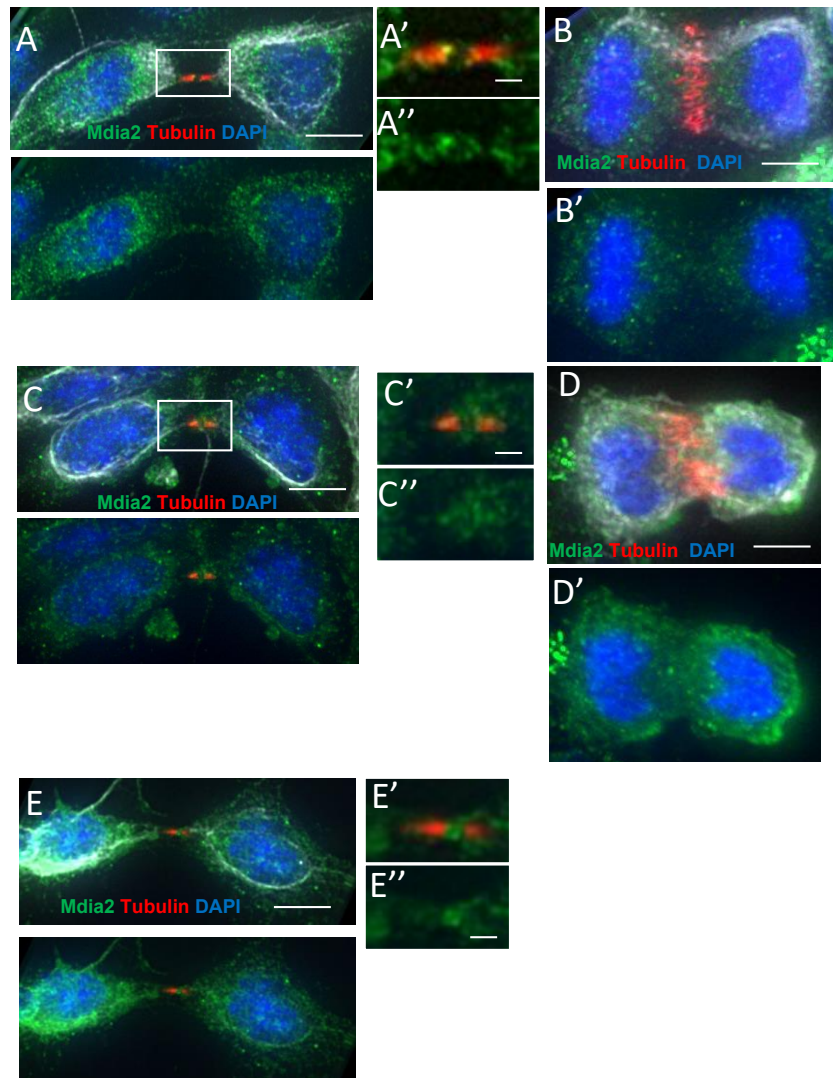


Figure App 4-3: Example images of mDia2 staining in E11.5 or E12.5 NSCs

A cultured NSC with a midbody (A,C, E) or a NSC in anaphase (B,D) is immunostained for mDia2 from proteintech (A,B), c-terminus (C,D) and n-terminus (E) serum antibodies.

Scale Bars 5 μm (A-E). Scale Bars 1 μm for insets A'-A'', C'-C'', E'-E''.

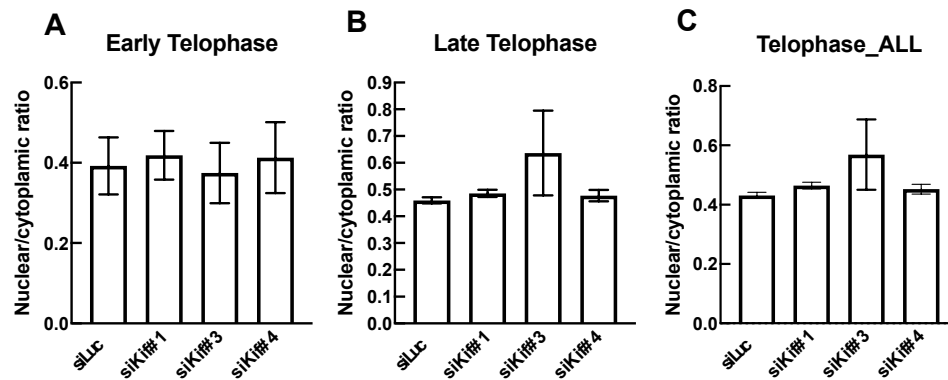


Figure App 4-4: The loss of Kif20b in HeLa cells does not increase mDIA2 nuclear localization

HeLa cells transfected with a control luciferase siRNA, or a Kif20b siRNA had their nuclear to cytoplasmic ratio of mDIA2 measured at early telophase **(A)** and late telophase **(B)**. **(C)** Combining both early and late stage telophase cells shows no difference in nuclear to cytoplasmic ratio. Early telophase was identified as a cell with midbody but the nuclear envelope had not reformed. Late telophase was identifies as a cell with a midbody and the nuclear envelope has reformed. Early telophase: n= siLuc 9, siKif1 8, siKif3 2, siKif4 7. Late telophase: n=siLuc n= 14, siKif1 14, siKif3 18, siKif4 19. Telophase: n= siLuc 23, siKif1 22, siKif3 20, siKif4 26

Appendix V: Kif20b mutant neuron outgrowth phenotypes differ on L1CAM and Laminin

Authors: Katrina McNeely, Sara Martin, and Noelle Dwyer

Introduction

Neurons are polarized cells with multiple dendrites and one axon that can extend the length of the human body. This polarized structure is essential for sending unidirectional signals down the axon. We have a limited understanding of the coordinated events that establish this important polarity. Previous studies have found that not only are the actin and microtubule cytoskeleton important, but intracellular signaling through kinases are involved (Lewis et al., 2013). The microtubule cytoskeleton is essential for establishing stable processes. Microtubules are continually switching between growing and shrinking phases and have an organization that is essential for neurite polarization, outgrowth, and axon/dendrite specification (Menon and Gupton, 2016; van Beuningen and Hoogenraad, 2016). This dynamic process underscores the complexity of establishing neuron polarity and axon outgrowth.

Microtubules play an essential role in axon outgrowth. Therefore, it is unsurprisingly that motor proteins are also vital (Hirokawa et al., 2010). Kif20b is a plus-end directed microtubule motor that can bind and bundle microtubules (Abaza et al., 2003). Kif20b localizes to the central spindle and midbody flanks of dividing cells (Abaza et al., 2003; Janisch et al., 2018). When Kif20b is lost in HeLa or neural stem cells, cytokinesis timing is perturbed ((Janisch et al., 2018), **Chapter II, III**). Recently, another lab and our lab found that Kif20b has a cell cycle independent role in brain development ((McNeely et al., 2017; Sapir et al., 2013), **Chapter IV**). A truncated Kif20b was shown to be able to localize into axons (Lipka et al., 2016). *Kif20b* mutant neurons have less Shootin1, a polarity protein, and difficulty polarizing *in vitro*. Axons of the neurons that can successfully polarize are shorter, wider, and retract more often ((McNeely et al., 2017), **Chapter IV**). Suggesting that microtubule instability may be the important commonality between the defects in the cell cycle and neurons.

In this Appendix, we further investigate Kif20b's role in microtubule stability. To do this, we grew *Kif20b* mutant neurons on two different substrates (L1CAM and Laminin). We

have previously shown that the loss of Kif20b disrupts microtubule organization within the axon and prevents efficient polarization. We had previously characterized neuronal defects in neurons grown on the standard neuronal substrate, poly-L-Lysine (PLL). We decided to explore the role of microtubule instability using L1CAM and Laminin because both substrates have been shown to cause microtubule bundling within the axon shaft (Burden-Gulley and Lemmon, 1996). One hypothesis was that the loss of Shootin1 in *Kif20b* mutants contributes to the polarization and axon outgrowth phenotype ((McNeely et al., 2017), **Chapter IV**). Here, we tested that hypothesis and found that when *Kif20b* mutant neurons were grown on L1CAM that Shootin1 localization was not restored, but the polarization was rescued and axon outgrowth phenotype was reversed into an overgrowth phenotype. Interestingly, on Laminin, there was a rescue of both polarization and axon outgrowth. These data allowed us to separate polarization and axon outgrowth as two separate processes. Interestingly, microtubule bundling can be rescued through substrate changes and microtubule bundling drugs but not localization of key polarity proteins.

Material and Methods

Cell culture

Neurons were cultured on 18 mm round coverslips that were washed twice every 10 minutes with distilled, UV-irradiated water and treated in nitric acid overnight. Before coverslips were placed in an oven at 160 °C overnight to dry and sterilize, they were washed 3 more times with distilled water. The next day after coverslips had cooled, each coverslip was treated with 200 µL poly-L-lysine (PLL) solution (1 µg/mL in borate buffer) and incubated overnight at 37 °C. This was followed by distilled water washes (2-hour washes were done twice following three quick rinses) and application of neuron plating media (.5 mL-1 mL). For L1CAM, coverslips were first coated with PLL as described above, then the next day, the coverslips were rinsed with distilled water for 3 times for 10 minutes and then the 2 hour long washes. The coverslips were then incubated in anti-human Fc antibody (Sigma Aldrich Cat#: I2136 1:500 in Sterile PBS (Cat#: Gibco 10010-023) for 2 hours at room temp in the cell culture hood. Coverslips were washed with sterile PBS 3 times quickly. Then incubate in FC-L1CAM (2µg/mL, cat # R&D Systems 777-NC-100) overnight in the 4°C fridge. The following day, the coverslips were rinsed 3 times quickly with sterile PBS. Next, neurons plating media was added. For Laminin

coating: coverslips were coated with 50µg/mL laminin (Sigma L2020-1mG) diluted in DPBS and incubated for 4 hours at 37°C. Coverslips were rinsed with DPBS and stored in DPBS until they were used. Neuron plating media is filter-sterilized and consists of 500 mL Minimum Essential Medium (MEM) with glutamine, 5 mL Penicillin/Streptomycin, 15 mL 20% glucose, 5 mL Sodium Pyruvate, and 10% Fetal Bovine Serum. At E14.5, pregnant females were sacrificed, and the embryos placed into cold HBSS mix (500 mL Hank's Balanced Salt Solution (HBSS) with 5 mL HEPES and 5 mL Penicillin/Streptomycin. Fine forceps were used to break apart the cortex, and then the pieces of cortex were collected and placed into a tube containing a 0.05% trypsin solution for 5-15 min in a 37 °C water bath. Following trypsin digestion, the resulting neuron pellets were rinsed 3 times every 5 min with HBSS mix and then treated with neuron plating medium during trituration. Appropriate volumes of the resulting solution of neuron plating medium and dissociated neurons were pipetted onto the PLL-coated coverslips to achieve a density of 50,000 cells/m. The media was switched from Neuron Plating Medium to Neurobasal and B27 (NB27) after three hours. NB27 is 49mL of neurobasal media and 1 mL of B27. 48 hours after being plated initially, the neurons were fixed in 2% Paraformaldehyde (PFA) for ten minutes and then in 2% PFA with 30% sucrose for 10 min. Finally, coverslips were rinsed in one time in Phosphate Buffer Saline (PBS) or MeOH for 10 min three times and kept at 4 °C until ready for immunofluorescent staining.

Immunocytochemistry

Following dissociation, neuron plating, and fixation, coverslips were incubated for an hour at room temperature in blocking buffer (0.1% Triton-X, 2% Normal Goat Serum in PBS) and then overnight at 4 °C or for 3 h at room temperature in appropriate primary antibody solution (antibody diluted in blocking solution). Primary antibodies used were a rabbit or mouse monoclonal antibody against neuron-specific beta-III tubulin (Tuj1) at a dilution of 1:500 in blocking buffer (Covance clone Cat# 1-15-79 D71G9 and MMS-435P, Abcam Cat# ab52623), a mouse monoclonal antibody against acetylated tubulin (Sigma Cat# T-6793) at a dilution of 1:800 in blocking buffer, and (green)-Phalloidin (Molecular Probes Cat# O7466) at a dilution of 1:50, Shootin1 (B627 and C094 from Orly Reiner 1:100). After primary incubation, coverslips were rinsed in PBS (every 10 minutes for 30 minutes) and then incubated at room temperature with appropriate secondary antibody solution (1:200 dilution) for 30 min in the dark. Species-specific secondary antibodies

were conjugated to Alexa fluorophores (Invitrogen) at a dilution of 1:200 in blocking buffer. After secondary incubation, coverslips were rinsed in PBS in a dark drawer (every 10 minutes for 20 minutes), and then nuclei were stained with DAPI (Invitrogen, Cat# D1306) at a concentration of 1:100 in a dark drawer. Following final washes of PBS in dark drawer, coverslips were mounted onto glass slides with Fluoromount.

Image acquisition and analysis

Fluorescent images were obtained on a Carl Zeiss widefield epi-fluorescence microscope via AxioVision camera and software. Low-magnification images for stage analyses were taken at 20x, while high-magnification images for neuron measurements were taken at 40x or 100x. Image analysis was completed through ImageJ software. Neurite lengths were measured from the base of the process at the soma to the tip of the beta-III tubulin stain. Stage 3 neurons' widths were measured in thickness at 10 μm and 25 μm from the edge of the soma.

Polarity stage analyses

Neurons were considered to be in Stage 1 if they extended broad lamellipodia with no clear, coalesced neurites. The neurites of Stage 2 neurons are all a similar length. A neuron was Stage 3 when one neurite was at least twice as long as the next longest neurite. Axonal branches were counted if they had significant microtubule invasion.

Acetylation and Shootin line-scan analysis

Either 40x or 100X images were taken at the same exposure time of Shootin, beta-III tubulin, or Acetylated Tubulin on Carl Zeiss widefield epi-fluorescence microscope via AxioVision camera and software, images were uploaded into Zen software for analysis. Lines were drawn from the base of the soma to the tip of the axon. Intensity values for each channel (acetylated tubulin, beta-III tubulin, or Shootin) were recorded for all points along the line.

Addition of Sir Tubulin

Neurons were grown for 24 hours at 37°C in an incubator with 2 mL of NB27 media. Then 1mL of NB27 media was removed, and 1 mL of 200nM SiR-Tubulin (from Cytoskeleton, Cat# CY-SC002) diluted in NB27 was added. The final concentration was 100nM of Sir Tubulin. After the addition of SiR-Tubulin was complete, neurons were allowed to grow for an additional 24hours before fixation.

Statistics

Significance was tested using Prism by GraphPad. One-way ANOVA was used for multiple comparisons, and Student's T-test was used to find significance between two variables when no other variables were compared.

Results

Kif20b mutant axons grow longer than controls on L1CAM

Kif20b interacts with the polarization protein Shootin1 (Sapir et al., 2013). We have previously shown that Shootin1 localization in the axons of *Kif20b* mutant neurons is disrupted in the axonal growth cone ((McNeely et al., 2017), **Chapter IV**). This loss of localization was present on the substrate poly-L-Lysine (PLL). Interestingly, when Shootin1 is knocked-down in neurons, a noticeable length change is only detectable on the substrate Cell Adhesion Molecule L1 (L1CAM), not PLL (Shimada et al., 2008). To further understand the *Kif20b* mutant phenotype, we grew *Kif20b* mutant neurons on the L1CAM instead of PLL. L1CAM is a cell adhesion molecule that promotes axon outgrowth (Doherty and Walsh, 1996; Kiryushko et al., 2004). L1CAM has been shown to interact with Shootin1 and hypothesized to be a part of the actin treadmilling force that allows axons to extend from the growth cone (Kubo et al., 2015; Shimada et al., 2008; Toriyama et al., 2013). We hypothesized that the reduction in Shootin1 in *Kif20b* mutants would be compounded when the neurons are grown on L1CAM. Surprisingly, we found that the *Kif20b* mutant neurons on L1CAM were able to grow axons that were 30% longer than controls, and twice the length of the *Kif20b* mutant axons on PLL (**Figure App 5-1A, B**).

This substantial outgrowth was very surprising to us. We wondered if this additional growth was due to neurons polarizing faster or more than controls. To measure neuron polarization, we classified neurons using the Banker staging criteria (Methods, (Dotti et al., 1988)). Simply, a stage 3 neuron has a neurite that is more than twice the length of any other neurite. We found that control neuron cultures were 40% polarized (Stage 3) by day 2 of culture when grown on PLL or L1CAM (**Figure App 5-1C, black bars**). Interestingly, the *Kif20b* mutants had decreased polarization on PLL (24% of neurons

polarized), which was partially rescued to 32% on L1CAM ((McNeely et al., 2017), **Figure App 5-1C**).

L1CAM partially rescues polarization and promotes axon outgrowth in the *Kif20b* mutants. We decided to look at Shootin1 localization in the axons of the *Kif20b* mutant neurons grown on L1CAM. We hypothesize this was due to the increase in the sequestering of Shootin1 in the axonal growth cones. To test this, we grew neurons on L1CAM and immunostained with Shootin1 antibodies from the Reiner lab. Shootin1 has two known isoforms, long (631 amino acids) and short (1- 456 amino acids). Shootin1 B627 is a polyclonal rabbit antibody made to the first 456 amino acids. It recognizes both the long and the short form of Shootin1 (Personal Communication with Tamir Sapir). Shootin1 C097 is a polyclonal rabbit antibody made against the C-terminal fragment (413 – 630 amino acids) and can recognize both long and short forms on western blot (Personal communication with Tamir Sapir). To determine if Shootin1 localization was restored in *Kif20b* mutant neurons, we drew a line down the axon and measured the raw intensity values of Shootin1 (as previously described in (McNeely et al., 2017)). There was still a significant decrease in Shootin1 expression in the growth cone of the *Kif20b* mutant neurons compared to the control (**Figure App 5-1D-F**) when we used the B627 antibody (**Figure App 5-1F**). There was a similar trend for the C094, but we did not reach significance most likely due to the small n (**Figure App 5-1G-I**). These data suggest that the enhanced axon extension we observe on L1CAM is through a different mechanism than Shootin1 localization to the growth cone.

We tried several other Shootin1 antibodies on *Kif20b* mutant neurons. We tried Shootin1 from Proteintech (KIAA1598) made to amino acids 399 to 631 of Shootin1. Immunostaining did not work on neurons, but this antibody worked well on western blot. We received a Shootin1 antibody made in the Inagaki lab and was raised to the full-length protein. We tried this antibody on *Shootin1* heterozygous and *Shootin1* mutant neurons. The immunostaining was very weak, even at a high concentration of 1:50. This antibody does lose specific staining in the *Shootin1* mutant neurons but was not bright enough to warrant trying on the *Kif20b* mutant neurons. We received a phospho-shootin1 antibody made by Inagaki Lab. Phospho-Shootin1 was of interest to us because it has enhanced interaction with F-actin, which promotes axonal outgrowth (Toriyama et al., 2013). We tried this antibody on control neurons, and there was no

visible immunostaining. It is worth noting that this antibody arrived at the Dwyer Lab warm from the Inagaki lab.

Kif20b mutant neurons grow longer processes on L1CAM

To determine if the enhanced axonal outgrowth on L1CAM was specific to the axon outgrowth, we examined dendrite length and number, axon branching, and filopodia of the axonal growth cone. There was a slight reduction in the number of dendrites per cell in the *Kif20b* mutants grown on L1CAM (**Figure App 5-2A**). Overall, the dendrites grew longer than controls on L1CAM, but when all the dendrite lengths were added together, control and *Kif20b* mutants were similar (**Figure App 5-2B, C**). The dendrite outgrowth data suggests that L1CAM supports neurite outgrowth in general, but does not alter *Kif20b* mutant dendrites outgrowth in the extreme. Since the axons seem to be the most altered process in the *Kif20b* mutant neuron, we focused on microtubule branching from the axon, next. The percent of neurons with a least one axon branch did not change between control and *Kif20b* mutant on L1CAM; neither did branch density (**Figure App 5-2D, E**). Branch length increased for both controls and *Kif20b* mutants on L1CAM, but the increase was greater in the *Kif20b* mutants (**Figure App 5-2F, G**). The increased branch growth further supports the idea that *Kif20b* mutants are more pro-growth on L1CAM.

If the *Kif20b* mutant microtubules are more splayed, we hypothesized that the bundling defect we see on PLL would be rescued on L1CAM. We found that *Kif20b* mutant axons are not wider at 10 μ m or 20 μ m from the soma when grown on L1CAM (**Figure App 5-2H**). Suggesting changing the substrate is sufficient to promote microtubule bundling. A striking finding from our previous paper showed an increase in the length of actin-rich filopodia in the *Kif20b* mutant axonal growth cones ((McNeely et al., 2017), **Chapter IV**). Control filopodia do not grow longer on L1CAM, and *Kif20b* mutant filopodia decrease in length about 7% on L1CAM (**Figure App 5-2I**); therefore, the filopodia phenotype seen on PLL was rescued on L1CAM. Axonal microtubules in control cells grown on L1CAM do reach the leading edge of the growth cone, possibly stabilizing the transient filopodial outgrowth (Burden-Gulley and Lemmon, 1996). This could be why in the case of the *Kif20b* mutants on L1CAM, the filopodia regain normal growth dynamics, which suggests a link between microtubule dynamics and filopodia outgrowth. As mentioned in the

previous section, Shootin1 is not rescued, therefore what about the L1CAM substrate is able to compensate for the loss of Kif20b in regards to polarization and filopodia length but allow for the enhanced outgrowth of axons. Since we previously proposed that *Kif20b* mutant axons had dynamic microtubules, maybe L1CAM can stabilize the microtubules (McNeely et al., 2017). We hypothesize that L1CAM can stabilize the microtubules just enough to enhance axon outgrowth. Therefore, we wondered if another commonly used substrate in culture, Laminin, would rescue similar phenotypes.

Kif20b mutant neuron polarization and axon length defects are rescued on Laminin

To investigate if polarization and axon morphology changes we see in *Kif20b* mutant neurons when grown in L1CAM are specific to this substrate or are a result of rescued microtubule stabilization we grew neurons on Laminin, an extracellular matrix protein. Laminin can also promote axon outgrowth (Powell and Kleinman, 1997). When neurons grow on Laminin, like L1CAM, the microtubules are tightly bundled in the axon shaft and then begin to splay out into the axonal growth cone (Burden-Gulley and Lemmon, 1996). The axonal growth cone microtubules on L1CAM are curved and may reach the leading edge of the cell and have a more splayed appearance. The microtubules on Laminin have a straight appearance and are confined to the central region of the growth cone (Burden-Gulley and Lemmon, 1996). Axons of both control and *Kif20b* mutants are longer on Laminin compared to PLL (increased length by 16% and 28%, respectively, **Figure App 5-3A, B**). However, the *Kif20b* mutants do not display the enhanced axon outgrowth, as seen on L1CAM (**Figure App 5-1B**). Control and *Kif20b* mutants have enhanced polarization on Laminin, with *Kif20b* mutant neurons having a 95% increase in polarized neurons (**Figure App 5-3C**). Neurons grown on Laminin have axons that are the same width as controls (**Figure App 5-3D**). There was an 18% decrease in filopodia length for the *Kif20b* mutants on Laminin, and even the control filopodia were shorter (**Figure App 5-3E**). However, there is a no difference between control and *Kif20b* mutant on Laminin. Further supporting the idea of microtubule placement within growth cones promoting filopodia growth and stabilization. In the case of neurons grown on Laminin, the microtubules make less contact with the leading edge and are not able to promote growth leading to shorter filopodia.

The mechanism for polarization, axon width, and filopodia length are dependent on something in common with Laminin and L1CAM. The "stickiness" of the substrate may promote a more natural environment allowing for increased polarization and regulated axon width and filopodia length. We can now separate polarization (axon initiation) and axon outgrowth as two independent phenotypes in the *Kif20b* mutant. The interaction between L1CAM and *Kif20b* mutant neurons that promotes excess axon growth remains elusive.

Axon stabilization on L1CAM: Finding a balance for outgrowth

One hypothesis is that L1CAM balances the microtubule dynamics of *Kif20b* mutant neurons enough to promote uninhibited axon growth. Acetylation of lysine 40 on alpha-tubulin is a post-translational modification (PTM) that marks more stable, long-lived microtubules (Janke and Montagnac, 2017). When the acetyltransferase, MEC-17, is lost, decreased acetylation in the neurons causes increased microtubule de-bundling, invasion of microtubules into the filopodia, and increased plus dynamics (Dan et al., 2018). This phenotype is reminiscent of our previous findings in the *Kif20b* mutant neurons on PLL ((McNeely et al., 2017), **Chapter IV**). To test if there are changes in the long-lived microtubules in *Kif20b* mutant cultures compared to controls, we immunostained for acetylated-tubulin and beta-III tubulin. The intensity of the acetylated tubulin and beta-III tubulin within the axon were measured similarly to Shootin1 (Methods). The raw intensity of acetylated tubulin and beta-III tubulin were increased in the axons of *Kif20b* mutants grown on L1CAM ((intensities were summed from 50 μ m of the axon starting from the growth cone) (**Figure App 5-4B**)). The ratio between acetylated tubulin and beta-III tubulin in the axon was also increased in the *Kif20b* mutants on both PLL and L1CAM. The proportion of acetylated tubulin and beta-III tubulin increased on L1CAM in the controls suggests that the change in the substrate was able to stabilize microtubules. There is a range of axon lengths within each culture. We hypothesized that axons that were the longest would have increased ratio of acetylated tubulin to beta-III tubulin compared to shorter axons. We found that the ratio is increased in *Kif20b* mutants compared to controls on both PLL and L1CAM at the shorter axon lengths (**Figure App 5-4D, E**). At the longer axon lengths, we find that the controls also have increased acetylated tubulin and are not significantly different

compared to the *Kif20b* mutants. We would hypothesize that on PLL, the increased acetylation is inhibitory, but on L1CAM, this inhibition is lost.

To try to determine if stabilizing microtubules can rescue both the polarization and axon outgrowth phenotypes in the *Kif20b* mutants, we decided to use a drug approach. We treated neurons grown for 24 hours *in vitro* with Silicone-Rhodamine Tubulin (SiR-Tub) at levels just below the known dose to inhibit mitosis (100nM (Lukinavicius et al., 2014)). Neurons were exposed to SiR-Tub for 24 hours before fixation. SiR-Tub is a live fluorescent microtubule marker that can bind to microtubules, based on Docetaxel (Lukinavicius et al., 2014). Neurons treated with a media change, a known neuron stressor, or a similar concentration of DMSO to the SiR-Tub served as a control to the SiR-Tub treatment. This paradigm allowed us to measure both the polarization and axon outgrowth at 48 hours *in vitro*. Polarization in the *Kif20b* mutant was rescued on both PLL and L1CAM when SiR-Tub was added (**Figure App 5A**) — adding further evidence to our hypothesis that stabilization of the *Kif20b* mutant microtubules was enough to rescue the polarization phenotype. We measured the axon length of control and *Kif20b* mutant neurons grown on PLL and treated with SiR-Tub, DMSO, or underwent a media change. Control axons grown on PLL were not affected by any of the treatments (**Figure App 5B, black bars**). Excitingly, only the SiR-Tub treatment in the *Kif20b* mutants rescued the axon growth defect on PLL (**Figure App 5B, white bars**). When control or *Kif20b* mutants were grown on L1CAM, axon lengths were longer than axons grown on PLL, as expected. Interestingly, the control neurons grew even longer on L1CAM when treated with SiR-Tub (**Figure App 5C, black bars**). However, in the *Kif20b* mutant axons grown on L1CAM, the axon length is decreased compared to controls or *Kif20b* mutant neurons that had a media exchange (**Figure App 5C**). Together these data suggest there is a delicate balance of microtubule stabilization that can promote axon growth, and the threshold for promoting polarization is more flexible than for axon outgrowth.

Discussion

The loss of *Kif20b* in neurons causes polarization and axon outgrowth defects. Interestingly, when *Kif20b* mutant neurons are grown on L1CAM and Laminin, many of these defects are rescued, and in fact mutant axons grow longer than controls' on

L1CAM (**Table App 5-1**). We have shown that polarization and axon outgrowth can be separated and require different levels of microtubule stability to complete successfully. Interestingly, a slight increase in microtubule stability using taxol is enough to induce polarity in hippocampal neurons (Witte et al., 2008), further supporting the idea that polarization needs less microtubule stability or can complete successfully within a broader range of microtubule stability, which is why it is the commonly rescued phenotype across L1CAM, Laminin, and SiR-Tub.

<i>Kif20b</i> mutant phenotype			
	PLL	L1CAM	Laminin
Shootin1 Localization	Reduced axon localization	Reduced axon localization	-
Polarization	Reduced	Rescued	Rescued
Axon Length	Shorter	Overgrowth	Rescued
Axon Branching	Not changed	Longer	-
Axon Width	Wider	Rescued	Rescued
Filopodia Length	Longer	Rescued	Rescued
Dendrite Length	Not changed	Not changed	-
Acetylated Tubulin	Increased in axon	Increased in axon	-
SiR-Tubulin Treatment	Rescued axon length	Rescued axonal overgrowth and polarization	-

Table App 5- 1: Summary of *Kif20b* mutant phenotypes on different substrates. Rescued means that the *Kif20b* mutants are statistically similar to controls.

Kif20b is an important microtubule motor in neuron morphogenesis and regulates microtubule stabilization to ensure controlled axon outgrowth. We have not determined how the loss of *Kif20b* tips the balance of microtubule stabilization. *Kif20b* is important for more than sequestering or delivery of Shootin1. *Kif20* appears to help facilitate tight bundling of microtubules in the axon (could be direct or indirectly). Other polarization or axon outgrowth proteins may be disturbed when *Kif20b* is lost. *Kif20b* mutant neurons have opposite outgrowth phenotypes on PLL versus L1CAM (short versus long). *Kif20b* mutant neurons treated with SiR-Tub grow longer on PLL. The overgrowth phenotype on L1CAM is prevented since there is no difference between *Kif20b* mutant axon length on PLL and L1CAM when treated with SiR-Tub. Control neurons are longer on L1CAM but are unchanged on PLL with the addition of SiR-Tub. These data suggest that there is a narrow window of microtubule stability in neurons that successfully promotes axon

outgrowth but not axonal overgrowth. Without Kif20b, this regulation is lost and causes defects in outgrowth.

Neurons grown on L1CAM and Laminin have different microtubule organization in the axonal growth cone (Burden-Gulley and Lemmon, 1996). The axonal growth cone microtubules on L1CAM are curved and may reach the leading edge of the cell and have a more splayed appearance. Microtubules of axons grown on Laminin have a straight appearance and are confined to the central region of the growth cone (Burden-Gulley and Lemmon, 1996). It is reasonable to speculate that more microtubules within the periphery of the growth cone may promote continued axon outgrowth. Interestingly, both L1CAM and Laminin were able to rescue the *Kif20b* mutant filopodia phenotype, so that could mean that these peripheral microtubules aren't necessary for filopodia outgrowth. However, they might promote axonal outgrowth since the filopodia grow longer on L1CAM compared to Laminin.

To better understand Kif20b's role in microtubule stability, we need to investigate Kif20b's localization as well as the microtubule dynamics with and without Kif20b. It would be nice to have a knockin mouse that has Kif20b tagged. This mouse might allow us to see where Kif20b resides within the axon and how closely it associated with microtubules in the growth cone. Since knockin mice can be difficult to make we could express HA-tagged Kif20b construct or the truncated Kif20b-GFP construct. We could stain for HA and hopefully find the possible localizations of Kif20b in neurons. Additionally, we could determine other binding partners of Kif20b in the axon. Having a tagged Kif20b would prove useful to try to determine how Kif20b fits into the already documented L1CAM/Shootin1 outgrowth process. To address the microtubule dynamics we could further explore two lines of inquiry that we have tried before, SiR-Tubulin labeling to look for microtubule looping and staining with EB1 or EB3. We have tried to look at the microtubules with SiR-Tubulin in neurons, the microtubules look beautiful but it is difficult to find the neurons. Therefore, combining with a live membrane marker like the MTMG mouse could prove useful. We have also previously stained for EB1 and did not see any striking differences but no quantification was done.

Figure App 5-1: Kif20b neurons polarize more and grow longer axons on L1CAM.

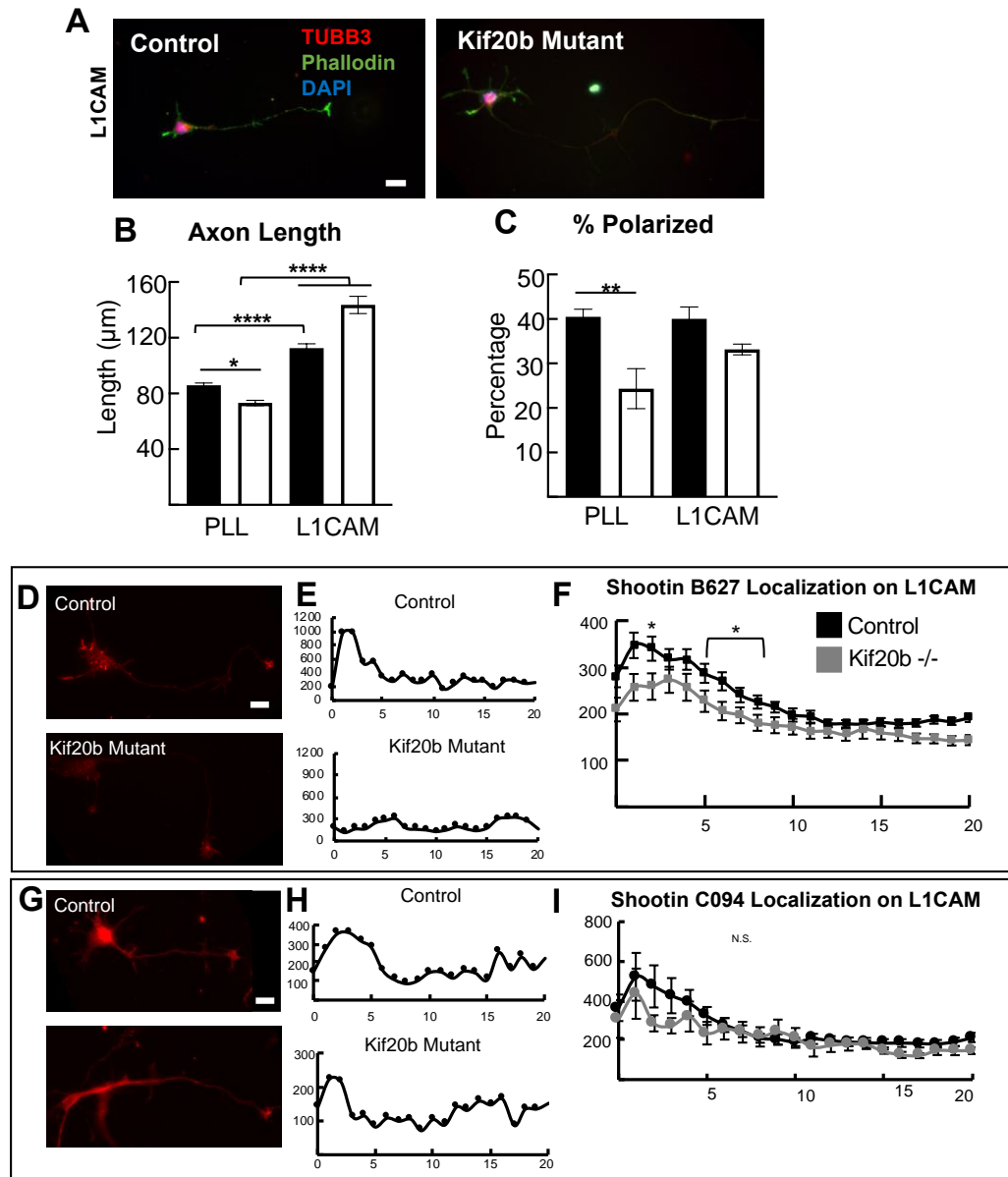


Figure App 5-1: Kif20b neurons polarize normally and grow longer axons on L1CAM

(A) Representative images of E14.5 stage 3 (polarized; having one neurite at least twice as long as any other) cortical neurons grown on L1CAM for 2 days and stained for neuron-specific beta-II tubulin (TUBB3, *red*), actin (phalloidin, *green*), and nuclei (DAPI, *blue*). Scale bar 1 μ m. **(B)** The average axon length (\pm s.e.m.) of control and Kif20b mutant (-/-) when grown on PLL (*black bars*) and L1 (*white bars*). Mutant cultures grow significantly longer than mutants on PLL and controls on L1. $n=397$ total control, and 260 total mutant neurons on PLL and $n=364$ total control and 270 total mutant neurons on L1. Neurons taken from 3 wild type, 4 heterozygous, and 4 mutant brains. ANOVA: * $p<0.05$, ** $p<0.01$ **** $p<.0001$. **(C)** The percent of stage three axons (\pm s.e.m.) are no longer significantly different between controls and mutants when grown on L1. PLL and L1: Ctrl $n=7$ brains Kif20b mutant $n=5$ brains. Stage 3 neurons grown on L1CAM were immunostained for Shootin B627 (**D**) or Shootin CO97 (**G**). There is less Shootin in the axons of Kif20b mutants compared to controls when using both antibodies (**E,F,H,I**). Scale bars for D, G 10 μ m. F,I: T-Test: * $p<0.05$. N: Shootin B627: Control (All HET) = 159, 4brains, Kif20b mutant =83, 4 brains; : Shootin C097: Control (WT and HET) = 30, brains, Kif20b mutant =12.

Figure App 5-2: Kif20b mutant neurons have longer axonal branches and rescue the filopodia defect on L1CAM.

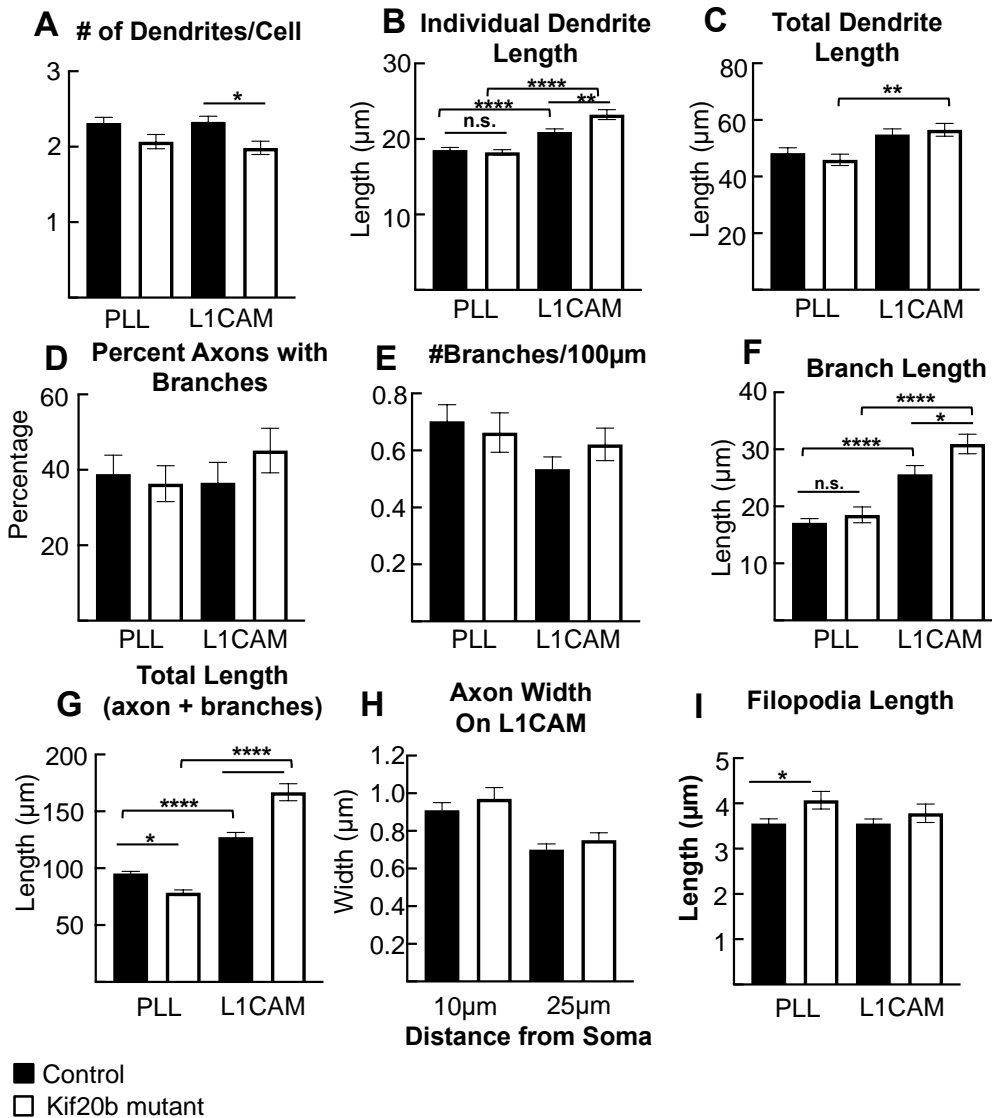


Figure App 5-2: Kif20b mutant neurons have longer axonal branches and rescue the filopodia defect on L1CAM

(A) Dendrite number N= cells PLL: Ctrl =364, Mutant =253, L1: Ctrl=356, Mutant=263
 (B) Individual Dendrites N= dendrites PLL Ctrl =842, Mutant=522, L1 Ctrl=828, Mutant =521
 (C) Total Dendrite length N= cells PLL Ctrl =324, Mutant =207, L1 Ctrl=317, Mutant =214
 F. Branch Length N= branches PLL: Ctrl = 229, Mutant =125; L1 Ctrl= 216, Mutant =213
 E, G #Branches/100 μ m and Total Length N= cells PLL: Ctrl =395, Mutant=259, L1: Ctrl=363, Mut=365. (H) Axon width (\pm s.e.m.) is not significantly different between controls and mutants on L1 at 10 or 20 μ m down the axon from the cell body. $n=81$ total control control and 80 total mutant neurons from 3 control and 3 mutant brains.. (I) Filopodia length (\pm s.e.m.) is not significantly different between controls and mutants when neurons are grown on L1. $n=335$ control and 170 mutant neurons from 4 and 3 brains respectively. ANOVAs A-G, I, H is T-test * p value < 0.05, **p value < 0.01, *** p value < 0.001 ****p value <0.0001, n.s. not significant

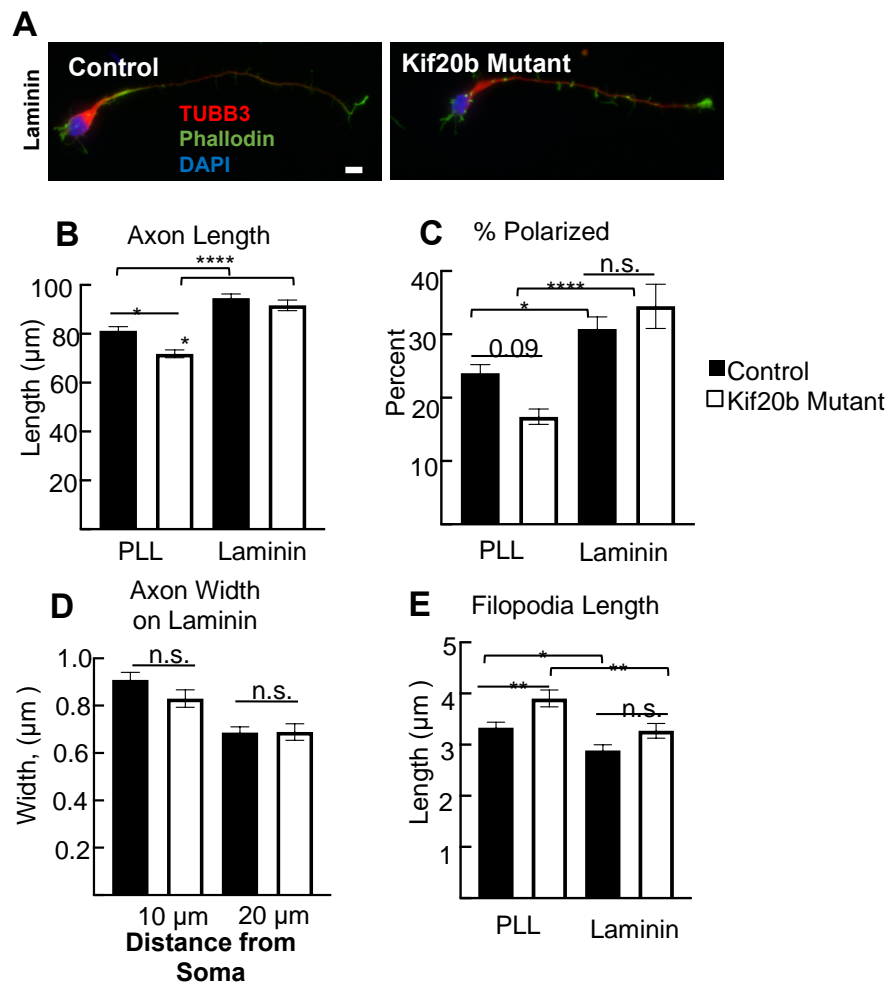


Figure App 5-3: Kif20b^{-/-} cortical neuron polarization and axon outgrowth is similar to controls when grown on laminin

(A) Control and Kif20b mutant neurons grown on laminin for 48 hours. **(B)** The average axon length (\pm s.e.m.) between control and mutant stage 3, polarized neurons is not significantly different on Laminin. $n=391$ control and 277 mutant neurons analyzed from 5 and 3 brains respectively. **(C)** The percent of stage three axons (\pm s.e.m.) are not significantly different between controls (*black bars*) and mutants (*white bars*) when grown on Laminin. PLL and Laminin Control $n=10$ coverslips, 5 brains; PLL and Laminin Mutant $n=6$ coverslips, 3 brains. **(D)** Axon width (\pm s.e.m.) is not significantly different between controls and mutants on Laminin at 10 or 20 μ m down the axon from the cell body. $n=100$ total control control and 60 total mutant neurons from 5 control and 3 mutant brains. **(E)** Filopodia length (\pm s.e.m.) is not significantly different between controls and mutants when neurons are grown on Laminin. PLL: control 245, Mutant 151 L1: control=183 Mutant =157 filopodia from 5 and 3 brains respectively. Significance found using ANOVA: * p value < 0.05, **p value < 0.01, ****p value < 0.0001, n.s. not significant

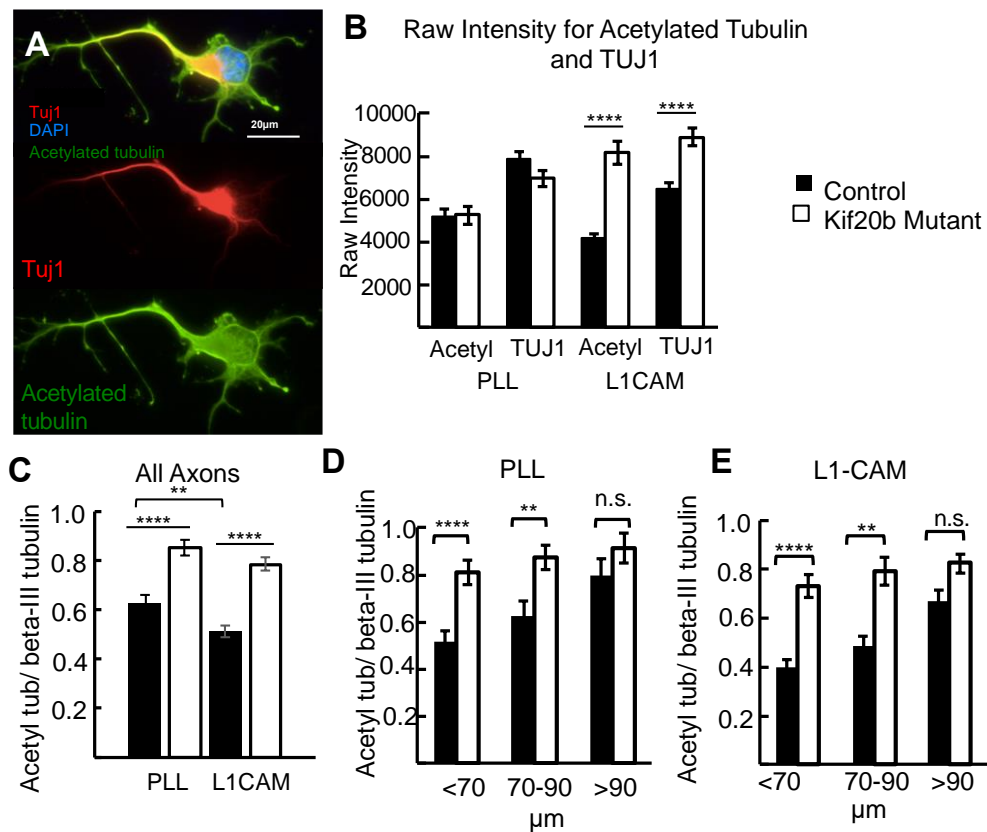


Figure App 5-4: Increased ratio of acetylated tubulin to tubulin found in mutant axons is independent of substrate.

(A) Example image of neuron stained for acetylated tubulin (green), neuron-specific beta-II tubulin (Tuj1, red), and nuclei (DAPI, blue). (B) Raw intensity values were summed from 50μm of the axon (measured from the axonal growth cone) for Acetylated Tubulin and TUJ1. (C-E) The total summed ratio of acetylated tubulin to tubulin down the axon (\pm s.e.m.) is increased in mutants (white bars) compared to controls (black bars) when grown on PLL or L1. Longer axons appear to have less acetylated tubulin compared to shorter axons (D,E). PLL: $n=145$ total control and 101 total mutant neurons analyzed from 6 and 4 brains respectively. L1: $n=141$ total control and 100 total mutant neurons analyzed from 6 and 4 brains respectively. Significance found using ANOVA ** $p < 0.01$ **** $p < .0001$

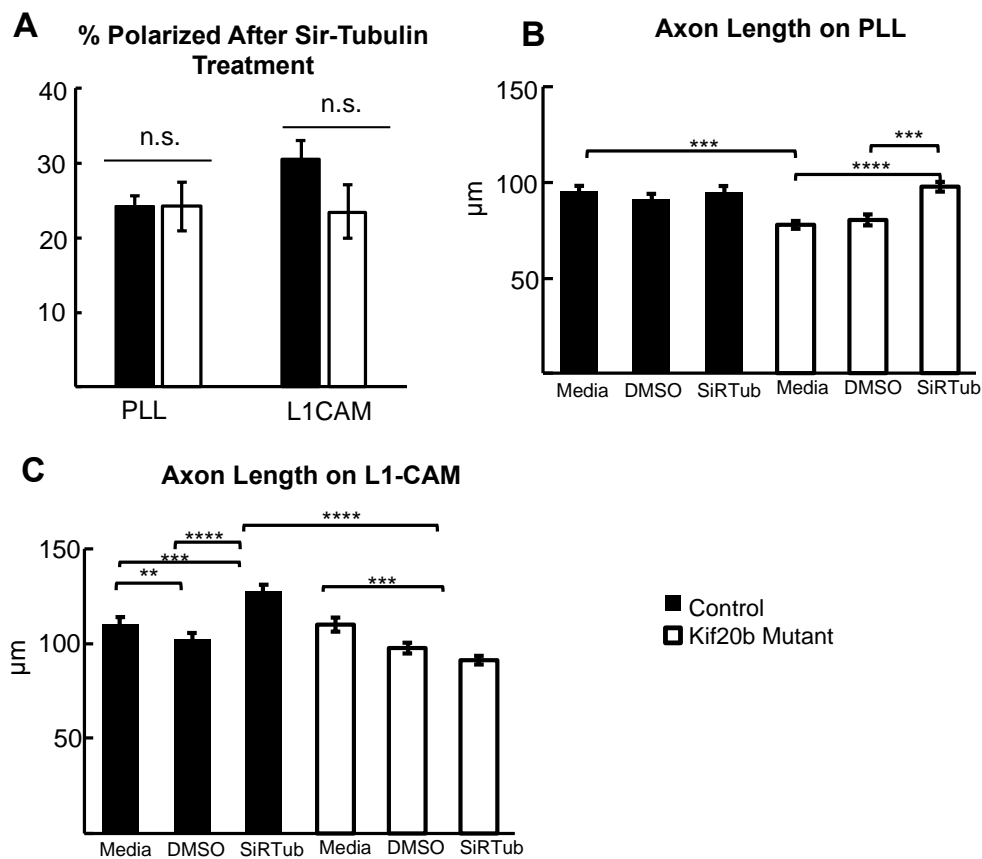


Figure App 5-5: SiR-Tubulin, a taxol derivative, treatment stops Kif20b mutant axon overgrowth on L1CAM

(A) Percentage of cells that were polarized after SiRTubulin treatment on PLL and L1CAM. N: PLL= 2 animals, 4 coverslips for control and Kif20b mutants. L1= 3 animals, 6 coverslips for control and Kif20b mutants. (B, C) Average neuron length of all treatments on PLL and L1. Media represents media change during neuron culture. DMSO serves as a control for SiRTubulin which is dissolved in DMSO. N: Ctrl, PLL: Media = 115, DMSO= 118, SiRTublin = 133; Kif20b mutant, PLL: Media= 110, DMSO =107, SiRTubulin =105; Ctrl, L1: Media = 178, DMSO =181, SiRTubulin =171; Kif20b mutant L1: Media 153, DMSO=167, SiRTubulin=158. ANOVA **p <0.01, *** p<0.001 ****p<.0001 , n.s. not significant

Appendix VI: *Shootin1* mutant neurons do not grow longer on L1-CAM

Shootin1 is a neuron polarization protein with 5 predicted isoforms, but only two isoforms (long and short) are detected in the rat and mouse (Higashiguchi et al., 2016). The short form is found in the embryonic and adult mouse and rat brain (Sapir et al., 2013; Toriyama et al., 2006). The long-form is not present in the adult brain but is present in peripheral developing and adult tissues (Higashiguchi et al., 2016). The expression pattern of *Shootin1* suggests both the long and short forms are important during development, specifically during the period of neurogenesis. However, all of the functional data on *Shootin1* is on the short-form (Kubo et al., 2015; Shimada et al., 2008; Toriyama et al., 2013; Toriyama et al., 2006). *Shootin1* expression fluctuates in the neurite growth cones of stage 2 neurons until it localizes into one neurite and promotes axon polarization (Toriyama et al., 2006). When *Shootin1* is knocked-down in the brains of mouse embryos, there was a reduction in the number of neurons reaching the cortical plate (Sapir et al., 2013). In cell culture, *Shootin1* knockdown neurons showed a defect in polarization on the substrate Poly-L-Lysine and axon outgrowth on the substrate L1-CAM (Sapir et al., 2013; Shimada et al., 2008). *Shootin1* has been proposed to be transported by actin waves into the neurite or by Kinesin-6 family member, Kif20b (Sapir et al., 2013; Shimada et al., 2008). Both *Shootin1* and Kif20b can be pulled down in a microtubule-associated fraction. This data suggests that *Shootin1* may directly or indirectly interact with microtubules. The indirect interaction could be through the association with the microtubule motor, Kif20b (Sapir et al., 2013).

We previously found in the *Kif20b* mutant neurons that *Shootin1* was reduced in the growth cone of axons (**Chapter IV**, (McNeely et al., 2017)). This data suggested to us that the *Kif20b* mutant polarization defect might be caused by the loss of *Shootin1* in the neurites, especially since Kif20b was proposed to localize *Shootin1* to the neurites. We wanted to investigate *Shootin1*'s role in axon outgrowth further, so we decided to do some preliminary experiments with a *Shootin1* mouse mutant. The *Shootin1* mouse mutant is a CRISPR mutant with a four base pair deletion (154-157aa) created in the lab of Jung-Bum Shin. By western blot using the Proteintech *Shootin1* (KIAA1598, raised against 399-631aa) antibody, there was no *Shootin1* (long or short form) present in the

cochlea or brains of these mice (Shin lab). These mice surprisingly have a grossly normal body and brain size at post-natal day 0 (Dwyer Lab).

We decided to use the *Shootin1* mutant to validate Shootin1 antibodies and to investigate polarization defects in these neurons. First, we tested the specificity of the antibodies we were using to assess Shootin1 localization in *Kif20b* mutant neurons. The two antibodies (C094 and B627, gifts from Orly Reiner) were both tested on *Shootin1* mutant neurons. C094 and B627 are both polyclonal rabbit antibodies made in the Reiner lab. C094 was raised against the c-terminal region (413 to 613 aa). B627 was raised against the N-terminus (1 to 456aa). On western blot, both antibodies recognize the long and the short form of Shootin1 (communication with Tamar Sapir, Reiner lab). Both antibody signals were significantly reduced in the *Shootin1* mutant (**Figure App 6-1A-C**). This confirmed the loss we see in *Kif20b* mutant neurons is specific to *Shootin1* protein. Second, we wanted to determine if a global loss of Shootin1 had similar axon outgrowth effects as knockdown in cultured neurons. E18.5 neurons were cultured on L1-CAM for 48 hours (as previously described in **Chapter IV**) and then measured the axon lengths for both *Shootin1* mutant and control neurons. The *Shootin1* mutant neurons were not significantly different from controls (**Figure App 6-1D, E**). This data was surprising since Shootin1 knockdown experiments showed that neurons without Shootin1 were significantly shorter compared to controls. This discrepancy suggests compensation for the loss of Shootin1 is happening early on in this mouse mutant.

In conclusion, the loss of Shootin1 localization in the *Kif20b* mutants was validated by the *Shootin1* mutant. This CRISPR mutant did not produce an expected phenotype, most likely due to early compensation of another neuron polarization protein. Recently, there has been a *Shootin1* mouse mutant created using CRISPR to delete 400 base pairs of the gene at the Jackson Laboratory. If the initial characterization of this mouse has distinct brain phenotypes, it would be worth further investigation into polarization and axon outgrowth of these neurons lacking Shootin1. There is still much to be learned about the role of Shootin1 in neuron outgrowth.

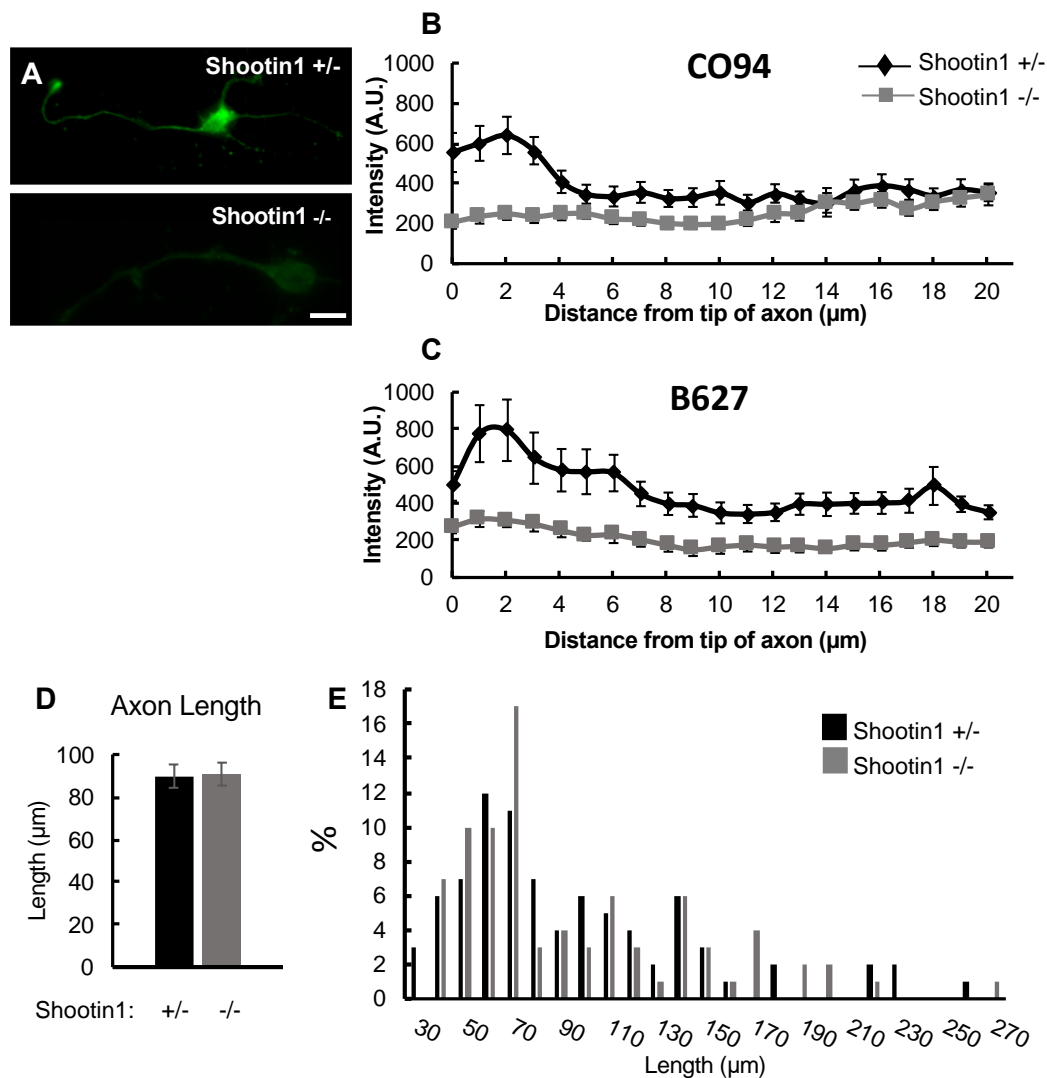


Figure App 6-1: *Shootin1* mutant neurons have normal axon outgrowth

(A) *Shootin1* heterozygous and mutant neurons were grown on L1-CAM for 48hours and immunostained for *Shootin1* (C094 and B627 *Shootin1* antibodies kind gift from Orly Reiner). Line scans were drawn along the axons from the growth cone to the cell body **(B)** C094 $n=20$ axons for both *Shootin1* +/- and *Shootin1* -/-. **(C)** B627 to measure the intensity of *Shootin1* staining. $n=10$ axons for both *Shootin1* +/- and *Shootin1* -/-. **(D)** *Shootin1* knockout neurons have similar length axons to the heterozygous controls. $n=$ *Shootin1* +/-: 84 neurons, *Shootin1* -/-: 84 neurons. 3 animals each. **(E)** Frequency distribution of axon length shows similar distribution between *Shootin1* +/- and *Shootin1* -/-. Scale bar $10\mu\text{m}$, *Shootin1* mice were a kind gift from Jung-Bum Shin.

References:

- Abaza, A., J.M. Soleilhac, J. Westendorf, M. Piel, I. Crevel, A. Roux, and F. Pirollet. 2003. M phase phosphoprotein 1 is a human plus-end-directed kinesin-related protein required for cytokinesis. *J Biol Chem.* 278:27844-27852.
- Addi, C., J. Bai, and A. Echard. 2018. Actin, microtubule, septin and ESCRT filament remodeling during late steps of cytokinesis. *Curr Opin Cell Biol.* 50:27-34.
- Addi, C., A. Presle, S. Frémont, F. Cuvelier, M. Rocancourt, F. Milin, S. Schmutz, J. Chamot-Rooke, T. Douché, M. Duchateau, Q.G. Gianetto, H. Ménager, M. Matondo, P. Zimmermann, N. Gupta-Rossi, and A. Echard. 2020. The Flemmingsome reveals an ESCRT-to-membrane coupling required for completion of cytokinesis. *bioRxiv:907857*.
- Alexandre, P., A.M. Reugels, D. Barker, E. Blanc, and J.D. Clarke. 2010. Neurons derive from the more apical daughter in asymmetric divisions in the zebrafish neural tube. *Nat Neurosci.* 13:673-679.
- Arai, Y., J.N. Pulvers, C. Haffner, B. Schilling, I. Nusslein, F. Calegari, and W.B. Huttner. 2011. Neural stem and progenitor cells shorten S-phase on commitment to neuron production. *Nat Commun.* 2:154.
- Arai, Y., J.L. Sampaio, M. Wilsch-Brauninger, A.W. Ettinger, C. Haffner, and W.B. Huttner. 2015. Lipidome of midbody released from neural stem and progenitor cells during mammalian cortical neurogenesis. *Frontiers in cellular neuroscience.* 9:325.
- Atilla-Gokcumen, G.E., E. Muro, J. Relat-Goberna, S. Sasse, A. Bedigian, M.L. Coughlin, S. Garcia-Manyes, and U.S. Eggert. 2014. Dividing cells regulate their lipid composition and localization. *Cell.* 156:428-439.
- Barnes, A.P., and F. Polleux. 2009. Establishment of axon-dendrite polarity in developing neurons. *Annu Rev Neurosci.* 32:347-381.
- Baron, R.D., and F.A. Barr. 2015. The Kinesin-6 Members MKLP1, MKLP2 and MPP1. *In Kinesins and Cancer.* F.S.B.F. Kozielski, editor. Springer Netherlands, Dordrecht. 193-222.
- Bartolini, F., J.B. Moseley, J. Schmoranzler, L. Cassimeris, B.L. Goode, and G.G. Gundersen. 2008. The formin mDia2 stabilizes microtubules independently of its actin nucleation activity. *The Journal of cell biology.* 181:523-536.

- Bastmeyer, M., and D.D. O'Leary. 1996. Dynamics of target recognition by interstitial axon branching along developing cortical axons. *J Neurosci.* 16:1450-1459.
- Bastos, R.N., and F.A. Barr. 2010. Plk1 negatively regulates Cep55 recruitment to the midbody to ensure orderly abscission. *The Journal of cell biology.* 191:751-760.
- Bernabe-Rubio, M., G. Andres, J. Casares-Arias, J. Fernandez-Barrera, L. Rangel, N. Reglero-Real, D.C. Gershlick, J.J. Fernandez, J. Millan, I. Correias, D.G. Miguez, and M.A. Alonso. 2016. Novel role for the midbody in primary ciliogenesis by polarized epithelial cells. *The Journal of cell biology.* 214:259-273.
- Bernabé-Rubio, M., M. Bosch-Fortea, E. García, J.B. de la Serna, and M.A. Alonso. 2019. The ciliary membrane of polarized epithelial cells stems from a midbody remnant-associated membrane patch with condensed nanodomains. *bioRxiv:667642.*
- Bianchi, F.T., C. Tocco, G. Pallavicini, Y. Liu, F. Verni, C. Merigliano, S. Bonaccorsi, N. El-Assawy, L. Priano, M. Gai, G.E. Berto, A.M. Chiotto, F. Sgro, A. Caramello, L. Tasca, U. Ala, F. Neri, S. Oliviero, A. Mauro, S. Geley, M. Gatti, and F. Di Cunto. 2017. Citron Kinase Deficiency Leads to Chromosomal Instability and TP53-Sensitive Microcephaly. *Cell Rep.* 18:1674-1686.
- Bizzotto, S., and F. Francis. 2015. Morphological and functional aspects of progenitors perturbed in cortical malformations. *Frontiers in cellular neuroscience.* 9:30.
- Bondeson, M.L., K. Ericson, S. Gudmundsson, A. Ameer, F. Ponten, J. Wesstrom, C. Frykholm, and M. Wilbe. 2017. A nonsense mutation in CEP55 defines a new locus for a Meckel-like syndrome, an autosomal recessive lethal fetal ciliopathy. *Clin Genet.* 92:510-516.
- Bultje, R.S., D.R. Castaneda-Castellanos, L.Y. Jan, Y.N. Jan, A.R. Kriegstein, and S.H. Shi. 2009. Mammalian Par3 regulates progenitor cell asymmetric division via notch signaling in the developing neocortex. *Neuron.* 63:189-202.
- Burden-Gulley, S.M., and V. Lemmon. 1996. L1, N-cadherin, and laminin induce distinct distribution patterns of cytoskeletal elements in growth cones. *Cell Motil Cytoskeleton.* 35:1-23.
- Caballe, A., D.M. Wenzel, M. Agromayor, S.L. Alam, J.J. Skalicky, M. Kloc, J.G. Carlton, L. Labrador, W.I. Sundquist, and J. Martin-Serrano. 2015. ULK3 regulates cytokinetic abscission by phosphorylating ESCRT-III proteins. *Elife.* 4:e06547.

- Carlton, J.G., M. Agromayor, and J. Martin-Serrano. 2008. Differential requirements for Alix and ESCRT-III in cytokinesis and HIV-1 release. *Proc Natl Acad Sci U S A.* 105:10541-10546.
- Carlton, J.G., A. Caballe, M. Agromayor, M. Kloc, and J. Martin-Serrano. 2012. ESCRT-III governs the Aurora B-mediated abscission checkpoint through CHMP4C. *Science.* 336:220-225.
- Casares-Arias, J., M.U. Gonzalez, A.S. Paulo, L.N. Ventimiglia, J.B.A. Sadler, D.G. Miguez, L. Labat-de-Hoz, A. Rubio-Ramos, L. Rangel, M. Bernabé-Rubio, J. Fernández-Barrera, I. Correas, J. Martín-Serrano, and M.A. Alonso. 2019. Midbody remnant inheritance is regulated by the ESCRT subunit CHMP4C. *bioRxiv:810523.*
- Chai, Y., D. Tian, Y. Yang, G. Feng, Z. Cheng, W. Li, and G. Ou. 2012. Apoptotic regulators promote cytokinetic midbody degradation in *C. elegans*. *The Journal of cell biology.* 199:1047-1055.
- Chaigne, A., C. Labouesse, M. Agnew, E. Hannezo, K.J. Chalut, and E.K. Paluch. 2019. Abscission couples cell division to embryonic stem cell fate. *bioRxiv:798165.*
- Chau, K.F., M.W. Springel, K.G. Broadbelt, H.Y. Park, S. Topal, M.P. Lun, H. Mullan, T. Maynard, H. Steen, A.S. LaMantia, and M.K. Lehtinen. 2015. Progressive Differentiation and Instructive Capacities of Amniotic Fluid and Cerebrospinal Fluid Proteomes following Neural Tube Closure. *Dev Cell.* 35:789-802.
- Christ, L., E.M. Wenzel, K. Liestol, C. Raiborg, C. Campsteijn, and H. Stenmark. 2016. ALIX and ESCRT-I/II function as parallel ESCRT-III recruiters in cytokinetic abscission. *The Journal of cell biology.* 212:499-513.
- Connell, J.W., C. Lindon, J.P. Luzio, and E. Reid. 2009. Spastin couples microtubule severing to membrane traffic in completion of cytokinesis and secretion. *Traffic.* 10:42-56.
- Crowell, E.F., A.L. Gaffuri, B. Gayraud-Morel, S. Tajbakhsh, and A. Echard. 2014. Engulfment of the midbody remnant after cytokinesis in mammalian cells. *J Cell Sci.* 127:3840-3851.
- Dagenbach, E.M., and S.A. Endow. 2004. A new kinesin tree. *J Cell Sci.* 117:3-7.
- Damiani, D., A.M. Goffinet, A. Alberts, and F. Tissir. 2016. Lack of Diaph3 relaxes the spindle checkpoint causing the loss of neural progenitors. *Nat Commun.* 7:13509.

- Dan, W., N. Gao, L. Li, J.X. Zhu, L. Diao, J. Huang, Q.J. Han, S. Wang, H. Xue, Q. Wang, Q.F. Wu, X. Zhang, and L. Bao. 2018. alpha-Tubulin Acetylation Restricts Axon Overbranching by Dampening Microtubule Plus-End Dynamics in Neurons. *Cereb Cortex*. 28:3332-3346.
- Daniel, E., M. Daude, I. Kolotuev, K. Charish, V. Auld, and R. Le Borgne. 2018. Coordination of Septate Junctions Assembly and Completion of Cytokinesis in Proliferative Epithelial Tissues. *Curr Biol*. 28:1380-1391 e1384.
- del Castillo, U., W. Lu, M. Winding, M. Lakonishok, and V.I. Gelfand. 2015. Pavarotti/MKLP1 regulates microtubule sliding and neurite outgrowth in *Drosophila* neurons. *Curr Biol*. 25:200-205.
- Di Cunto, F., S. Imarisio, E. Hirsch, V. Broccoli, A. Bulfone, A. Migheli, C. Atzori, E. Turco, R. Triolo, G.P. Dotto, L. Silengo, and F. Altruda. 2000. Defective neurogenesis in citron kinase knockout mice by altered cytokinesis and massive apoptosis. *Neuron*. 28:115-127.
- Dionne, L.K., E. Peterman, J. Schiel, P. Gibieza, V.A. Skeberdis, A. Jimeno, X.J. Wang, and R. Prekeris. 2017. FYCO1 regulates accumulation of post-mitotic midbodies by mediating LC3-dependent midbody degradation. *J Cell Sci*. 130:4051-4062.
- Dionne, L.K., X.J. Wang, and R. Prekeris. 2015. Midbody: from cellular junk to regulator of cell polarity and cell fate. *Curr Opin Cell Biol*. 35:51-58.
- Doherty, P., and F.S. Walsh. 1996. CAM-FGF Receptor Interactions: A Model for Axonal Growth. *Mol Cell Neurosci*. 8:99-111.
- Dotti, C.G., C.A. Sullivan, and G.A. Banker. 1988. The establishment of polarity by hippocampal neurons in culture. *J Neurosci*. 8:1454-1468.
- Douglas, M.E., T. Davies, N. Joseph, and M. Mishima. 2010. Aurora B and 14-3-3 coordinately regulate clustering of central spindle during cytokinesis. *Curr Biol*. 20:927-933.
- Dubreuil, V., A.M. Marzesco, D. Corbeil, W.B. Huttner, and M. Wilsch-Brauninger. 2007. Midbody and primary cilium of neural progenitors release extracellular membrane particles enriched in the stem cell marker prominin-1. *The Journal of cell biology*. 176:483-495.
- Dwivedy, A., F.B. Gertler, J. Miller, C.E. Holt, and C. Lebrand. 2007. Ena/VASP function in retinal axons is required for terminal arborization but not pathway navigation. *Development*. 134:2137-2146.

- Dwyer, N.D., B. Chen, S.J. Chou, S. Hippenmeyer, L. Nguyen, and H.T. Ghashghaei. 2016. Neural Stem Cells to Cerebral Cortex: Emerging Mechanisms Regulating Progenitor Behavior and Productivity. *J Neurosci.* 36:11394-11401.
- Dwyer, N.D., D.K. Manning, J.L. Moran, R. Mudbhary, M.S. Fleming, C.B. Favero, V.M. Vock, D.D. O'Leary, C.A. Walsh, and D.R. Beier. 2011. A forward genetic screen with a thalamocortical axon reporter mouse yields novel neurodevelopment mutants and a distinct *Emx2* mutant phenotype. *Neural Dev.* 6:3.
- Elia, N., R. Sougrat, T.A. Spurlin, J.H. Hurley, and J. Lippincott-Schwartz. 2011. Dynamics of endosomal sorting complex required for transport (ESCRT) machinery during cytokinesis and its role in abscission. *Proc Natl Acad Sci U S A.* 108:4846-4851.
- Englund, C., A. Fink, C. Lau, D. Pham, R.A. Daza, A. Bulfone, T. Kowalczyk, and R.F. Hevner. 2005. *Pax6*, *Tbr2*, and *Tbr1* are expressed sequentially by radial glia, intermediate progenitor cells, and postmitotic neurons in developing neocortex. *J Neurosci.* 25:247-251.
- Estey, M.P., C. Di Ciano-Oliveira, C.D. Froese, M.T. Bejide, and W.S. Trimble. 2010. Distinct roles of septins in cytokinesis: SEPT9 mediates midbody abscission. *The Journal of cell biology.* 191:741-749.
- Ettinger, A.W., M. Wilsch-Brauninger, A.M. Marzesco, M. Bickle, A. Lohmann, Z. Maliga, J. Karbanova, D. Corbeil, A.A. Hyman, and W.B. Huttner. 2011. Proliferating versus differentiating stem and cancer cells exhibit distinct midbody-release behaviour. *Nat Commun.* 2:503.
- Fabbro, M., B.B. Zhou, M. Takahashi, B. Sarcevic, P. Lal, M.E. Graham, B.G. Gabrielli, P.J. Robinson, E.A. Nigg, Y. Ono, and K.K. Khanna. 2005. Cdk1/Erk2- and Plk1-dependent phosphorylation of a centrosome protein, Cep55, is required for its recruitment to midbody and cytokinesis. *Dev Cell.* 9:477-488.
- Falk, S., S. Bugeon, J. Ninkovic, G.A. Pilz, M.P. Postiglione, H. Cremer, J.A. Knoblich, and M. Gotz. 2017. Time-Specific Effects of Spindle Positioning on Embryonic Progenitor Pool Composition and Adult Neural Stem Cell Seeding. *Neuron.* 93:777-791 e773.
- Farkas, L.M., and W.B. Huttner. 2008. The cell biology of neural stem and progenitor cells and its significance for their proliferation versus differentiation during mammalian brain development. *Curr Opin Cell Biol.* 20:707-715.

- Fazeli, G., M. Trinkwalder, L. Irmisch, and A.M. Wehman. 2016. C. elegans midbodies are released, phagocytosed and undergo LC3-dependent degradation independent of macroautophagy. *J Cell Sci.* 129:3721-3731.
- Fededa, J.P., and D.W. Gerlich. 2012. Molecular control of animal cell cytokinesis. *Nat Cell Biol.* 14:440-447.
- Feng, Y., and C.A. Walsh. 2004. Mitotic spindle regulation by Nde1 controls cerebral cortical size. *Neuron.* 44:279-293.
- Fietz, S.A., I. Kelava, J. Vogt, M. Wilsch-Brauninger, D. Stenzel, J.L. Fish, D. Corbeil, A. Riehn, W. Distler, R. Nitsch, and W.B. Huttner. 2010. OSVZ progenitors of human and ferret neocortex are epithelial-like and expand by integrin signaling. *Nat Neurosci.* 13:690-699.
- Frosk, P., H.H. Arts, J. Philippe, C.S. Gunn, E.L. Brown, B. Chodirker, L. Simard, J. Majewski, S. Fahiminiya, C. Russell, Y.P. Liu, F.C. Consortium, M. Canadian Rare Diseases, N. Mechanisms, R. Hegele, N. Katsanis, C. Goerz, M.R. Del Bigio, and E.E. Davis. 2017. A truncating mutation in CEP55 is the likely cause of MARCH, a novel syndrome affecting neuronal mitosis. *J Med Genet.* 54:490-501.
- Fu, X., K.J. Brown, C.C. Yap, B. Winckler, J.K. Jaiswal, and J.S. Liu. 2013. Doublecortin (Dcx) family proteins regulate filamentous actin structure in developing neurons. *J Neurosci.* 33:709-721.
- Fujikura, K., T. Setsu, K. Tanigaki, T. Abe, H. Kiyonari, T. Terashima, and T. Sakisaka. 2013. Kif14 mutation causes severe brain malformation and hypomyelination. *PLoS One.* 8:e53490.
- Fung, S.Y.S., M. Kitagawa, P.J. Liao, J. Wong, and S.H. Lee. 2017. Opposing Activities of Aurora B Kinase and B56-PP2A Phosphatase on MKlp2 Determine Abcission Timing. *Curr Biol.* 27:78-86.
- Gai, M., P. Camera, A. Dema, F. Bianchi, G. Berto, E. Scarpa, G. Germena, and F. Di Cunto. 2011. Citron kinase controls abscission through RhoA and anillin. *Mol Biol Cell.* 22:3768-3778.
- Gallo, G. 2013. Mechanisms underlying the initiation and dynamics of neuronal filopodia: from neurite formation to synaptogenesis. *International review of cell and molecular biology.* 301:95-156.
- Gao, P., M.P. Postiglione, T.G. Krieger, L. Hernandez, C. Wang, Z. Han, C. Streicher, E. Papusheva, R. Insolera, K. Chugh, O. Kodish, K. Huang, B.D. Simons, L. Luo, S.

- Hippenmeyer, and S.H. Shi. 2014. Deterministic progenitor behavior and unitary production of neurons in the neocortex. *Cell*. 159:775-788.
- Geng, A., R. Qiu, K. Murai, J. Liu, X. Wu, H. Zhang, H. Farhoodi, N. Duong, M. Jiang, J.K. Yee, W. Tsark, and Q. Lu. 2018. KIF20A/MKLP2 regulates the division modes of neural progenitor cells during cortical development. *Nat Commun*. 9:2707.
- Gershony, O., T. Pe'er, M. Noach-Hirsh, N. Elia, and A. Tzur. 2014. Cytokinetic abscission is an acute G1 event. *Cell Cycle*. 13:3436-3441.
- Gershony, O., S. Sherman, S. Adar, I. Segal, D. Nachmias, I. Goliand, and N. Elia. 2017. Measuring abscission spatiotemporal dynamics using quantitative high-resolution microscopy. *Methods in cell biology*. 137:205-224.
- Glotzer, M. 2005. The molecular requirements for cytokinesis. *Science*. 307:1735-1739.
- Goldstein, A.Y., Y.N. Jan, and L. Luo. 2005. Function and regulation of Tumbleweed (RacGAP50C) in neuroblast proliferation and neuronal morphogenesis. *Proc Natl Acad Sci U S A*. 102:3834-3839.
- Goliand, I., S. Adar-Levor, I. Segal, D. Nachmias, T. Dadosh, M.M. Kozlov, and N. Elia. 2018. Resolving ESCRT-III Spirals at the Intercellular Bridge of Dividing Cells Using 3D STORM. *Cell Rep*. 24:1756-1764.
- Goliand, I., D. Nachmias, O. Gershony, and N. Elia. 2014. Inhibition of ESCRT-II-CHMP6 interactions impedes cytokinetic abscission and leads to cell death. *Mol Biol Cell*. 25:3740-3748.
- Gotz, M., and W.B. Huttner. 2005. The cell biology of neurogenesis. *Nat Rev Mol Cell Biol*. 6:777-788.
- Green, R.A., J.R. Mayers, S. Wang, L. Lewellyn, A. Desai, A. Audhya, and K. Oegema. 2013. The midbody ring scaffolds the abscission machinery in the absence of midbody microtubules. *The Journal of cell biology*. 203:505-520.
- Green, R.A., E. Paluch, and K. Oegema. 2012. Cytokinesis in animal cells. *Annu Rev Cell Dev Biol*. 28:29-58.
- Gromley, A., A. Jurczyk, J. Sillibourne, E. Halilovic, M. Mogensen, I. Groisman, M. Blomberg, and S. Doxsey. 2003. A novel human protein of the maternal centriole is required for the final stages of cytokinesis and entry into S phase. *The Journal of cell biology*. 161:535-545.
- Gromley, A., C. Yeaman, J. Rosa, S. Redick, C.T. Chen, S. Mirabelle, M. Guha, J. Sillibourne, and S.J. Doxsey. 2005. Centriolin anchoring of exocyst and SNARE

- complexes at the midbody is required for secretory-vesicle-mediated abscission. *Cell*. 123:75-87.
- Gruenberg, J., and H. Stenmark. 2004. The biogenesis of multivesicular endosomes. *Nat Rev Mol Cell Biol*. 5:317-323.
- Gruneberg, U., R. Neef, R. Honda, E.A. Nigg, and F.A. Barr. 2004. Relocation of Aurora B from centromeres to the central spindle at the metaphase to anaphase transition requires MKlp2. *The Journal of cell biology*. 166:167-172.
- Gruneberg, U., R. Neef, X. Li, E.H. Chan, R.B. Chalamalasetty, E.A. Nigg, and F.A. Barr. 2006. KIF14 and citron kinase act together to promote efficient cytokinesis. *The Journal of cell biology*. 172:363-372.
- Guizetti, J., L. Schermelleh, J. Mantler, S. Maar, I. Poser, H. Leonhardt, T. Muller-Reichert, and D.W. Gerlich. 2011. Cortical constriction during abscission involves helices of ESCRT-III-dependent filaments. *Science*. 331:1616-1620.
- Hansen, D.V., J.H. Lui, P.R. Parker, and A.R. Kriegstein. 2010. Neurogenic radial glia in the outer subventricular zone of human neocortex. *Nature*. 464:554-561.
- Harding, B.N., A. Moccia, S. Drunat, O. Soukarieh, H. Tubeuf, L.S. Chitty, A. Verloes, P. Gressens, V. El Ghouzzi, S. Joriot, F. Di Cunto, A. Martins, S. Passemard, and S.L. Bielas. 2016. Mutations in Citron Kinase Cause Recessive Microlissencephaly with Multinucleated Neurons. *Am J Hum Genet*. 99:511-520.
- Hatanaka, Y., and F. Murakami. 2002. In vitro analysis of the origin, migratory behavior, and maturation of cortical pyramidal cells. *The Journal of comparative neurology*. 454:1-14.
- Hayashi, S., P. Lewis, L. Pevny, and A.P. McMahon. 2002. Efficient gene modulation in mouse epiblast using a Sox2Cre transgenic mouse strain. *Mech Dev*. 119 Suppl 1:S97-S101.
- Herszterg, S., D. Pinheiro, and Y. Bellaiche. 2014. A multicellular view of cytokinesis in epithelial tissue. *Trends Cell Biol*. 24:285-293.
- Higashi, T., T.R. Arnold, R.E. Stephenson, K.M. Dinshaw, and A.L. Miller. 2016. Maintenance of the Epithelial Barrier and Remodeling of Cell-Cell Junctions during Cytokinesis. *Curr Biol*. 26:1829-1842.
- Higashiguchi, Y., K. Katsuta, T. Minegishi, S. Yonemura, A. Urasaki, and N. Inagaki. 2016. Identification of a shootin1 isoform expressed in peripheral tissues. *Cell and tissue research*. 366:75-87.

- Hill, E., M. Clarke, and F.A. Barr. 2000. The Rab6-binding kinesin, Rab6-KIFL, is required for cytokinesis. *EMBO J.* 19:5711-5719.
- Hirokawa, N., S. Niwa, and Y. Tanaka. 2010. Molecular motors in neurons: transport mechanisms and roles in brain function, development, and disease. *Neuron.* 68:610-638.
- Hirokawa, N., and Y. Noda. 2008. Intracellular transport and kinesin superfamily proteins, KIFs: structure, function, and dynamics. *Physiol Rev.* 88:1089-1118.
- Hu, C.K., M. Coughlin, and T.J. Mitchison. 2012. Midbody assembly and its regulation during cytokinesis. *Mol Biol Cell.* 23:1024-1034.
- Hummer, S., and T.U. Mayer. 2009. Cdk1 negatively regulates midzone localization of the mitotic kinesin Mklp2 and the chromosomal passenger complex. *Curr Biol.* 19:607-612.
- Insolera, R., H. Bazzi, W. Shao, K.V. Anderson, and S.H. Shi. 2014. Cortical neurogenesis in the absence of centrioles. *Nat Neurosci.* 17:1528-1535.
- Isogai, T., R. van der Kammen, S.S. Goerdayal, A.J. Heck, A.F. Altelaar, and M. Innocenti. 2015. Proteomic analyses uncover a new function and mode of action for mouse homolog of Diaphanous 2 (mDia2). *Mol Cell Proteomics.* 14:1064-1078.
- Jaffe, A.B., N. Kaji, J. Durgan, and A. Hall. 2008. Cdc42 controls spindle orientation to position the apical surface during epithelial morphogenesis. *The Journal of cell biology.* 183:625-633.
- Janisch, K.M., and N.D. Dwyer. 2016. Imaging and quantitative analysis of cytokinesis in developing brains of Kinesin-6 mutant mice. *Methods in cell biology.* 131:233-252.
- Janisch, K.M., K.C. McNeely, J.M. Dardick, S.H. Lim, and N.D. Dwyer. 2018. Kinesin-6 KIF20B is required for efficient cytokinetic furrowing and timely abscission in human cells. *Mol Biol Cell.* 29:166-179.
- Janisch, K.M., V.M. Vock, M.S. Fleming, A. Shrestha, C.M. Grimsley-Myers, B.A. Rasoul, S.A. Neale, T.D. Cupp, J.M. Kinchen, K.F. Liem, Jr., and N.D. Dwyer. 2013. The vertebrate-specific Kinesin-6, Kif20b, is required for normal cytokinesis of polarized cortical stem cells and cerebral cortex size. *Development.* 140:4672-4682.
- Janke, C., and G. Montagnac. 2017. Causes and Consequences of Microtubule Acetylation. *Curr Biol.* 27:R1287-R1292.

- Jayaraman, D., B.-I. Bae, and C.A. Walsh. 2018. The Genetics of Primary Microcephaly. *Annual Review of Genomics and Human Genetics*. 19:177-200.
- Jeffery, J., C. Neyt, W. Moore, S. Paterson, N.I. Bower, G. Chenevix-Trench, H. Verkade, B.M. Hogan, and K.K. Khanna. 2015. Cep55 regulates embryonic growth and development by promoting Akt stability in zebrafish. *FASEB J*. 29:1999-2009.
- Johnson, C.A., C.E. Wright, and H.T. Ghashghaei. 2017. Regulation of Cytokinesis during Corticogenesis: Focus on the Midbody. *FEBS Lett*.
- Kaindl, A.M., S. Passemard, P. Kumar, N. Kraemer, L. Issa, A. Zwirner, B. Gerard, A. Verloes, S. Mani, and P. Gressens. 2010. Many roads lead to primary autosomal recessive microcephaly. *Progress in neurobiology*. 90:363-383.
- Kamimoto, T., T. Zama, R. Aoki, Y. Muro, and M. Hagiwara. 2001. Identification of a novel kinesin-related protein, KRMP1, as a target for mitotic peptidyl-prolyl isomerase Pin1. *J Biol Chem*. 276:37520-37528.
- Kanehira, M., T. Katagiri, A. Shimo, R. Takata, T. Shuin, T. Miki, T. Fujioka, and Y. Nakamura. 2007. Oncogenic role of MPHOSPH1, a cancer-testis antigen specific to human bladder cancer. *Cancer Res*. 67:3276-3285.
- Kim, S., M.K. Lehtinen, A. Sessa, M.W. Zappaterra, S.H. Cho, D. Gonzalez, B. Boggan, C.A. Austin, J. Wijnholds, M.J. Gambello, J. Malicki, A.S. LaMantia, V. Broccoli, and C.A. Walsh. 2010. The apical complex couples cell fate and cell survival to cerebral cortical development. *Neuron*. 66:69-84.
- Kinoshita, M., C.M. Field, M.L. Coughlin, A.F. Straight, and T.J. Mitchison. 2002. Self- and actin-templated assembly of Mammalian septins. *Dev Cell*. 3:791-802.
- Kiryushko, D., V. Berezin, and E. Bock. 2004. Regulators of neurite outgrowth: role of cell adhesion molecules. *Ann N Y Acad Sci*. 1014:140-154.
- Kitagawa, M., S.Y. Fung, N. Onishi, H. Saya, and S.H. Lee. 2013. Targeting Aurora B to the equatorial cortex by MKlp2 is required for cytokinesis. *PLoS One*. 8:e64826.
- Kittler, R., G. Putz, L. Pelletier, I. Poser, A.K. Heninger, D. Drechsel, S. Fischer, I. Konstantinova, B. Habermann, H. Grabner, M.L. Yaspo, H. Himmelbauer, B. Korn, K. Neugebauer, M.T. Pisabarro, and F. Buchholz. 2004. An endoribonuclease-prepared siRNA screen in human cells identifies genes essential for cell division. *Nature*. 432:1036-1040.
- Kittler, R., V. Surendranath, A.K. Heninger, M. Slabicki, M. Theis, G. Putz, K. Franke, A. Caldarelli, H. Grabner, K. Kozak, J. Wagner, E. Rees, B. Korn, C. Frenzel, C.

- Sachse, B. Sonnichsen, J. Guo, J. Schelter, J. Burchard, P.S. Linsley, A.L. Jackson, B. Habermann, and F. Buchholz. 2007. Genome-wide resources of endoribonuclease-prepared short interfering RNAs for specific loss-of-function studies. *Nat Methods*. 4:337-344.
- Konig, J., E.B. Frankel, A. Audhya, and T. Muller-Reichert. 2017. Membrane remodeling during embryonic abscission in *Caenorhabditis elegans*. *The Journal of cell biology*. 216:1277-1286.
- Konno, D., G. Shioi, A. Shitamukai, A. Mori, H. Kiyonari, T. Miyata, and F. Matsuzaki. 2008. Neuroepithelial progenitors undergo LGN-dependent planar divisions to maintain self-renewability during mammalian neurogenesis. *Nat Cell Biol*. 10:93-101.
- Kosodo, Y., K. Roper, W. Haubensak, A.M. Marzesco, D. Corbeil, and W.B. Huttner. 2004. Asymmetric distribution of the apical plasma membrane during neurogenic divisions of mammalian neuroepithelial cells. *Embo J*. 23:2314-2324.
- Kosodo, Y., K. Toida, V. Dubreuil, P. Alexandre, J. Schenk, E. Kiyokage, A. Attardo, F. Mora-Bermudez, T. Arii, J.D. Clarke, and W.B. Huttner. 2008. Cytokinesis of neuroepithelial cells can divide their basal process before anaphase. *Embo J*. 27:3151-3163.
- Kremer, B.E., T. Haystead, and I.G. Macara. 2005. Mammalian septins regulate microtubule stability through interaction with the microtubule-binding protein MAP4. *Mol Biol Cell*. 16:4648-4659.
- Kriegstein, A., and A. Alvarez-Buylla. 2009. The glial nature of embryonic and adult neural stem cells. *Annu Rev Neurosci*. 32:149-184.
- Kubo, Y., K. Baba, M. Toriyama, T. Minegishi, T. Sugiura, S. Kozawa, K. Ikeda, and N. Inagaki. 2015. Shootin1-cortactin interaction mediates signal-force transduction for axon outgrowth. *The Journal of cell biology*. 210:663-676.
- Kuo, T.C., C.T. Chen, D. Baron, T.T. Onder, S. Loewer, S. Almeida, C.M. Weismann, P. Xu, J.M. Houghton, F.B. Gao, G.Q. Daley, and S. Doxsey. 2011. Midbody accumulation through evasion of autophagy contributes to cellular reprogramming and tumorigenicity. *Nat Cell Biol*. 13:1214-1223.
- Kwan, K.Y., N. Sestan, and E.S. Anton. 2012. Transcriptional co-regulation of neuronal migration and laminar identity in the neocortex. *Development*. 139:1535-1546.

- Lafaurie-Janvore, J., P. Maiuri, I. Wang, M. Pinot, J.B. Manneville, T. Betz, M. Balland, and M. Piel. 2013. ESCRT-III assembly and cytokinetic abscission are induced by tension release in the intercellular bridge. *Science*. 339:1625-1629.
- Lambrus, B.G., V. Daggubati, Y. Uetake, P.M. Scott, K.M. Clutario, G. Sluder, and A.J. Holland. 2016. A USP28-53BP1-p53-p21 signaling axis arrests growth after centrosome loss or prolonged mitosis. *The Journal of cell biology*. 214:143-153.
- LaMonica, B.E., J.H. Lui, D.V. Hansen, and A.R. Kriegstein. 2013. Mitotic spindle orientation predicts outer radial glial cell generation in human neocortex. *Nat Commun*. 4:1665.
- Lee, H.H., N. Elia, R. Ghirlando, J. Lippincott-Schwartz, and J.H. Hurley. 2008. Midbody targeting of the ESCRT machinery by a noncanonical coiled coil in CEP55. *Science*. 322:576-580.
- Lenhart, K.F., and S. DiNardo. 2015. Somatic cell encystment promotes abscission in germline stem cells following a regulated block in cytokinesis. *Dev Cell*. 34:192-205.
- Lewis, T.L., Jr., J. Courchet, and F. Polleux. 2013. Cell biology in neuroscience: Cellular and molecular mechanisms underlying axon formation, growth, and branching. *The Journal of cell biology*. 202:837-848.
- Li, H., S.L. Bielas, M.S. Zaki, S. Ismail, D. Farfara, K. Um, R.O. Rosti, E.C. Scott, S. Tu, N.C. Chi, S. Gabriel, E.Z. Erson-Omay, A.G. Ercan-Sencicek, K. Yasuno, A.O. Caglayan, H. Kaymakcalan, B. Ekici, K. Bilguvar, M. Gunel, and J.G. Gleeson. 2016. Biallelic Mutations in Citron Kinase Link Mitotic Cytokinesis to Human Primary Microcephaly. *Am J Hum Genet*. 99:501-510.
- Lie-Jensen, A., K. Ivanauskiene, L. Malerod, A. Jain, K.W. Tan, J.K. Laerdahl, K. Liestol, H. Stenmark, and K. Haglund. 2019. Centralspindlin Recruits ALIX to the Midbody during Cytokinetic Abscission in *Drosophila* via a Mechanism Analogous to Virus Budding. *Curr Biol*. 29:3538-3548 e3537.
- Lin, S., M. Liu, O.I. Mozgova, W. Yu, and P.W. Baas. 2012. Mitotic motors coregulate microtubule patterns in axons and dendrites. *J Neurosci*. 32:14033-14049.
- Lipka, J., L.C. Kapitein, J. Jaworski, and C.C. Hoogenraad. 2016. Microtubule-binding protein doublecortin-like kinase 1 (DCLK1) guides kinesin-3-mediated cargo transport to dendrites. *EMBO J*. 35:302-318.
- Little, J.N. 2019. Mutations of key cytokinetic abscission mediators cause microcephaly. *Dissertation in Cell Biology at the University of Virginia*.

- Little, J.N., and N.D. Dwyer. 2019. p53 deletion rescues lethal microcephaly in a mouse model with neural stem cell abscission defects. *Hum Mol Genet.* 28:434-447.
- Liu, X., Y. Zhou, X. Liu, A. Peng, H. Gong, L. Huang, K. Ji, R.B. Petersen, L. Zheng, and K. Huang. 2014. MPHOSPH1: a potential therapeutic target for hepatocellular carcinoma. *Cancer Res.* 74:6623-6634.
- Lujan, P., T. Rubio, G. Varsano, and M. Kohn. 2017. Keep it on the edge: The post-mitotic midbody as a polarity signal unit. *Commun Integr Biol.* 10:e1338990.
- Lujan, P., G. Varsano, T. Rubio, M.L. Henrich, T. Sachsenheimer, M. Galvez-Santisteban, F. Martin-Belmonte, A.C. Gavin, B. Brugger, and M. Kohn. 2016. PRL-3 disrupts epithelial architecture by altering the post-mitotic midbody position. *J Cell Sci.* 129:4130-4142.
- Lukinavicius, G., L. Reymond, E. D'Este, A. Masharina, F. Gottfert, H. Ta, A. Guther, M. Fournier, S. Rizzo, H. Waldmann, C. Blaukopf, C. Sommer, D.W. Gerlich, H.D. Arndt, S.W. Hell, and K. Johnsson. 2014. Fluorogenic probes for live-cell imaging of the cytoskeleton. *Nat Methods.* 11:731-733.
- Mackay, D.R., M. Makise, and K.S. Ullman. 2010. Defects in nuclear pore assembly lead to activation of an Aurora B-mediated abscission checkpoint. *The Journal of cell biology.* 191:923-931.
- Maliga, Z., M. Junqueira, Y. Toyoda, A. Ettinger, F. Mora-Bermudez, R.W. Klemm, A. Vasilj, E. Guhr, I. Ibarlucea-Benitez, I. Poser, E. Bonifacio, W.B. Huttner, A. Shevchenko, and A.A. Hyman. 2013. A genomic toolkit to investigate kinesin and myosin motor function in cells. *Nat Cell Biol.* 15:325-334.
- Marthiens, V., and C. French-Constant. 2009. Adherens junction domains are split by asymmetric division of embryonic neural stem cells. *EMBO Rep.* 10:515-520.
- Matuliene, J., and R. Kuriyama. 2002. Kinesin-like protein CHO1 is required for the formation of midbody matrix and the completion of cytokinesis in mammalian cells. *Mol Biol Cell.* 13:1832-1845.
- McNeely, K.C., T.D. Cupp, J.N. Little, K.M. Janisch, A. Shrestha, and N.D. Dwyer. 2017. Mutation of Kinesin-6 Kif20b causes defects in cortical neuron polarization and morphogenesis. *Neural Dev.* 12:5.
- Meitinger, F., J.V. Anzola, M. Kaulich, A. Richardson, J.D. Stender, C. Benner, C.K. Glass, S.F. Dowdy, A. Desai, A.K. Shiau, and K. Oegema. 2016. 53BP1 and USP28 mediate p53 activation and G1 arrest after centrosome loss or extended mitotic duration. *The Journal of cell biology.* 214:155-166.

- Menon, M.B., A. Sawada, A. Chaturvedi, P. Mishra, K. Schuster-Gossler, M. Galla, A. Schambach, A. Gossler, R. Forster, M. Heuser, A. Kotlyarov, M. Kinoshita, and M. Gaestel. 2014. Genetic deletion of SEPT7 reveals a cell type-specific role of septins in microtubule destabilization for the completion of cytokinesis. *PLoS Genet.* 10:e1004558.
- Menon, S., and S.L. Gupton. 2016. Building Blocks of Functioning Brain: Cytoskeletal Dynamics in Neuronal Development. *International review of cell and molecular biology.* 322:183-245.
- Mierzwa, B., and D.W. Gerlich. 2014. Cytokinetic abscission: molecular mechanisms and temporal control. *Dev Cell.* 31:525-538.
- Mierzwa, B.E., N. Chiaruttini, L. Redondo-Morata, J.M. von Filseck, J. Konig, J. Larios, I. Poser, T. Muller-Reichert, S. Scheuring, A. Roux, and D.W. Gerlich. 2017. Dynamic subunit turnover in ESCRT-III assemblies is regulated by Vps4 to mediate membrane remodelling during cytokinesis. *Nat Cell Biol.* 19:787-798.
- Miki, H., Y. Okada, and N. Hirokawa. 2005. Analysis of the kinesin superfamily: insights into structure and function. *Trends Cell Biol.* 15:467-476.
- Miki, T., K. Okawa, T. Sekimoto, Y. Yoneda, S. Watanabe, T. Ishizaki, and S. Narumiya. 2009. mDia2 shuttles between the nucleus and the cytoplasm through the importin- α / β - and CRM1-mediated nuclear transport mechanism. *J Biol Chem.* 284:5753-5762.
- Mishima, M., V. Pavicic, U. Gruneberg, E.A. Nigg, and M. Glotzer. 2004. Cell cycle regulation of central spindle assembly. *Nature.* 430:908-913.
- Miyata, T., A. Kawaguchi, H. Okano, and M. Ogawa. 2001. Asymmetric inheritance of radial glial fibers by cortical neurons. *Neuron.* 31:727-741.
- Moawia, A., R. Shaheen, S. Rasool, S.S. Waseem, N. Ewida, B. Budde, A. Kawalia, S. Motameny, K. Khan, A. Fatima, M. Jameel, F. Ullah, T. Akram, Z. Ali, U. Abdullah, S. Irshad, W. Hohne, A.A. Noegel, M. Al-Owain, K. Hortnagel, P. Stobe, S.M. Baig, P. Numberg, F.S. Alkuraya, A. Hahn, and M.S. Hussain. 2017. Mutations of KIF14 cause primary microcephaly by impairing cytokinesis. *Ann Neurol.* 82:562-577.
- Mollinari, C., J.P. Kleman, W. Jiang, G. Schoehn, T. Hunter, and R.L. Margolis. 2002. PRC1 is a microtubule binding and bundling protein essential to maintain the mitotic spindle midzone. *The Journal of cell biology.* 157:1175-1186.

- Morita, E., V. Sandrin, H.Y. Chung, S.G. Morham, S.P. Gygi, C.K. Rodesch, and W.I. Sundquist. 2007. Human ESCRT and ALIX proteins interact with proteins of the midbody and function in cytokinesis. *EMBO J.* 26:4215-4227.
- Mukhina, S., Y.L. Wang, and M. Murata-Hori. 2007. Alpha-actinin is required for tightly regulated remodeling of the actin cortical network during cytokinesis. *Dev Cell.* 13:554-565.
- Mullins, J.M., and J.J. Biesele. 1977. Terminal phase of cytokinesis in D-98s cells. *The Journal of cell biology.* 73:672-684.
- Muzumdar, M.D., B. Tasic, K. Miyamichi, L. Li, and L. Luo. 2007. A global double-fluorescent Cre reporter mouse. *Genesis.* 45:593-605.
- Nahse, V., L. Christ, H. Stenmark, and C. Campsteijn. 2017. The Abcission Checkpoint: Making It to the Final Cut. *Trends Cell Biol.* 27:1-11.
- Neef, R., C. Preisinger, J. Sutcliffe, R. Kopajtich, E.A. Nigg, T.U. Mayer, and F.A. Barr. 2003. Phosphorylation of mitotic kinesin-like protein 2 by polo-like kinase 1 is required for cytokinesis. *The Journal of cell biology.* 162:863-875.
- Neumann, B., T. Walter, J.K. Heriche, J. Bulkescher, H. Erfle, C. Conrad, P. Rogers, I. Poser, M. Held, U. Liebel, C. Cetin, F. Sieckmann, G. Pau, R. Kabbe, A. Wunsche, V. Satagopam, M.H. Schmitz, C. Chapuis, D.W. Gerlich, R. Schneider, R. Eils, W. Huber, J.M. Peters, A.A. Hyman, R. Durbin, R. Pepperkok, and J. Ellenberg. 2010. Phenotypic profiling of the human genome by time-lapse microscopy reveals cell division genes. *Nature.* 464:721-727.
- Nishimura, Y., and S. Yonemura. 2006. Centralspindlin regulates ECT2 and RhoA accumulation at the equatorial cortex during cytokinesis. *J Cell Sci.* 119:104-114.
- Nishizawa, Y., H. Imafuku, K. Saito, R. Kanda, M. Kimura, S. Minobe, F. Miyazaki, S. Kawakatsu, M. Masaoka, M. Ogawa, and T. Miyata. 2007. Survey of the morphogenetic dynamics of the ventricular surface of the developing mouse neocortex. *Dev Dyn.* 236:3061-3070.
- Noctor, S.C., V. Martinez-Cerdeno, L. Ivic, and A.R. Kriegstein. 2004. Cortical neurons arise in symmetric and asymmetric division zones and migrate through specific phases. *Nat Neurosci.* 7:136-144.
- Noctor, S.C., V. Martinez-Cerdeno, and A.R. Kriegstein. 2008. Distinct behaviors of neural stem and progenitor cells underlie cortical neurogenesis. *The Journal of comparative neurology.* 508:28-44.

- Normand, G., and R.W. King. 2010. Understanding cytokinesis failure. *Adv Exp Med Biol.* 676:27-55.
- Ou, G., C. Gentili, and P. Gonczy. 2014. Stereotyped distribution of midbody remnants in early *C. elegans* embryos requires cell death genes and is dispensable for development. *Cell Res.* 24:251-253.
- Pacheco, A., and G. Gallo. 2016. Actin filament-microtubule interactions in axon initiation and branching. *Brain Res Bull.* 126:300-310.
- Paridaen, J.T., and W.B. Huttner. 2014. Neurogenesis during development of the vertebrate central nervous system. *EMBO Rep.* 15:351-364.
- Paridaen, J.T., M. Wilsch-Brauninger, and W.B. Huttner. 2013. Asymmetric inheritance of centrosome-associated primary cilium membrane directs ciliogenesis after cell division. *Cell.* 155:333-344.
- Peterman, E., P. Gibieza, J. Schafer, V.A. Skeberdis, A. Kaupinis, M. Valius, X. Heiligenstein, I. Hurbain, G. Raposo, and R. Prekeris. 2019. The post-abscission midbody is an intracellular signaling organelle that regulates cell proliferation. *Nat Commun.* 10:3181.
- Petsalaki, E., T. Akoumianaki, E.J. Black, D.A. Gillespie, and G. Zachos. 2011. Phosphorylation at serine 331 is required for Aurora B activation. *The Journal of cell biology.* 195:449-466.
- Petsalaki, E., and G. Zachos. 2019. Building bridges between chromosomes: novel insights into the abscission checkpoint. *Cell Mol Life Sci.* 76:4291-4307.
- Pilaz, L.J., J.J. McMahon, E.E. Miller, A.L. Lennox, A. Suzuki, E. Salmon, and D.L. Silver. 2016. Prolonged Mitosis of Neural Progenitors Alters Cell Fate in the Developing Brain. *Neuron.* 89:83-99.
- Pollarolo, G., J.G. Schulz, S. Munck, and C.G. Dotti. 2011. Cytokinesis remnants define first neuronal asymmetry in vivo. *Nat Neurosci.* 14:1525-1533.
- Polleux, F., and W. Snider. 2010. Initiating and growing an axon. *Cold Spring Harb Perspect Biol.* 2:a001925.
- Postiglione, M.P., C. Juschke, Y. Xie, G.A. Haas, C. Charalambous, and J.A. Knoblich. 2011. Mouse inscuteable induces apical-basal spindle orientation to facilitate intermediate progenitor generation in the developing neocortex. *Neuron.* 72:269-284.
- Powell, S.K., and H.K. Kleinman. 1997. Neuronal laminins and their cellular receptors. *Int J Biochem Cell Biol.* 29:401-414.

- Qian, X., S.K. Goderie, Q. Shen, J.H. Stern, and S. Temple. 1998. Intrinsic programs of patterned cell lineages in isolated vertebrate CNS ventricular zone cells. *Development*. 125:3143-3152.
- Qiu, R., Q. Runxiang, A. Geng, J. Liu, C.W. Xu, M.B. Menon, M. Gaestel, and Q. Lu. 2019. SEPT7 Interacts with KIF20A and Regulates the Proliferative State of Neural Progenitor Cells During Cortical Development. *Cereb Cortex*.
- Reilly, M.L., M.F. Stokman, V. Magry, C. Jeanpierre, M. Alves, M. Paydar, J. Hellinga, M. Delous, D. Pouly, M. Failler, J. Martinovic, L. Loeuillet, B. Leroy, J. Tantau, J. Roume, C.Y. Gregory-Evans, X. Shan, I. Filges, J.S. Allingham, B.H. Kwok, S. Saunier, R.H. Giles, and A. Benmerah. 2019. Loss-of-function mutations in KIF14 cause severe microcephaly and kidney development defects in humans and zebrafish. *Hum Mol Genet*. 28:778-795.
- Renshaw, M.J., J. Liu, B.D. Lavoie, and A. Wilde. 2014. Anillin-dependent organization of septin filaments promotes intercellular bridge elongation and Chmp4B targeting to the abscission site. *Open Biol*. 4:130190.
- Said Halidi, K.N., E. Fontan, A. Boucharlat, L. Davignon, M. Charpentier, M. Boulle, R. Weil, A. Israel, E. Laplantine, and F. Agou. 2019. Two NEMO-like Ubiquitin-Binding Domains in CEP55 Differently Regulate Cytokinesis. *iScience*. 20:292-309.
- Salzberg, A., D. D'Evelyn, K.L. Schulze, J.K. Lee, D. Strumpf, L. Tsai, and H.J. Bellen. 1994. Mutations affecting the pattern of the PNS in *Drosophila* reveal novel aspects of neuronal development. *Neuron*. 13:269-287.
- Salzmann, V., C. Chen, C.Y. Chiang, A. Tiyaboonchai, M. Mayer, and Y.M. Yamashita. 2014. Centrosome-dependent asymmetric inheritance of the midbody ring in *Drosophila* germline stem cell division. *Mol Biol Cell*. 25:267-275.
- Sapir, T., T. Levy, A. Sakakibara, A. Rabinkov, T. Miyata, and O. Reiner. 2013. Shootin1 acts in concert with KIF20B to promote polarization of migrating neurons. *J Neurosci*. 33:11932-11948.
- Sarkisian, M.R., W. Li, F. Di Cunto, S.R. D'Mello, and J.J. LoTurco. 2002. Citron-kinase, a protein essential to cytokinesis in neuronal progenitors, is deleted in the flathead mutant rat. *J Neurosci*. 22:RC217.
- Schiel, J.A., K. Park, M.K. Morphew, E. Reid, A. Hoenger, and R. Prekeris. 2011. Endocytic membrane fusion and buckling-induced microtubule severing mediate cell abscission. *J Cell Sci*. 124:1411-1424.

- Schiel, J.A., and R. Prekeris. 2010. Making the final cut - mechanisms mediating the abscission step of cytokinesis. *ScientificWorldJournal*. 10:1424-1434.
- Schiel, J.A., G.C. Simon, C. Zaharris, J. Weisz, D. Castle, C.C. Wu, and R. Prekeris. 2012. FIP3-endosome-dependent formation of the secondary ingression mediates ESCRT-III recruitment during cytokinesis. *Nat Cell Biol*. 14:1068-1078.
- Shaheen, R., A. Hashem, G.M. Abdel-Salam, F. Al-Fadhli, N. Ewida, and F.S. Alkuraya. 2016. Mutations in CIT, encoding citron rho-interacting serine/threonine kinase, cause severe primary microcephaly in humans. *Hum Genet*. 135:1191-1197.
- Shen, Q., Y. Wang, J.T. Dimos, C.A. Fasano, T.N. Phoenix, I.R. Lemischka, N.B. Ivanova, S. Stifani, E.E. Morrisey, and S. Temple. 2006. The timing of cortical neurogenesis is encoded within lineages of individual progenitor cells. *Nat Neurosci*. 9:743-751.
- Shen, Q., W. Zhong, Y.N. Jan, and S. Temple. 2002. Asymmetric Numb distribution is critical for asymmetric cell division of mouse cerebral cortical stem cells and neuroblasts. *Development*. 129:4843-4853.
- Shimada, T., M. Toriyama, K. Uemura, H. Kamiguchi, T. Sugiura, N. Watanabe, and N. Inagaki. 2008. Shootin1 interacts with actin retrograde flow and L1-CAM to promote axon outgrowth. *The Journal of cell biology*. 181:817-829.
- Shitamukai, A., D. Konno, and F. Matsuzaki. 2011. Oblique radial glial divisions in the developing mouse neocortex induce self-renewing progenitors outside the germinal zone that resemble primate outer subventricular zone progenitors. *J Neurosci*. 31:3683-3695.
- Singh, D., and C. Pohl. 2014a. Coupling of rotational cortical flow, asymmetric midbody positioning, and spindle rotation mediates dorsoventral axis formation in *C. elegans*. *Dev Cell*. 28:253-267.
- Singh, D., and C. Pohl. 2014b. A function for the midbody remnant in embryonic patterning. *Commun Integr Biol*. 7:e28533.
- Skop, A.R., H. Liu, J. Yates, 3rd, B.J. Meyer, and R. Heald. 2004. Dissection of the mammalian midbody proteome reveals conserved cytokinesis mechanisms. *Science*. 305:61-66.
- Spiliotis, E.T., M. Kinoshita, and W.J. Nelson. 2005. A mitotic septin scaffold required for Mammalian chromosome congression and segregation. *Science*. 307:1781-1785.

- Steigemann, P., C. Wurzenberger, M.H. Schmitz, M. Held, J. Guizetti, S. Maar, and D.W. Gerlich. 2009. Aurora B-mediated abscission checkpoint protects against tetraploidization. *Cell*. 136:473-484.
- Stoten, C.L., and J.G. Carlton. 2018. ESCRT-dependent control of membrane remodelling during cell division. *Semin Cell Dev Biol*. 74:50-65.
- Takahashi, T., R.S. Nowakowski, and V.S. Caviness, Jr. 1995. The cell cycle of the pseudostratified ventricular epithelium of the embryonic murine cerebral wall. *J Neurosci*. 15:6046-6057.
- Tan, X., and S.H. Shi. 2013. Neocortical neurogenesis and neuronal migration. *Wiley Interdiscip Rev Dev Biol*. 2:443-459.
- Tanaka, E.M., and M.W. Kirschner. 1991. Microtubule behavior in the growth cones of living neurons during axon elongation. *The Journal of cell biology*. 115:345-363.
- Thoresen, S.B., C. Campsteijn, M. Vietri, K.O. Schink, K. Liestol, J.S. Andersen, C. Raiborg, and H. Stenmark. 2014. ANCHR mediates Aurora-B-dependent abscission checkpoint control through retention of VPS4. *Nat Cell Biol*. 16:550-560.
- Toriyama, M., S. Kozawa, Y. Sakumura, and N. Inagaki. 2013. Conversion of a signal into forces for axon outgrowth through Pak1-mediated shootin1 phosphorylation. *Curr Biol*. 23:529-534.
- Toriyama, M., T. Shimada, K.B. Kim, M. Mitsuba, E. Nomura, K. Katsuta, Y. Sakumura, P. Roepstorff, and N. Inagaki. 2006. Shootin1: A protein involved in the organization of an asymmetric signal for neuronal polarization. *The Journal of cell biology*. 175:147-157.
- van Beuningen, S.F., and C.C. Hoogenraad. 2016. Neuronal polarity: remodeling microtubule organization. *Curr Opin Neurobiol*. 39:1-7.
- Wang, X., J.W. Tsai, J.H. Imai, W.N. Lian, R.B. Vallee, and S.H. Shi. 2009. Asymmetric centrosome inheritance maintains neural progenitors in the neocortex. *Nature*. 461:947-955.
- Watanabe, S., Y. Ando, S. Yasuda, H. Hosoya, N. Watanabe, T. Ishizaki, and S. Narumiya. 2008. mDia2 induces the actin scaffold for the contractile ring and stabilizes its position during cytokinesis in NIH 3T3 cells. *Mol Biol Cell*. 19:2328-2338.

- Watanabe, S., T. De Zan, T. Ishizaki, and S. Narumiya. 2013a. Citron kinase mediates transition from constriction to abscission through its coiled-coil domain. *J Cell Sci.* 126:1773-1784.
- Watanabe, S., T. De Zan, T. Ishizaki, S. Yasuda, H. Kamijo, D. Yamada, T. Aoki, H. Kiyonari, H. Kaneko, R. Shimizu, M. Yamamoto, G. Goshima, and S. Narumiya. 2013b. Loss of a Rho-regulated actin nucleator, mDia2, impairs cytokinesis during mouse fetal erythropoiesis. *Cell Rep.* 5:926-932.
- Watanabe, S., K. Okawa, T. Miki, S. Sakamoto, T. Morinaga, K. Segawa, T. Arakawa, M. Kinoshita, T. Ishizaki, and S. Narumiya. 2010. Rho and anillin-dependent control of mDia2 localization and function in cytokinesis. *Mol Biol Cell.* 21:3193-3204.
- Westendorf, J.M., P.N. Rao, and L. Gerace. 1994. Cloning of cDNAs for M-phase phosphoproteins recognized by the MPM2 monoclonal antibody and determination of the phosphorylated epitope. *Proc Natl Acad Sci U S A.* 91:714-718.
- Witte, H., D. Neukirchen, and F. Bradke. 2008. Microtubule stabilization specifies initial neuronal polarization. *The Journal of cell biology.* 180:619-632.
- Yamashita, Y.M., A.P. Mahowald, J.R. Perlin, and M.T. Fuller. 2007. Asymmetric inheritance of mother versus daughter centrosome in stem cell division. *Science.* 315:518-521.
- Yanagi, K., R. Sone, R. Ohga, and A. Kawahara. 2019. Involvement of the centrosomal protein 55 (cep55) gene in zebrafish head formation. *Genes Cells.* 24:642-649.
- Yang, D., N. Rismanchi, B. Renvoise, J. Lippincott-Schwartz, C. Blackstone, and J.H. Hurley. 2008. Structural basis for midbody targeting of spastin by the ESCRT-III protein CHMP1B. *Nat Struct Mol Biol.* 15:1278-1286.
- Yingling, J., Y.H. Youn, D. Darling, K. Toyo-Oka, T. Pramparo, S. Hirotsune, and A. Wynshaw-Boris. 2008. Neuroepithelial stem cell proliferation requires LIS1 for precise spindle orientation and symmetric division. *Cell.* 132:474-486.
- Yu, W., C. Cook, C. Sauter, R. Kuriyama, P.L. Kaplan, and P.W. Baas. 2000. Depletion of a microtubule-associated motor protein induces the loss of dendritic identity. *J Neurosci.* 20:5782-5791.
- Zhao, W.M., A. Seki, and G. Fang. 2006. Cep55, a microtubule-bundling protein, associates with centralspindlin to control the midbody integrity and cell abscission during cytokinesis. *Mol Biol Cell.* 17:3881-3896.

- Zhu, C., E. Bossy-Wetzel, and W. Jiang. 2005a. Recruitment of MKLP1 to the spindle midzone/midbody by INCENP is essential for midbody formation and completion of cytokinesis in human cells. *Biochem J.* 389:373-381.
- Zhu, C., E. Lau, R. Schwarzenbacher, E. Bossy-Wetzel, and W. Jiang. 2006. Spatiotemporal control of spindle midzone formation by PRC1 in human cells. *Proc Natl Acad Sci U S A.* 103:6196-6201.
- Zhu, C., J. Zhao, M. Bibikova, J.D. Levenson, E. Bossy-Wetzel, J.B. Fan, R.T. Abraham, and W. Jiang. 2005b. Functional analysis of human microtubule-based motor proteins, the kinesins and dyneins, in mitosis/cytokinesis using RNA interference. *Mol Biol Cell.* 16:3187-3199.